論文 / 著書情報
Article / Book Information

題目(和文)	
Title(English)	Performance of River levee reinforced with Steel Drainage Pipes against Flooding
著者(和文)	SinghJenisha
Author(English)	Jenisha Singh
出典(和文)	学位:博士(学術), 学位授与機関:東京工業大学, 報告番号:甲第11534号, 授与年月日:2020年3月26日, 学位の種別:課程博士, 審査員:髙橋 章浩,北詰 昌樹,竹村 次朗,笠間 清伸,WIJEYEWICKREMA ANIL
Citation(English)	Degree:Doctor (Academic), Conferring organization: Tokyo Institute of Technology, Report number:甲第11534号, Conferred date:2020/3/26, Degree Type:Course doctor, Examiner:,,,,
学位種別(和文)	博士論文
Type(English)	Doctoral Thesis

Performance of River levee reinforced with Steel Drainage Pipes against Flooding

Jenisha Singh

THESIS

Submitted in partial fulfilment of the requirements for the degree of

DOCTOR OF PHILOSOPHY

at

DEPARTMENT OF CIVIL ENGINEERING

TOKYO INSTITUTE OF TECHNOLOGY

Tokyo, Japan

November 2019

Acknowledgements

I would like to first and foremost express my gratitude to Professor Akihiro Takahashi, my academic supervisor for my study here at the Tokyo Institute of Technology. His constant encouragement, guidance and support throughout my research helped me in achieving the research goals. The role he played in completion of this dissertation cannot be overstated. I have learned a lot from him not only from his role as my academic supervisor but also as a researcher and teacher by attending his lectures.

I am grateful to my thesis committee, Professor Masaki Kitazume, Associate Professor Jiro Takemura, Associate Professor Kiyonobu Kasama and Associate Professor Anil C. Wijeyewickrema, for their valuable suggestions on my research. Their comments and recommendation have certainly improved the quality of the dissertation.

I want to extend my thanks to Assistant Professor Kazuki Horikoshi for helping me with the experiments and numerical analysis during my research. I am immensely grateful to our lab technician Mr Sakea Seki for guiding me through the centrifuge experiment. He was extremely patient and kind in teaching me every aspect of the experiments. I am also very thankful for my labmates from the Geotechnical Engineering group who have contributed to my research through their valuable suggestions. I would like to specially mention Uemura, Koito, Vijay, Partha, Kusaka, Ritesh, and Max for their contribution to my research. This research was conducted as part of the collaboration with Nippon Steel and Sumitomo Metal, Research and Engineering Centre. I am grateful to team in the research centre for their contribution to research. I acknowledge the Ministry of Education, Culture, Sports, Science and Technology, Japan (MEXT) for granting me Monbukagakusho scholarship.

I want to thank my friends Anuja and Keshav for being moral support and being like my family away from family here in Tokyo. Also, my Nepalese community here at Tokyo Tech for making this journey beautiful. Finally, I would like to thank my parents and my brother for always being the source of motivation and unconditional love.

Abstract

Increased seepage flow in levees during the flood can cause destabilization by an increase in self-weight of soil and reduction of shear strength due to the decrease of effective stress. Reduction of effective stress is due to loss of matric suction when the soil is saturated. Reduction of soil strength in slope caused due to the decrease in effective stress can cause soil mass movement making the slope unstable. Additional protection measures in the levees subjected to the seepage flow is expected enhance the level of safety against seepage induced failure. Additional protection in the levee can be provided either in the form of drainage which would limit the rise of phreatic surface or in the form of the reinforcement which would compensate the loss of the shear strength caused due to seepage flow through mobilization of additional strength.

Drainage pipes are one of the standard methods of protection, used mostly in existing levees, to limit the decrease in effective stress by limiting development of the positive pressure. Soil nails are also used as other option of protection measure in the slope stability problems by mobilization of additional strength. Soil nails predominantly with the development of axial force increase the shear resistance in the slope. However, slope protection measures with only either of drainage or by reinforcement has shown its limitation when subjected to seepage flow. Combining both functions of drainage and increasing reinforcement provide better solution against seepage-induced failure. The presence of reinforcement along with the drainage provides additional protection in the cases drainage in pipes cannot function.

In this study, therefore, the possibility of use of the steel drainage pipe in the levee for the protection against seepage-induced failure is investigated through the series of the centrifugal test. Steel drainage pipes are newly designed protection measures which are capable of providing both functions of the drainage and reinforcement. Steel drainage pipes can provide these dual function because of its tubular structure with numerous holes on the surface and the spiral blades at the end included in design. During the course of

study the working mechanism of steel drainage pipes is identified. Through the series of centrifuge test and 1g physical model test results, it is confirmed that quick drainage of the seepage water can restrict the development of positive pore water pressure in the slope and mobilization of the axial force and bending moment in the pipes minimizes flood-induced deformation of the levee. In addition drainage aides the force mobilisation in pipes. Test results also reveal that installation of the steel drainage pipes (1) allows the levee to withstand the higher flood water head and extended flood duration and (2) is effective to limit the continuation of slip line in the slope.

After the working mechanism of the steel drainage pipes is confirmed, the performance of the levee reinforced with the steel drainage pipe under the varying condition such as soil properties, flood rising rate and arrangement of pipes is discussed.

From the parametric studies using numerical analysis it is confirmed that deformation in levee with steel drainage pipes remains consistent in soil within large range of hydraulic conductivity. In the soil with very low hydraulic conductivity (less than 4.5E-5 m/s), installation of the steel drainage pipes do not contribute to the lowering of pore water pressure and consequently to the deformation as well.

In unreinforced levee, speed of rising of flood level effects the progression of phreatic surface within the levee whereas in the case provided with steel drainage pipes progression is minimally affected by the speed of rising of flood level. Speed of the rise of flood level in unreinforced case cause the change in the final deformation. Final deformation in levee with steel drainage pipe is found to be independent of the speed of rising of flood level; rather, it is dependent on the flood level only.

From the study about arrangement of steel drainage pipes in levee, it is found that overall deformation of the slope is more controlled by the location of the phreatic surface within the slope. Thus installation of the steel drainage pipe at lower elevation would be more effective in minimizing deformation in slope subjected to flooding. Spacing of steel drainage pipes controls the deformation experienced by levee. If pipes are installed at very large spacing, the installation of steel drainage pipes will provide no improvement in deformation control.

Table of Contents

List of Figures

List of Tables

List of Symbols and Acronyms

σ' : Effective normal stress

σ_x : Normal stress in x direction

σ_y : Normal stress in y direction

σ_z : Normal stress in z direction

τ_{xy} : Shear stress on x-plane pointing in y direction

τ_{xz} : Shear stress on x-plane pointing in z direction

τ_{yx} : Shear stress on y-plane pointing in x direction

τ_{yz} : Shear stress on y-plane pointing in z direction

τ_{zx} : Shear stress on z-plane pointing in x direction

τ_{zy} : Shear stress on z-plane pointing in y direction

u_w: Pore water pressure

χ : Soil parameter related to degree of saturation

u_a : Pore air pressure

σ : Total stress

S_e : Effective degree of saturation

θ: Volumetric water content

θ_r : Residual volumetric content.

θ_s : Saturated volumetric water content

SWCC: Soil water characteristic curve

α : Soil fitting parameter in van Genuchten model function

ψ : Pressure head

n' : Soil fitting parameter in van Genuchten model function

m : Soil fitting parameter in van Genuchten model function

k_{wr} : Specific permeability coefficient

k_{wu} : Unsaturated permeability

k_{ws} : Saturated permeability

PPT: Pore water pressure transducer

LDT: Laser displacement transducer

USCS: Unified soil classification system

1 Introduction

Slope failure has always been one of the leading causes of the damage to the property and human lives. Levees constructed on the river bank are susceptible to the seepage failure during the flooding in the river channel. Under the normal condition, the majority of the slopes are composed of unsaturated soil. Such slopes due to the presence of the suction in the soil above the line of the saturation remain stable even when the slopes are steeper than what is supported by the saturated soil mechanics.

The instantaneous rise in the water level in the river channel during the event of flood cause the increase of the water table in the slope, thus increasing the pore water pressure. The increase in pore water pressure cause loss of the effective stress in soil and eventually leading to the failure.

Many incidents of levee failure and in worst case scenario breaching of the levee has been reported in the past. Breaching of the levees can cause the catastrophic damage when the cities are spread below the high flood water level like the cases in the major cities of the Japan which can be seen in an example cross section of Tokyo shown in Fig 1.1. Figure 1.2 shows some of the incidents of the levee breaching and damage caused. The Niigata Flood in 2004, the breaching of the levee constructed on the Kariyata River caused inundation of the protected area (Sato et al., 2006). Also, the torrential rain and subsequent flooding in the Ikarashi River in 2004 resulted in the breaching of the levee leading to the flood in Sanjo City (Nobuyuki, 2004). Very recently, in 2015 flooding in the Kinugawa River of the Ibaraki prefecture caused by the typhoon Etau also caused breaching of the levee and subsequent inundation of the protected area (Chappell, 2015). This kind of the reported cases highlights the need for understanding the response of the levees against the seepage flow. Understanding the failure of river levee when subjected to the flood induced seepage, requires the understanding of the unsaturated soil mechanics and seepage flow in unsaturated slope.

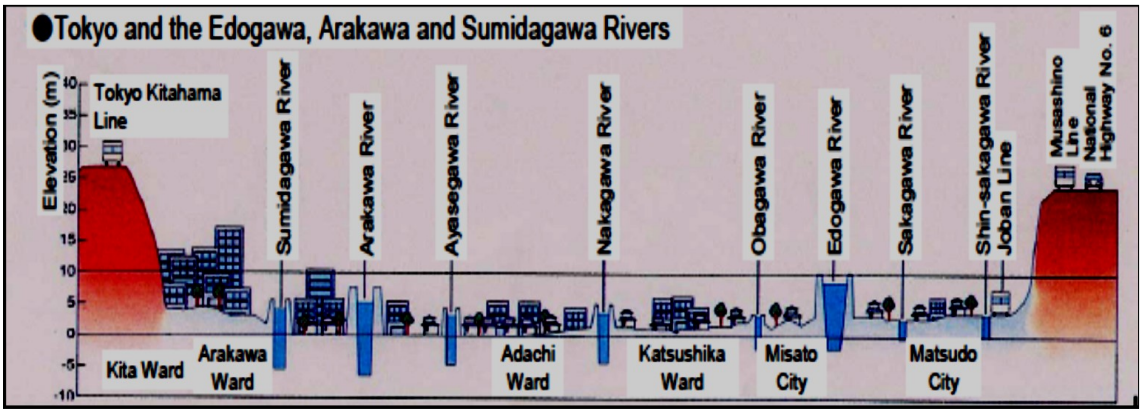

Figure 1.1 Cross-section of Tokyo showing the level of river (Source: River Bureau, Minister of Land, Infrastructure, Transport and Tourism, Japan)

Figure 1.2 Damages caused by the breaching of the levee (Chappell, 2015; Nobuyuki, 2004; Sato et al., 2006)

1.1 Unsaturated Soil Mechanics

Unsaturated soil can be defined as soil having four different phases: (1) solid (2) water (3) air and (4) air-water interface also called contractile skin (Fredlund and Morgenstern, 1977). Out of these two phases, air and water flow under the stress gradient and other remaining two solid and contractile skin stay in equilibrium under the stress gradient (D. G. Fredlund & Rahardjo, 1993). Stress state changes in any of the phases can lead the unsaturated soil to change its water content, volume and shear strength (Fredlund et al., 2012).

1.1.1 Stress state variable.

State variables are the variables which are defined in the context of the continuum mechanics, remains independent of soil properties (Fredlund et al., 2012) and are required to explain a system or mixture of phases (Fung, 1965). A set of independent stress state variable is termed as suitable stress state variable when there is no deformation or volume change in the element considered when there is a change in the individual component of stress state variable by keeping state variable itself constant (Fredlund and Morgenstern, 1977).

For the saturated soil stress, state was defined by Terzaghi in terms of the effective stress as (Terzaghi, 1936)

$$\left[\sigma'\right]=\begin{bmatrix}\left(\sigma_x-u_w\right) & \tau_{yx} & \tau_{zx}\\ \tau_{xy} & \left(\sigma_y-u_w\right) & \tau_{zy}\\ \tau_{xz} & \tau_{yz} & \left(\sigma_z-u_w\right)\end{bmatrix} \quad \text{.....[1.1]}$$

where: σ': effective normal stress

$\sigma_x, \sigma_y, \sigma_z$, : Normal stress in x, y, and z-direction respectively.

$\tau_{xy}, \tau_{xz}, \tau_{yx}, \tau_{yz}\ \ \tau_{zx}\ \tau_{zy}$: Shear stress

u_w: Pore water pressure

For saturated soil, from much experimental evidence has ensured the viability of effective stress variable for defining the physical behaviour. However, this is not the case when the soil is unsaturated. In the unsaturated soil void between soils are not only occupied by the incompressible liquid but also highly compressible air, so only the effective stress is not enough as stress state variable. Various researchers have made a contribution towards defining the stress state variable for unsaturated soil. Two independent stress state variable $(\sigma - u_w)$ and u_w was proposed by Biot (1941) based on the general theory of consolidation identifying the fact that effective stress and pore water pressure needs to be separated. After this Colman (1962), suggested the idea of three stress state variable; $\sigma - u_a$ and $u_w - u_a$ based on the triaxial experiments. Based on the laboratory test results, soil behaviour change with respect to the normal stress and matric suction which was found to be independent of each other, net normal stress and matric suction were presented as independent state variable by Bishop & Blight (1963). Also, citing the characterization of the volume-mass behaviour Matyas & Radhakrishna (1968); Barden et al. (1969), proposed the idea of the independent component of net normal stress and the matric suction as the stress parameter.

Fredlund & Morgenstern (1977) justified the use of the independent stress state variable through the equilibrium analysis on an unsaturated soil assuming soil particle as incompressible and chemically inert. The analysis also proposed the use of three possible combinations of the stress variable; (1) $\sigma - u_a$ and $u_a - u_w$, (2) $\sigma - u_w$ and $u_a - u_w$, and (3) $\sigma - u_a$ and $\sigma - u_w$. Out of these, the first combination is widely accepted in the formulation of the unsaturated problem.

1.1.2 Effective stress equation

One of the oldest and single-valued effective stress relationships was proposed by Bishop (1960) and often referred as the Bishop's effective stress equation for the unsaturated soil which has the form as shown in equation [1.2].

$$\sigma' = (\sigma - u_a) + \chi(u_a - u_w) \quad \text{..... [1.2]}$$

here, χ is soil parameter related to the degree of the saturation ranging from 0 to 1.

Based on the definition proposed by Vanapalli et al. (1996) for the shear strength applied for the failure criterion, χ can be replaced by the effective saturation. Effective saturation (S_e) is defined as following:

$$S_e = \frac{\theta - \theta_r}{\theta_s - \theta_r} \quad \text{..... [1.3]}$$

In the equation θ is volumetric water content, θ_s is the saturated volumetric water content which can be taken approximately equal to the porosity and θ_r is the residual volumetric content.

In this way, effective stress of the unsaturated soil is related to the soil water characteristic curve (SWCC) which is the variation of the matric suction with the change in moisture content/ degree of the saturation of the soil.

The rate of change of the shear strength of the unsaturated soil appears to depend on the area of menisci in contact with the soil; it is, therefore, appropriate to relate the effective stress to the SWCC. Details of SWCC are explained in subsection 1.1.4

1.1.3 Hydraulic properties

Understanding the stability of slopes subjected to the seepage flow needs the understanding of the pore water pressure development before, during and after the seepage flow. Pore water pressure and the strength parameters govern the stability of the slope subjected to the seepage flow. In the unsaturated soil, development of the pore water pressure depends on both the intrinsic and external parameters. Intrinsic factors mainly deal with the hydraulic properties such as water retention characteristics and water coefficient of permeability. External factors refer to many factors such as climatic condition, slopes geometries, flux parameters and much more.

Many researchers have studied about the factors influencing the pore water response of the soil subjected to seepage flow. Heber Green & Ampt (1911), concluded the dependence of the pore water pressure reliance on the saturated coefficient of permeability and specific storage. To this Gavin & Xue (2008) added the concept of varying coefficient of the permeability rather than constant value. Kasim et al. (1998)

studied the response of the pore water pressure considering coefficient of the permeability and concluded that the pore water pressure evolution in the soil depends on the saturated permeability, approximate air entry value, and desaturation coefficient. Zhan & Ng (2004) and Rahimi et al. (2015) from their studies came to the conclusion that the storage capacity defined by the soil water characteristic curve and water coefficient of the permeability of the soil are most important hydraulic properties for the seepage flow in the unsaturated soil.

Flow in the unsaturated soil, like in the saturated soil is governed by Darcy's law (Fredlund et al., 2012). However, there exist some major difference in the unsaturated soil when compared to the saturated soil flow. These major differences are the storage term which indicates the variation of the moisture content with the matric suction and water coefficient of permeability which is very much influenced by the variation of moisture content. The SWCC can determine the storage term. So, SWCC and coefficient of the permeability are the most important hydraulic parameter in the unsaturated soil.

1.1.4 Soil Water Characteristic Curve (SWCC)

Soil water characteristic curve can be defined as the variation of water storage capacity within the macro and micro pores of soil with respect to the suction (Zapata, 1999). This relationship is plotted as a change of gravimetric water content, volumetric water content or degree of the saturation with respect to the soil suction. Soil suction consists of both matric and osmotic suction. However, it is the matric suction that governs the engineering properties of the unsaturated soil in the low suction range which is most encountered in field situation (Fredlund, 1995). Therefore, SWCC is often plotted in terms of the matric suction rather than the total suction.

Figure 1.3 shows the typical soil water characteristic curve for drying process along with the different stages of the desaturation. With the increase in the matric suction, soil starts to desaturate. There are three steps of the desaturation; boundary effect stage, transition stage and the residual stage of unsaturation. Transition stage can further be divided into primary transition and secondary transition stage.

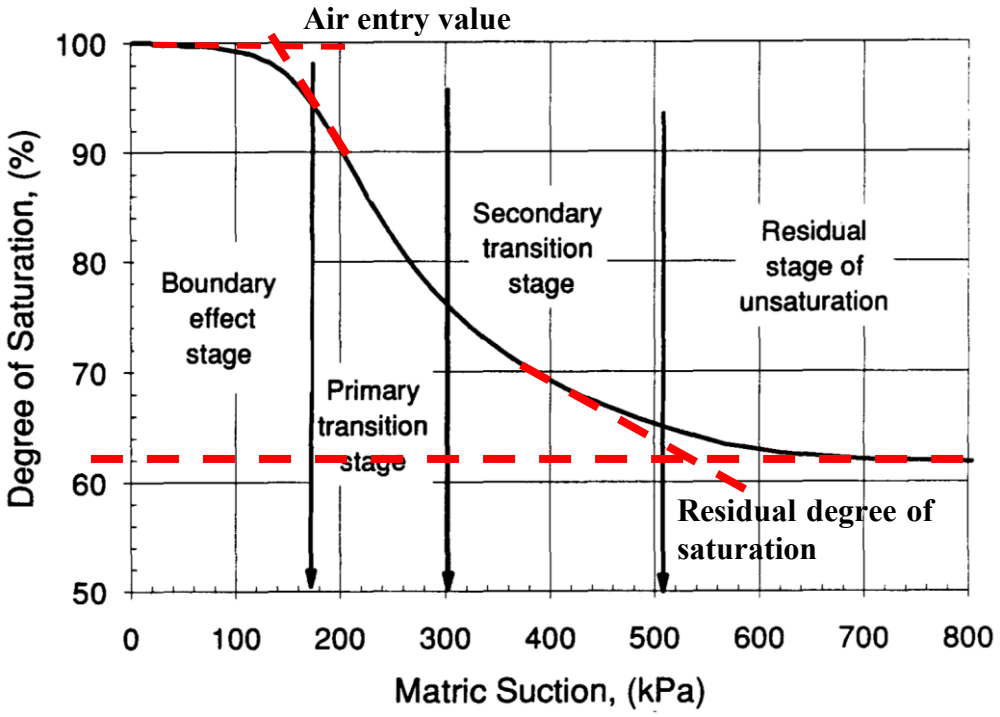

Figure 1.3 Soil water characteristics curve showing different stages of the desaturation (after Fredlund, 1995)

Figure 1.4 demonstrates the variation of the wetted area of contact during the various stages of the desaturation. During the boundary effect stage, almost all the void space between the soil particles is filled with the water. At this stage, soil is saturated. Air entry point in this stage is the value of suction at which air enters the largest pores of the soil. Soil starts to desaturate in the transition stage. At this stage, saturation changes significantly even at the small change in the matric suction. As the suction is increased, connectivity between the pores or voids decreases thus water flow through increasingly small pores. On further increasing the suction, the change in saturation is not drastic like in primary transition stage. On further increasing the suction, leads to a subtle variation in the degree of the saturation. This stage is referred as the residual stage of the unsaturation. At this stage, the soil has very less water content and has no or very less contribution in the flow. Moisture content at this stage is referred as residual moisture

content. At this stage, the wetted contact area is reduced significantly, and soil suction is not very effective in contributing to shear strength.

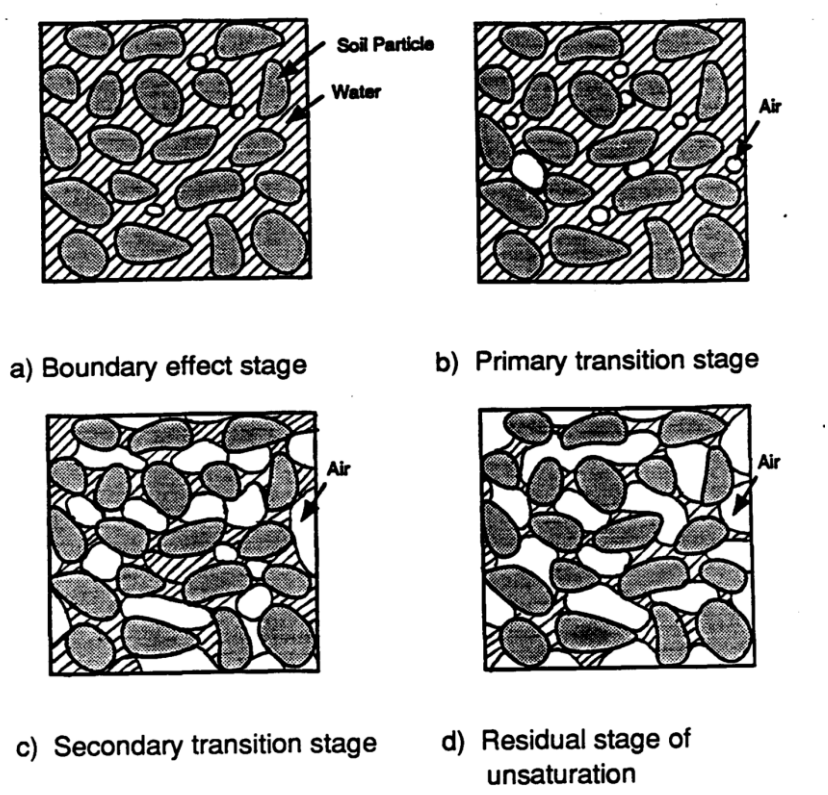

Figure 1.4 Variation of the wetted contact area for different stages of soil water characteristic curve (after Fredlund, 1995)

Parameters required to describe the SWCC include the saturated volumetric water content which can be treated as the porosity of the soil. The other parameter required is the air entry value. Air entry value is the minimum suction to be exceeded for air to recedes into soil pore. Residual water content or the saturation is next parameter required to describe SWCC. Residual Saturation is the degree of saturation at which increase in suction does not produce a significant change in the level of the saturation. Soil suction can be expressed in term of energy per unit mass, energy per unit volume or the energy per unit weight of the soil water. Common units to express the suction are kPa or MPa and cm or m of the water. The development of the SWCC for a particular soil needs lots of test and

time to obtain all the required information. To solve this issue, several mathematical models have been developed to estimate the SWCC. The mathematical model facilitates the description of SWCC for the particular soil with just a few points.

Many mathematical equations have been proposed to represent the SWCC. Most of the proposed equations are empirical in nature and based on the shape of SWCC. Some researchers established the empirical relation between the soil properties and fitting parameters of SWCC (Ahuja et al., 1985; Chin et al., 2010). Some researchers used approaches involving the grain size distribution into pore size distribution of the soil to estimate the SWCC (Arya and Paris, 1981; Fredlund et al., 1997). Fredlund & Xing (1994) proposed the empirical equation based on the assumption that shape of SWCC depends on pore size distribution of the soil. Leong & Rahardjo (1997) from their study concluded that the empirical equation proposed by Fredlund & Xing (1994) provided the best fit. Zhang & Chen (2005) extended the model suggested by the Fredlund & Xing (1994) and van Genuchten (1980) to the bimodal and the multimodal SWCC.

Mathematical model proposed by the van Genuchten in (1980) is four parameter equation is widely used especially for predicting the hydraulic conductivity. van Genuchten model even though do not address the hysteresis in the SWCC and has been reported to be not very suitable within the high suction region fairs quite well in the low suction region which common in the field. Here, in this study van Genuchten model is used for estimating the SWCC.

The relation proposed by van Genuchten as represented in Equation [1.4] shows the relationship between effective saturation and pressure head ψ .

$$S_e = \left\{1+(\alpha\psi)^{n'}\right\}^{-m} \qquad [1.4]$$

here, α, n' are fitting parameters. Here, α is a function of the air entry value and n' is soil parameter controlling the slope of SWCC at the inflection point. m is calculated as following

$$m = 1 - 1/n' \qquad [1.5]$$

The fitting parameters were determined from the experimental data of wetting soil moisture characteristic curve obtained by column test in this study.

1.1.5 Coefficient of permeability

For the unsaturated soil, unlike in the case of the saturated soil, the coefficient of permeability is not a constant value. In the unsaturated soil, the coefficient of the permeability depends on the degree of the saturation or the negative pore water pressure of the soil. In the unsaturated soil, water flows only through the pore space filled with water as air-filled pores are not conductive to the water. So, the percentage of the void which is occupied by the water which is indicated by the degree of the saturation is a major factor in the determination of the coefficient of permeability of the unsaturated soil. The coefficient of the permeability with respect to the negative pore water pressure holds the relationship with SWCC, which is the representation of the relationship between the degree of the saturation and negative pore water pressure. The coefficient of the permeability in the unsaturated soil, therefore, can be estimated with the saturated permeability and SWCC (Brooks and Corey, 1964; Fredlund et al., 1994; Van Genuchten, 1980).

Figure 1.5 shows a typical hydraulic conductivity curve for the two types of the soil; namely sandy soil and clayey soil. In the figure, it can be seen that even though saturated hydraulic conductivity of the sandy soil is initially larger than the clayey soil, because of the sharp change in the conductivity with respect to the change in the matric suction unsaturated permeability of sandy soil eventually is less than the clayey soil. This behaviour is related to the high desaturation rate in the sandy soil. By high desaturation rate, it indicates that with the small change in the matric suction, there is a very sharp change in the moisture content. To put in the other word, it can be said that with a small increase in the matric suction, a large area of the void is occupied by the air. Since the voids filled with air are nonconductive to the flow of water, there is a sharp change in the coefficient of permeability with an increase in the matric suction.

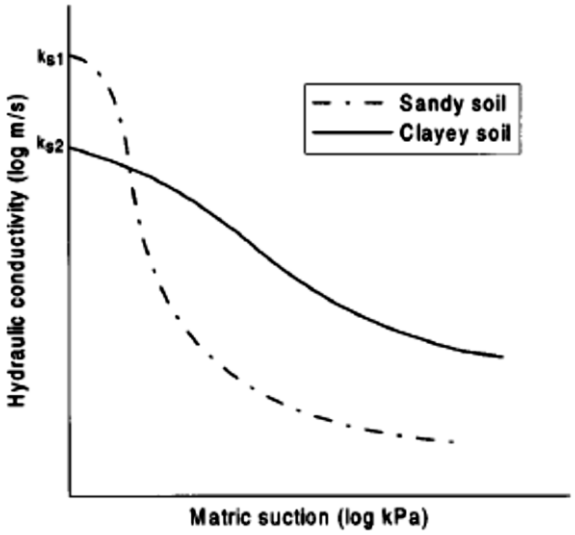

Figure 1.5 Relationship between water permeability and matric suction for different soil [based on (Zhan et al., 2004)]

In this study, relation proposed by Kosugi (1999) which relates the coefficient of the permeability with SWCC and the saturated hydraulic permeability is used. The proposed relation is as following

$$k_{wr} = S_e^{\xi}\left(\frac{\int_0^{S_e}|\psi|^{-\beta}\,dS_e}{\int_0^{1}|\psi|^{-\beta}\,dS_e}\right)^{\eta} \qquad [1.6]$$

Here $\xi, \beta, \eta =$ fitting parameters and using the values equal to $\xi = 0.5, \beta = 1, \eta = 2$ relationship thus obtained is used in the numerical analysis,

$$k_{wr} = S_e^{0.5}\left\{1-\left(1-S_e^{1/m}\right)^{m}\right\}^{2} \qquad [1.7]$$

Here, k_{wr} is the specific permeability coefficient which is the ratio of unsaturated permeability k_{wu} to saturated permeability k_{ws},

$$k_{wr} = \frac{k_{wu}}{k_{ws}} \qquad [1.8]$$

1.2 Seepage flow in the unsaturated soil slope

The structural integrity of the river levee is crucial for the protection of life and other assets. Water content/ moisture content in the soil significantly affects the behaviour of the slope under the broad range of the loading and external conditions. An event such as flooding often causes the damage of the levee. During the case of the flooding, levee can fail due to numerous factors such as overtopping, scouring of the foundation, seepage in levee/foundation, or the sliding of the foundation. Among these, a failure which is influenced by the levee's geometrical configuration, hydraulic conditions and material properties caused by the seepage is considered one of the predominant cause of the failure (Camici et al., 2015). Seepage flow in such earthen structure like river levee, therefore, demands the greater attention when considered the stability of the river levee.

Understanding the effect of the seepage flow in the unsaturated soil slope is important because seepage flow in the slope may reduce the effective stress in the soil. It also can affect the stability of the bank by reducing the resistance force in the potential failure surface or by increasing the driving force above it. Reduction in the resistance force on the soil slope can occur through the combination of the initial toe erosion or by the loss of the matric suction. The increment in the driving force can be the result of the increment of the soil weight or the increment in pore water pressure (Vandamme and Zou, 2013). Negative pore water pressure which is also coined as the matric suction provides the apparent cohesion to the soil slope and thus increases the stability of the slope significantly. However, with the seepage flow, this negative pressure is removed which substantially decreases the stability of slope and may lead to failure of the slope.

1.2.1 Cases of levees/ embankment failure due to flooding induced seepage

Many cases of the levee/embankment failures are reported annually which are caused due to seepage flow. Here in this section few of such situations are discussed along with the reasons for the failure showing the different areas where such failure affects the life and assets.

1.2.1.1 Failure of the Acquaviva railway embankment

Figure 1.6 Breaching of the Acquaviva railway embankment, Southern Italy after 5 October 2005 flooding (taken from Polemio & Lollino, 2011)

Figure 1.6 shows the breaching of the Acquaviva railway embankment which was the embankment of the National Railway connecting Bari and Taranto in the Southern Italy after the flash flooding that occurred on 5 October 2005 (Polemio & Lollino, 2011). The embankment which was made of two type of material, inner highly gap graded rock fill and an outer layer of fine soil which ranged between sand and silt and had the slope angle of the 45º. The embankment collapsed after about the 6 hours from the beginning of the rainfall event which created the reservoir of the maximum head of the 6.3m. After 2-3 hour of reaching the maximum head, embankment failed with dispersion embankment material in the downstream.

It was reported that shallow slope failures were observed along both the downstream and upstream slope. Shallow slope failure was caused by the high pore water pressure induced by the transient seepage flow in the embankment body. These shallow failure enhanced the internal erosion in the embankment. Internal erosion possibly consisting the suffusion of the soil along with the concentrated pipe erosion along the contact between the rock fill and the concrete culvert caused the global failure of the significant portion of the

structure within the few hours. Apart from this major breaching, shallow sliding failures were also observed along the slopes of the remaining part of the Acquaviva embankment.

1.2.1.2 Failure of the New Orleans 17Th Street Canal levee during the Hurricane Katrina

Figure 1.7 Breach in 17th Street Canal Levee in New Orleans, Louisiana showing inundated neighbourhood (Bea, 2008)

Figure 1.7 shows the satellite image of the breaching of the levee on the 17th Street Canal, New Orleans, which occurred on August 29, 2005. The failure caused the inundation of the nearby neighbourhood causing the huge loss. The failure of the levee resulted from the combined effect of numerous factor. Before the storm surge, a strong wind caused the uprooting of the vegetation thus creating the cracks on the surface. This accelerated the seepage in the levee. The water pushed the floodwall on the flood side creating the gap and allowing the flow of the water (see **Fig.1.8**) through the gap. The failure eventually occurred due to the sliding as the strength parameter of the soil which was expected in design was reduced to a lower value due to the seepage flow. This reduced strength

parameter caused the breaching even though flood level was lower than the design flood level.

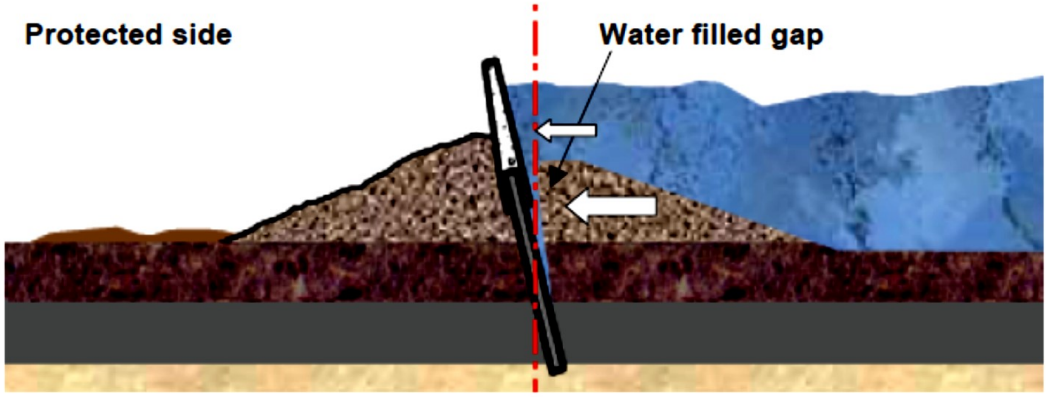

Figure 1.8 Cross-section of the levee in failure mode (Bea, 2008)

1.2.1.3 Failure of the levee along the Foenna stream

Figure 1.9 shows the different stages of the failure of the levee along the Foenna stream located in the central Italy which occurred on the 1st January 2006 which caused the flooding in the industrial-urban area of Sinalunga, a town in Tuscany region of Italy. **Figure 1.9** (a) and (b) shows the outflow of the water in landside caused due to the seepage flow and start of the subsidence of the levee crest respectively facilitated by the increased outflow in the landside. **Figure 1.9** (c) and (d) shows the evolution of the breach failure and flood entering the protected side. The breaching of the levee was quick and extended to the width of 40m. The breach evolution lasted only a few hours and caused huge damage. Reasons for the failure were attributed to channelized seepage flow through the discontinuity present within the levee body. Discontinuities within the levee body were created by the presence of the burrows made by the animal which provided a preferential path of flow, thus creating a zone of high pore water pressure. The failure started from such weak point and finally led to 40m wide breach in the levee.

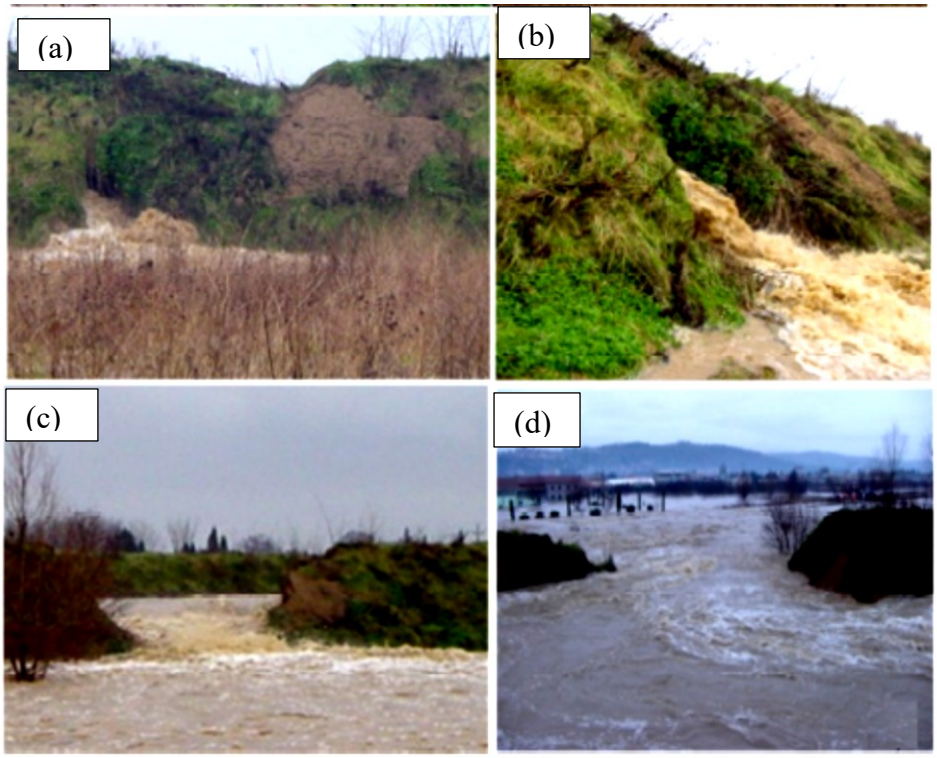

Figure 1.9 Failure of the levee in Foenna stream, Italy (a) Outflow due to seepage located on the landslide of the levee face (b) onset of the subsidence of the levee crest (c), (d) breach evolution for the Foenna stream levee. (After Camici et al. (2015))

1.2.1.4 Failure of levee at Edgecumbe, New Zealand

Figure 1.10 shows the inundation at the Edgecumbe, New Zealand on April, 2017. The failure was caused by the sliding of the ground containing the cribwall and some of ground behind it and followed by the sliding failure of the flood wall. The levee was subjected to long duration flood, which caused the rise in pore water pressure. The pore water pressure exerted both lateral load against the ground and uplift pressure under the flood wall, consequently reducing the resistance of ground and fall and leading to slide forward.

Figure 1.10 Breach of levee at Edgecumbe, New Zealand, April 2017 (*Rangitaiki River Scheme Review- April 2017 Flood Event*, 2017)

From all the cases presented here, it is evident, that seepage flow in the levee/embankment causes the significant loss in the strength of soil. The failure caused by seepage in river levee can be broadly categorised to two groups as following:

- → Slip/sliding failure caused by the rise of the pore water pressure within the embankment caused by the rain water or by the penetration flood water
- → Piping failure caused due to rise of pore water pressure within the foundation or embankment.

In this study, slip/ sliding failure will be taken in consideration for the study.

1.2.2 Reinforcement against seepage flow

Levees need to be reinforced against the seepage flow for the better performance. There are various methods of the reinforcement that can be used in the levee body against seepage. Traditionally there are two different approaches for designing the protection

measures in the levee. In first method, additional strength is provided to levee by providing the levee with soil nail, geo-membrane, etc. to compensate the strength loss caused due to the seepage of flood water in levee. This is termed as protection by reinforcement in the study. Second method is method of protection in which extent of strength reduction caused due to rise of the pore water pressure is minimized. This is achieved through drainage which can be provided through drain pipe, toe drain, etc. This is termed as protection by drainage in this study.

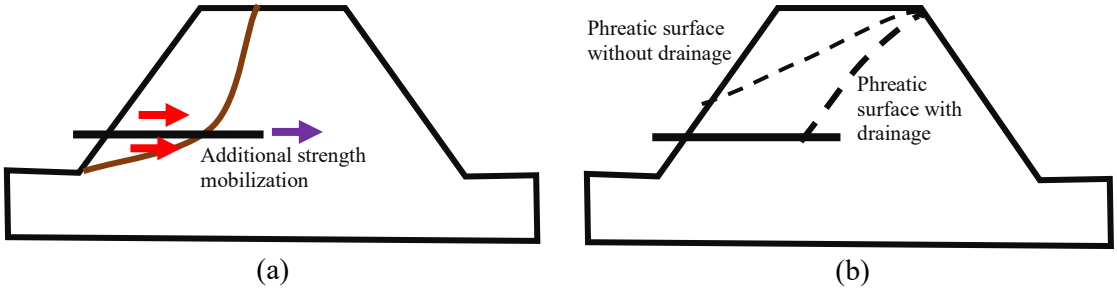

Figure 1.11 Two methods of protection of river levee (a) protection by reinforcement (b) protection by drainage

Figure 1.11 summarise the two methods of protection i.e. protection by reinforcement and protection by drainage that can be provided in river levee against the flood induced deformation. Various studies have been made in effort to understand the seepage flow in river levee and protection measures in river levee against flood induced deformation which is discussed in the following section

1.2.3 Previous studies on seepage flow in river levee and protection against flood induced deformation.

In this section, some of the physical modelling and numerical studies done in the seepage flow in the slope and the protection mechanism against seepage induced failure is discussed.

1.2.3.1 Seepage induced failure in levee/embankment

Increased seepage flow in levees during the flood cause destabilization by an increase in self-weight of soil and reduction of shear strength due to the decrease of effective stress by reduction of matric suction.

Krahn et al., (1989) from their field observation and labortaory experiment and Ng et al., (2003) from their field onservation emphasised on the importance of the suction in the stability of soil slopes. Study also emphasised on the importance of understanding of the unsaturated soil behaviour in terms of suction as supposed to using the water content.

Timpong et al. (2007) conducted the geotechnical centrifuge test on homogenous soil slope having the slope angle of 50^{o} made of the mixture of river sand and Fujinomori Clay and using in-flight ground water table control system. From this study, it was concluded that generation of the positive pore water pressure and increase of the saturation of model slope due to rise in ground water level is sufficient to trigger the slope failure. Chu-Agor et al., (2008) studied the seepage mechanism of hillslope, gully and streambanks through the physical model test. From the study it was concluded that slope failure occurs either by the tension failure or by the erosion of the soil. The failure mechanism is controlled by soil property such as bulk density, hydraulic conductivity, effective cohesion, internal angle of friction and critical shear stress. Ling et al., (2009a) from their centrifuge experiment in slopes of varying geometry and soil properties also confirmed the reduction of matric suction as cause of failure subjected to seepage flow. This study also generated threshold rainfall intensity curve for stability of their test slope.

Schnellmann et al. (2010) conducted 1g physical model and numerical studies and Hamdhan & Schweiger, (2011) performed fully coupled flow –deformation analysis of unsaturated soil slope to investigate the effect of the rising groundwater table in pore water pressure in unsaturated soil slope. The research showed that rise of the phreatic surface is delayed by low permeability in the unsaturated zone. It was concluded that different soil types, geometries and boundary condition would yield different delay in the rise of the water table. Thus, the time of failure will vary accordingly.

Rahimi et al. (2015) conducted the series of the parametric studies to explore the effect of hydraulic parameters in the stability of the slope against the rainfall induced seepage flow. From the study, it was concluded that soil with higher saturated permeability is affected more by the external flux compared to soil with lower saturated permeability. It was also found that the SWCC fitting parameters influence the stability of poor drainage soil (having saturated permeability less than 10^{-6} m/s) more significantly than the good drainage soil. It was also concluded that if the external flux is less than the saturated permeability, soils with different permeability and same SWCC parameter have similar stability level for all the slopes.

1.2.3.2 Protection by drainage

Drainage pipes are one of the standard methods of protection, used mostly in existing levees, to limit the decrease in effective stress by limiting development of the positive pressure. (Choi, 1984; Rahardjo et al., 2011, 2003; Resnick and Znidarcic, 1990; Saran and Viswanadham, 2018). However, drainage pipes also have some limitation towards protection of levee. Its performance is affected by the hydraulic properties of the soil, cannot increase the performance beyond the critical length of drainage and have limited zone of influence (Cai et al., 1998; Chen and Chen, 2016; Ghiassian and Ghareh, 2008; Yang and Deng, 2019).

1.2.3.3 Protection by reinforcement

Soil nails are also used as other option of protection measure in the slope stability problems by mobilization of additional strength. Soil nails predominantly with the development of axial force increase the shear resistance in the slope (Allersma and Bartsch, 2004; Cai and Ugai, 2003; Tei et al., 1998; Zhang et al., 2001). Ng et al. (2006) and Rotte and Viswanadham (2012) through the series of the centrifuge experiments and Li et al. (2008) and Zhou et al. (2009) from full-scale test confirmed the effectiveness of soil nail in the global stability of the slope subjected to seepage flow. However, in these studies, limitation of soil nail performance was also shown, as soil nails were capable of only minimizing the formation of the crack and local failure, but could not prevent them.

1.3 Objectives of study

From the previous research work, it is evident that seepage flow in the levee is one of the predominant causes of the failure of the levee. The need of the protection against the seepage flow failure is also clearly presented in the previous works. However, different factors such as the flooding condition and soil permeability which make the levee more vulnerable towards the seepage flow needs to be studied more rigorously. While much research has been done in the protection mechanism in the levee, the system that can be used not only in the new levees but also in the existing embankment still needs to be studied. Mostly the protection used against the seepage flow in levee are evaluated for their ability to either lower down the water table in the levee or for the reinforcing ability i.e. providing the external strength to the soil slope. These two protection mechanism is seldom used in combination which in fact could provide the improved protection in levee against seepage induced failure. Therefore, in this study use of the "steel drainage pipe" is proposed. Steel drainage pipe are the tubular steel pipe which by its unique design and material of composition could not only lower the water table but also increasing the overall strength of levee. With this hypothesis of the use of steel drainage pipes and to know the scope of use following objectives were set out for this study;

- → To demonstrate the failure mechanism of the levee subjected to the seepage flow under the various level of protection.
- → To understand the working mechanism of the proposed steel drainage pipes which uses the function of drainage and reinforcement in combination (how does steel drainage pipe works?).
- → To determine the performance of levee reinforced with steel drainage pipe under the varying condition of flooding, soil permeability, and arrangement of steel drainage pipes in the levee (where can be steel drainage pipe used?)
- → To make comparative study of the performance of steel drainage pipes with other protection measures such as pipes with only drainage and pipes with only reinforcement function (why steel drainage pipe should be used?).

1.4 Outline of dissertation

This dissertation has additional 6 chapters. Short description of the each chapter is described in following section which encompass the main body of research work. Acknowledgement and references are added in the beginning and end respectively to complete dissertation.

Chapter 2 describes the details of the centrifuge experiment and result of various test cases used in the study.

Chapter 3 describes the details of the 1g physical model test and results of the test cases used in the study.

Chapter 4 describes the details of the finite element numerical model used in study along with the verification with comparison with the centrifuge model test result.

Chapter 5 describes the working mechanism of steel drainage pipe based on the results of physical model test and numerical analysis.

Chapter 6 identifies the scope of the use of steel drainage pipe based on the numerical analysis result.

Conclusion and recommendations are presented in chapter 7.

2 Centrifuge experiments and results

2.1 Introduction

Geotechnical centrifuge modeling was used to study the behavior of soil slope when subjected to the seepage flow. The objective of the centrifuge modeling was also to understand the behavior of the slope subjected to seepage flow when it is reinforced with the proposed steel drainage pipe and compare with performance of the levee reinforced with pipes having only drainage, pipes having only reinforcement and unreinforced levee. This chapter presents the specifics of the geotechnical centrifuge modeling of the seepage flow in the soil slope. The centrifuge facility, equipment used, and instrumentation for data acquisition are explained in this chapter. This chapter also gives the details of the experiment procedure, assumptions, and the difficulties faced during the centrifuge modeling.

2.2 Geotechnical Centrifuge Modelling

Geotechnical centrifuge modeling has been extensively used to study the various type of geotechnical problem. Seepage and slope stability problems are also extensively studied using geotechnical centrifuge modeling (Ling et al., 2009; Tei et al., 1998; Timpong et al., 2007; Zhang et al., 2001). Seepage flow problem in the soil is a complex issue; understanding this behavior only through the analytical solution has its set of limitations, and could be misleading. The obvious best way to understand these seepage flow problems is the full-scale modeling, which is not always feasible considering various aspects. The reduced scale modeling has difficulty in modeling the body force, which is the governing factor in such seepage flow problems. Also, in the reduced scale modeling, capillary rise becomes the predominant influencing factor for seepage flow, which is not the actual representation of the prototype condition. In the prototype scale, the capillarity has minimal influence on the seepage flow. Geotechnical centrifuge modeling can

overcome the problem of modeling the body forces and influence of the capillarity effectively (Cargill and Ko, 1983; Sutherland and Rechard, 1984), thus helps in the better understanding of the seepage flow problem.

The geotechnical centrifugal model enables to replicate the stress state in the model similar to the prototype by providing the increased gravity environment. The ability to create the same stress state in the model have allowed the use of this modeling technique in the study the problem of slope stability. The scaling law derived and effectively verified for these two phenomena of slope stability, and seepage is similar. This allows the simultaneous modeling of both problems and thus making it possible to study the influence of the seepage flow on the slope stability (Resnick and Znidarcic, 1990).

Geotechnical centrifuge model, therefore, can be effectively used to model the real case scenario of the failure of the river levees and embankments during the flooding. This situation, which involves the problem of slope stability subjected to the seepage flow, can be visualized better with use this technique.

2.3 Scaling law

The basic principle of the geotechnical centrifuge modeling is that it establishes the same stress state condition of the prototype in the model. This is achieved by placing the model in an increased gravity environment. **Figure 2.1** summarises the principle of centrifuge modeling. The figure shows that a model which is scaled down by the factor ‘n’ when placed in normal gravity field at any point will experience reduced stress state. However, when the reduced model is placed in centrifuge, providing the accelerated gravity by the same factor ‘n’ will experience the same stress state as in prototype at any point. For example, if the soil surface of height 20 m is to be modelled, 1 m model soil surface will experience the same vertical stress at the bottom as the prototype when it is placed in centrifuge environment with gravity increased by 20 times. . For modelling of the drainage pipe, the dimensionally similar model pipes are used as they can give proportional drainage capacity in the model ground.

The scaling rule for the seepage and slope stability problem is summarised in **Table 2-1**. For the model, three types of similarities is considered viz. geometric similarity, kinematic similarity and dynamic similarity (Kumar, 2007). Geometric similarity is satisfied whenever constant ratio of length is satisfied. In addition to geometric similarities, ratio of velocities is kept same to maintain kinematic similarity. Dynamic similarities is ensured by keeping pressure constant in both model and prototype.

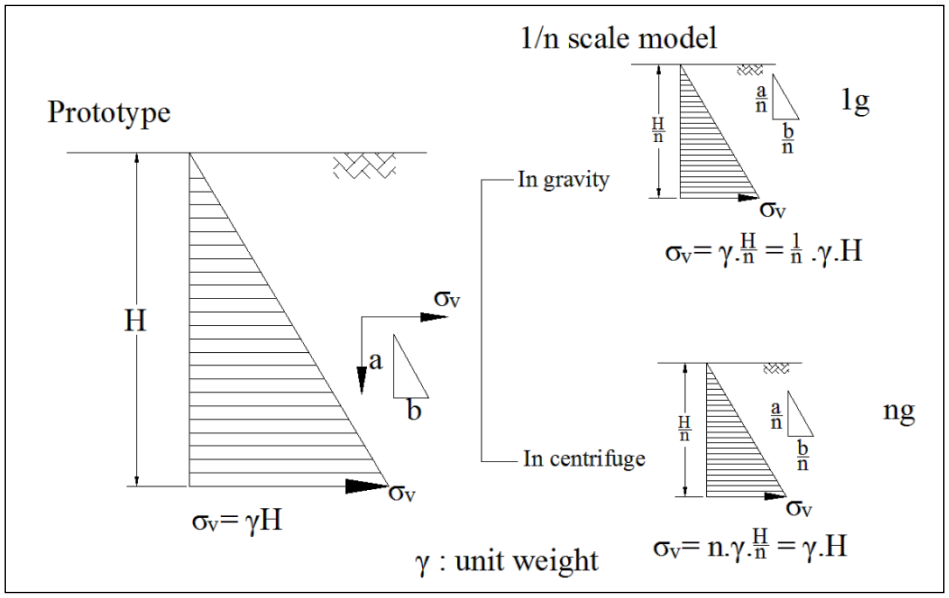

Figure 2.1 Schematic representation of Principle of the geotechnical centrifuge.

Table 2-1 Scaling law(Cargill and Ko, 1983; Thusyanthan and Madabhushi, 2003)

Parameters	Ratio of model to prototype
Length	1/N
Area	$1/N^2$
Volume	$1/N^3$
Velocity	N
Pressure	1
Head	1/N
Intrinsic permeability	1
Time	$1/N^2$

2.4 Geotechnical centrifuge facility

2.4.1 Tokyo Tech Mark III centrifuge.

All the physical model test is carried out using the Tokyo Tech Mark III centrifuge (Takemura et al., 1999) (see **Fig.2.2**). All the test is carried out at 20g centrifugal acceleration. This centrifuge is the beam type of centrifuge consisting of two parallel arms which hold the platforms for the model container and the counterweight in the opposite ends as shown in **Fig.2.3**. Distance from the rotating shaft to the platform bottom is 2.45m (2.32m at the platform base), which is the radius of the rotation. The swinging platforms are always normal to the resultant acceleration of the centrifugal acceleration, ng, and the earth's gravity. The specification of the centrifuge is listed in **Table 2-2**.

In the Tokyo Tech Mark III centrifuge, two types of signal transmission methods are used for the data acquisition. The first method of transmission uses electrical slip rings. In this method, transducers are connected to the slip rings via a junction box, and then signals are transferred to the amplifier on the laboratory floor. The other type is a Wi-Fi connection. In this case, transducers are connected to signal conditioners on the centrifuge. Analog signal from the transducer is amplified and then converted to the digital signal by A/D converters. A computer on the lab floor can manage gains, filters, and other conditions of the signal conditioners. The digital signals are transferred to the computer through the Wi-Fi connection. The rotary hydraulic joint facilitates the supply of the air and water to the centrifuge during the spinning with a maximum pressure of 1 MPa, which is mounted on the centrifuge.

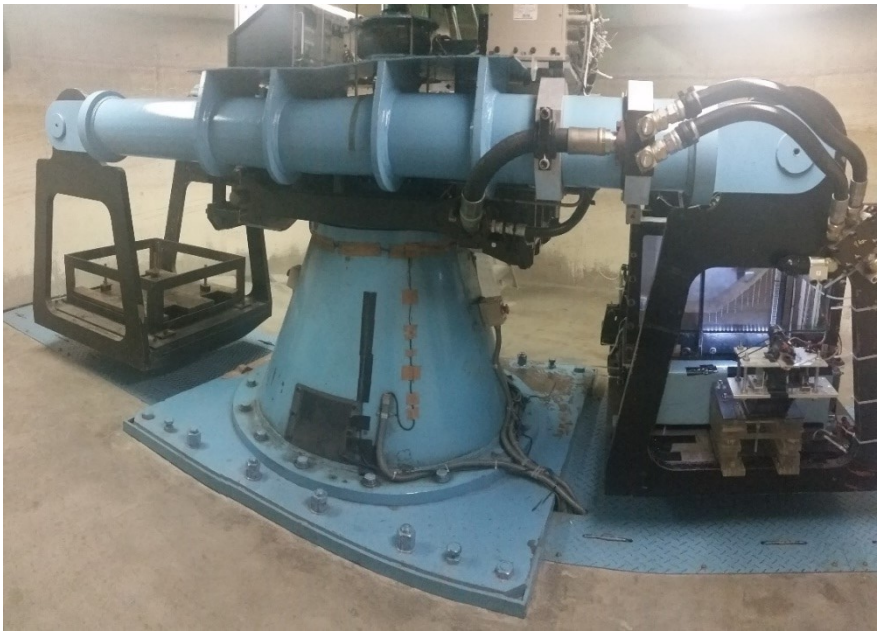

Figure 2.2 Tokyo Tech Mark III centrifuge

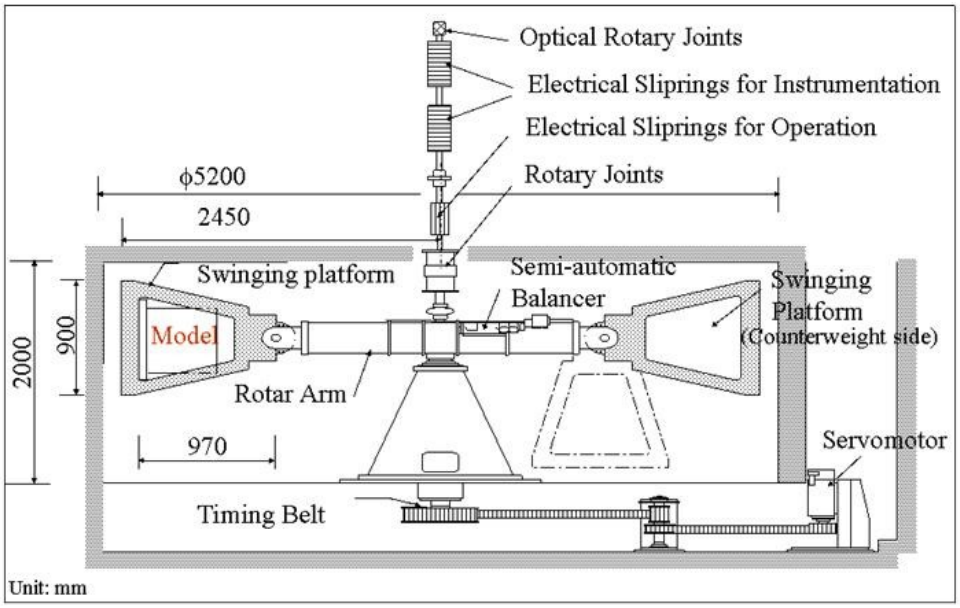

Figure 2.3 Sectional view of Tokyo Tech Mark III centrifuge (Takahashi, 2002)

Table 2-2 Specification of Tokyo Tech Mark III centrifuge.

Radius	Platform radius	2.45m
	Effective radius	1.95 m
Platform dimensions	Width	0.9m
	Depth	0.9m
	Maximum Height	0.97m
Capacity	Maximum payload	50g.ton
	Maximum number of rotation	300 rpm
Electrical Slip Rings	For instrumentation	72 channel
	For operation	18 channel
Rotary joint	Number of ports for air and water	2
	Working pressure for air and water	1 MPa
	Number of ports for oil	2
	Working pressure for oil	21 MPa

2.4.2 Model container

All the centrifuge test was carried using an aluminum model container with the inner dimensions of 700mm in width, 150mm in breadth and 450 mm in height. The front face of the container was a transparent window which allowed the observation of ground deformation during the test. The container was divided into three sections. The first section was 50mm in width to serve as the water supply reservoir during the test. The second section was a model section of the width 600 mm where the ground model was prepared, and the third section of width 50mm served as the drainage section to drain out water accumulated to drainage tank through pipe connection as shown in **Fig.2.4**

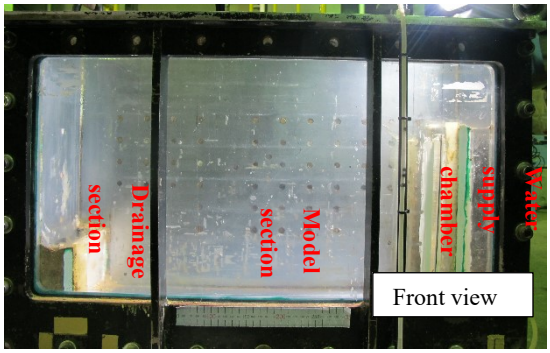

(a)

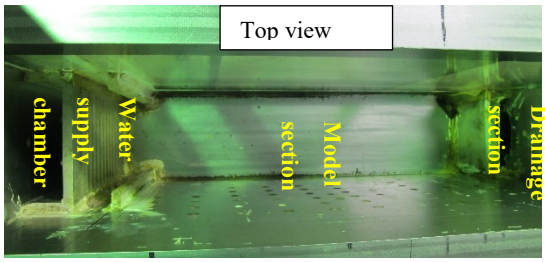

(b)

(c)

Figure 2.4 Model container (a) Front view (b) Top view showing different sections. (c) Pipe connection from container to drainage tank

The boundary between the model section and the water supply section was made of the perforated steel wall covered with the geomembrane, which allowed inflow of water to the model ground without migrating soil. Perforated steel wall consisted two layer of steel plate with slots made in vertical in one layer and horizontal direction in other layer of plate. These two plates was screwed together with geomembrane in middle. The steel wall separated the drainage section and the model section. In the model section, 570mm width was utilized to make a model slope, and 30 mm width was used for incorporating filter layer made of Silica no.3 (with same density as levee soil) to ensure uniform flow of water from the water supply chamber to the model slope. At the boundary of this silica layer and model ground 10 mm thick, 20 mm breadth and 280 mm high acrylic plate was

attached to two faces of the container (see **Fig. 2.10**). The purpose of using the acrylic plate was to prevent the channelization of the flow at the boundaries of the container. Rubber membrane was also attached to the steel walls towards the front face of the container to prevent any leakage of water from the seam of the steel walls.

2.4.3 Instrumentation

The behavior of the model during the experiment was monitored by using different types of transducers. The number and type of the transducers were selected such that placement of transducers does not cause much change in the natural behavior of the model and also was able to capture the key behavior of the model ground. In all the experiment cases, three types of transducers were used in the model. Pore pressure transducer, earth pressure transducer, and laser displacement transducer were used to measure pore water pressure, earth pressure, and settlement, respectively.

Figure 2.5 (a-c) shows the earth pressure transducer, pore water pressure transducer, and laser displacement transducer respectively used in the experiment. Apart from this transducers, model steel pipe with the attached strain gauge was also used. Two types of strain gauge to measure the bending moment and axial force was employed in the steel pipe. All the transducers were calibrated to convert the voltage output to the engineering units.

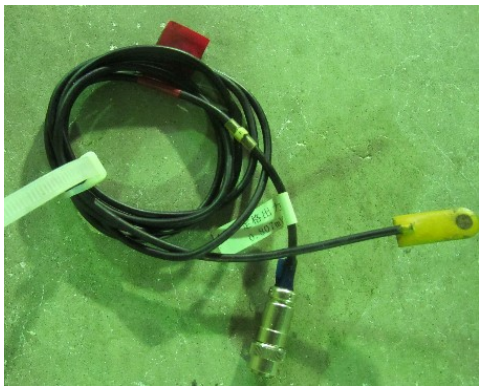

(a)

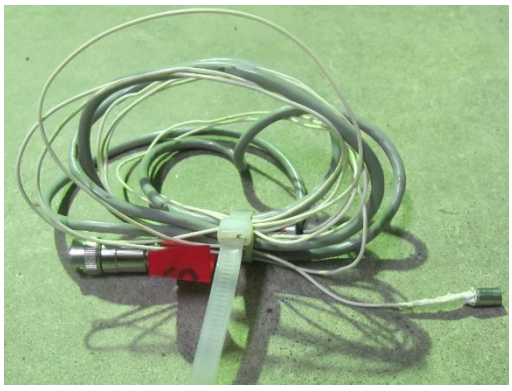

(b)

(c)

Figure 2.5 Transducers used in centrifuge experiment (a) Earth pressure transducer (b) Pore water pressure transducer (c) Laser displacement transducer

In the experiment, six numbers of the pore water pressure transducers (PPT), one earth pressure transducer, and two laser displacement transducers (LDT) were used. The PPTs used in the experiments were SSK Micro Pressure Transducer P306V-02 supplied with the wire mesh at the head and having the maximum capacity of 200 kPa. Earth pressure transducer used was PS-1KC of Kyowa Electronic Instruments Co. Ltd. having a standard maximum capacity of 100 kPa. The laser displacement transducers used in the experiment were of two types. Both the LDT had the sensor head of LB-02 series manufactured by Keyence. However, the amplifier used were of two types of LB60 and LB62 series with the measurement range of ±40mm and ±10mm, respectively. In the steel pipe, two sensors were used to measure axial force, and four sensors were used to measure the bending moment. The change in pore water pressure in the model ground with the seepage flow was recorded using the PPTs and surface settlement was measured using LDTs. The change in earth pressure during the experiment was recorded using earth pressure transducer.

The location of each transducer was carefully measured to ensure the target placement of the transducer. Transducers which were placed inside the model ground were placed perpendicular to the direction of the flow and wires were arranged such that minimum obstruction was caused by wires to the flow of water.

Apart from these transducers, marked noodles were used in the front face of the model ground to observe the deformation pattern during the experiment.

2.4.4 Visual observation

For the visual observation of the model ground during the experiment, two video cameras, and one still camera were used. Out of the two video cameras, one placed in front was used to observe the front view of the model, and another top camera was used to observe the slope of the model ground. The still camera was also placed to observe the front face of the model ground. The still camera recorded the image at every twenty seconds. **Figure 2.6** shows the cameras used in the experiment.

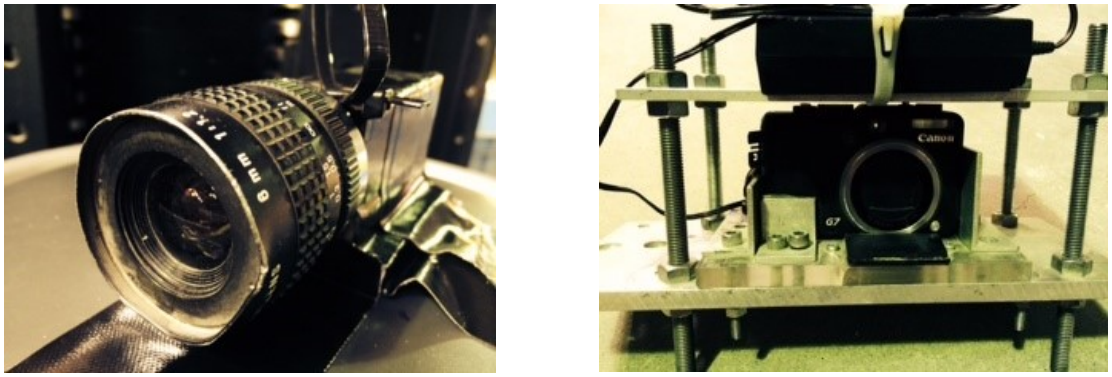

(a) (b)

Figure 2.6 Cameras used in experiment (a) Video camera placed in front of model and above the model (b) Still camera put in front of model

2.4.5 In-flight water supply and drainage system

Flooding during the experiment was simulated by increasing the water table in the water supply chamber during the experiment. When the centrifuge acceleration was set to the target value of 20g, at first steady state was achieved by letting model spin in target acceleration till pore water pressure became stable. After that water was supplied to the water supply chamber during the flight by monitoring through the valve control on the lab floor. The water table was increased to the target value and then kept constant by observing the pore water pressure transducers placed in water supply chamber and by visual inspection of standpipe attached on the front face of the container through real-time video camera record. The water accumulated after the seepage flow was drained out

through a drainage chamber to drainage tank placed on the platform via pipe connection. The electrical valve controlled the passage of water to the drainage tank. The water level in the drainage tank was also monitored through the pore water pressure record obtained during the experiment. **Figure 2.7** shows the schematic diagram showing the water supply and drainage system used in the experiment.

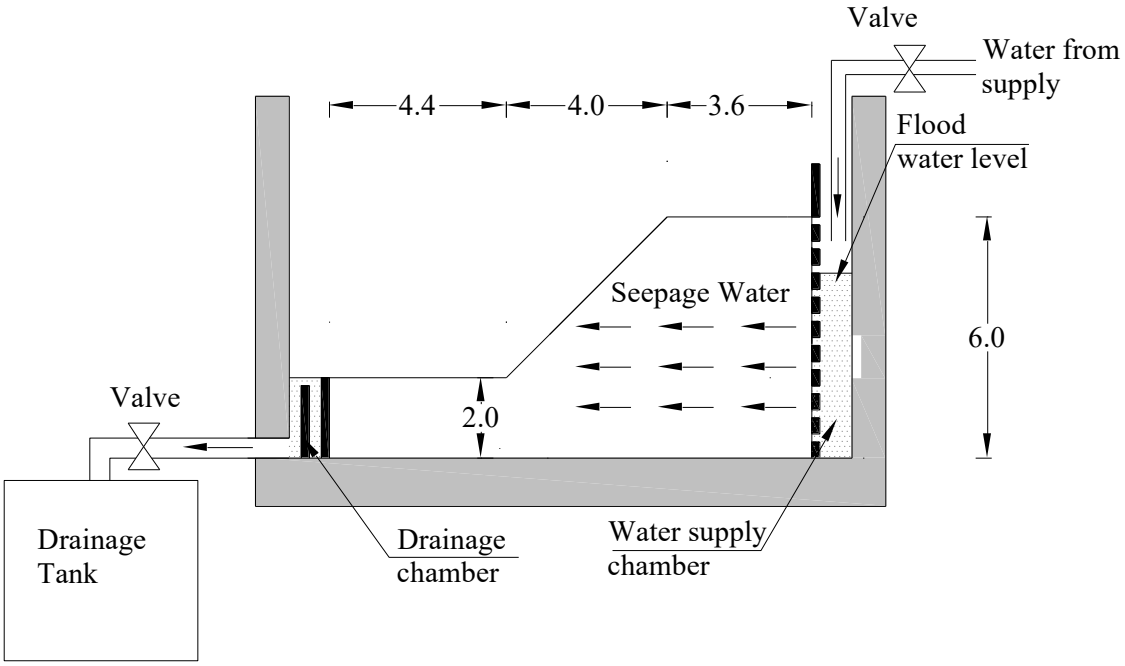

Figure 2.7 Schematic diagram showing inflight water supply and drainage system

2.5 Material properties

All the centrifuge experiments are conducted using the Edosaki sand. The index properties of the Edosaki sand is shown in **Table 2-3**. **Figure 2.9** shows the particle size distribution of Edosaki sand. Strength parameter for soil without fiber are obtained from standard undrained triaxle test and the angle of shearing resistance and cohesion for the soil with fiber is obtained from direct shear test. The classification of the soil based on particle size is shown in **Table 2-4.** The material is classified as silty sand (SM) according to USCS. Foundation and embankment are prepared with soil with a degree of compaction (Dc) of 95% (1.72 Mg/m^3) and 80% (1.45 Mg/m^3) of maximum dry density determined from Standard Proctor Compaction test respectively. **Figure 2.8** shows the

result of Standard Proctor Compaction test for the Edosaki sand. **Figure 2.10** shows the soil water characteristic curve (SWCC) for the embankment along with the principal parameters for the van Genuchten model. SWCC here plotted is the wetting curve obtained from column test as proposed by Fredlund et al. (2012). The figure also shows the change in hydraulic conductivity with change in the volumetric water content calculated based on Kosugi model [ref. Equation 1.7 and 1.8]. In this study hysteresis of SWCC is neglected as the objective of study is only limited to wetting of slope surface. The soil used in experiment to prepare model ground has the volumetric water content of 21.25% and matric suction of 2.98 kPa (obtained from SWCC). The surface layer on the slope is prepared by soil mixed with fiber to replicate the grass cover often found in the real levee and to prevent the occurrence of unrealistic surface erosion during the experiment. The content of the fiber is 1% (for Cases 1-4, see the following subsection for details) or 2% (for Cases 5 & 6) of the dry weight of sand. The polyester fibers named Teijin RA04FN, approximately 39 μm in diameter and 5 mm in length is used in the test.

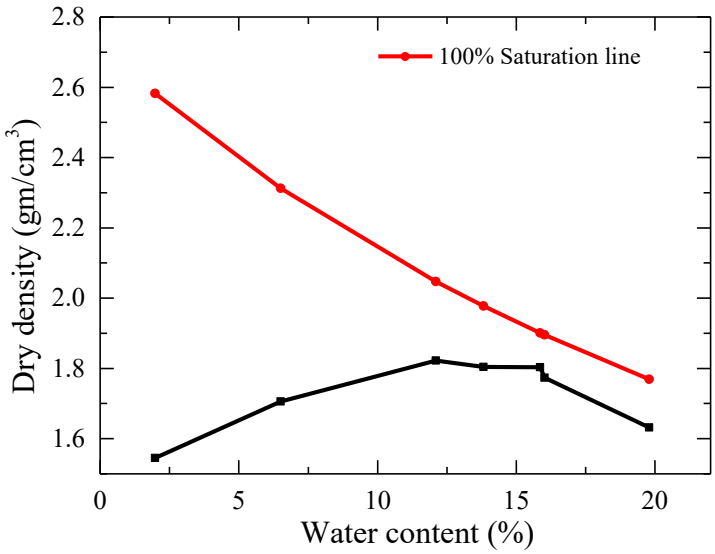

Figure 2.8 Compaction curve for Edosaki sand based on Standard Proctor Compaction test

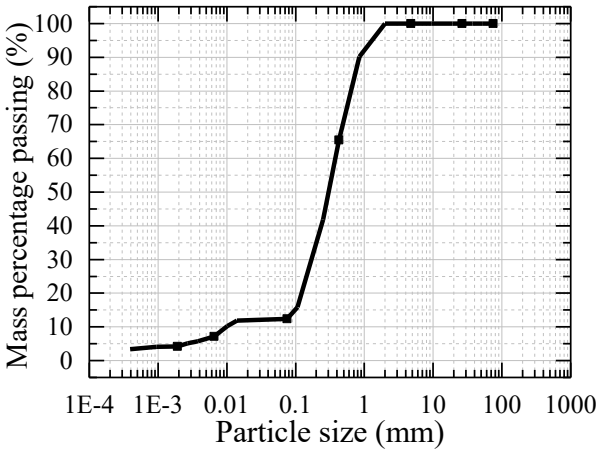

Figure 2.9 Particle size distribution of Edosaki sand

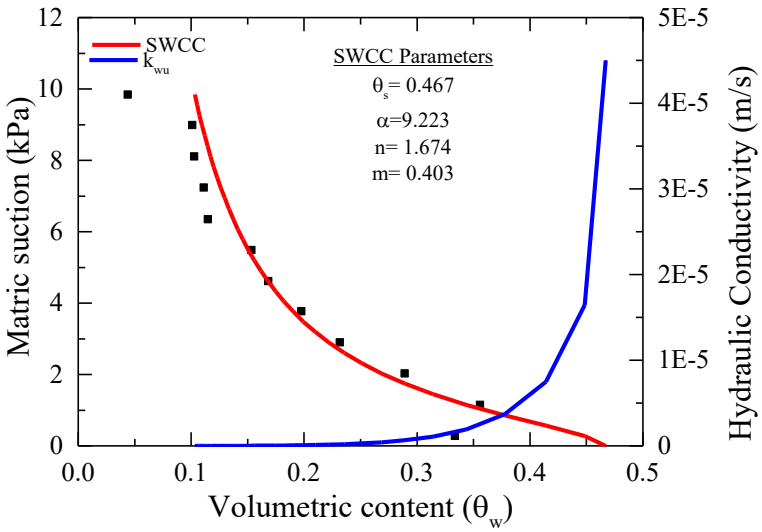

Figure 2.10 Soil water characteristics curve (SWCC) along with hydraulic conductivity for embankment

Table 2-3 Index properties of the soil

Soil properties	Values
D_{50} (mm)	0.30
D_{10} (mm)	0.010
Coefficient of uniformity	38
Coefficient of gradation	8.53
Soil particle density (Mg/m^3)	2.72
Optimum moisture content	14.5%
Average initial water content of model ground	14.7%
Angle of shearing resistance [Degree of compaction Dc= 80%] (degrees)	
Soil without fiber	29
Soil with 1% fiber	31
Soil with 2% fiber	33
Cohesion [Dc= 80 %](kN/m^2)	
Soil without fiber	2.5
Soil with 1% fiber	4.2
Soil with 2% fiber	6.0
Saturated coefficient of permeability (m/s)	
Foundation	1.5E-6
Embankment	4.5E-5
Dry density of embankment (Mg/m^3)	1.45
Dry density of foundation (Mg/m^3)	1.72
Modulus of Elasticity (N/m^2)	2.55E5

Table 2-4 Classification of the soil

Type	Mass percentage
Coarse gravel %	0.00
Medium gravel %	0.00
Fine gravel %	0.00
coarse sand %	9.80
medium sand %	48.41
fine sand %	29.41
silt %	6.38
clay%	6.00

Steel drainage pipes, steel pipes filled with glue and flexible pipes made of the Silicone are used as protection in levee against seepage induced deformation for different cases of the test (described later). **Figure 2.11** shows the dimensions of the steel drainage pipe used in the test on the prototype scale. The longitudinal section of the pipes with the

spacing of the drainage holes, spiral blade, and location of the strain gauges are shown in **Fig.2.1** (a). **Figure 2.11** (b) and (c) show the cross-sections of the steel drainage pipe and steel pipe with only reinforcement. Steel drainage pipes are tubular steel pipes with holes of the diameter 24 mm at the spacing of 0.16 m on the surface. The end one-meter length of the pipe is provided with the spiral blade of the external diameter 0.16 m. The spiral blade provides better anchorage to pipes with the soil. These pipes provide both drainage and reinforcement functions. Properties of the steel drainage pipes used in the experiment in the prototype scale are summarized in **Table 2-5**. The tubular steel pipes with the same configuration and material but filled with glue (Shin-Etsu RE45T) are used to model steel pipes with only reinforcement function. The added glue in the pipe increases the overall weight of the pipe. However, only reinforcement pipe, which is mostly solid is expected to have larger weight compared to drainage pipes. Flexible Silicone tube (Young's modulus =5.0E7 N/m2) with same internal dimension as the steel drainage pipes (keeping drainage capacity similar) and without the spiral blades are used to model the pipe with drainage function only. The external dimension of the drainage pipe, however, is 100 mm compared to 80 mm of steel drainage pipe. This difference in external dimension is not expected to cause a significant difference in behavior. These pipes could be easily bent and are expected not to provide significant additional reinforcement.

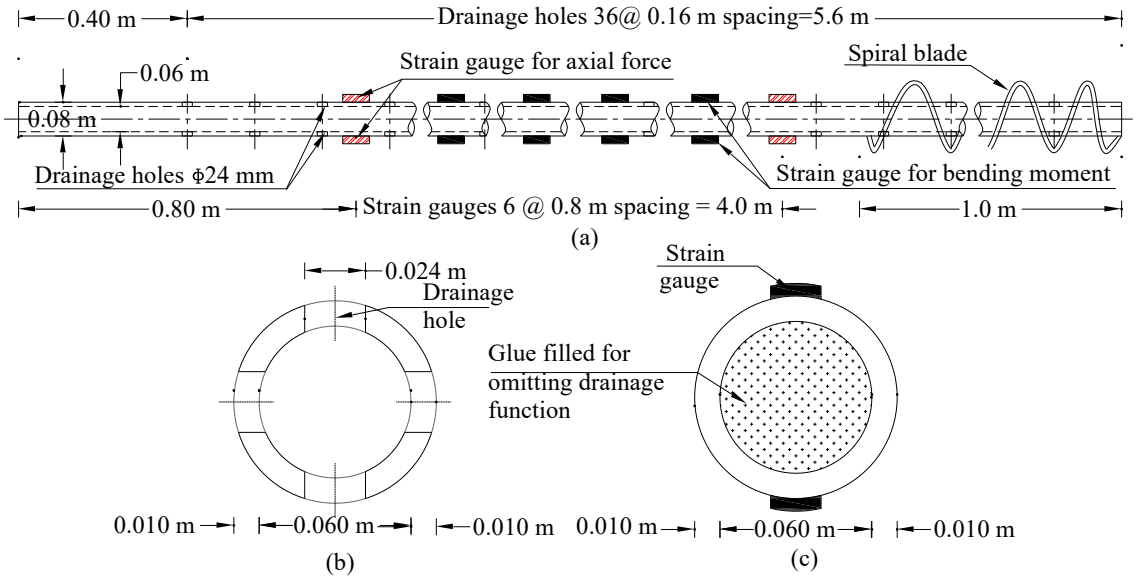

Figure 2.11 Steel drainage pipe (a) longitudinal section with locations of strain gauges and drainage holes; (b) cross-section of steel drainage pipe (c) cross-section of only reinforcement pipe with strain gauge

Table 2-5 Properties of Steel Drainage Pipe

Parameters	Values
Internal diameter (mm)	60
External diameter (mm)	80
Length (m)	6
Pitch of the screw (mm)	160
Thickness of plate forming screw (mm)	20
External diameter of screw part (mm)	160
Young's Modulus, E (N/m^2)	2.10E+11
Poisson's ratio, v	0.3

2.6 Test conditions

Six different cases of varying level of protection are investigated during the study. **Figure 2.12** shows the geometry of model slope and arrangement of pipes in the centrifuge models (Cases 1-6). Here all the dimensions are discussed in prototype scale unless mentioned otherwise. The model consists of the 2 m thick foundation layer and 4 m high embankment with the 1H: 1V slope. The total length of the model ground is 12 m, and

the width of the model is 3 m. **Figure 2.12 (a)** shows the cross-section of the model with pipes. In Cases 2-6, the pipes are installed at a 1m height from the toe of the slope. **Figure 2.12 (b)** shows the arrangement of the pipes in the plan view for the Cases 2-4 and 6. In all these cases, the slope is provided with three pipes. The pipes are installed at the spacing of the 1 m. In Cases 2-4, steel pipes are used, whereas in Case 6, pipes made of flexible Silicone pipe is used. In Case 5, two pipes are installed at the spacing of 2 m, as shown in **Fig. 2.1 (c)** In all the cases, the surface layer of 0.2 m made of soil mixed with the fiber is provided on the slope. The test conditions are summarized in **Table 2-6**. These cases are designed to study the effectiveness of the steel drainage pipes in slope stabilization and also to understand the contribution of drainage function and reinforcement function separately.

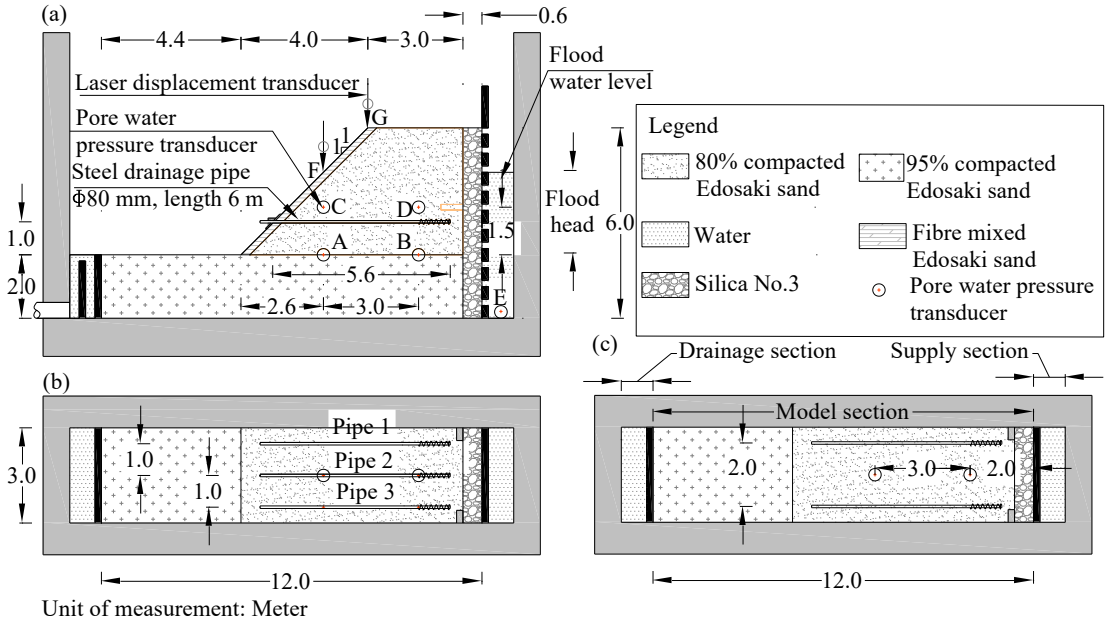

Figure 2.12 Model Configuration (a) sectional view with geometry and location of sensors (b) plan view for Case 2-4, 6 (c) plan view for Case 5

Table 2-6 Protection conditions in models

Cases	Level of protection	Description of protection					
		Pipe 1		Pipe 2		Pipe 3	
		R	D	R	D	R	D
Case 1	Unreinforced	N/A	N/A	N/A	N/A	N/A	N/A
Case 2	Reinforced (3 steel drainage	○	○	○	○	○	○
Case 3	Reinforced (2 steel drainage pipes + 1 steel pipe)	○	○	○[a]	×	○	○
Case 4	Reinforced (3 steel pipes)	○	×	○[a]	×	○	×
Case 5	Reinforced (2 steel drainage	○	○	N/A	N/A	○	○
Case 6	Reinforced (3 drainage	×	○	×	○	×	○

Note: R= reinforcement function, here pipe made of steel; D= drainage function, here pipes is tubular with holes on surface; ○ = present; × = not present N/A= not available, pipes not used; a= with strain gauges to measure axial force and bending moment

2.7 Model preparation

All models are constructed in the container with the inner dimension of 1.4 × 3.0 × 9.0 m in the prototype scale and equipped with a transparent window made of acrylic. The container is divided into three sections; upstream supply section, model section, and downstream drainage section. Supply section and drainage section both has a width of 1 m and the model section has 12 m width on the prototype scale. In the container special arrangement of the acrylic plate is made to prevent the channelization of flow along the interface between the container wall and model ground. In the model section, 1:20 scaled down the model ground was prepared by dynamic compaction and excavation technique. At first, ground with the uniform cross section 11.4 x 3 x 6 m (prototype scale) is prepared by placing and compacting the Edosaki sand in 12 layers of an equal thickness of 0.5 m to the target density (95% for foundation layer and 80% for levee layer) using temporary support. Each soil layer is compacted at the average moisture content of 14.7% which is near to the optimum moisture content of the soil. Layers of the soil are compacted using hand-held vibrator over the flat acrylic plate. Miniature pore water pressure transducers (PPTs) with wire mesh head are also placed in predetermined locations (locations A, B, C and D in **Fig. 2.1**) with precise measurement while preparing the model ground. After

making the uniform model ground using Edosaki sand, a layer of Silica no. 3 layer of 0.6 × 3 × 6 m (prototype scale) is prepared, by pouring the Silica No. 3 in the gap between Edosaki ground and supply tank resulting model ground of dimensions of 12 × 3 × 6 m in prototype scale. The model ground is then excavated to the designed configuration by placing the acrylic guide having dimensions same as the embankment over the container and using a T-shaped blade.

The slope portion of the model is then further excavated resulting slope to 0.2 m deeper than the required dimension. In excavated slope surface, Edosaki sand mixed with fiber layer is compacted with a degree of compaction of 80% to form required model geometry. Two laser displacement transducers (LDT) are used to measure the settlement at locations F and G (see **Fig. 2.1 a**). Both the LDTs have the sensor head of LB-02 series manufactured by Keyence. However, the amplifiers used are two types of LB60 and LB62 series with the measurement range of ±40 mm and ±10 mm respectively. Marked noodles are placed on the side face of the model for visual observation of the deformation pattern through the transparent window. Apart from this, in the Cases 3 and 4, the central pipe (Pipe 2) is equipped with strain gauges to measure axial force with axial force sensor (sensor giving the average of strain value of the strain gauge placed on top and bottom of pipe) at two locations and bending moment with bending moment sensor (sensor giving the difference of strain value of the strain gauge placed on top and bottom of pipe) at four locations. The wires of these sensors are passed inside the pipes to prevent the channelization of flow if present on the surface of the pipes.

In Cases 2-6, the steel pipes/drainage pipes are driven at the specified location using the acrylic guide after making a hole using the auger drill bit. Embedment length is kept 5.6 m for all the pipes. After the pipes have been installed, aluminum facing plates with the dimensions 0.6 × 0.6 × 0.04 m are installed and fixed with caps made of the acrylic. Water is supplied to the supply section and collected from drainage section through the pipe connection. Drained water is then collected in a separate drainage tank. Additional PPTs are installed in the supply section of the container and drainage tank for measuring the supply flood water head and the amount of drainage water, respectively. For the visual observations of slope during the test, two high definition video recorders (top and side)

along with one high-resolution digital camera (side) is used. Steps of model preparation is summarised in the **Fig. 2.13**

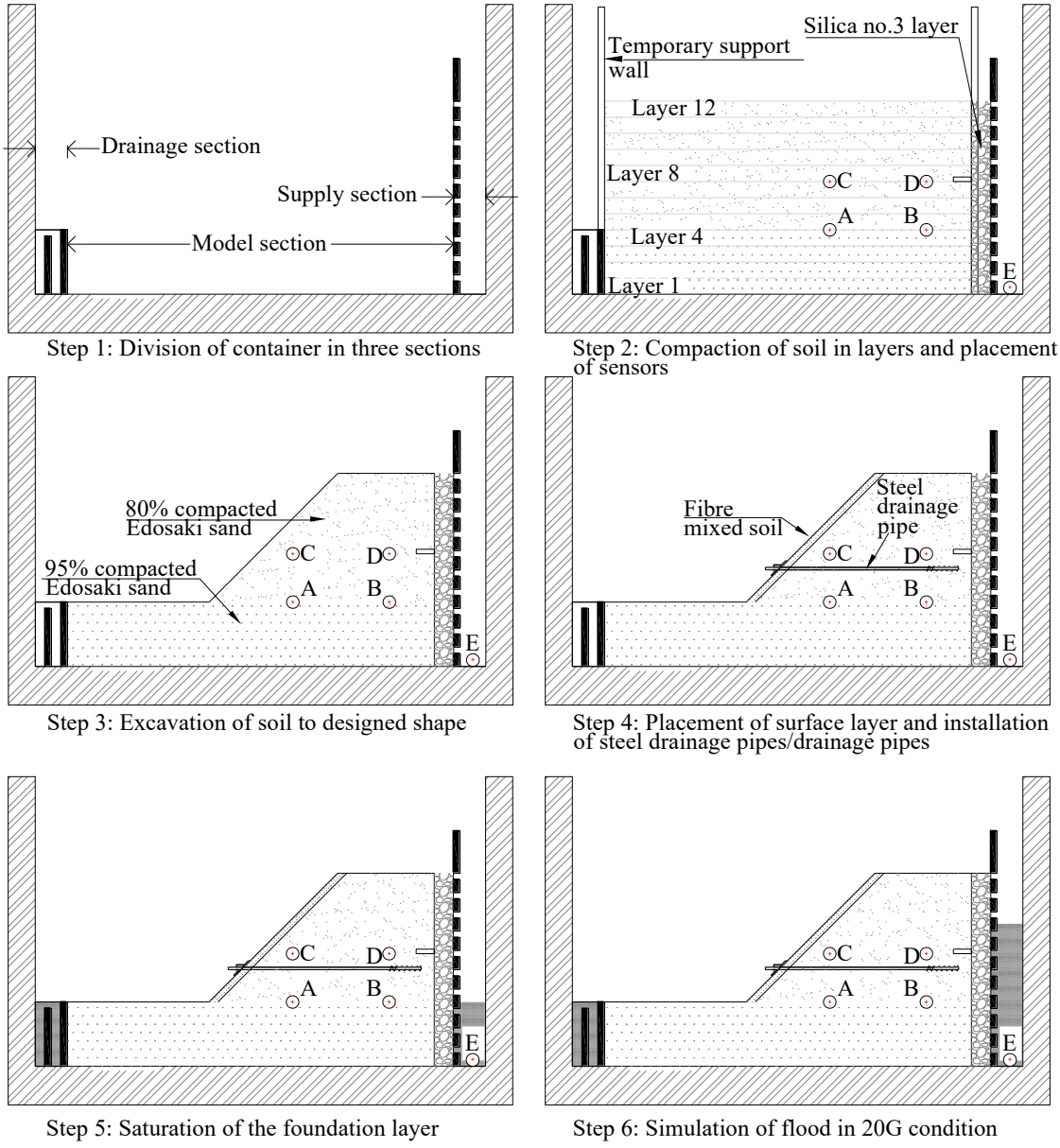

Figure 2.13 Steps of model preparation

2.8 Testing Procedure

After all the set-up has been completed, saturation of foundation layer is carried out. For saturation, de-aired water is supplied to the supply section until the volume of the water supplied exceeded the calculated volume of the pores of the foundation layer. At this stage, the apparent water level in the model is slightly higher than the top of the foundation. After the completion of saturation of the foundation at 1g, centrifugal acceleration is increased in steps to the target 20g. After the centrifugal acceleration has reached to 20g, steady state is ensured by allowing the pore water pressure measurement to become stable. At this stage, the water level in the model is near to the top of the foundation and unaffected by the presence or absence of the protection. The phenomenon of the flood in the river channel is then simulated by raising the water level in the supply section as in experiment conducted by Horikoshi and Takahashi (2015) and Koito et al. (2016). **Figure 2.14** shows the time history of flood water head supplied in the supply tank. Flood water head is the difference between the supply water level and drainage water level (equal to top of foundation) (**see Fig 2.10**). In Cases 1-4 the rising rate of the flood water is small and is in a range of 0.03-0.06 m/hr, while that is large and is around 0.3 m/hr in Cases 5 & 6. This unintentional difference in rising rate did not allow direct comparison on time reference among all the cases. In Cases 1-4 nearly steady state of seepage is achieved whereas in Cases 5 and 6 steady state seepage flow is not achieved. Therefore, comparison of the Cases 1-4 where similar seepage condition is achieved is made to understand the effectiveness of the steel drainage pipe and comparative performance of steel drainage pipes with the pipes with only reinforcement function in slope protection. Comparison of Cases 5 and 6 is made to understand the comparative

performance of the steel drainage pipes with dual function and pipes with only drainage function in slope protection. The water level is continuously monitored through the transducers' record and visual observation of the standpipe through video camera record. The flow of water is controlled manually by a valve from the centrifuge control room.

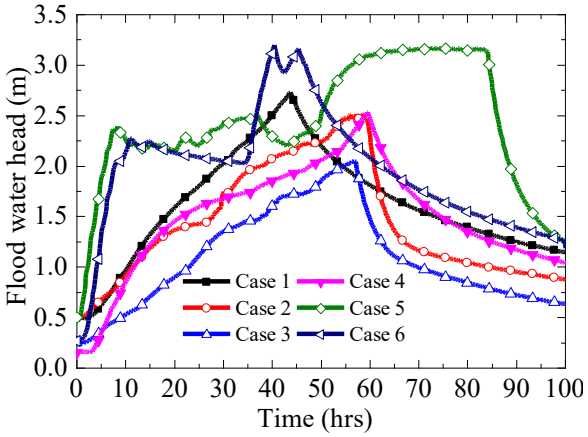

Figure 2.14 Time histories of supply flood water head.

2.9 Centrifuge Test Result

The six different test cases have been provided with varying level of protections. Case 1 is the unreinforced case, which acts as the base case for comparison with other cases to understand the relative performances of the provided protection. Cases 2, 3, and 5 are provided with the proposed steel drainage pipes. Cases 4 and 6 protection mimics the traditional protection which provides only reinforcement and only drainage respectively. Observations made for each test cases based on the visual observation through the transparent window and LVDT sensors are summarised in following section.

2.9.1 Case 1(Unreinforced)

In Case 1 model ground has no additional protection. The model ground when subjected to the flood with rising rate 0.056m/hr, it experiences gradual deformation starting from the toe of the slope. The failure starts from the toe region and progressively extends to the crest causing the complete collapse of the levee, i.e., the retrogressive failure mode

occurs (Wang and Sassa, 2003)as shown in **Fig. 2.15.** Failure initiation started after 22 hours of seepage flow when the flood head was 1.67 m. The complete collapse was observed after 35 hours of seepage flow at flood head of 2.2 m

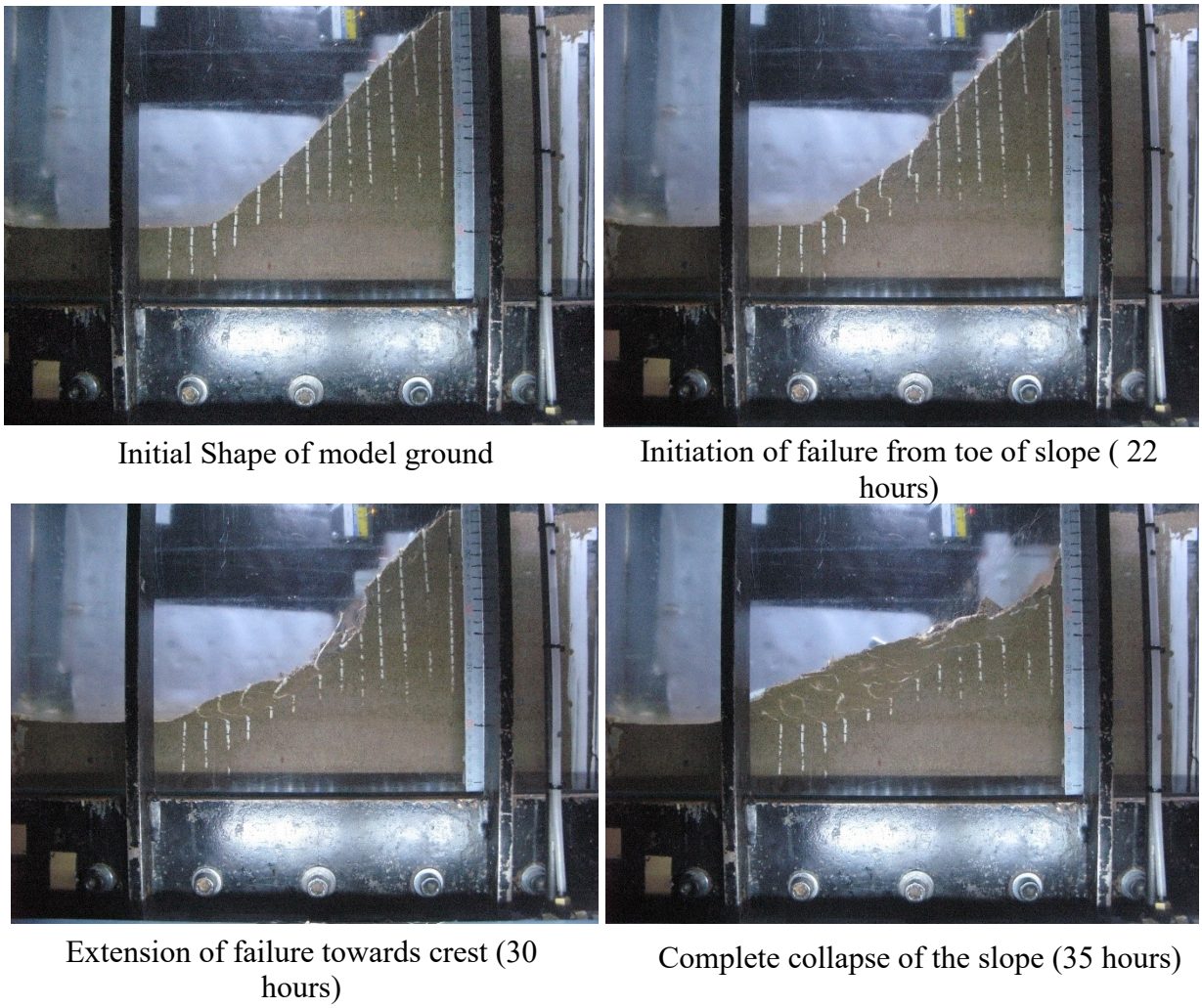

Initial Shape of model ground

Initiation of failure from toe of slope (22 hours)

Extension of failure towards crest (30 hours)

Complete collapse of the slope (35 hours)

Figure 2.15 Model ground behavior in Case 1

Figure 2.16 shows the time history of pore water pressure at the location A and B (see **Fig. 2.1**) along with the supply flood water head. From the figure it can be observed that with the increase in flood water head pore water pressure increases uniformly throughout the model ground. The change in pore water pressure is quicker than the change in the flood water head. With no protection provided in the model ground, this rise in the pore

water pressure causes the decrease in effective stress of soil and consequently strength of the levee structure initiating the failure.

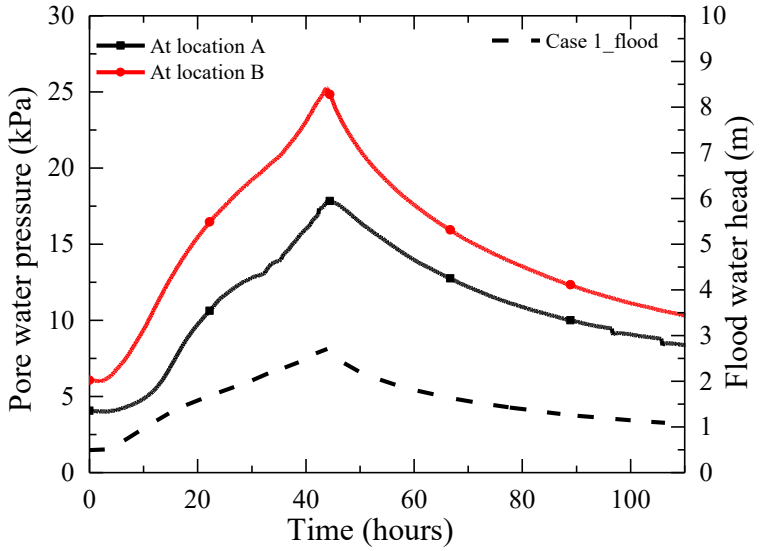

Figure 2.16 Time history of pore water pressure and flood water head for Case 1

2.9.2 Case 2 (With steel drainage pipes)

In Case 2 model ground is the provided with three steel drainage pipes at the spacing of 1m and at a height of 1 m from the toe of the slope. In this case, slope performs well when it is subjected to the flood with the rising rate of 0.04m/hr. In this case, no significant deformation was observed as shown in **Fig.2.17.**

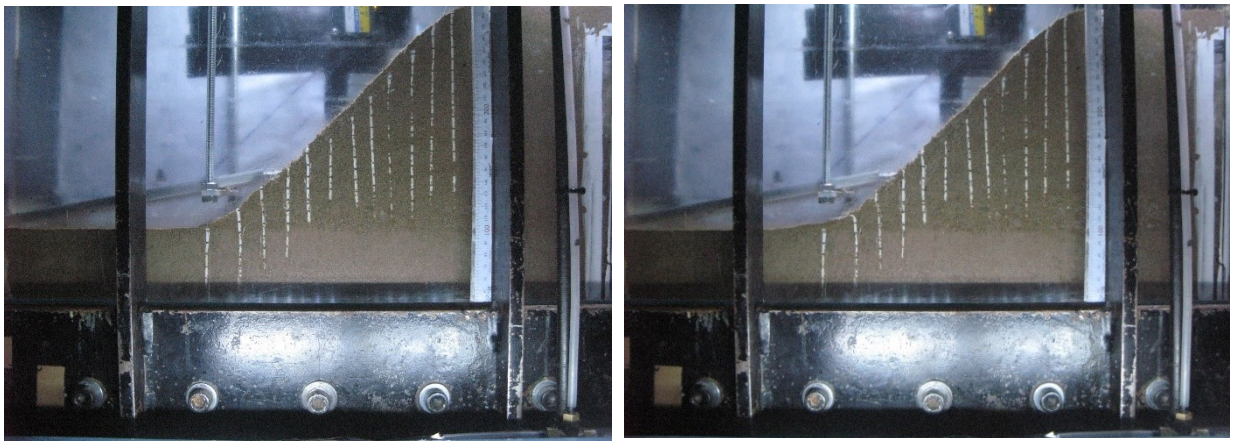

Initial Shape of model ground Final Shape of model ground

Figure 2.17 Model ground behavior in Case 2

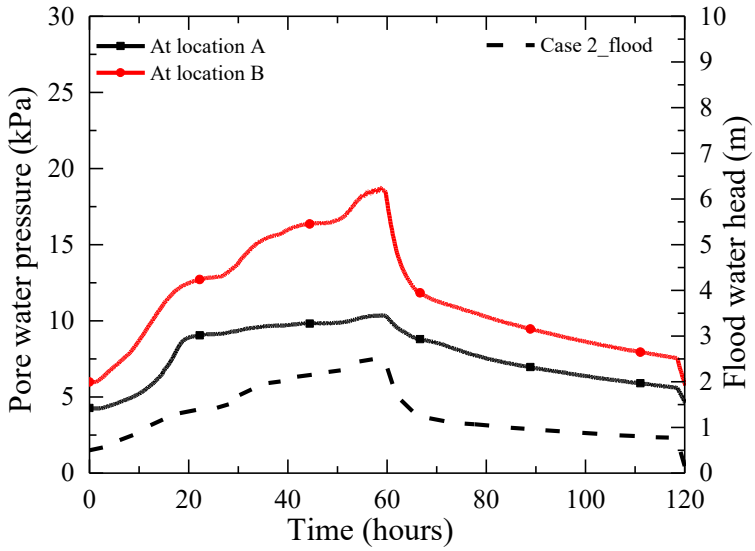

Figure 2.18 Time history of pore water pressure and flood water head for Case 2

Figure 2.18 shows the change in pore water pressure at two locations A and B (see **Fig.2.1**) with time along with the time history of flood water head for Case 2. From the figure it can be observed that with increase in flood water head rise in pore water pressure is not uniform in the model ground. The rise of pore water pressure near the supply (at location B) follows the similar trend as the rise in the flood water head whereas rise of pore water pressure near the slope surface (at location A) is limited. The pore water pressure near the slope remains maintained around 9 kPa. The effect of drainage of seepage water through the steel drainage pipe causes this limited rise of the pore water

pressure near the slope surface. Since the pore water pressure near the slope is limited, no deformation is observed in the model ground.

2.9.3 Case 3 (with steel drainage pipes)

In Case 3 model ground is provided with three steel drainage pipes at the spacing of 1 m at the height of 1 m above the toe of the slope. Since the central pipe was provided with the sensors to measure axial force and bending moment, drainage function was not available in this pipe. So, the central pipe provides the only drainage. In this case, flooding rising rate is about 0.04 m/hr. In Case 3, even though levee suffered surface erosion below the location of the pipe before the seepage test (while increasing centrifugal acceleration as the increasing rate of the centrifugal acceleration rather larger compared to the other cases), the large deformation of the levee is prevented. The surface erosion in Case 3 is attributed to insufficient manual control over the rate of increase of centrifugal acceleration. The presence of erosion below the toe region before seepage test facilitated the continuation of erosion, especially above the pipe 1 and pipe 3 (see **Fig. 2.1 (b)** for location) during the rise of the flood water. Along with this, tension cracks are observed on the crest of the levee. However, significant movement of the soil mass is prevented, as shown in **Fig. 2.19.**

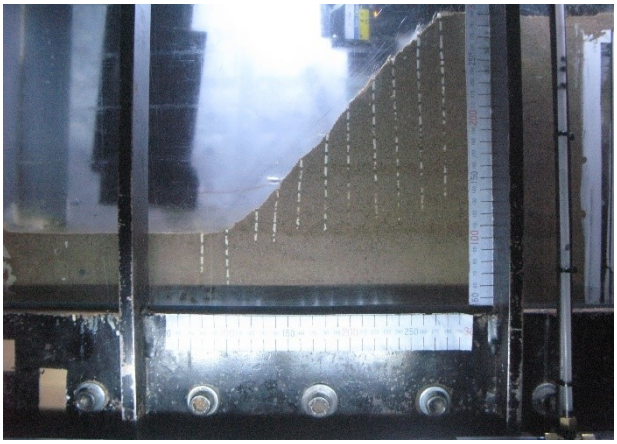

Initial Shape of model ground

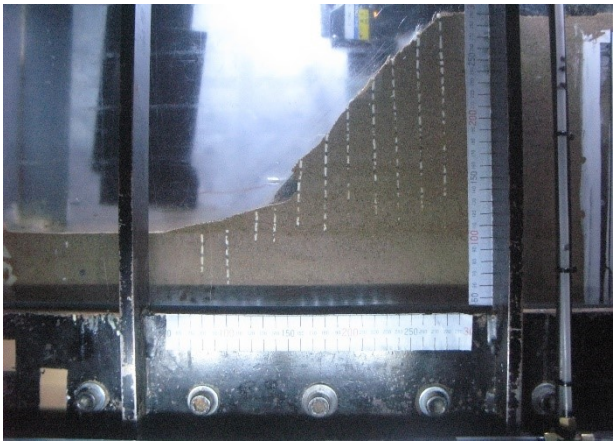

Surface erosion below pipe while increasing centrifugal acceleration

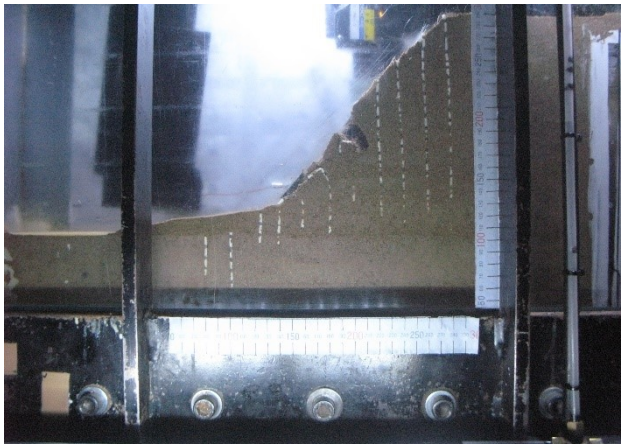

Continuation of erosion above the pipe (30 hours)

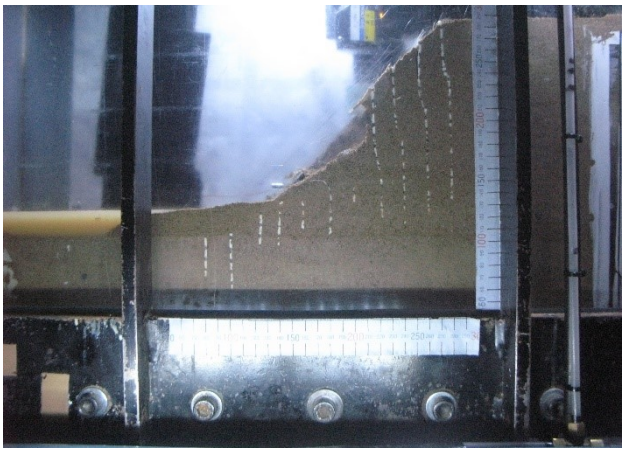

Final deformed shape of model ground

Figure 2.19 Model ground behavior in Case 3

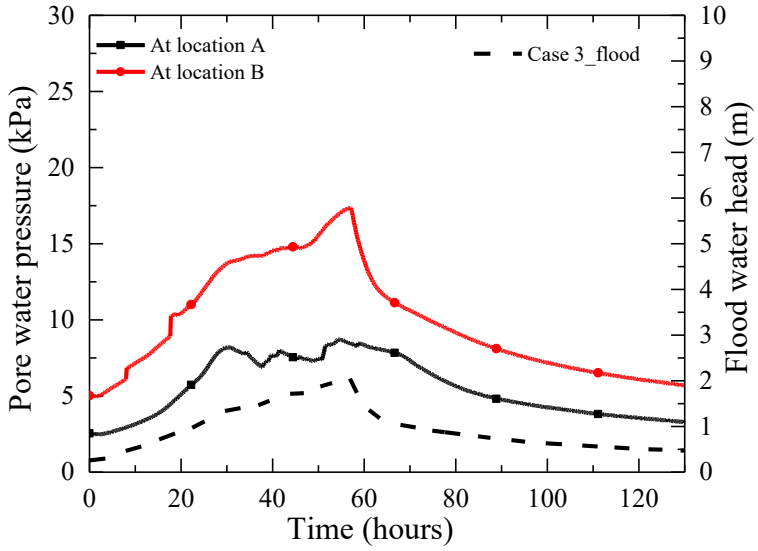

Figure 2.20 Time history of pore water pressure and flood water head for Case 3

Figure 2.20 shows the time history of pore water pressure at two locations A and B (see **Fig.2.1**) with time along with the time history of flood water head for Case 3. From the figure it can be observed that with increase in flood water head rise in pore water pressure is not uniform in the model ground. The rise of pore water pressure near the supply (at location B) follows the similar trend as the rise in the flood water head as observed in Case 2. Rise of pore water pressure near the slope surface (at location A) is maintained at maximum value around 8 kPa. Despite the surface erosion near the toe erosion during the increment of the centrifugal acceleration, the maintenance of the pore water pressure at lower level near the slope surface and presence of reinforcement prevents the collapse of the slope.

2.9.4 Case 4 (Only reinforcement)

In Case 4 model ground is provided with three steel pipes with its tubular structure filled with glue. In this case, pipes only provide reinforcement function. Pipes here are also installed at a spacing of 1 m at the height of 1 m from the toe of the slope. The model ground, in this case, is subjected to flood with the rising rate of 0.03m/hr. With the increase in flood head deformation is observed above the location of pipe but the continuation of slip line below the location of the pipe is stopped. However, the formation

of deeper tension cracks on the crest and consequent large deformation of the levee is not prevented as shown in **Fig.2.21.** The other unique result during the experiment was that continuous deposition of eroded soil near the location of pipe was observed. The soil was eroded from around the location of pipe from the slope surface, as shown in **Fig. 2.22.**

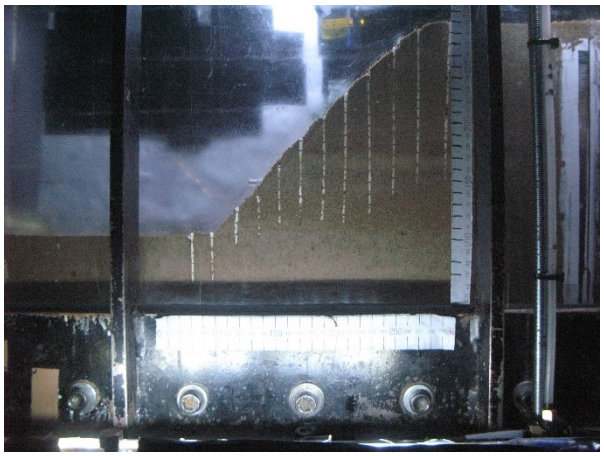

Initial Shape of model ground

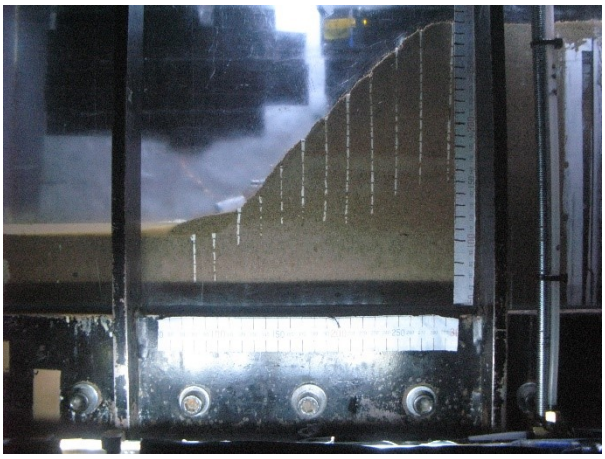

Deposition of eroded soil from near pipe at toe region of slope (40 hours)

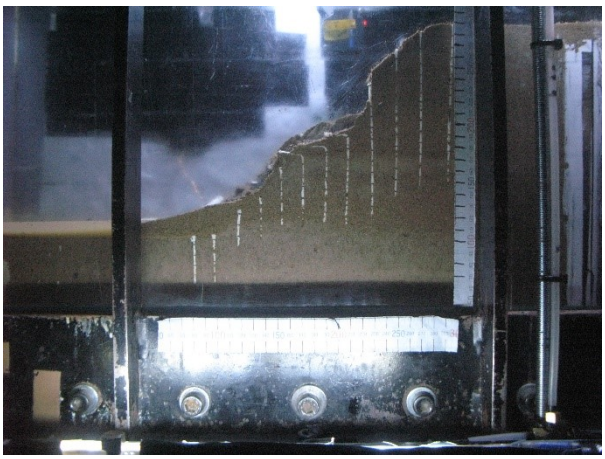

Movement of slope above pipe (55 hours)

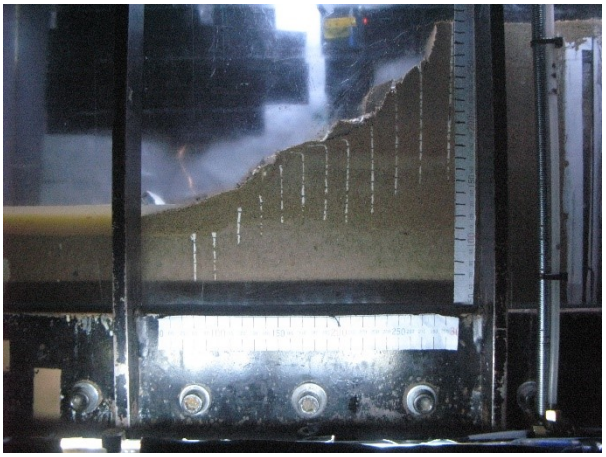

Formation of cracks on crest showing large deformation

Figure 2.21 Model ground behavior in Case 4

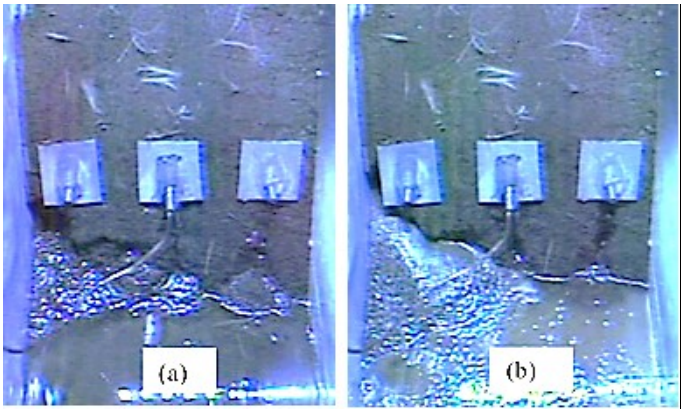

Figure 2.22 Erosion of soil near the slope surface in Case 4 (a) at 37 hours (b) 52 hours of seepage flow

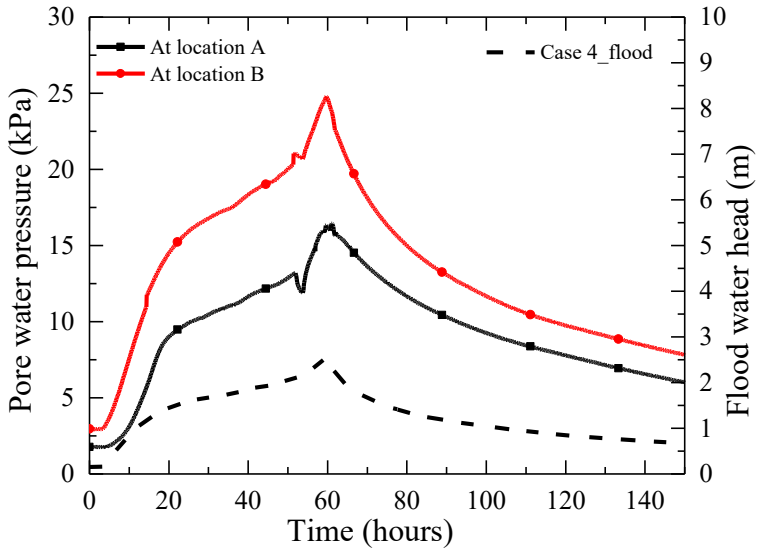

Figure 2.23 Time history of pore water pressure and flood water head for Case 4

Figure 2.23 shows the time history of pore water pressure at the location A and B (see **Fig. 2.1**) along with the supply flood water head in Case 4. From the figure it can be observed that with the increase in flood water head pore water pressure increases uniformly throughout the model ground as in the unreinforced model ground in Case 1. With reinforcement provided in the model ground, it could withstand development of higher pore water pressure within the model ground. At the high pore water pressure condition starting at 37 hours of seepage flow duration, erosion of soil near the location of pipe is observed. Under the high pore water pressure the channelized flow of seepage water below the rigid pipe causes the erosion of the soil around pipe. So, the presence of

steel pipe without drainage can create weak region around the pipe through removal of soil around the pipe especially under the high flood water head. This creation of weak region eventually can cause large deformation in the levee.

2.9.5 Case 5 (With steel drainage pipe)

In Case 5 model ground is provided with two steel drainage pipe at the spacing of 1.5m at the height of 1m from above the toe of the slope. The model ground is subjected to flood head rising at a rate of about 0.3m/hr. In this case, no significant deformation was observed as shown in **Fig. 2.24.**

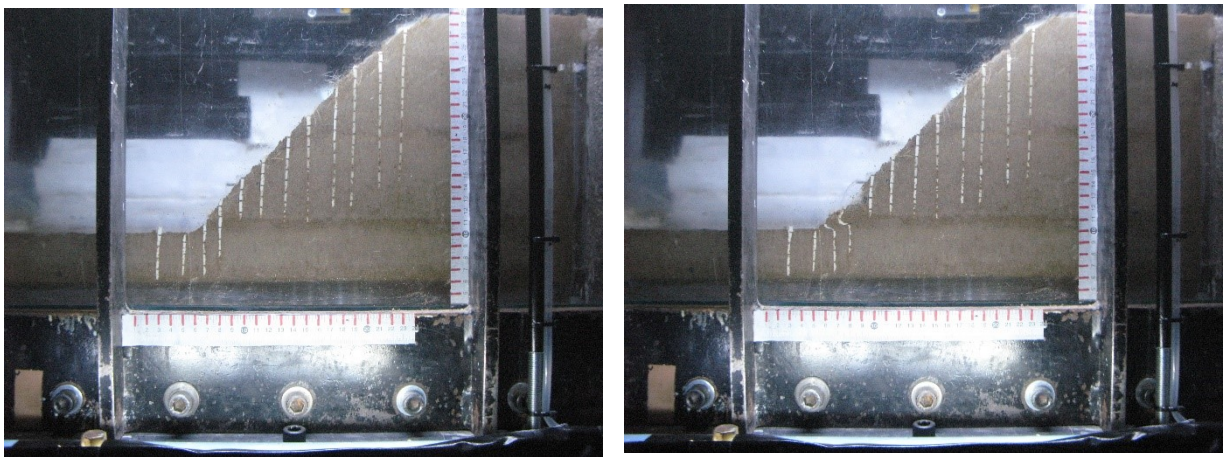

Initial shape of model ground

Final deformed shape of model ground

Figure 2.24 Model ground behavior in Case 5

Figure 2.25 shows the change in pore water pressure at two locations A and B (see **Fig.2.1**) with time along with the time history of flood water head for Case 5. The pore water pressure near the slope remains maintained around 10 kPa. The effect of drainage of seepage water through the steel drainage pipe causes this limited rise of the pore water pressure near the slope surface. Even though in this case the number of the drainage pipes is only two, pore water pressure near the slope surface is maintained at lower level indicating the sufficient capacity of the steel drainage pipes.

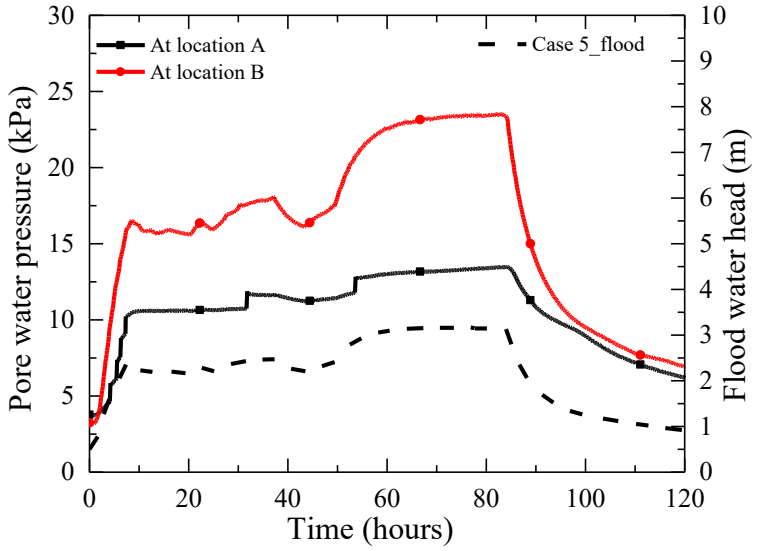

Figure 2.25 Time history of pore water pressure and flood water head for Case 5

2.9.6 Case 6 (Only drainage)

In Case 6 model ground is provided with three drainage pipe made of flexible silicone tube. The model ground is subjected to the flood head at a rising rate of 0.3m/hr. In this case slip line continued from the toe of the levee to the crest of the levee. The progression of the failure begins with the settlement of the pipe (after 36 hrs seepage flow) leading to the eventual large deformation of the levee (at 43 hrs of seepage flow duration) as shown in **Fig. 2.26.**

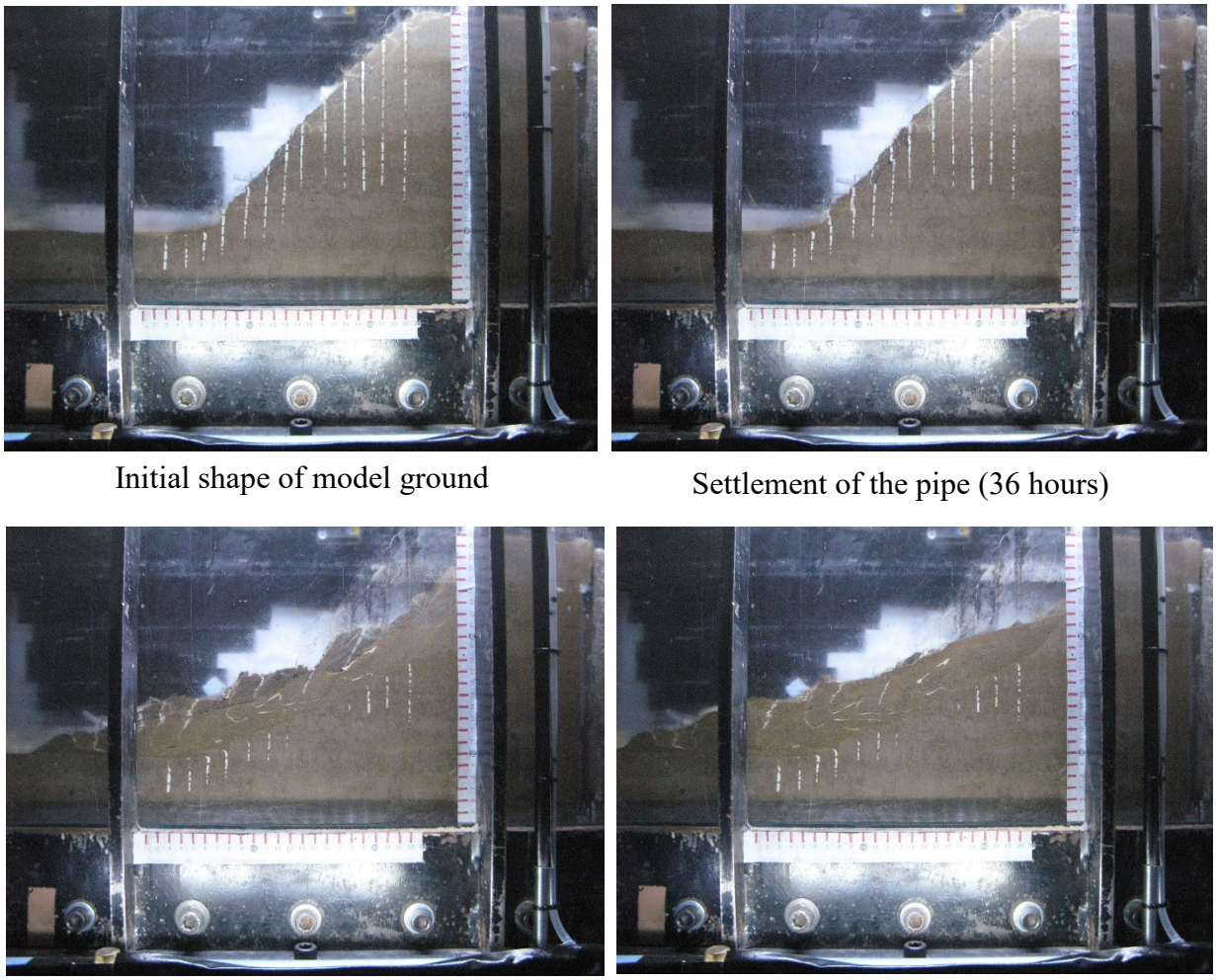

Initial shape of model ground

Settlement of the pipe (36 hours)

Sudden development of deep seated failure (43 hours)

Complete collapse of the slope (at the end of experiment)

Figure 2.26 Model ground behavior in Case 6

Figure 2.27 shows the time history of pore water pressure at the location A and B (see **Fig. 2.1**) along with the supply flood water head in Case 6. From the figure it can be observed that initially with rise in flood water head by 2 m the rise in pore water pressure near slope surface is about 10 kPa, however on further raising flood water head by 1 m also cause the rise of the pore water pressure by further 9.6 kPa (almost 10 kPa). So under the large flood water head, drainage capacity of pipe is not enough to limit the pore water pressure sufficiently. Since in this case no reinforcement is provided under the larger flood head only presence of drainage is not sufficient enough to limit the deformation in slope. In this case under the larger flood head collapse of the slope is observed.

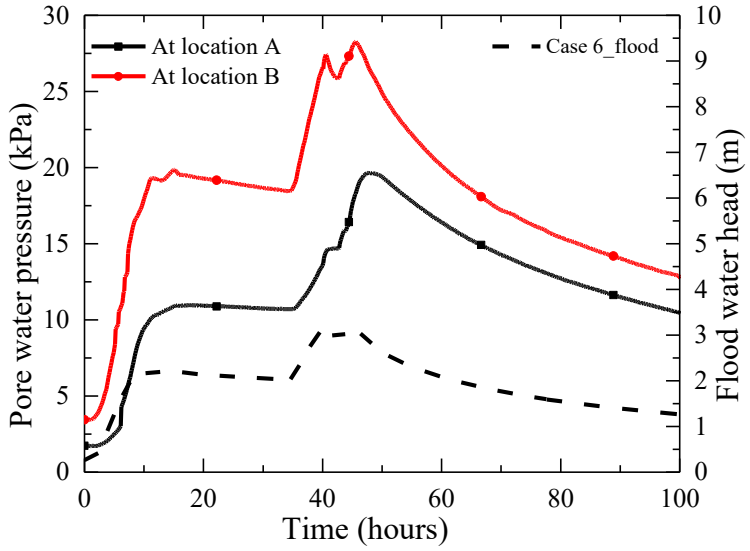

Figure 2.27 Time history of pore water pressure and flood water head for Case 6

2.10 Comparative performance in different cases

Observation can be summarised as follows. Failure is prevented in Cases 2 and 5 completely. In Case 3, a slight movement of the slope is observed with no large deformation of the slope. In all these cases (Cases 2, 3 and 5), protection in levee is provided by steel drainage pipes. In Case 4, the more extensive movement of soil slope is observed; however, the large deformation of the slope as observed in Case 1 is prevented. In Case 6, the slope has large deformation compared to no significant deformation in Case 5. In Case 1 and 4 the pore water pressure development is quicker and uniform throughout the model ground. For the cases with the drainage pore water pressure development near the slope surface is limited. In Case 6 where only drainage is provided, drainage is sufficient at low flood water head in preventing the deformation whereas at large flood water head drainage capacity is not enough to limit the rise of pore water pressure and prevent deformation. In Case 4, presence of reinforcement allows the model ground to withstand large pore water pressure development. However, at the large flood head due to the channelized flow around the pipe cause erosion of soil and thereby creating the weak zone. At large flood head thus pipe with only reinforcement cannot prevent large flood head.

2.11 Limitation of the centrifuge test

In the series of the centrifuge test, the major limitation was in the control of the supply flood water head. Ideally, the supply water head in all cases if could be maintained same could provide better condition for comparison among the cases. Also, the maintenance of the same initial condition among all the cases was also not particularly achieved. In Case 3 during the spinning of the centrifuge surface erosion was observed. This created difference in initial condition. While the initial water level was targeted to be at the top of foundation level, in Case 3 initial value of supply flood head is slightly higher compared to Case 4. Hence, providing higher seepage velocity which created inclined phreatic surface in Case 3. In Case 4 seepage velocity is small considering the smaller head difference between the upstream and the downstream. However, it should be considered that initially water level within model slope is near to the foundation and certainly unaffected by the presence of the pipes placed above 1m height from foundation as shown in **Fig. 2.28**. The main objective was to achieve the similar initial condition in all the cases which is unaffected by the different drainage and reinforcement condition among the cases which is fairly achieved in all the cases.

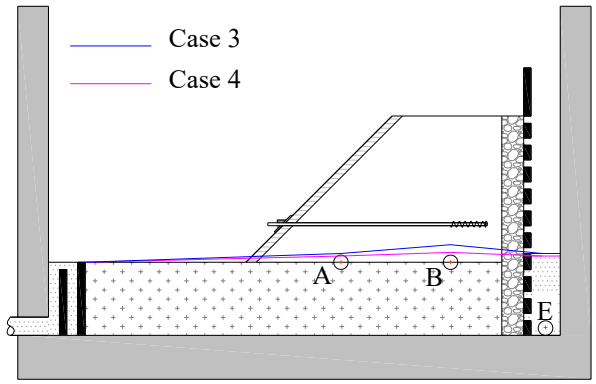

Figure 2.28 Initial water level in Case 3 and Case 4

2.12 Summary

In this chapter, the details of the centrifuge experiment are discussed. The scaling law, material properties, testing conditions, testing procedures, and observation made during the experiment are presented in detail. Details of different test condition and observation made in each case are presented, which demonstrates the overall performance of the protection provided in the model ground. From the series of experiment following observations are made:

- From the experiment result, it is observed that with the increase in flood head, large deformation is induced and eventually cause failure when no protection is provided.
- Protection, when provided in the form of either drainage or reinforcement only, can delay the failure; however, cannot be prevented.
- With the use of the steel drainage pipe, large deformation due to increased seepage flow during the flood is prevented.
- From the experiment it is observed that, on the condition pore water pressure near the toe region is limited within 10 kPa, slope failure is prevented even in absence of reinforcement.
- With the use of the reinforcement, levee can with stand higher pore water pressure, however higher pore water pressure can cause erosion of soil especially near pipes. This erosion of soil near pipes creates weak zone making levees vulnerable.

3 1g Physical model test and results

3.1 Introduction

The centrifuge test had the limitation of the inconsistency in the supply flood water level and the initial condition among the cases. 1g physical model test of soil slope was conducted with the objective of understanding the behavior of the slope subjected to seepage flow when it is reinforced with the proposed steel drainage pipe and compare its performance with levee of different protection under similar condition of seepage flow. This scaled down single gravity model is expected to give a better understanding of the working mechanism of the steel drainage pipe. This chapter presents the specifics of the geotechnical physical modeling of the seepage flow in the soil slope. The experiment facility, equipment used, and instrumentation for data acquisition are explained in this chapter. This chapter also gives the details of the experiment procedure, assumptions, and the results.

3.2 Mid-scale physical model

Midscale physical model used in this study give great advantages of better control of the boundary condition and loading condition of the model. Loading condition here being the supply flood head for the seepage flow through the physical model. This type of well-defined and well-controlled boundary conditions provides reliable data for supporting numerical modeling and back analysis. The well-defined loading condition helps in maintaining similar conditions among the test in different cases and making the comparative study more reliable. The models used are relatively larger. Therefore, the space available for sensors and instrumentation is larger. Also, better control of observation is feasible. In this study, mid-scale single gravity physical model test cases are conducted with the objective of having better control for the rise of flood head in all cases, which is not completely achieved in centrifuge model. Many studies have been made in understanding slope behavior during the seepage flow using the single gravity

physical model (Chen and Huang, 2011; Hori et al., 2011; Jia et al., 2009; P. Orense et al., 2006; Zhang and Maeda, 2014). This study can confirm the slope behavior under seepage flow and study the failure condition of the slope. While the scaled physical model ground experience obvious different stress level compared to natural slope; however, the suitable large scale model, this difference can be minimized and also make the numerous testing feasible. Nevertheless, in this study, the main objective is to confirm the working mechanism of proposed steel drainage pipe and also make a study of relative performance for different protection degree in slope which can be achieved by using the scaled down physical model mimicking the real river levee.

3.3 Testing facility.

For the single gravity physical model, the testing facility at Nippon and Sumitomo Metal, Research and Engineering Centre was used. The physical model used in this study used was in 1:6 scale of the prototype model used in the centrifuge. This scale of the model was large enough to avoid the effect of the capillary rise and also small to enough to finish the experiment within adequate time frame and resources. The details of the testing facility and instruments and material used are explained in the following sections

3.3.1 Model container

The model container used in the study is of 1.5m length, 0.7m width, and 1.0 m height. The model container was provided with one transparent window for visual observation. The container was divided into two sections. The first section of 0.1 m length served as the supply section and the second section of the length 1.4 m provide the space to construct the physical model. The boundary between the model section and the water supply section was made of the perforated steel wall covered with the geomembrane, which allowed inflow of water to the model ground without migrating soil. The steel wall separated the drainage section and the model section. In the non-transparent wall of the container, holes were made and connected to the pipes, which allowed to visually observe the location of the water level at each point. In addition to this main container, the

arrangement was made to collect and measure the drained seepage water in a separate tank. The special arrangement was made to collect the seepage water from the model container and pass to the drainage tank in the form of the open cylindrical channel. The drainage tank was placed over the load cell to measure the quantity of the seepage water continuously. **Figure 1** shows the arrangement of the model container and the drainage tank.

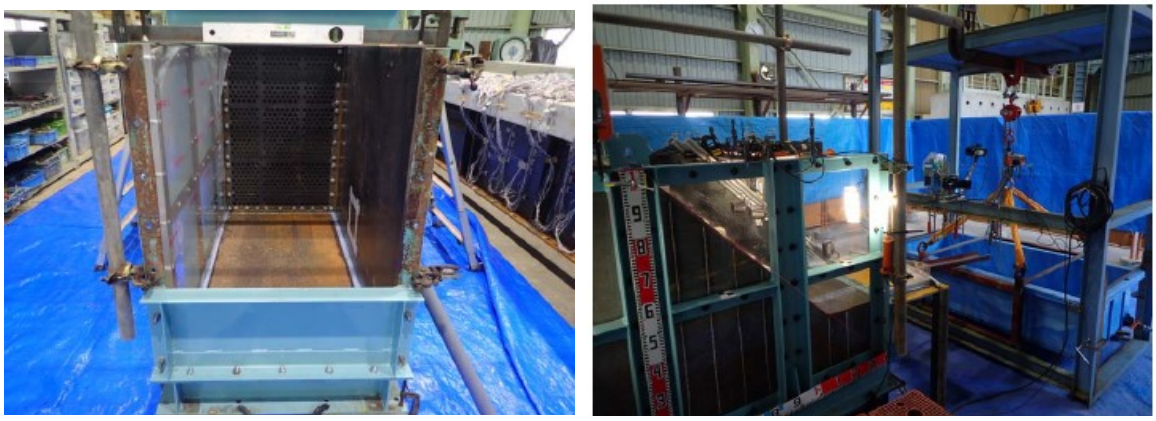

Figure 3.1 Model container and drainage tank arrangement for the experiment

3.3.2 Instrumentation

The behavior of the model during the experiment was monitored by using different types of transducers. In all the experiment cases, four types of transducers were used in the model. Pore pressure transducer, earth pressure transducer, potentiometer, and laser displacement transducer were used to measure pore water pressure, earth pressure, and settlement, respectively.

Figure 3.2(a-c) shows the pore water pressure transducer, potentiometer, and laser displacement transducer respectively used in the experiment. Apart from this transducers, model steel pipe with the attached strain gauge was also used. The strain gauge measurement is used in the calculation of the bending moment, and axial force mobilized in the steel pipe. All the transducers were calibrated to convert the voltage output to the engineering units.

In the experiment, ten numbers of the pore water pressure transducers (PPT), three potentiometer, and twelve laser displacement transducers (LDT) were used. The PPTs used in the experiments were pressure transducer BPR-A-50KPS supplied with stainless filter (10 μm) at the head and having the maximum capacity of 50 kPa and rated output of 0.4mV/V from KYOWA. The laser displacement transducers used in the experiment were with model name IL-300 manufactured by KEYENCE with the measurement range of 160 to 450 mm and reference distance of 300 mm. The potentiometer used is the model is general purpose displacement called SDP-200E with capacity of 200 mm. In the steel pipe, strain gauge sensor was used to measure strain at ten different locations. The change in pore water pressure in the model ground with the seepage flow was recorded using the PPTs and surface settlement was measured using LDTs and potentiometer.

The location of each transducer was carefully measured to ensure the target placement of the transducer. Transducers which were placed inside the model ground were placed perpendicular to the direction of the flow and wires were arranged such that minimum obstruction was caused by wires to the flow of water.

Apart from these transducers, marked noodles were used in the front face of the model ground to observe the deformation pattern during the experiment. Also, the arrangement of standpipes (manometer) was made on the non-transparent window of the container to locate the phreatic surface visually during the experiment. Line laser was also arranged to measure the profile of slope which could be moved during the test.

(a)

(b)

(c)

Figure 3.2 Sensors used in the experiment (a) pore water pressure transducer (b) potentiometer (c) laser displacement transducer

3.3.3 Visual observation

For the visual observation of the model ground during the experiment, three video cameras, and three still cameras were used. Still camera used was Power Shot G3 X from CANON, and video camera used EX-100PRO from CASIO. The three video cameras and still camera were placed in three different faces of the model container. One placed in front of transparent window was used to observe the front view of the model and the movement of marked noodle, one set of video and still camera was used to observe the slope of the model ground and last set of cameras were used in front on non-transparent wall of container to observe the manometer for location of phreatic surface. Also to observe the flow inside the pipe, the industrial endoscope with model code P-QV-

MTC39703 from J-Scope having head of 4 mm was used. Figure 1.6 shows the cameras used in the experiment.

3.3.4 Water supply and drainage system

Flooding during the experiment was simulated by increasing the water table in the water supply section during the experiment. The flood water level was measured using the water level meter of model name FL-001 from KEYENCE. **Figure 3.3** shows the arrangement of a water level meter for measurement. The water table was increased to the target value and then kept constant by observing the reading of water level meter placed in water supply section and by visual inspection of standpipe attached on the non-transparent face of the container. The water accumulated after the seepage flow was drained out through the cylindrical open channel to drainage tank. The water collected in the drainage tank was also monitored through the load cell measurement continuously throughout the experiment. **Figure 3.4** shows the arrangement for collecting and measuring the drained seepage water during the experiment.

Figure 3.3 Water level meter (FL-001) used for measuring flood water level.

Figure 3.4 Arrangement for collecting and measuring the drained seepage water

3.4 Material properties

All the experiments were conducted using the Kasimigaura sand. The index properties of the Kasimigaura sand was shown in **Table 3-1**. The strength parameters were determined from standard undrained triaxial test. Foundation and embankment were prepared with soil with a degree of compaction (Dc) of 90% (1.49 Mg/m3) of maximum dry density determined from the Standard Proctor Compaction test. The classification of the soil based on particle size was shown in **Table 3-2**. **Figure 3.5** shows the soil water characteristic curve (SWCC) for the embankment along with the principal parameters for the van Genuchten model. The surface layer on the slope was prepared by soil mixed with fiber to replicate the grass cover often found in the real levee and to prevent the occurrence of unrealistic surface erosion during the experiment. The content of the fiber is 1% of the dry weight of sand. The polyester fibers, approximately 39 μm in diameter and 5 mm in length was used in the test.

Table 3-1 Properties of Kasimigaura Sand

Soil properties	Values
Soil particle density (Mg/m^3)	2.71
Young's Modulus (N/m^2)	1.6E+04
D_{50} (mm)	0.5015
D_{10} (mm)	0.2535
Coefficient of uniformity	2.414
Coefficient of gradation	0.82
Saturated coefficient of permeability (m/s)	1.2E-04
Internal angle of friction	33
Initial void ratio	0.91
Cohesive strength (N/m^2)	0
Dry density of embankment (Mg/m3)	1.49
Optimum moisture content	19.43%
Poisson's ratio	0.33

Table 3-2 Classification of the soil

Type	Mass percentage
Coarse gravel %	0.00
Medium gravel %	0.00
Fine gravel %	7.10
coarse sand %	18.9
medium sand %	64.4
fine sand %	9.4
Silt and clay%	0.2

+

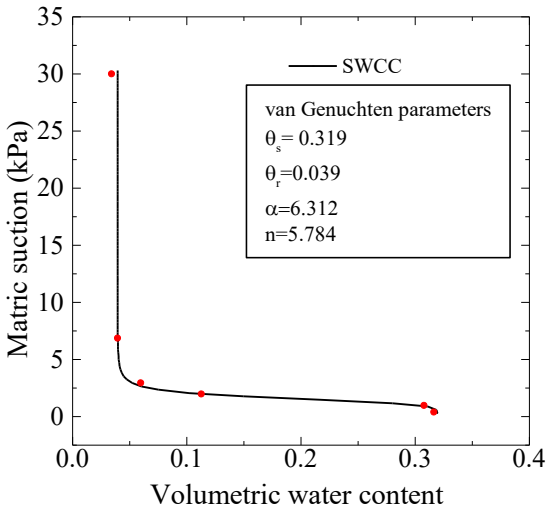

Figure 3.5 Soil water characteristics curve (SWCC) of Kasimigaura sand

Pipes used in the experiment are 0.9 m long with an internal diameter of 10mm, and external diameter of 12 mm. Pipe is tubular in structure with the holes on the surface on end 0.3 m portion. To mimic the function of spiral blade present in prototype pipes, pipes are attached to the end of the container with wire. The properties of the pipe used in the experiment are listed in **Table 3-3**.

Table 3-3 Properties of Steel drainage pipe

Parameters	Values
Internal diameter (mm)	10
Length (m)	0.9
Young's Modulus, E (N/m^2)	6.90E+10
Poisson's ratio, v	0.2

3.5 Test Conditions

Series of the three test cases of the physical model test is performed with a half section of the river levee made of Kasimigaura sand with the side slope of 1H: 1V is used. The test conditions are summarized in **Table 3-4**. **Figure 3.6** shows the geometry of model slope and arrangement of pipes in the experiment (Cases AT.1-AT.3). Figure 1 (a) shows the cross-section of the model with pipes and arrangement of sensors. In Cases AT.2 and

AT.3, the pipes are installed at the height of 0.05m from the toe of the slope. Figure 1 (b) shows the arrangement of the pipes in the plan view for the Cases AT.2 and AT.3. In Case AT.2 and AT.3, the slope is provided with five pipes. The pipes are installed at the spacing of the 0.14 m. Steel pipes used in the experiment are 0.9m long with an internal diameter of 10mm, and external diameter of 12 mm. Pipe is tubular in structure with the holes on the surface on end 0.3 m portion. To mimic the function of spiral blade present in prototype pipes, pipes are attached to the end of the container with wire. For the test with only reinforcement (i.e., Case AT.2) opening of the pipe was plugged so that it could not provide drainage.

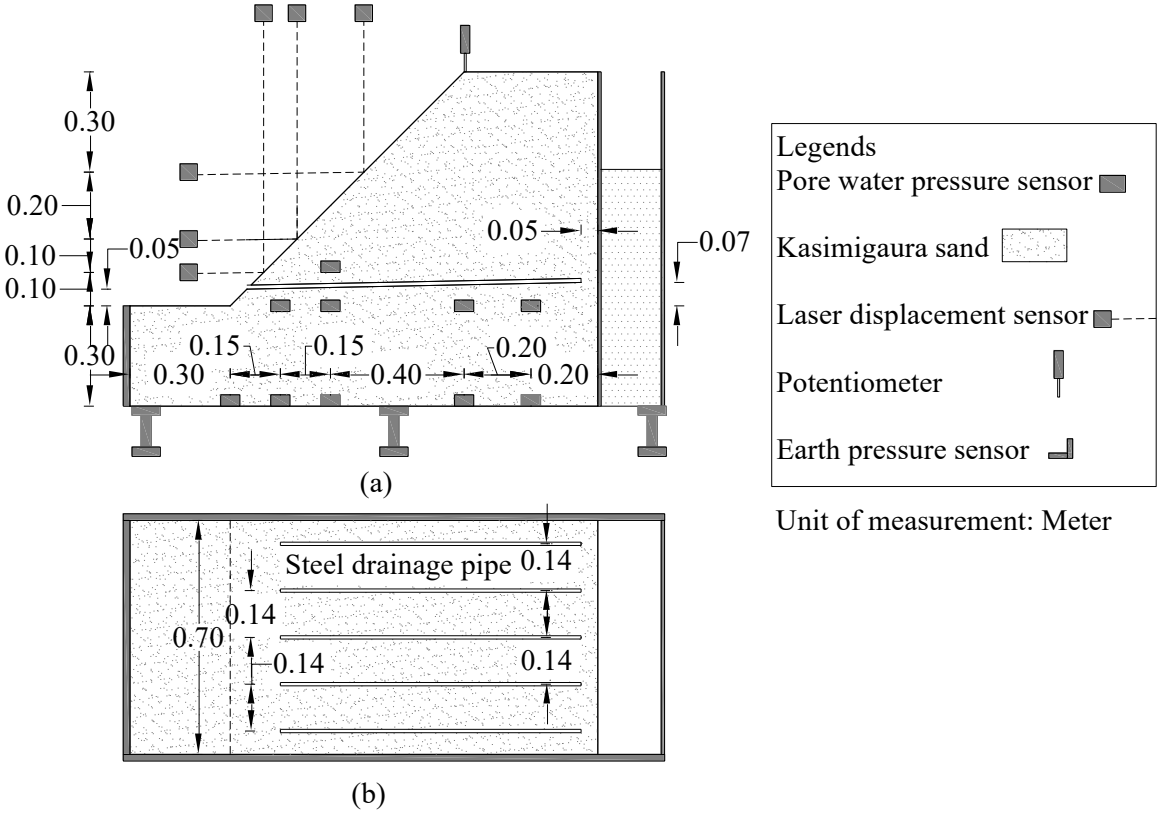

Figure 3.6 Model ground for the test (a) Cross-section with location of sensors and pipes (b) Plan view with location of pipes of the model ground

Table 3-4 Test condition for the experiment

Test Condition	Number of pipes	Height of pipe location from toe of slope
Case AT.1 (Unreinforced)	N/A	N/A
Case AT.2 (Only reinforcement)	5	0. m
Case AT.3 (Reinforcement +drainage)	5	0.05 m

3.6 Model preparation

All models are constructed in the container with the inner dimension of 1.5 x 0.7x 1.0 m and equipped with a transparent window made of acrylic. The container is divided into two sections; upstream supply section and model section. Supply section has a width of 0.1 m, and the model section has 1.4 m width. In the model section, 1:6 scaled down the model ground was prepared by manual compaction and excavation technique (see **Fig.3.7 b**). Steps of model preparation are summarised in **Fig. 3.7**. At first, ground with the varying cross-section is prepared by placing and compacting Kasimigaura sand in 10 layers of an equal thickness of 0.1 m to the target density. Each soil layer is compacted at the average moisture content of 12 %, which is near to the optimum moisture content of the soil. Layers of the soil are compacted manually by standing over the flat surface. Pore water pressure transducers (PPTs) are also placed in predetermined locations with precise measurement while preparing the model ground (see **Fig.3.7 c**). The location of the sensors in model ground is summarised in the **Table 3-5**. At the predetermined height of 0.05 m, pipes are placed at the spacing of 0.14 m in Cases AT.2 and AT.3. The model ground is then excavated to the designed shape.

The slope portion of the model is then further excavated resulting slope to 0.05 m deeper than the required dimension. In excavated slope surface, Kasimigaura sand mixed with fiber (1% by weight) is compacted with the same degree of compaction of the embankment to form required model geometry. Twelve laser displacement transducers (LDT) are used to measure the settlement at two different planes of slope (at ½ span and ¼ span of model ground). In each plane, six LDTs are used to measure vertical and horizontal displacement at three different locations (see **Fig. 3.6 a**). Marked noodles are

placed on the side face of the model for visual observation of the deformation pattern through the transparent window. Apart from this, in the Cases AT.2 and AT.3, the central pipe is equipped with strain gauges to measure strain at ten different locations. The wires of these sensors are passed from outside of the pipes to prevent the blockage of drainage through pipes.

Water is supplied to the supply section and passed to drainage tank after seepage through the cylindrical channel connection. Drainage tank is connected to the load cell to measure the drained water continuously. Water level meter is installed in water supply section to measure the supply flood water level. Standpipe with the floating balls is arranged on the non-transparent wall of the container to visually observe the location of the phreatic surface during the test. Line laser was also placed to measure the slope profile during the test. For the visual observations of model ground during the test, three high definition video recorders along with three high-resolution digital cameras (side) are placed in front of the transparent wall, non-transparent wall and in front of slope.

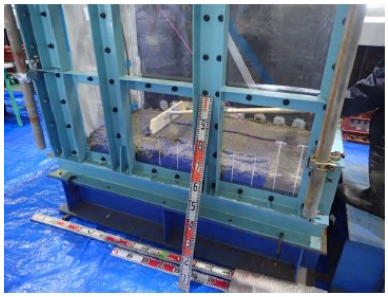

(a) Placing of the soil

(b) Manual compaction of the soil layer

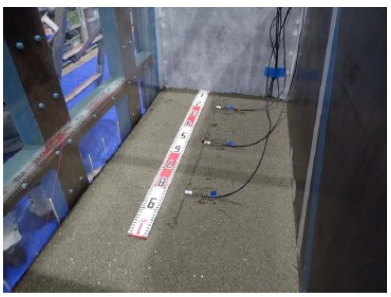

(c) Placement of sensor

(d) Construction of layer of soil

(e) Placement of pipe

(f) Completion of compaction of soil layers

(g) Soil Slope after excavation

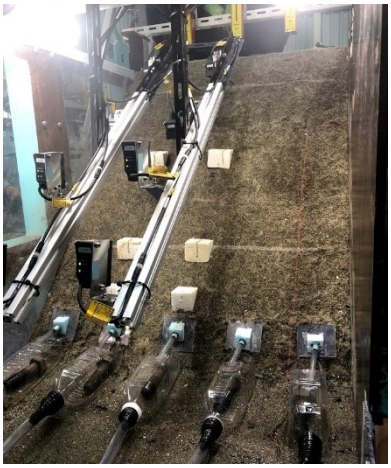

(h) Model ground after placement of cover soil and LDTs

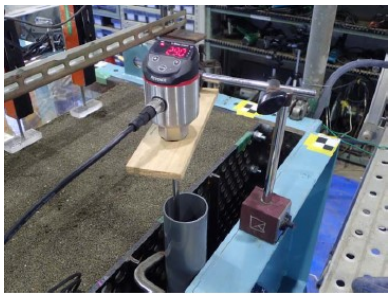

(i) Placement of water level meter

(j) Arrangement of drainage tank

Figure 3.7 Steps of model preparation

Table 3-5 Locations of sensors in model ground

Sensor ID	Type of sensor	Height from bottom of model	Distance from supply tank
01_200	Pore water pressure transducer	100 mm	200 mm
01_400	Pore water pressure transducer	100 mm	400 mm
01_800	Pore water pressure transducer	100 mm	800 mm
01_950	Pore water pressure transducer	100 mm	950 mm
01_1100	Pore water pressure transducer	100 mm	1100 mm
03_200	Pore water pressure transducer	300 mm	200 mm
03_400	Pore water pressure transducer	300 mm	400 mm
03_800	Pore water pressure transducer	300 mm	800 mm
03_950	Pore water pressure transducer	300 mm	950 mm
04_800	Pore water pressure transducer	400 mm	800 mm
LDT_H_04	Laser displacement transducer (for horizontal movement)	400 mm	1000 mm
LDT_H_05	Laser displacement transducer (for horizontal movement)	500 mm	900 mm
LDT_H_07	Laser displacement transducer (for horizontal movement)	700 mm	700 mm
LDT_V_04	Laser displacement transducer (for settlement)	400 mm	1000 mm
LDT_V_05	Laser displacement transducer (for settlement)	500 mm	900 mm
LDT_V_07	Laser displacement transducer (for settlement)	700 mm	700 mm
P_V_1	Potentiometer (for settlement at shoulder)	1000 mm	400 mm

3.7 Testing procedure

After the setup of the model ground is complete, the foundation layer is saturated. For the saturation, water is allowed to seep through the foundation layer for sufficient time, and attainment of water level at the top of the foundation layer is confirmed through visual observation. After that water level is raised in stepwise. In each step flood level is increased by 100 mm and the level is maintained for certain time to allow the steady state. In Case AT.1 and AT.3, the water level is maintained for the 30 minutes, and in Case AT.2 water level is maintained for 15 minutes. **Figure 3.8** shows the time history of the flood level for all the cases. The water level is continuously monitored through the water level meter record and visual observation of the standpipe. The flow of water is controlled manually by a tap.

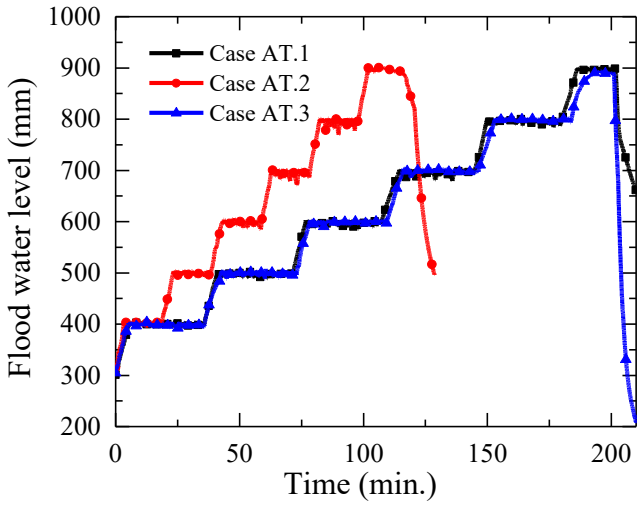

Figure 3.8 Time history of flood water level for Cases AT.1-AT.3

3.8 Results

In this series of the experiments, three different cases are studied. The three different test cases have been provided with varying level of protections. Case AT.1 is the unreinforced case, which acts as the base case for comparison with other cases to understand the relative performances of the provided protection. Cases AT.2 and AT.3 are provided with

the proposed steel drainage pipes. In Case AT.2, the end of the pipes are closed in the outlet so the pipes can provide only reinforcement. The main objective of this series of the experiments is to understand the behavior of the reinforcement function of the pipe when it is provided in isolation and in a combination of the drainage. Observations made for each test cases based on the visual observation through the transparent window and LVDT sensors are summarised in the following section.

3.8.1 Case AT.1 (Unreinforced)

In Case AT.1, the model ground is not provided any protection in terms of the pipe. In this case, water level is raised in steps at the average rate of 20 mm per minute. At each step, the water level is raised by 100 mm, and the level is maintained for 30 minutes. In this test, first sign of deformation in the form of the cracks appear when the water level is raised to 700 mm, and big collapse leading to the complete failure of the slope occurs when the water level is raised from 800 mm to 900 mm. Since in this case there is no protection provided, once the crack formation is initiated, failure is progressively moved towards upper portion of the slope. In this test also very similar to the centrifuge test (discussed in Chapter 2), failure starts from the toe region and extends to the upper portion. Hence, retrogressive sliding, which was also observed in the centrifuge test, is also observed in this test.

Figure 3.9 shows the progression of the failure in the Case AT.1. From the figure, it can be observed that failure started from the toe region with the crack. The failure then proceeds to the upper region. The sliding surface gets deeper, and ultimately, the total collapse of the slope occurs. Initially, one the account of the unsaturated state of the soil, slope remains stable, but when the phreatic surface is raised sufficiently high with the seepage flow, slope fails. In the absence of the protection, failure progression happens even with the small fluctuation of the level of phreatic surface within the slopes. With the progression of the failure, large soil mass movement is observed, which results in deposition of large soil mass near the toe region.

(a) Initial shape of the model ground

(b) Appearance of the crack near the toe region (at 700 mm water level)

(c) Progression of failure to upper region of the slope (800mm-900 mm water level)

(d) Soil mass movement with deep sliding surface ((800mm-900 mm water level)

(e) Complete collapse of the soil slope (900 mm water level)

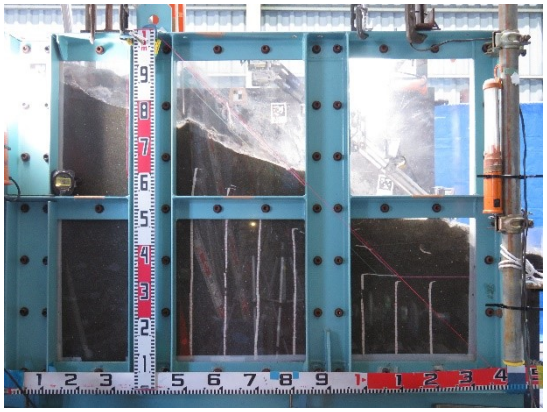

(f) Side profile showing collapse of the slope

Figure 3.9 Progression of failure in Case AT.1 (unreinforced case)

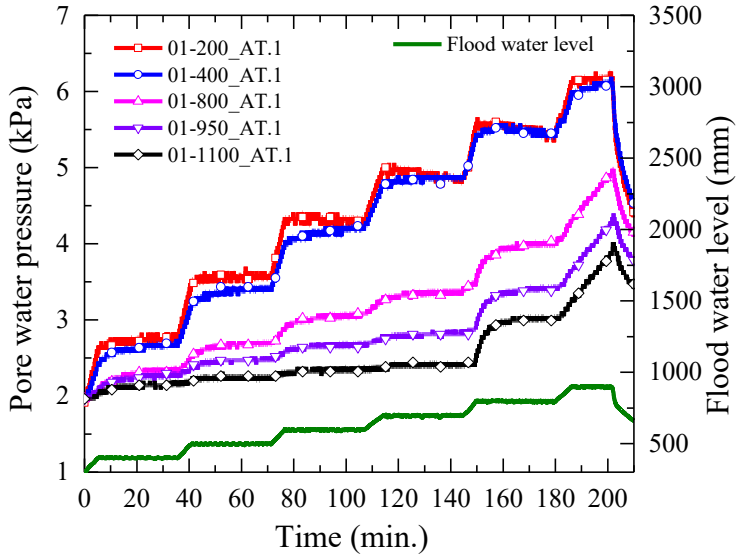

Figure 3.10 Time history of pore water pressure at foundation level in Case AT.1

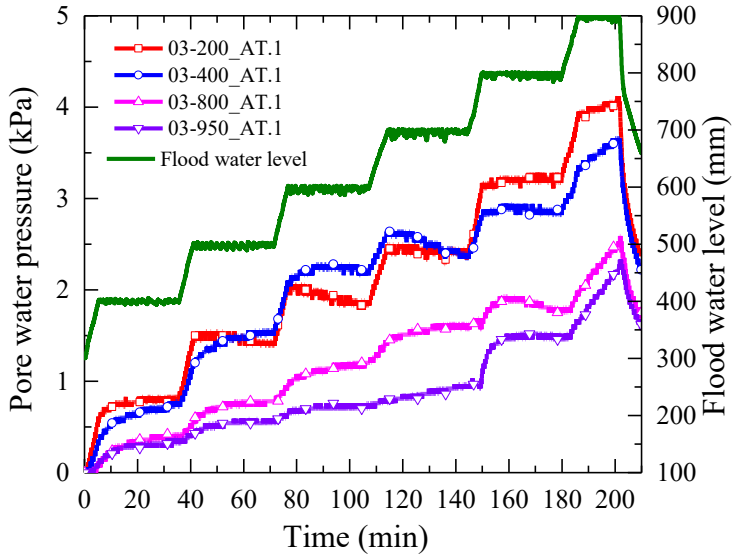

Figure 3.11 Time history of pore water pressure at top of foundation in Case AT.1

Figure 3.10 shows the time history of pore water pressure at different locations in the foundation level and **Fig. 3.11** shows the same at the top of the foundation level along with flood water level. From the figure it can be observed that pore water pressure is raised in steps as the rise in flood water level. In each step, steady state of seepage flow is achieved indicated by the achievement of steady pore water pressure. The failure is initiated when the pore water pressure reaches almost 1kPa near the toe region

(03_950_AT.1). With the further increase in pore water pressure complete collapse of soil occurs starting from the deformation near toe of slope.

Figure 3.12 shows the slope surface at the beginning of the seepage flow and the final shape of deformed slope along with the outline of levee. The dashed line in the figure is indicates the slip surface of model ground. In the absence of any protection slip surface extends from toe of slope to the crest of the slope. At the crest of the slope, settlement of about 216 mm is observed. Slip surface is also about 200 mm deep from the slope surface.

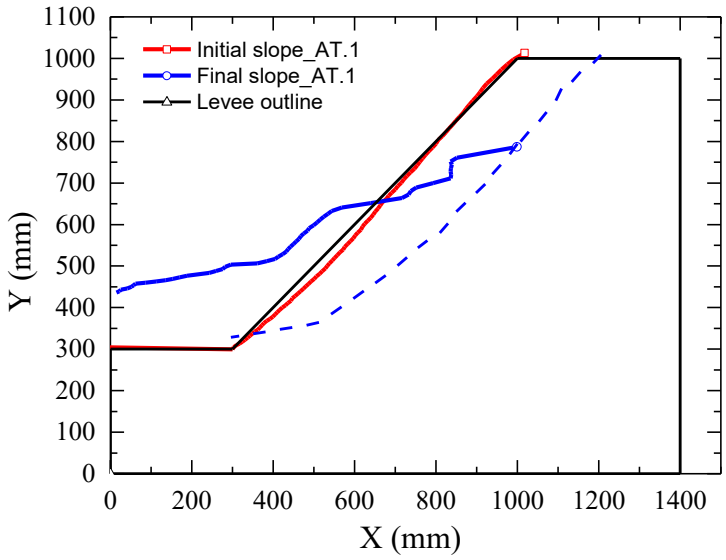

Figure 3.12 Change in slope surface with the seepage flow in Case AT.1

3.8.2 Case AT.2 (Only reinforcement)

In Case AT.2, the model ground is provided with the five pipes, which can function as reinforcement pipe only. In this case, also water level is raised in steps at an average rate of 20 mm per minute. In each step water level is raised by 100 mm and then the level is maintained for 15 minutes. In this case, water level is maintained only for 15 minutes as a steady state was achieved within this time period. The deformation starts when the water level is increased from 700 mm to 800 mm. During the progression of seepage flow, the soil mass movement is restricted by the reinforcement action of the pipe. The retained mass of soil above the location of pipe forms the arch. The differential settlement between

the location where there is pip, and there is no pipe is observed, which results in the formation of arch. Also, with seepage flow, soil below the location of pipe move away from the slope, which causes the facing plate to compress the soil above the pipe. With the further progression of the seepage flow, cracks are observed on the slope surface at a much higher position of the location of the pipes. Nevertheless, collapse of the slope is prevented in this case by the reinforcing effect of pipes.

(a) Initial shape of the model ground

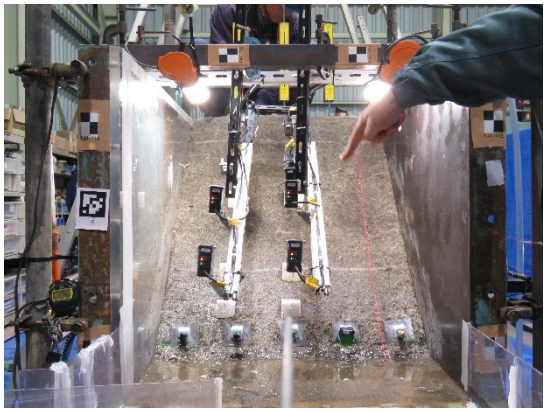

(b) Appearance of small cracks above near toe (700 mm to 800 mm water level)

(c) Formation of arch above the pipe location (800 mm water level)

(d) Deepening of the cracks on upper surface with limited soil mass movement (800 mm water level)

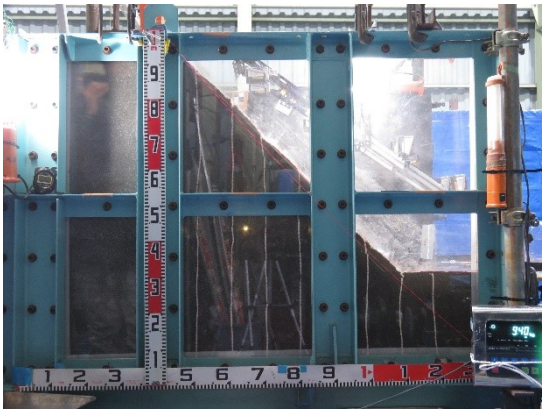

(e) Side profile of the soil slope at beginning of experiment

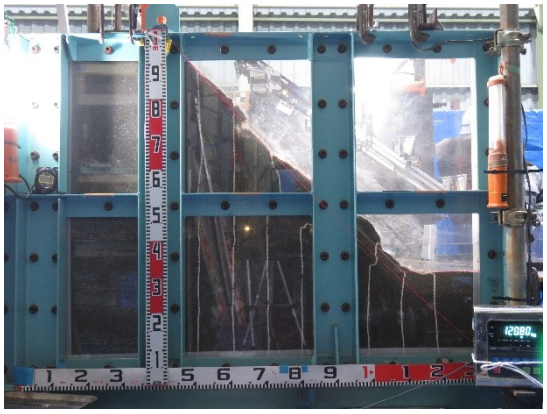

(f) Side profile of the soil slope at the end of experiment

Figure 3.13 Evolution of deformation in the model ground in Case AT.2

Figure 3.13 shows the progression of the soil movement in Case AT.2. In the figure, it can be observed that initially with the seepage flow arch is formed above the location of the pipes caused due to differential settlement across the plane of slopes. With the progression of the seepage, flow cracks are observed, but the collapse of the soil as such observed in Case AT.1 is prevented.

Figure 3.14 shows the time history of pore water pressure at different locations in the foundation level and **Fig.3.15** shows the same at the top of the foundation level for Case AT.2 along with the flood water level. In each step, steady state of seepage flow is achieved indicated by the achievement of steady pore water pressure. The level of the pore water pressure developed in this case is also similar to the Case AT.1. However, due to the presence of the reinforcement the deformation is limited.

.

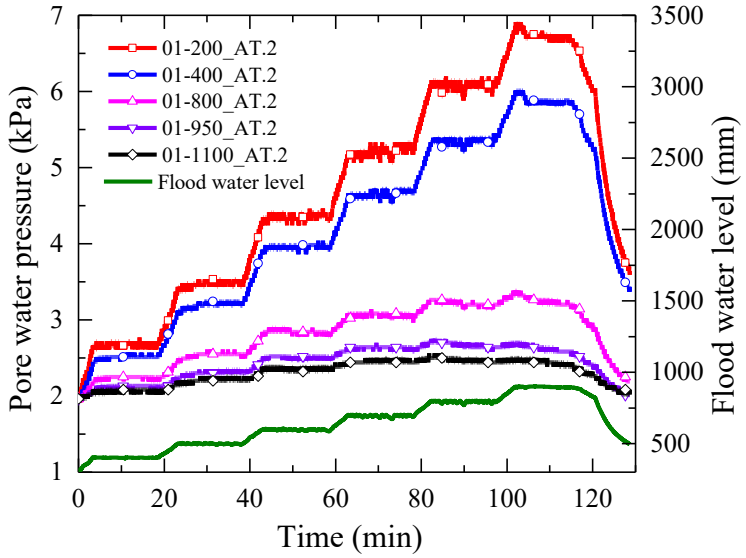

Figure 3.14 Time history of pore water pressure at foundation level in Case AT.2

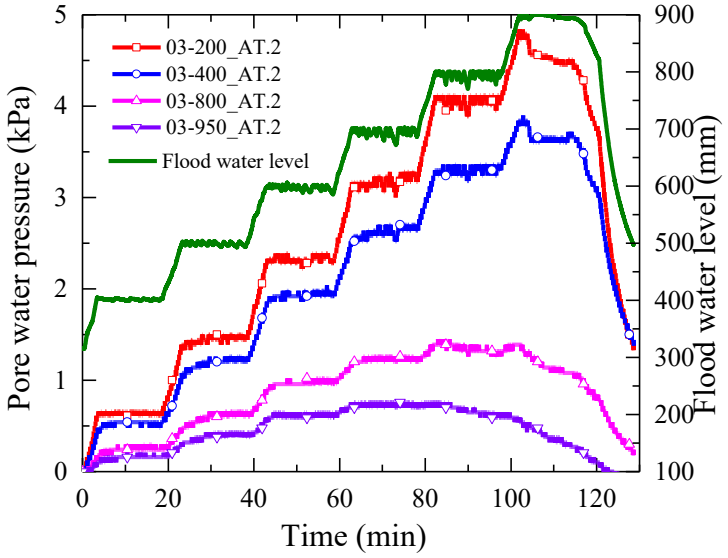

Figure 3.15 Time history of pore water pressure at top of foundation in Case AT.2

Figure 3.16 shows the slope surface at the beginning of the seepage flow and the final shape of deformed slope along with the outline of levee in Case AT.2. The dashed line in the figure is indicates the slip surface of model ground. Presence of the reinforcement limits the extension of the slip surface. At the crest of the slope, no significant settlement is observed is observed. Slip surface is also about 62 mm (70% reduction) deep from the

slope surface. The presence of pipe restrain the movement of slope forming the arch near the location of the pipe.

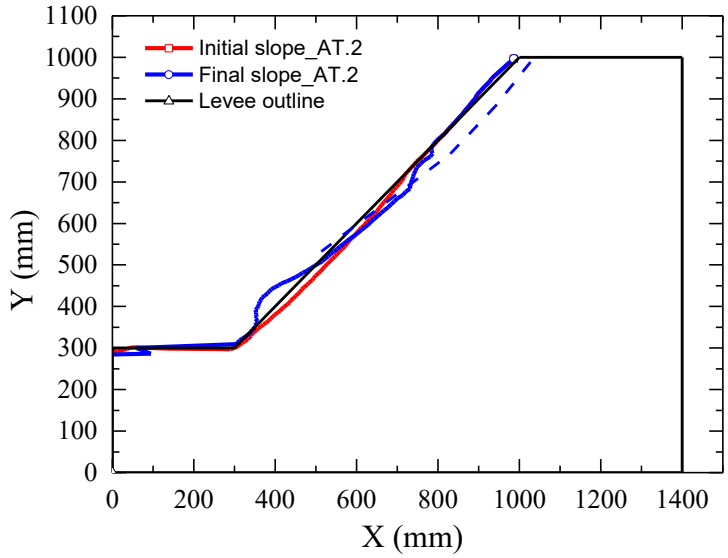

Figure 3.16 Change in slope surface with the seepage flow in Case AT.2

3.8.3 Case AT.3 (Reinforcement and drainage)

In Case AT.3, the model ground is provided with the five pipes which can function as both as reinforcement and drainage pipe. In this case, also water level is also raised in steps at an average rate of 20 mm per minute. In each step water level is raised by 100 mm and then the level is maintained for 30 minutes. In this case, water level is maintained for 30 minutes in which steady state was achieved. In this case, with the availability of the drainage function in pipe limits the rise in phreatic surface within the embankment. Also, with combined effect with the reinforcement, the deformation in Case AT.3 is completely prevented even at high flood water level.

Figure 3.17 shows the model ground before and after the experiment. As observed in the pictures, no deformation is observed in the model ground, which is due to the combined effect of the drainage and reinforcement.

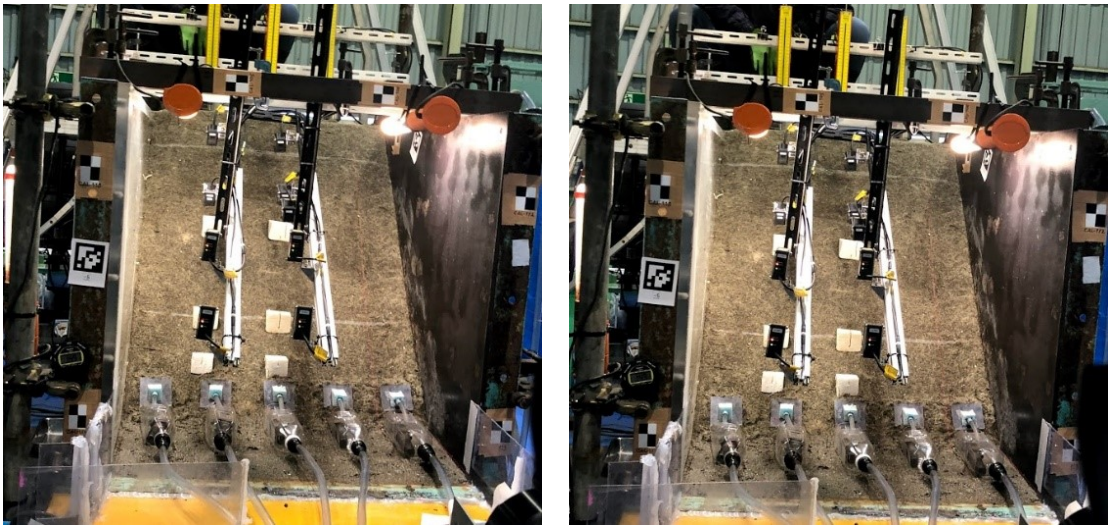

(a) Initial shape of model ground (b) Final shape of model ground

Figure 3.17 Model ground before and after the experiment in Case AT.3

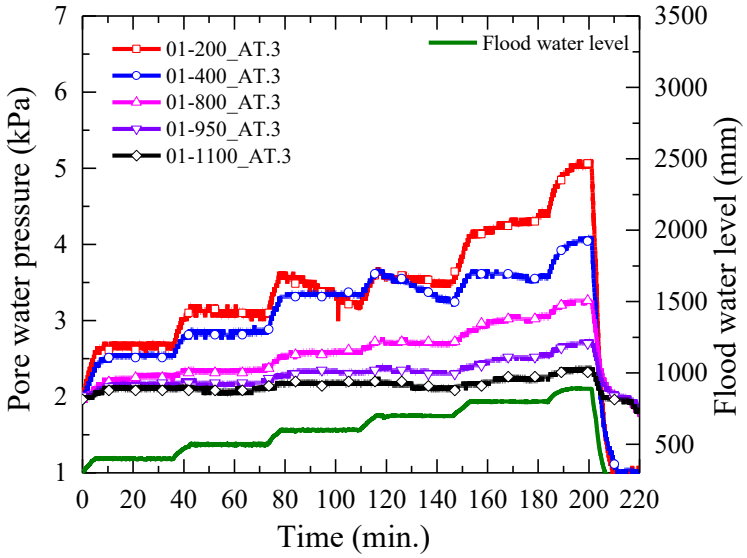

Figure 3.18 Time history of pore water pressure at foundation level in Case AT.3

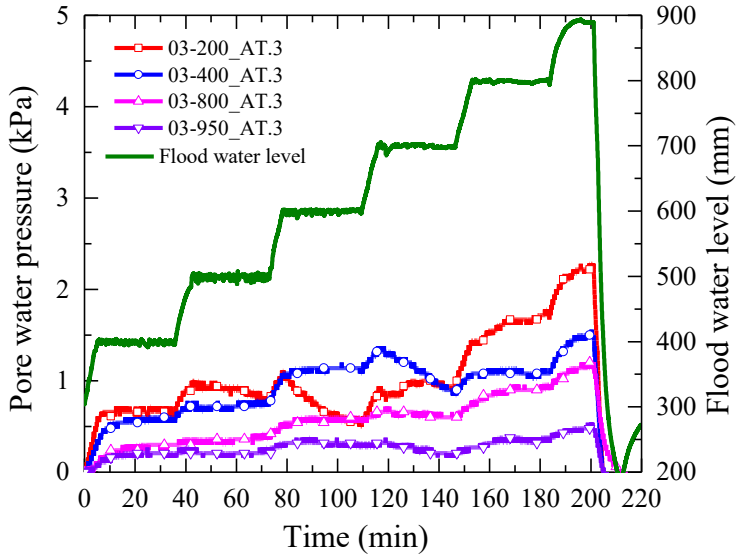

Figure 3.19 Time history of pore water pressure at top of foundation in Case AT.3

Figure 3.18 shows the time history of pore water pressure at different locations in the foundation level and **Fig.3.19** shows the same at the top of the foundation level for Case AT.3 along with the flood water level. In this case as well in each step, steady state of seepage flow is achieved indicated by the achievement of steady pore water pressure. In this case due to presence of the drainage pore water pressure is limited to lower value more significantly near the toe of the slope (see 03_800_AT.3, 03_950_AT.3). This lower pore water pressure development and also presence of additional reinforcement prevent deformation in Case AT.3. The value of the maximum pore water pressure developed in this case is reduced by 19% compared to the unreinforced case (Case AT.1)

3.9 Comparative performance among the cases

On comparing the performance of model ground in three cases, it can be observed that in unreinforced case, once the deformation starts, failure happens in quick progression and eventually cause complete collapse. In case where only reinforcement is provided, model ground is able to withstand the higher phreatic surface because of added reinforcing force mobilized through the pipe. In case where both drainage and reinforcement are provided deformation is completely prevented. **Figure 3.20** shows the change in the settlement at

the height of 0.7 m in mid-span of model ground with the rise of flood level in Cases AT.1 –AT.3. From the figure, it can be observed with the use of the pipe which can provide only reinforcement, the model ground can with stand the larger flood level compared to unreinforced case. In the case with both drainage and reinforcement provided in pipe (i.e., case AT.3) deformation is completely prevented.

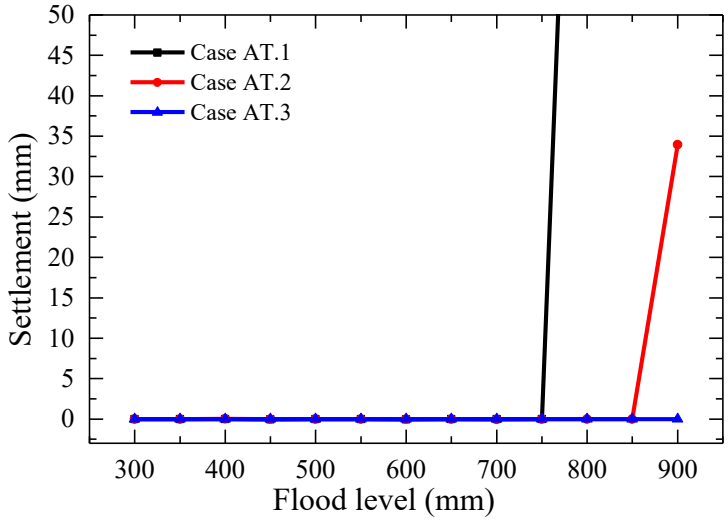

Figure 3.20 Change in settlement at height of 0.7 m in mid-span of model ground with rise of flood level

Figure 3.21 shows the change in horizontal displacement at the height of 0.5 m in mid-span of model ground with the rise of flood level in Cases AT.1 –AT.3. Here the positive value represents the movement of soil away from the slope and negative value represent caving or removal of soil mass from the target location of LDT. In Case AT.1, when the flood reaches 650 mm, there is a slight movement of soil away from the slope and then sudden slide, thus removing soil mass from the location. In Case AT.2 movement start much later when flood level is 750 mm, which continuously increases with an increase in the flood level. In Case AT.3, no significant deformation is observed.

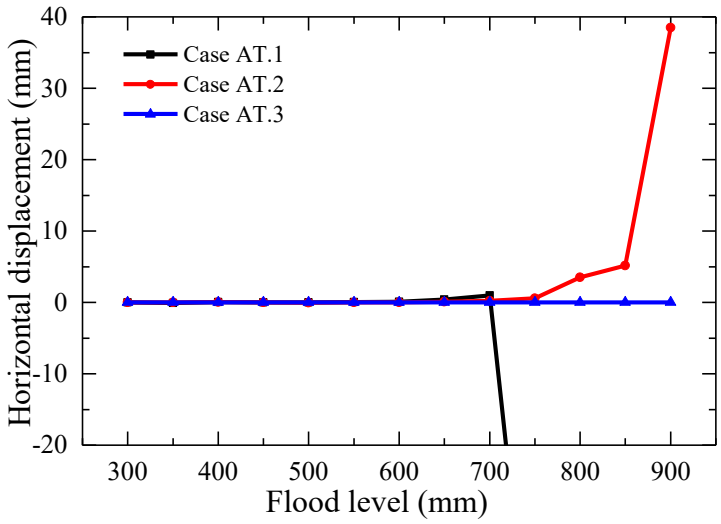

Figure 3.21 Change in horizontal displacement at height of 0.5 m in mid-span model ground with rise of flood.

3.10 Summary

In this chapter, the details of the single gravity experiment are discussed. The material properties, testing conditions, testing procedures, and observation made during the experiment are presented in detail. Details of different test condition and observation made in each case are presented, which gives the idea of the overall performance of the protection provided in the model ground. The observation from this chapter can be mobilised as following:

- In this series of the experiment, rising rate flood level is maintained equal through all test, making it possible for direct comparison among the cases.
- From the experiment result, it is observed that with the increase in flood head, large deformation is induced and eventually cause failure when no protection is provided. Protection, when provided in the form of reinforcement only, can delay the failure; making model ground able to withstand the larger flood level. Presence of pipe with both drainage and reinforcement can provide complete protection.

- The presence of only reinforcement reduced the depth of the slip surface by 70% compared to unreinforced case.
- The steel drainage pipe with the presence of the drainage and reinforcement reduced the maximum pore water pressure by 19% and deformation was completely prevented.

4 Numerical simulation of physical model tests

Numerical analysis was conducted using the finite element numerical programme developed by Prof. Akihiro Takahashi, 2016. Finite element deformation analysis was performed for comparative studies of the numerical analysis and physical modeling. The analysis was also conducted for the levees with reinforcement measures to evaluate the performance of the proposed reinforcing measure in improving the performance of the river levees when subjected to the seepage flow. In this chapter, validation of finite element model is performed by comparing the numerical result with the centrifuge test result.

4.1 Analysis conditions and assumption

Three-dimensional finite element deformation analysis was performed for a series of levees subjected to seepage flow with different reinforcement conditions. Both steady state and transient state calculations were made. Equations solved in the numerical analysis are described here.

Equilibrium equation for soil is expressed as

$$\frac{\partial \sigma_{ji}}{\partial x_j} + \bar{\rho} b_i = 0 \qquad [4.1]$$

where, density with soil, water, and air mixture $\bar{\rho}$ is given by

$$\bar{\rho} \equiv n S_r \rho_w + (1-n)\rho_s. \qquad [4.2]$$

Here, σ_{ij}= total stress, ρ_w= the density of water, ρ_s = soil particle density, n = porosity, S_r = degree of saturation.

Governing equation for pore water is expressed as

$$S_r \dot{\varepsilon}_{jj} + C\dot{h}_p + \frac{\partial}{\partial x_i}\left(-k_{wu}\frac{\partial h}{\partial x_i}\right) = 0. \quad [4.3]$$

In Equation [3] C is referred as specific moisture capacity from moisture characteristic curve (corresponds to the slope of relationship between pressure head with volumetric water content). In the equation, h and h_p represent the total head and pressure head respectively. k_{wu} is unsaturated hydraulic conductivity.

In the computation Drucker-Prager model (Drucker and Prager, 1952) is used for the yield surface, which is as shown in Equation [4.4]

$$f = \alpha I_1 + \sqrt{J_2} - k = -3\alpha p + \bar{s} - k = 0 \quad [4.4]$$

This is termed as the Drucker-Prager model. For α and k, it can be determined from the comparison with the failure criterion (yield criterion) of the Mohr-Coulomb.

$$I_1 = \sigma_{ij} = \sigma_{11} + \sigma_{22} + \sigma_{33} = \sigma_1 + \sigma_2 + \sigma_3 \quad [4.5]$$

$$\bar{s} = \sqrt{J_2} = \sqrt{\frac{1}{6}\{(\sigma_1 - \sigma_2)^2 + (\sigma_2 - \sigma_3)^2 + (\sigma_3 - \sigma_1)^2\}} \quad [4.6]$$

where $\sigma_1, \sigma_2, \sigma_3$ are the principal stresses.

When the yield surface of Drucker-Prager is inscribed in the failure criterion of Mohr-Coulomb, we get,

$$\alpha = \frac{\sin\phi}{\sqrt{3(3+sin^2\phi)}} \quad k = \frac{\sqrt{3}c\cos\phi}{\sqrt{3(3+sin^2\phi)}} \quad (If\ inscribed) \quad [4.7]$$

Effective stress $\sigma_{ij}^{'}$, is modeled as proposed by (Bishop, 1960) shown in Equation [1.2]. van Genuchten model (Van Genuchten, 1980) was used for modeling soil moisture characteristic curve (SWCC) of the unsaturated soil. The relation proposed by van Genuchten as represented in Equation [1.4] shows the relationship between effective saturation and pressure head ψ.

The permeability of unsaturated soil, unlike saturated soil, is not the constant value; it varies with the change in the degree of the saturation. This variation of the hydraulic conductivity in the numerical analysis is modeled based on the relation proposed by Kosugi, (Kosugi, 1999), which is shown in Equation [1.6]. The properties of the soil used in numerical analysis are presented in **Table 4-1.**

Table 4-1 Properties of soil from numerical analysis

Properties	Values
Soil particle density (Mg/m^3)	2.72
Average initial water content of model ground	14.7%
Angle of shearing resistance [Degree of compaction Dc= 80%] (degrees)	29
Cohesion [Dc= 80 %](kN/m^2)	2.5
Saturated hydraulic conductivity (m/s)	
Foundation	1.5E-6
Embankment	4.5E-5
SWCC parameters for van Genuchten model	
Saturated volumetric water content θ_s	0.467
Fitting parameters n	1.674
Fitting parameters α	9.223
Fitting parameters m	0.403
Dry density of embankment (Mg/m^3)	1.45
Dry density of foundation (Mg/m^3)	1.72
Modulus of Elasticity (N/m2)	2.55E5

4.2 Geometry and boundary condition

4.2.1 Modeling of the river levee

River levees in the analysis are modeled as in centrifuge experiment condition. Only a section of prototype river levee on the protected side is modeled as in a centrifuge test with the boundary condition similar to experiment condition. The foundation bottom was modeled as an impermeable layer and fixed rigid connection (displacement and rotation were constrained to zero). The sides of the foundation on the protected side are modeled as impervious surface, and all other boundary was considered permeable for the analysis.

As for the displacement constraint, vertical side boundaries were constrained in horizontal displacement direction to the value zero. The boundary condition and the geometry with mesh used in the analysis are shown in **Fig. 4.1**. The mesh has the 8 nodes element. The uniform size of mesh is used in the analysis. The uniform size of the mesh is used in the analysis as far as possible. In the mesh, the number of nodes and elements are 3393 and 2688 respectively.

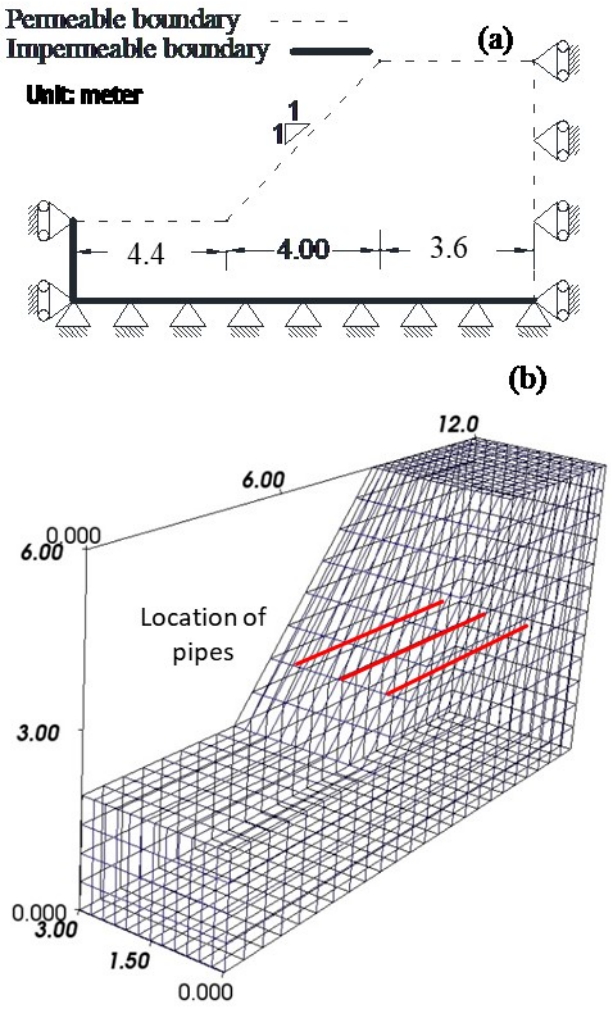

Figure 4.1 Finite element analysis condition (a) Boundary condition for analysis (b) Mesh for model ground

4.2.2 Modeling of steel drainage pipe

The proposed steel drainage pipe is 6 meters long, with two different sections. These two sections are; 1m long section having the spiral ring made of 1 cm thick metal plate having a pitch of 16 cm at the end and 5-meter long section without a spiral ring. For the numerical analysis, the spiral ring is not considered. The dimension and properties of the steel drainage pipe used in the analysis are listed in **Table 4-2**. The drainage function is modelled as the line of the nodes with a pressure head ceiling of the elevation of the nodes. Reinforcement function in the slope is modelled by adding the series of the elastic member, beam elements at the location of the drain pipe. The spiral blade section of steel drainage pipe is not considered in the analysis. The steel pipes is modelled as the rod element, each beam connection is modelled as two node element and calculation is made in each node. Pipes with only either of one function is also modelled using drainage or reinforcement function only.

Table 4-2 Properties of steel drainage pipe for analysis

Parameters	Values
Internal diameter (mm)	60
External diameter (mm)	80
Length (m)	6
Young's Modulus, E (N/m^2)	2.10E+11
Poisson's ratio, v	0.3

4.3 Flood conditions

Test conditions are kept similar to the experiment condition. So, six different cases with varying degree of reinforcement (ref. **Table 1-3**) with the same material properties as in experiment is analyzed. Each analysis is divided into two phases. In the first step, a steady state is achieved by giving input of water table at the top of the foundation. Hydrostatic condition after the end of the steady state calculation is considered as the initial condition

for the second state, which simulates the saturation of foundation conducted during the test before flooding. Seepage flow is simulated in the second step of the analysis, which is a transient analysis. In this step, the flood is simulated by increasing the water level on the right side of the model to the assumed flood elevation. During this step, the result of the analysis can be monitored at any time step considered. For flood, simulation water is raised numerous steps to achieve the flooding condition similar to that of the experiment.

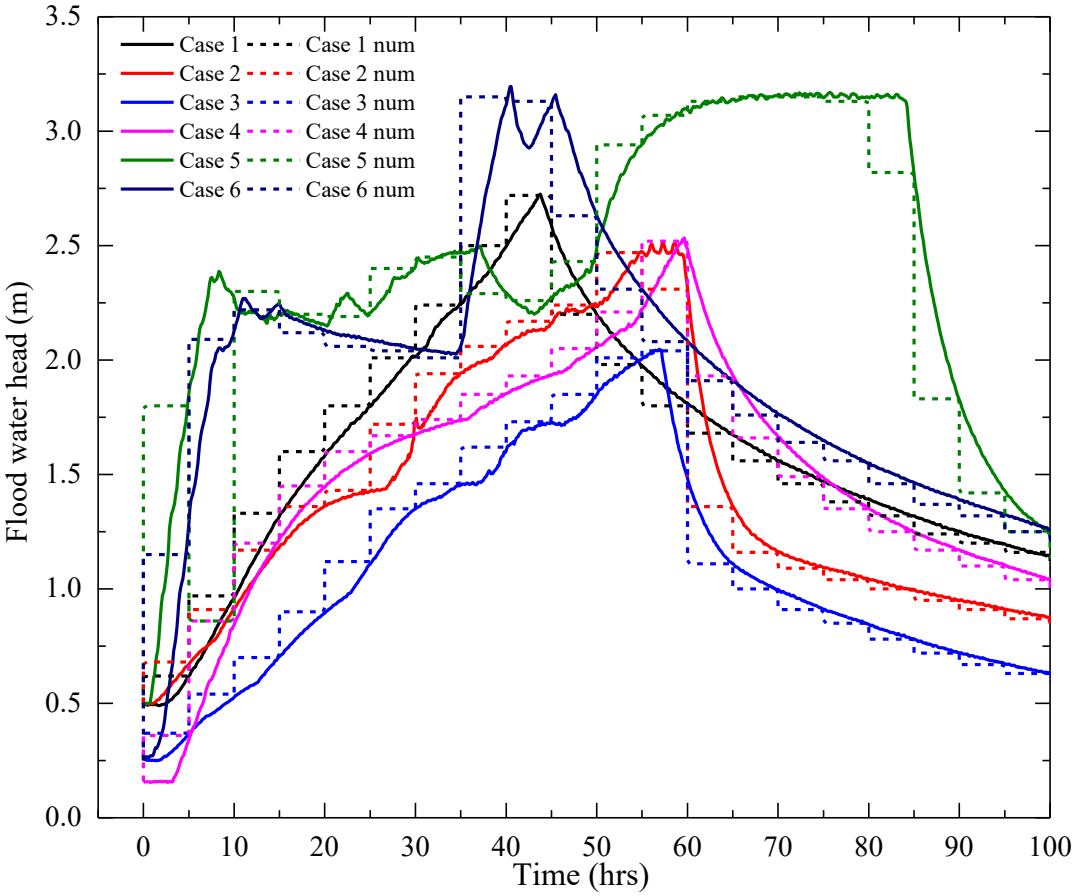

Figure 4.2 Comparison of time history of flood water head in the experiment and numerical

Figure 4.2 shows the flooding condition both in the centrifuge experiment and in the finite element numerical analysis. The solid line and broken line in the figure represent flood head time history in centrifuge experiment and numerical analysis, respectively. In the numerical analysis, the flood is modeled in a stepwise manner. Each step was 5 hours long. The rise of the flood water level in the multiple steps allowed to achieve similar condition as in the experiment thus making it possible to compare the results of numerical analysis with the experiment result in more fair condition.

4.4 Results and discussions

4.4.1 Comparison with centrifuge result

The hydraulic behavior in the centrifuge test is captured through pore water pressure record at different locations such as A, B, C, D and E as shown in **Fig.4.3** The force developed in pipe is measured through the sensors on the pipe.

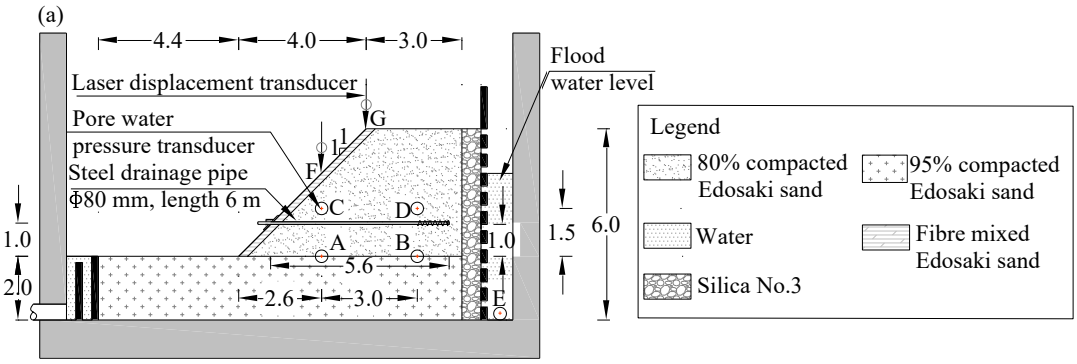

Figure 4.3 Location of sensors in centrifuge test

Figure 4.4 shows the comparison for the time history of pore water pressure recorded at two different locations; at A (below slope) and at B (below crest) in experiment and numerical analysis for Case 1, 2, 4 and 6 respectively. Here only these four cases are shown as they represent the different types of the protection provided in the levee. The results for the comparison for remaining other cases are also comparable to these results. In the figure, it can be observed that the trend of rising and fall of pore water pressure with increase and decrease flood head is captured by the numerical analysis. The magnitude is not exactly similar to the experiment result; however, from the results, it can be observed that the effect of drainage and the consequent change in pore water pressure is predicted by numerical analysis (as in Case 2 and 6). The comparison here shows that the numerical analysis in both cases of absence of drainage (Case 1 and Case 4) and in presence of drainage (Case 2 and Case 6) can fairly predict the development of the pore water pressure in the levee.

Figure 4.5 shows the comparison of the axial force observed near the slope in the experiment and numerical analysis in Cases 3 and 4 along with flood water head used in numerical simultion. Axial forces measurement from the experiment are available only for these two cases. Axial force here in both experiment and numerical analysis is shown by considering the axial force at the start of the seepage flow as zero. Thus, axial force represent as increase and decrease of the tensile force. Axial force predicted in both the cases is similar in the trend and magnitude. The change in the axial force with the seepage flow is well captured by numerical analysis in the both cases when drainage is present (i.e. Case 3) and when drainage is not present (i.e. Case 4).

Figure 4.6 shows the comparison of the time history of settlement at location F for Cases 1 and 6. In Cases 2 and 5 no significant deformation were recorded in the experiment. In the Case 3 the initial erosion near toe during the spinning of the centrifuge is observed and in Case 6, erosion of soil around the pipe is observed which could not be modelled in the present numerical analysis, hence no comparison is shown for these cases. From the figure it can be observed that the trend of the increase of settlement and also point of initiation of failure indicated by sharp change in value of settlement is well predicted by the numerical programme.

Thus, the numerical programme used in the study can simulate the flood-induced seepage in river levee and also the effect of the drainage and reinforcement with considerable reliability. Hence, the finite element programme is used in parametric studies and make the comparative study of the steel drainage pipes later in this study.

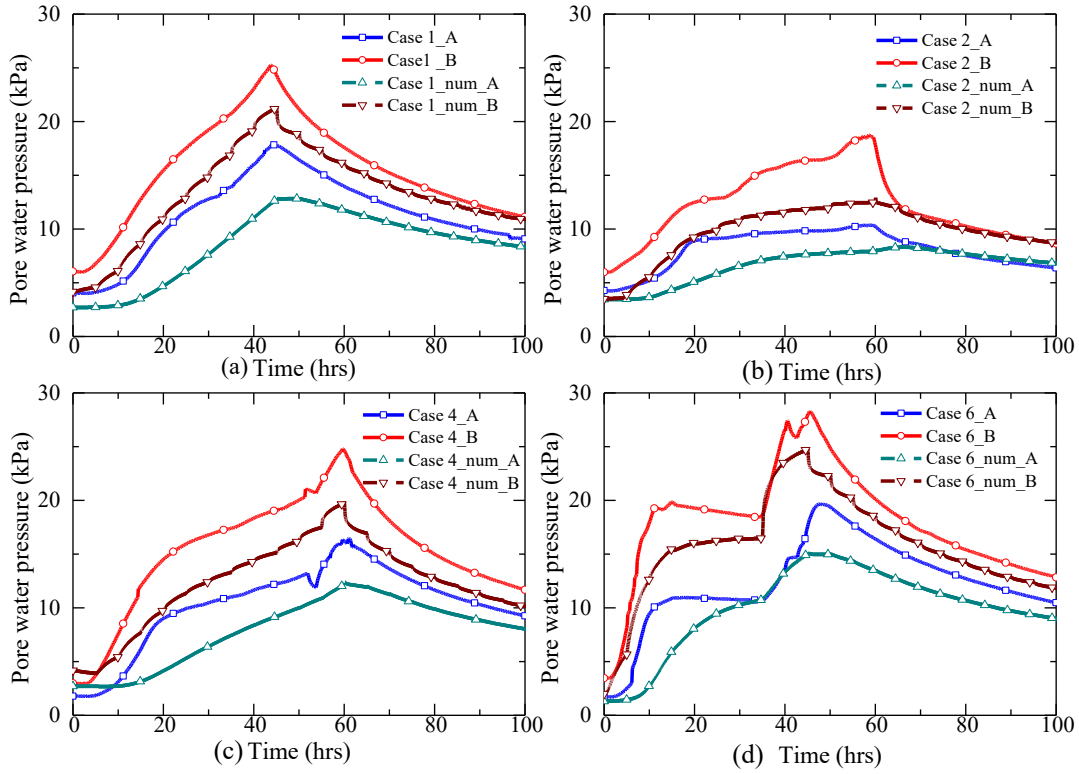

Figure 4.4 Comparison of time history of pore water pressure at location A and B in (a) Case 1 (b) Case 2 (c) Case 4 and (d) Case 6

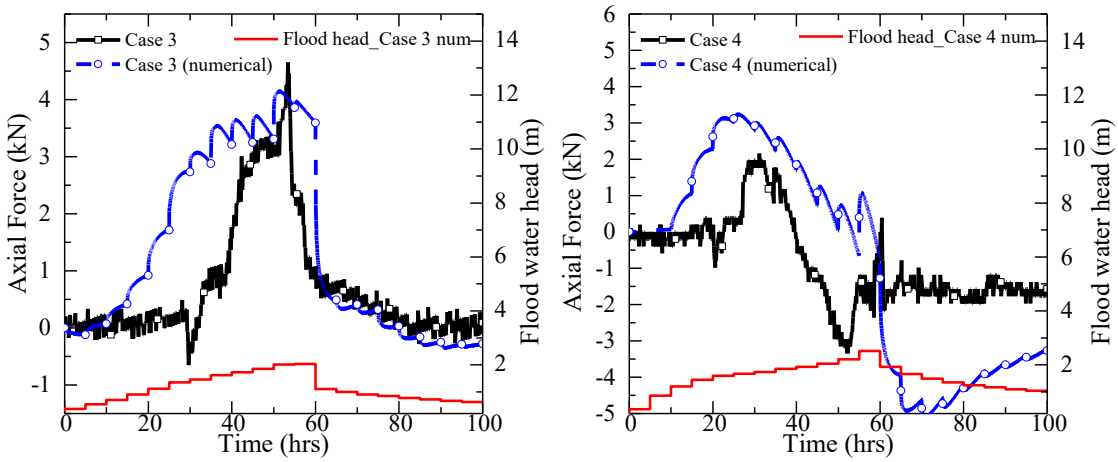

Figure 4.5 Comparison of the time history of axial force near the slope surface (a) for Case 3 (b) for Case 4

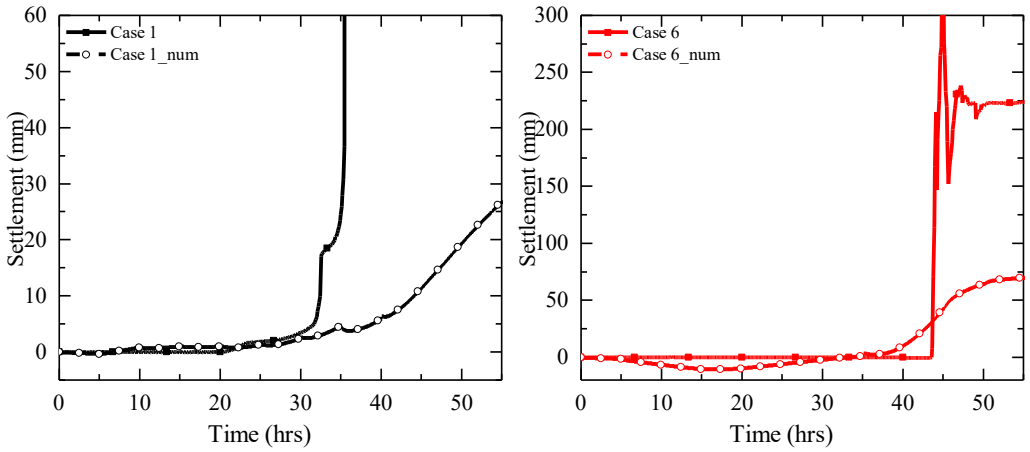

Figure 4.6 Comparison of the time history of settlement at location F (a) Case 1 (b) Case 6

4.4.2 Hydraulic behaviour

Hydraulic behavior in different cases here is evaluated on the basis of the pressure head developed inside the levee structure. Higher pressure head indicates the higher position of the water level (phreatic surface) inside the levee. The lower pressure head is desired inside the levee allowing the soil to remain in unsaturated condition so that loss of the soil shear strength is minimum.

- **Case 1**

Distribution of the pore water pressure at the mid-section of levee after 20, 40, 60, 80 and 100hrs of seepage flow in Case 1 is shown in **fig.4.7**. In the Case 1 flood water level is increased from 0 to 44hrs (ref: **fig**.**4.2**), during this phase increase in water level within the levee body could be observed. As there is no drainage in this case larger area develops the positive pore water pressure. From the distribution of pore water pressure in the levee, it can be observed that phreatic surface is very near levee slope surface.

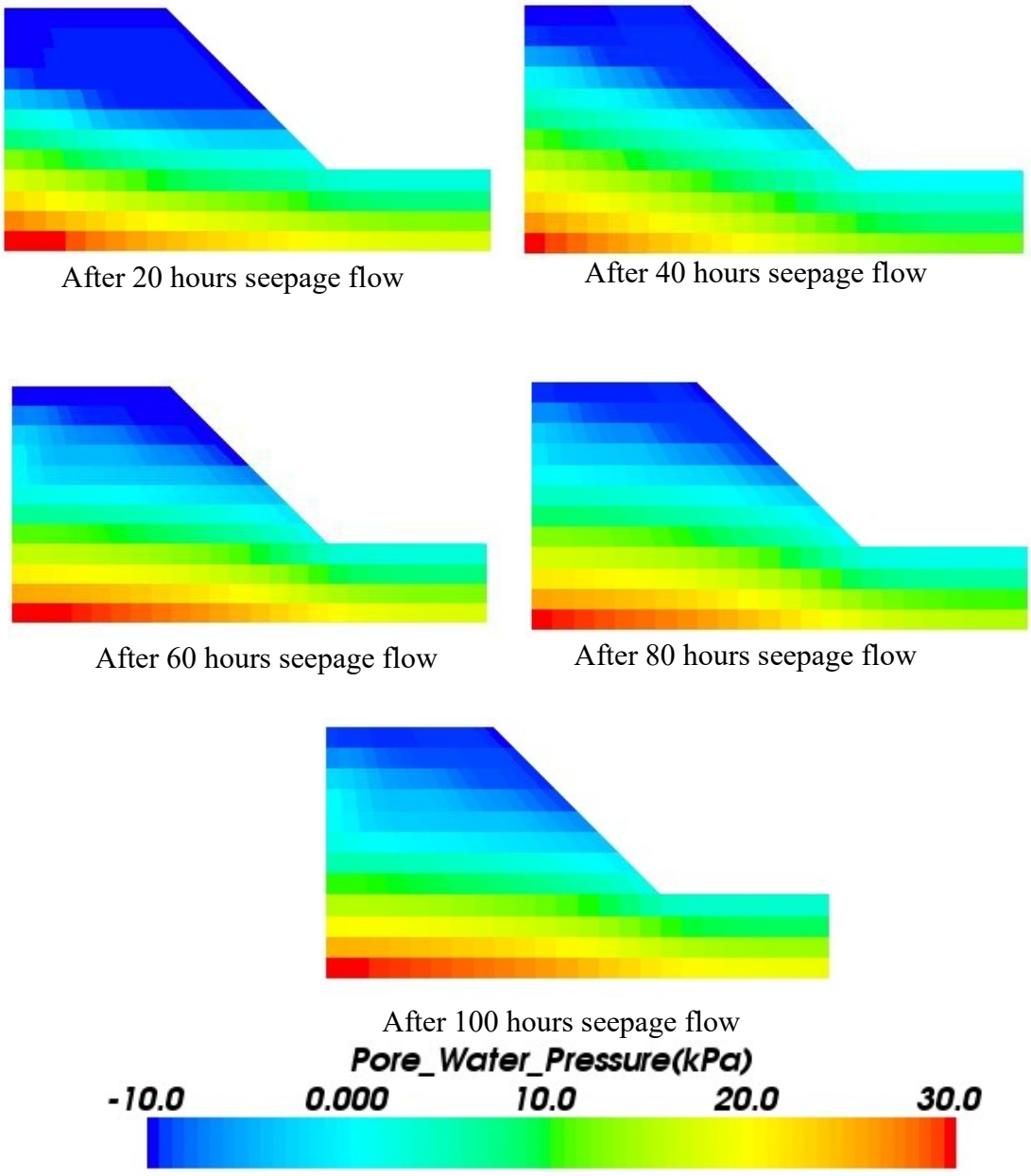

Figure 4.7 Distribution of the pore water pressure at mid-section of levee for Case 1 at different stages of seepage flow

- **Case 2**

Distribution of the pore water pressure at the mid-section of levee after 20, 40, 60, 80 and 100hrs of seepage flow in Case 2 with location of pipe is shown in **Fig**.**4.8**. In the Case 2 flood water level is increased from 0 to 60 hrs (ref: **Fig.4.2**). As there is drainage in this case development of the positive pressure inside the levee body is limited.

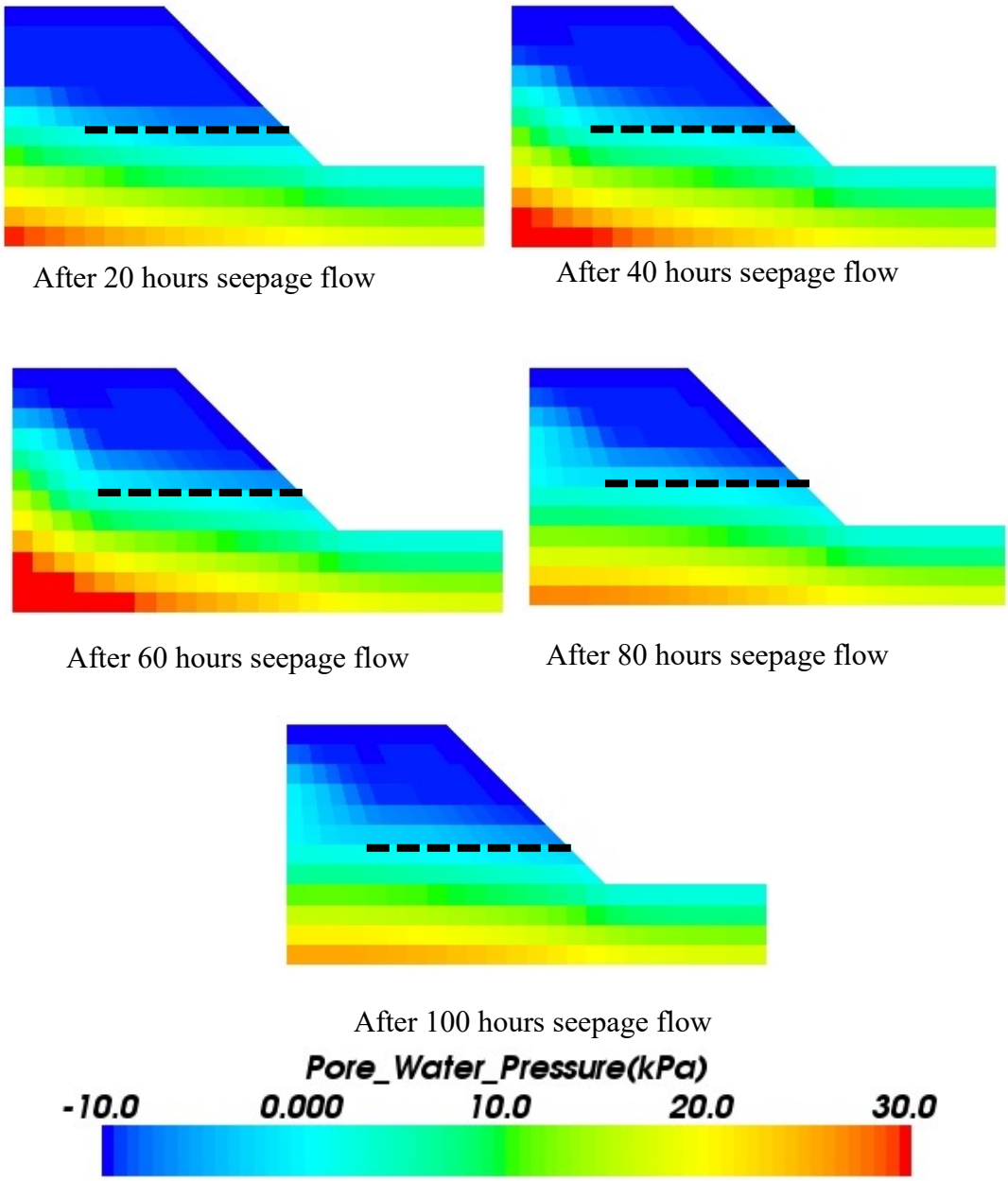

Figure 4.8 Distribution of the pore water pressure at mid-section of levee for Case 2 at different stages of seepage flow

From the figures of the distribution of pore water pressure in the section after 20hrs, 40hrs and 60 hrs of the seepage flow, it can be observed that water level near the slope remains lower as indicated by the presence of negative pore water pressure. Here, drainage is effective in minimizing the rise of the water level especially near the slope thus contributing to minimization of the loss of the shear strength of the soil. Also, with the installation of the drainage, flow path inside the levee is changed, flow is directed towards the location of the drainage pipe thus retaining phreatic surface well below the slope.

Gradient of the flow path is also lowered due to presence of the pipe at lower depth (1m above the foundation).

- **Case 3**

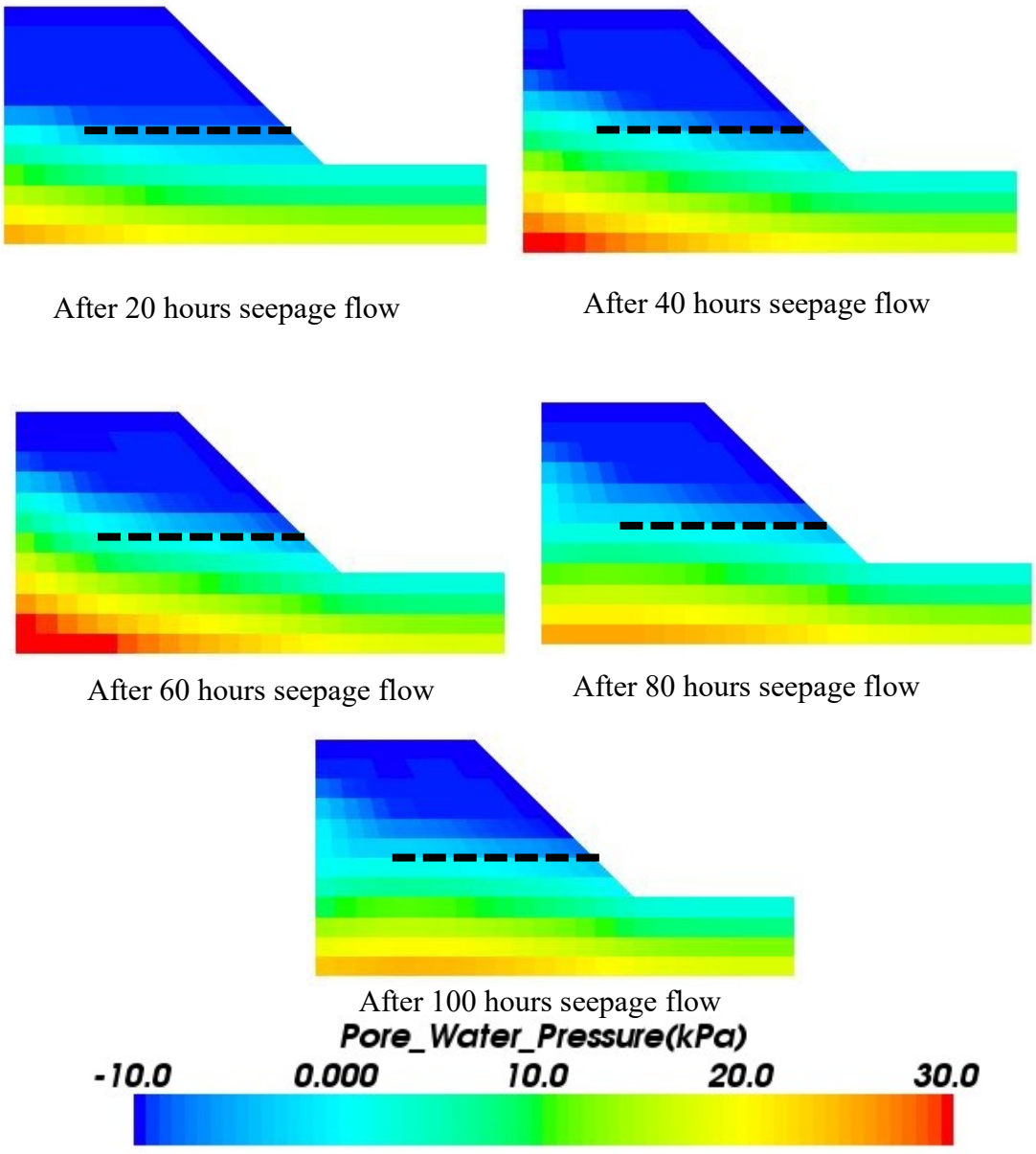

Figure 4.9 Distribution of the pore water pressure at mid-section of levee for Case 3 at different stages of seepage flow

Distribution of the pore water pressure at the mid-section of levee after 20, 40, 60, 80 and 100hrs of seepage flow in Case 3 with location of pipe is shown in **Fig.4.9**. In the Case 3 flood water level is increased from 0 to 60 hrs (ref: **Fig.4.2**). As there is drainage in this

case development of the positive pressure inside the levee body is limited. Drainage performance is very similar to the Case 2 even though the drainage is in only two pipes.

- **Case 4**

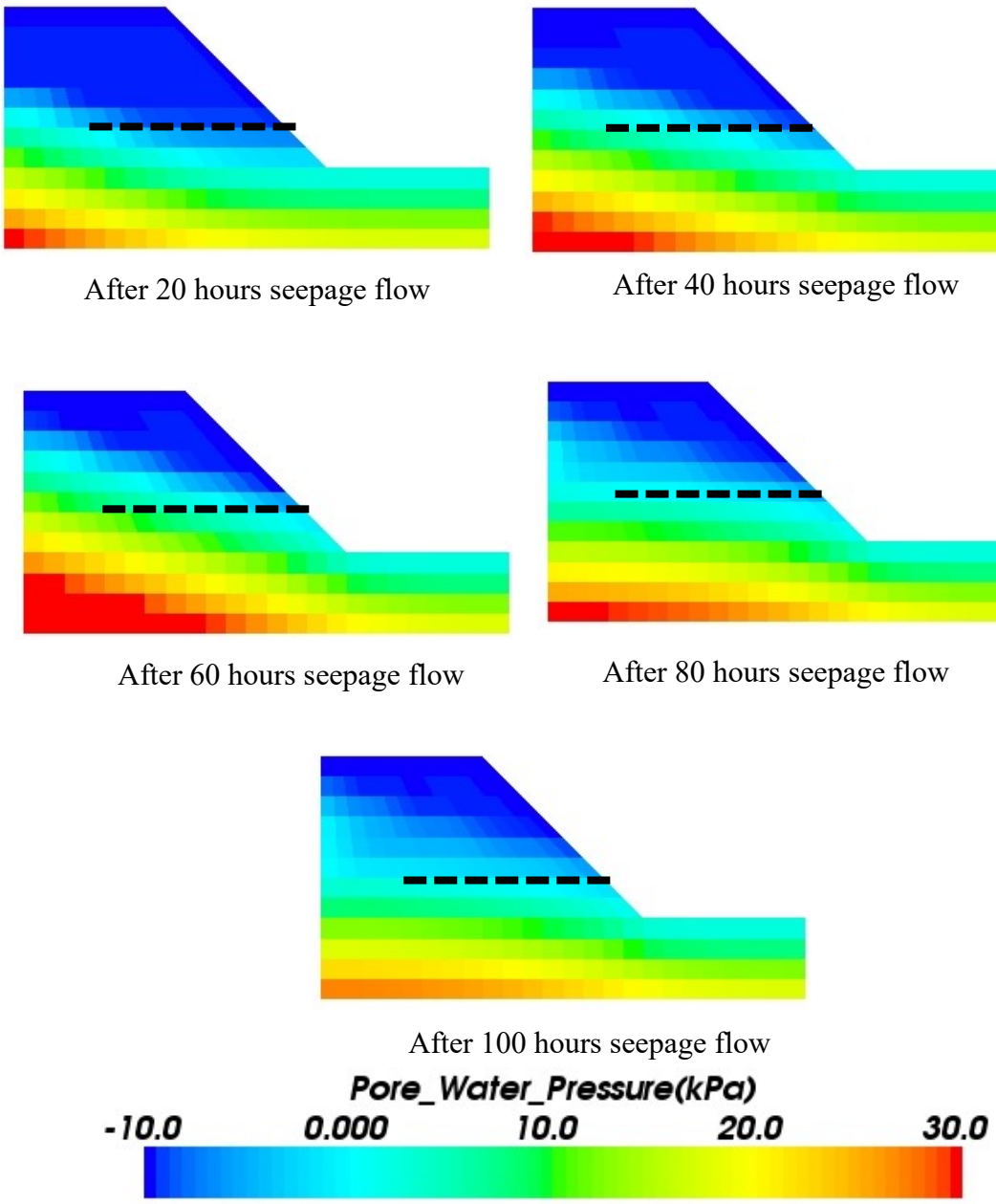

Figure 4.10 Distribution of the pore water pressure at mid-section of levee for Case 4 at different stages of seepage flow

Distribution of the pore water pressure at the mid-section of levee after 20, 40, 60, 80 and 100hrs of seepage flow in Case 4 is shown in with location of pipe **Fig.4.1.** In the Case 4

flood water level is increased from 0 to 60 hrs (ref: **Fig.4.2**). In this case there is no drainage provided hence the performance is similar to the Case 1.

- **Case 5**

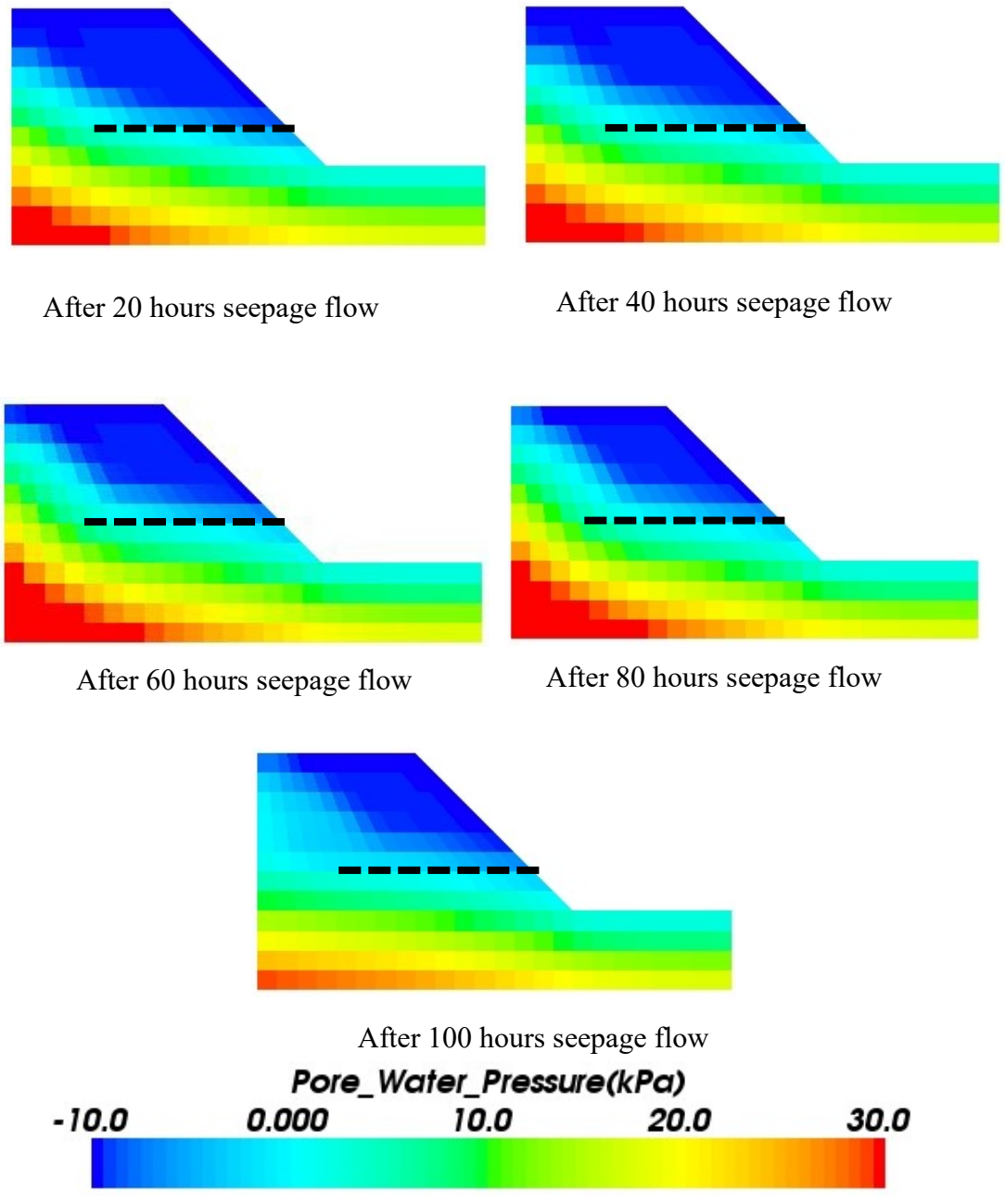

Figure 4.11 Distribution of the pore water pressure at mid-section of levee for Case 5 at different stages of seepage flow

Distribution of the pore water pressure at the mid-section of levee after 20, 40, 60, 80 and 100hrs of seepage flow in Case 5 with location of pipe is shown in **Fig.4.11**. In the Case 5 flood water level is increased from 0 to 80 hrs (ref: **Fig.4.2**). As there is drainage in this case development of the positive pressure inside the levee body is limited. In Case 5 even though number of the drainage pipes used is limited to 2 nos., similar to Case 3 the drainage performance is different from Case 3. In this case rate of the rising the flood water is much larger compared to other cases, hence different drainage performance is observed from the Case 3 which also had two drainage pipe. Here, larger area of the levee develops the positive pressure.

- **Case 6**

Distribution of the pore water pressure at the mid-section of levee after 20, 40, 60, 80 and 100hrs of seepage flow in Case 6 is with location of pipe shown in **Fig.4.12**. In the Case 6 flood water level is increased from 0 to 45 hrs (ref: **Fig.4.2**) with the rate of rising flood water similar to the Case 5.

Three numbers of the drainage pipes are used in Case 6 similar to Case 2. Since the rate of rising of the flood water head and flood water head at any instant is greater than Case 2, drainage behavior is notably different. Here, the drainage pipes capacity seems to be insufficient which cause the development of the positive pore water pressure (>0) in much larger area. The distribution of pore water pressure inside the levee body appears to be very similar to case without any drainage (i.e. Case 1) clearly indicating insufficient drainage of the seepage water from the levee body.

In the centrifuge experiment failure pattern for the Case 6 was very similar to the unreinforced case (Case 1) which could be because of this very similar distribution of the pore water pressure observed in both cases.

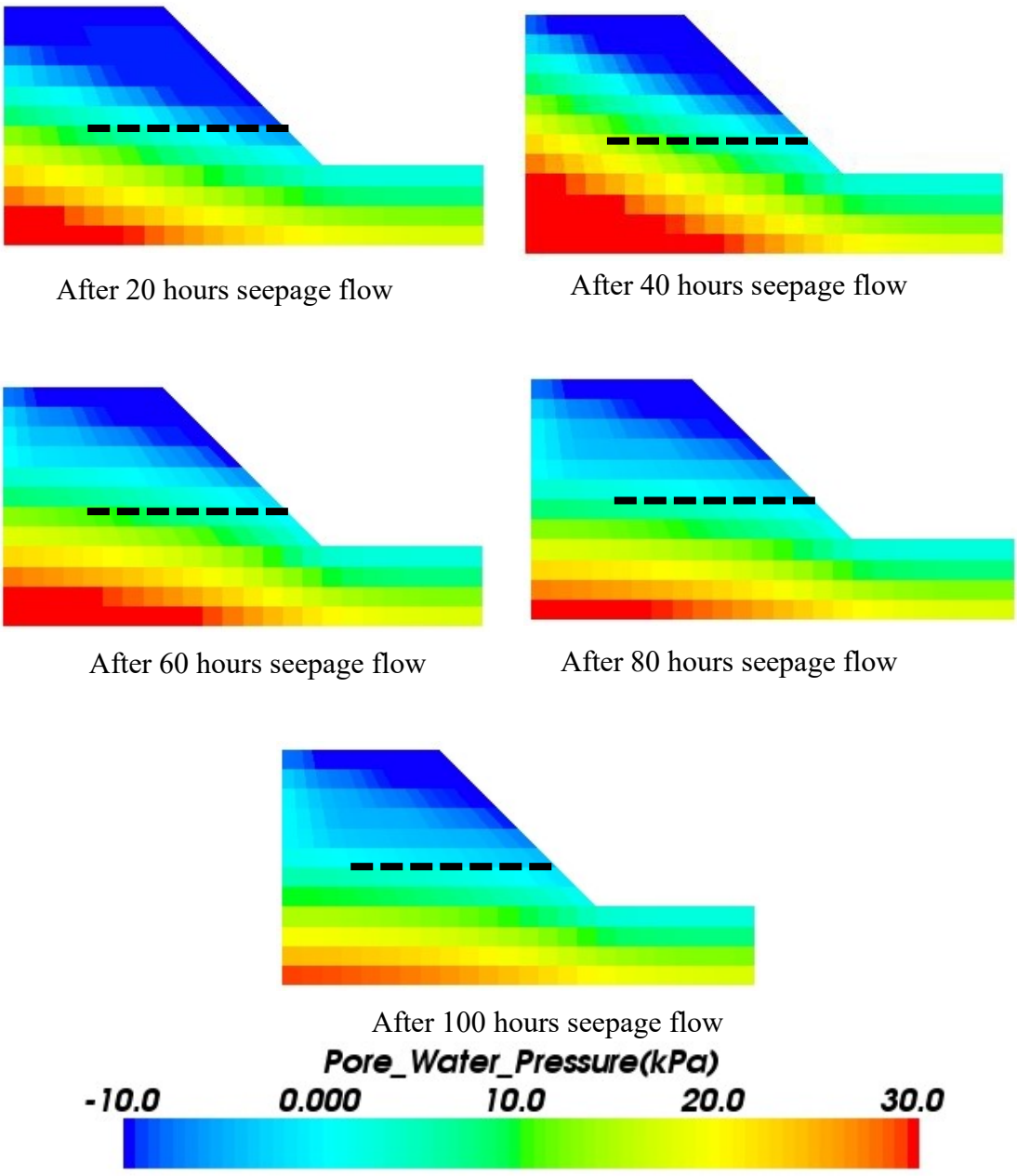

Figure 4.12 Distribution of the pore water pressure at mid-section of levee for Case 6 at different stages of seepage flow

4.4.3 Strain distribution

Deformation behavior in different cases here is evaluated on the basis of the deviatoric strain developed inside the levee structure. Higher values indicates the larger deformation inside the levee. In the case with the steel drainage pipe, it is expected that deformation in levee is minimized with the combined effect of the drainage and reinforcement.

- **Case 1**

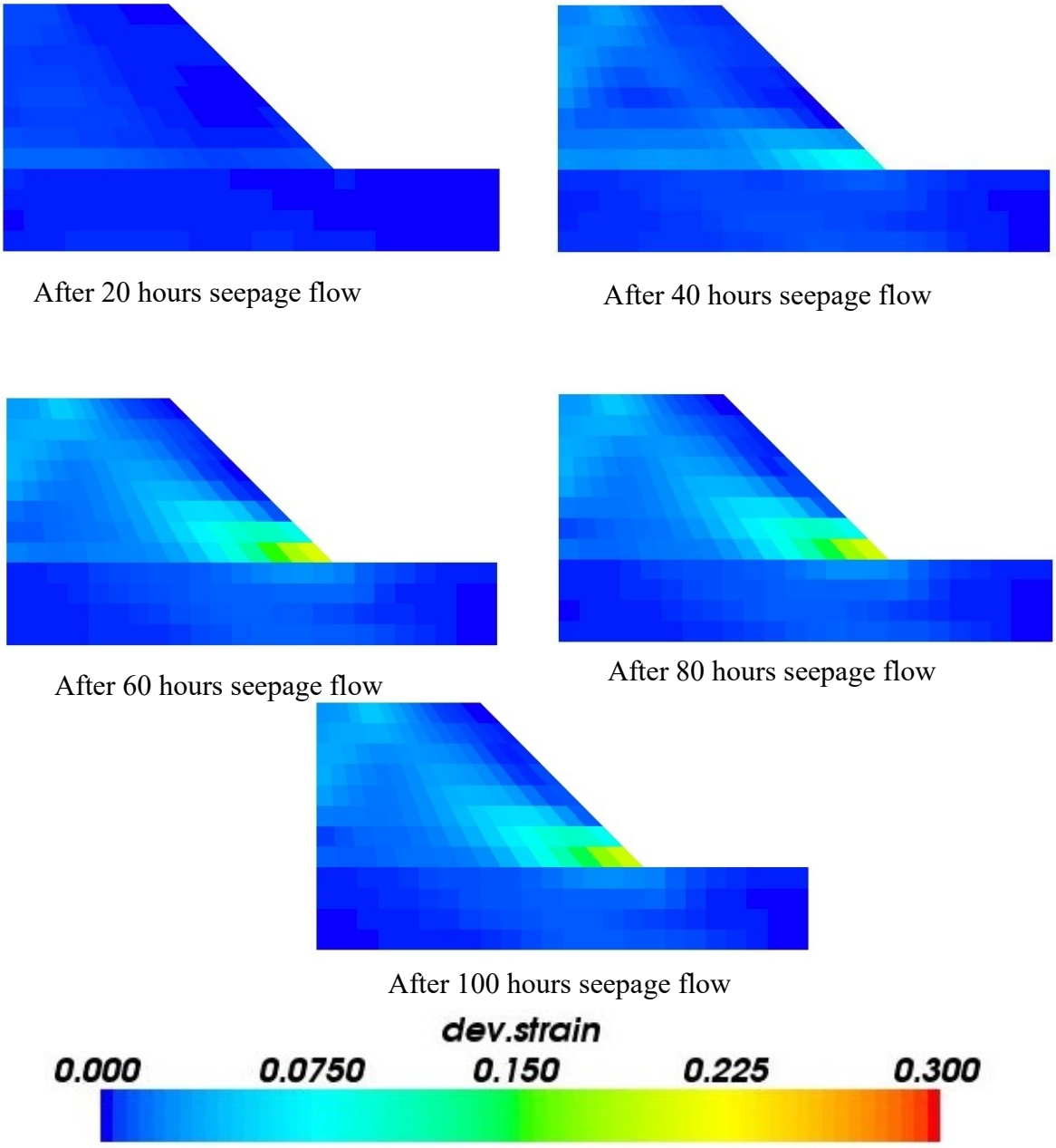

Figure 4.13 Distribution of the deviatoric strain at mid-section of levee for Case 1 at different stages of seepage flow

Figure 4.13 shows the distribution of the deviatoric strain at mid-section of the levee for Case 1 at different stages of the seepage flow. In the figure it can be observed that with increase in seepage flow duration, larger deviatoric strain is developed near the toe of the slope and subsequently towards the upper portion of slope. This behavior similar to that observed in the centrifuge experiment.

- **Case 2**

Figure 4.14 shows the distribution of the deviatoric strain at mid-section of the levee with location of pipe for Case 2 at different stages of the seepage flow. In the figure it can be observed that with increase in seepage flow duration, change in the distribution of the deviatoric strain is not very significant indicating no large deformation occurred in levee.

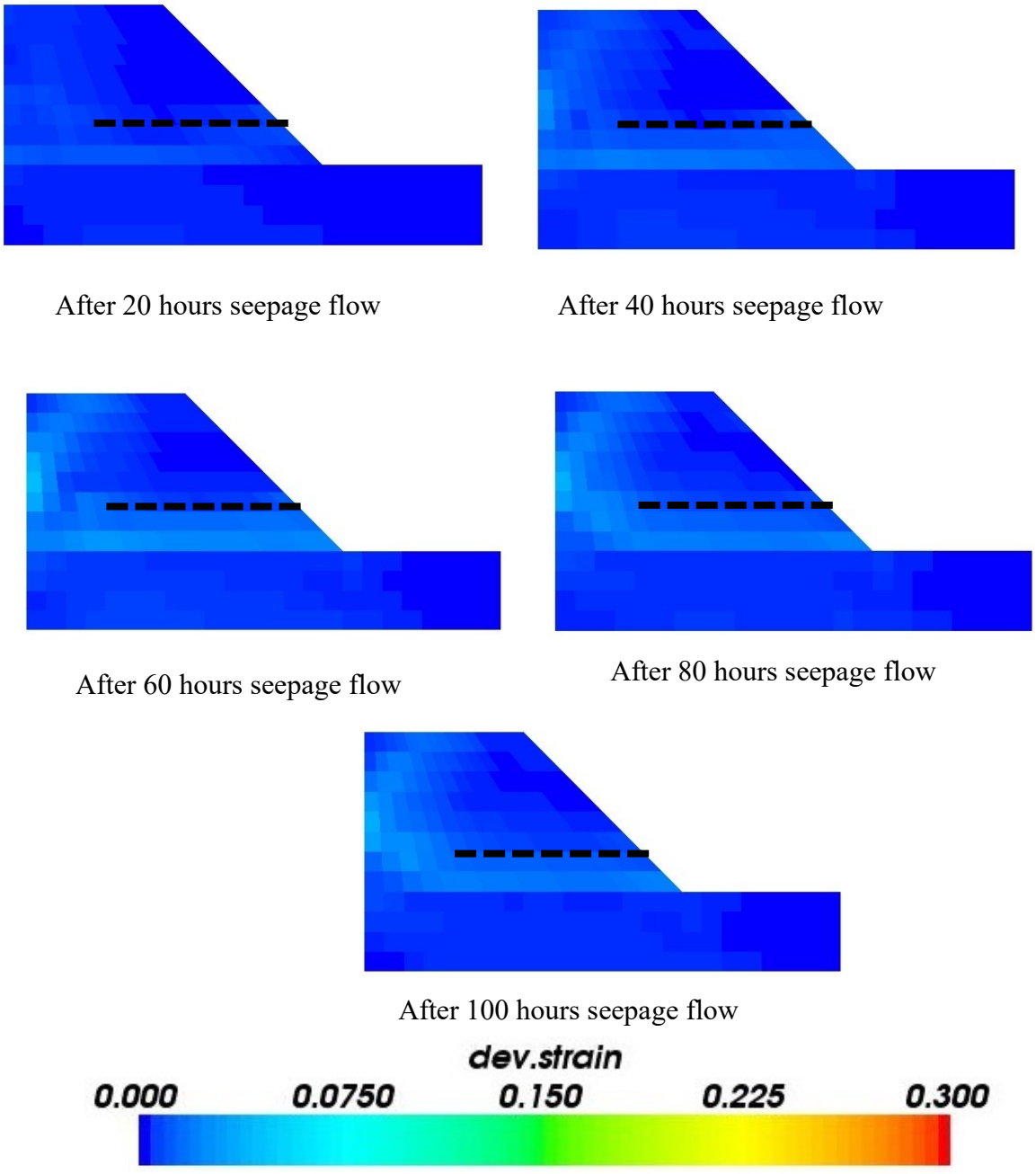

Figure 4.14 Distribution of the deviatoric strain at mid-section of levee for Case 2 at different stages of seepage flow

- **Case 3**

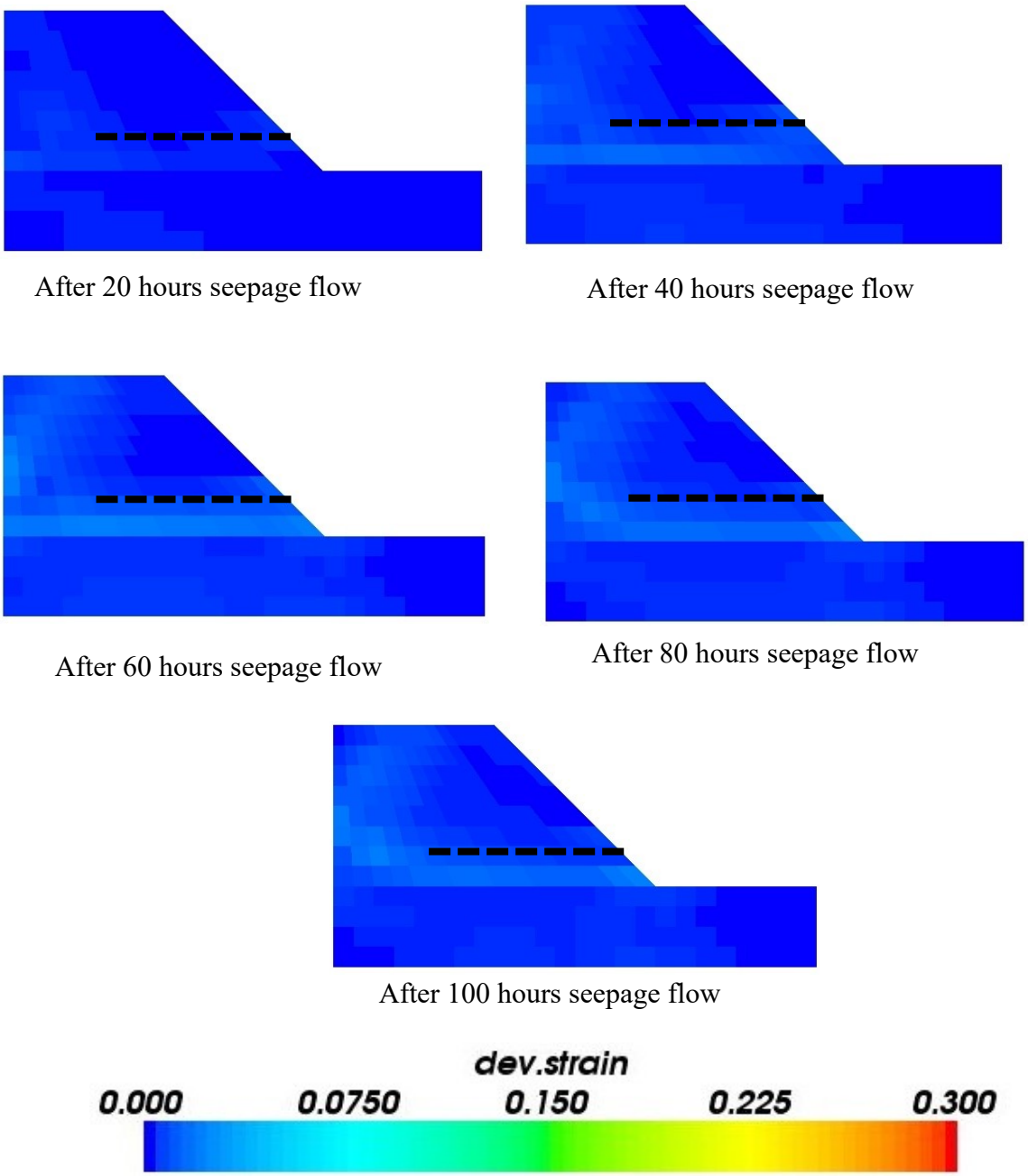

Figure 4.15 Distribution of the deviatoric strain at mid-section of levee for Case 3 at different stages of seepage flow

Figure 4.15 shows the distribution of the deviatoric strain at mid-section of the levee with location of pipe for Case 3 at different stages of the seepage flow. In the figure it can be observed that with increase in seepage flow duration, change in the distribution of the deviatoric strain is not very significant indicating no large deformation occurred in levee similar to Case 2.

- **Case 4**

Figure 4.16 shows distribution of deviatoric strain at mid-section of the levee with location of pipe for Case 4 at different stages of the seepage flow. In this case as there is no drainage provided, with the increase in seepage flow duration increase in deviatoric strain can be observed in levee body. The relatively larger strain values are observed near the toe of the slope of levee.

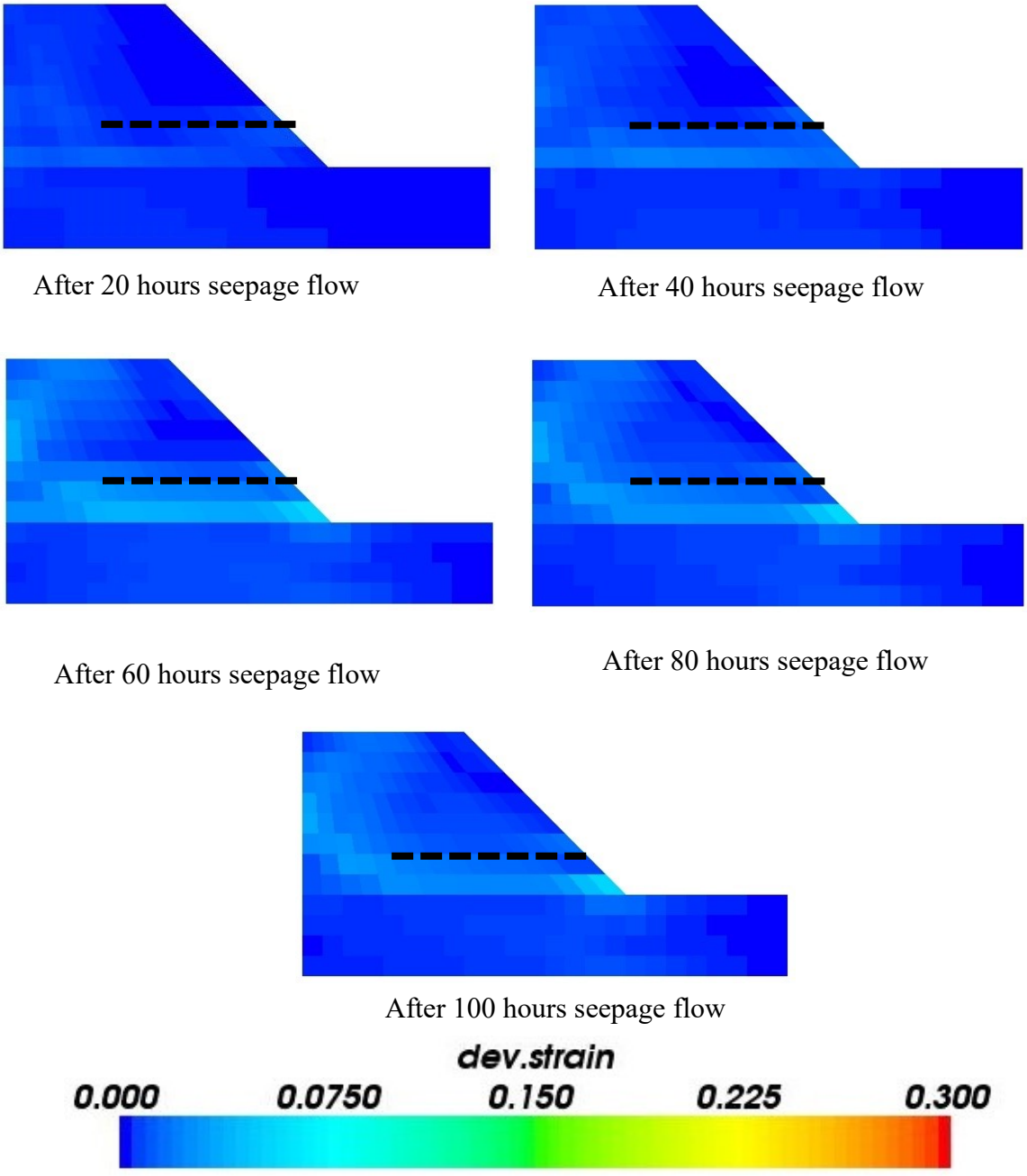

Figure 4.16 Distribution of the deviatoric strain at mid-section of levee for Case 4 at different stages of seepage flow

- **Case 5**

Figure 4.17 shows distribution of deviatoric strain at mid-section of the levee with location of pipe for Case 5 at different stages of the seepage flow. In this case as there are only two pipes and rate of rising the flood water level is high, with the increase in seepage flow duration increase in deviatoric strain can be observed in levee body. The relatively larger strain values are observed in the area parallel to the slope surface of the levee initially and subsequently in larger area.

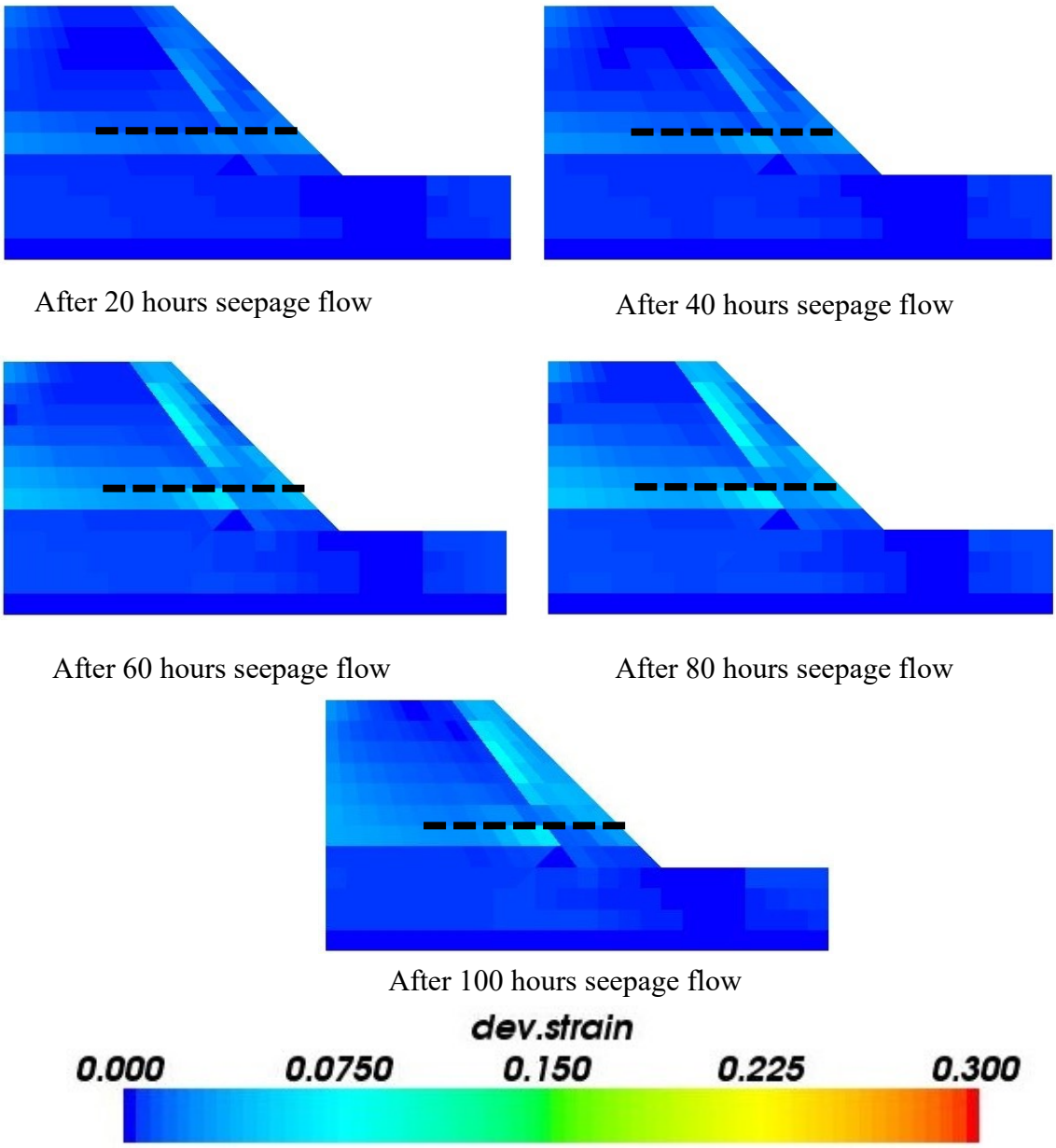

Figure 4.17 Distribution of the deviatoric strain at mid-section of levee for Case 5 at different stages of seepage flow

- **Case 6**

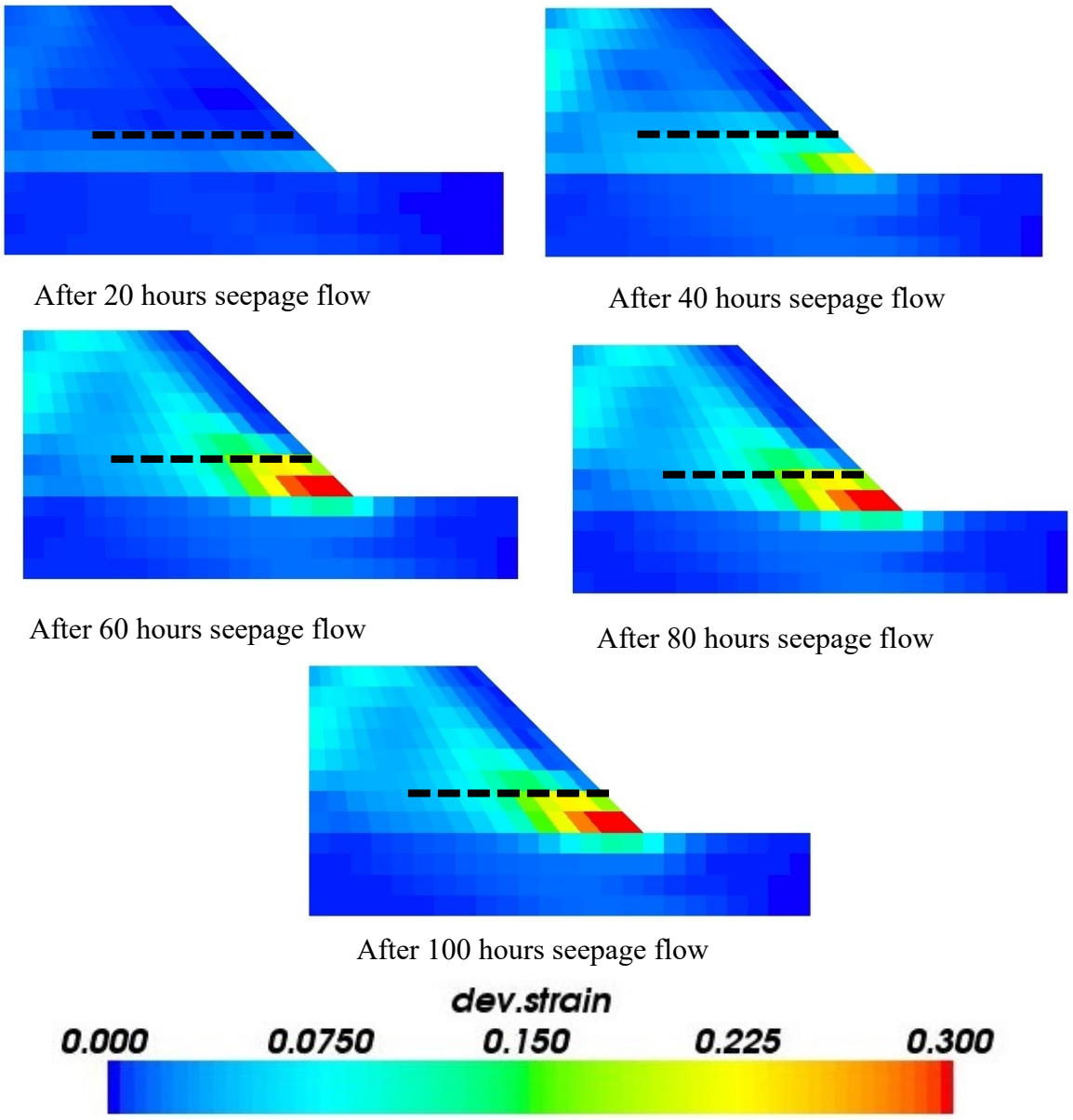

Figure 4.18 Distribution of the deviatoric strain at mid-section of levee for Case 6 at different stages of seepage flow

Figure 4.18 shows the distribution of the deviatoric strain at mid-section of the levee with location of pipe for Case 6 at different stages of the seepage flow. In the figure it can be observed that with increase in seepage flow duration, larger deviatoric strain is developed near the toe of the slope and subsequently towards the upper portion of slope. This behavior similar to that observed in unreinforced case. In this case due to larger rate of

rising flood water head and higher flood head, drainage capacity becomes insufficient to lower the phreatic surface significantly. Also, since pipes in this case did not provide the reinforcement larger strain values are observed.

4.5 Summary

In this chapter numerical and the centrifuge results are compared. Three-dimensional finite element analysis is carried out on the centrifuge model tests. Six test cases which included the unreinforced slope and slope with varying degree of protection is analyzed in numerical analysis. From this chapter following observation are made:

- The comparison between the results of experiment and numerical analysis shows the agreement in the trend of development of pore water pressure under the various condition of protection.
- The reinforcing action of the pipe by the mobilization of axial force is also well predicted through numerical analysis.
- The initiation point of the failure is also predicted through numerical analysis thus it is considered numerical analysis is suitable for the parametric studies.

5 Working mechanism of steel drainage pipe

5.1 Introduction

In this chapter, the working mechanism of the steel drainage pipe is discussed based on the centrifuge test results (Chapter 2) and single gravity physical model test result (Chapter 3). The main objective of this chapter is to discuss how the steel drainage pipe works in minimizing the deformation when the model ground is subjected to the flood. This chapter will also highlight the performance of pipes with drainage function and reinforcement function and also compare the performance with pipes with dual function of the drainage and reinforcement.

5.2 Discussion based on Centrifuge Test Results

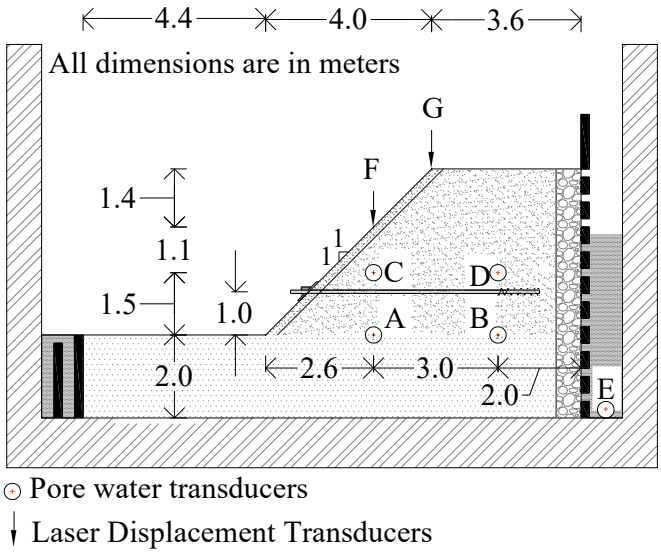

Figure 5.1 Locations of sensors in model ground

In series of six centrifuge tests which has been discussed in Chapter 2, numerous sensors were installed. Based on the observation of these sensors, working mechanism is discussed in this section. **Figure 5.1** shows the cross-section of the model ground with

the locations of the sensors. Working mechanism of the steel drainage pipe is discussed on account of their dual function of the reinforcement and drainage. In addition to this performance of the pipes with only drainage and only reinforcement are also discussed in following section based on centrifuge results.

5.2.1 Effect of Steel Drainage Pipes on Propagation of Sliding

The effectiveness of the steel drainage pipe on minimizing the propagation of slip line and comparative performance of steel drainage pipes along with pipes provided with only reinforcement function is investigated by comparison of reinforced cases (Cases 2-4) with the unreinforced case (Case 1). The comparative performance of steel drainage pipes with pipes provided with only drainage function is made from the comparative study of Cases 5 and 6. Deformation of the levee is evaluated through the observations of marked noodles through transparent window and measured displacement using the LVDTs.

Figure 5.2 shows the superimposed images of the levee at initial condition and after the seepage test for all the cases along with initial shape, deformed shape, and slip line. Superimposed images show the overall performance of the model ground among the different cases under varying level of the protection provided in model ground. In Case 1, the failure starts from the toe region and progressively extends to the crest causing the complete collapse of the levee, i.e., the retrogressive failure mode occurs (Wang and Sassa, 2003)as shown in **Fig. 5.2(a)**. In Cases 2 and 5, with the presence of the steel drainage pipes, seepage-induced failure is prevented, as shown in **Figs.5.2(b) and (e)** respectively. In Case 3, even though levee suffered surface erosion below the location of the pipe before the seepage test (while increasing centrifugal acceleration as the increasing rate of the centrifugal acceleration rather larger compared to the other cases), the large deformation of the levee is prevented. The surface erosion in Case 3 is attributed to insufficient manual control over the rate of increase of centrifugal acceleration. The presence of erosion below the toe region before seepage test facilitated the continuation of erosion, especially above the pipe 1 and pipe 3 during the rise of the flood water. Along with this, tension cracks are observed on the crest of the levee. However, significant movement of the soil mass is prevented, as shown in **Fig. 5.2 (c)**. In Case 4, in which protection on the levee is provided by steel pipes without drainage function, the

continuation of slip line below the location of the pipe is stopped. However, the formation of deeper tension cracks on the crest and consequent large deformation of the levee is not prevented, as shown in **Fig. 5.2 (d).** In Case 6, in which protection in the levee is provided by flexible tubular pipes without reinforcement function; slip line continued from the toe of the levee to the crest of the levee. The progression of the failure begins with the settlement of the pipe leading to the eventual large deformation of the levee as shown in **Fig.5.2 (f).**

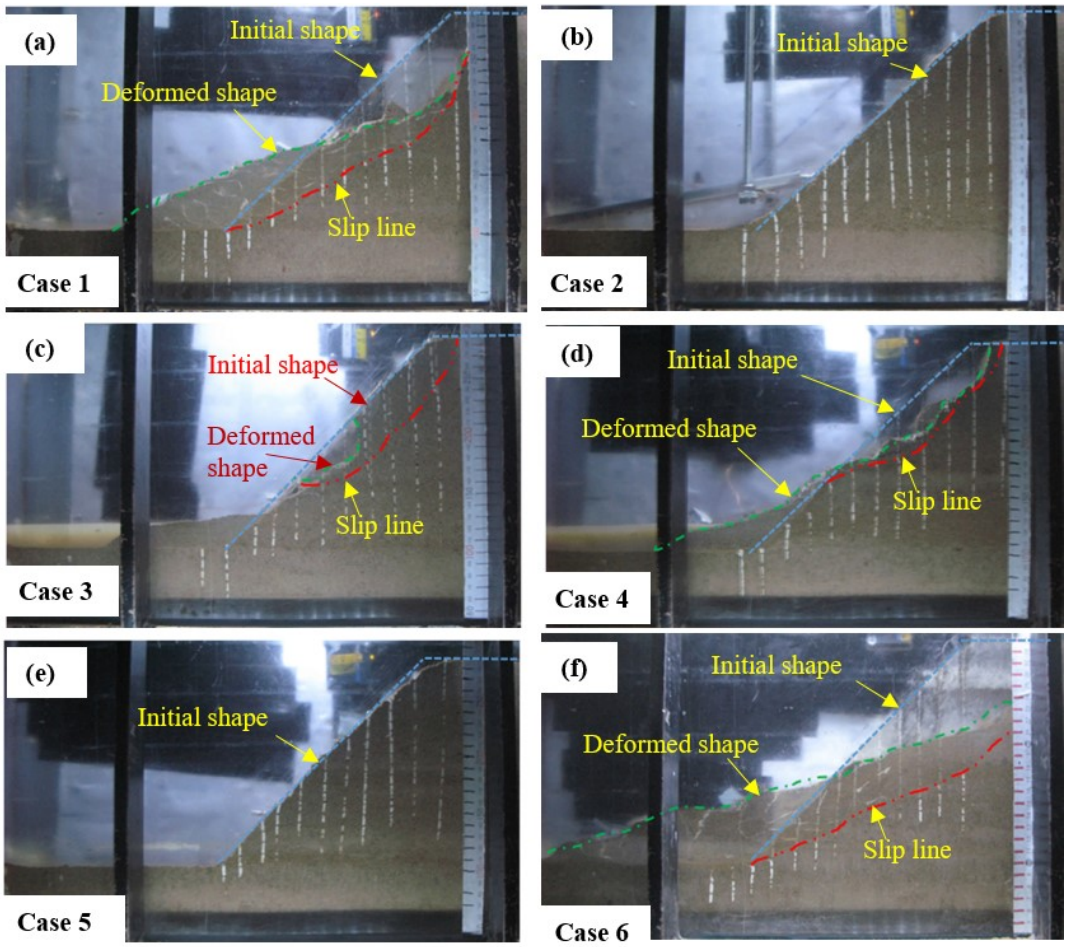

Figure 5.2 Superimposed image of initial condition (before seepage test) of slope with deformed shape of slope after experiment (after test completion) (a) Case 1; (b) Case 2; (c) Case 3; (d) Case 4; (e) Case 5; (f) Case 6

5.2.2 Effect of Steel Drainage Pipes on Resistance against Flood

Figure 5.3 shows the time histories of the settlement at the location F (location shown in **Fig. 3**) along with the indication of the flood head at initiation of the movement represented by the numbers on vertical line for Case 1 (unreinforced), Case 3 (both reinforcement and drainage), Case 4 (only reinforcement) and Case 6 (only drainage). In the figure, Cases 2 and 5 are not shown as in these cases, no significant movement is observed.

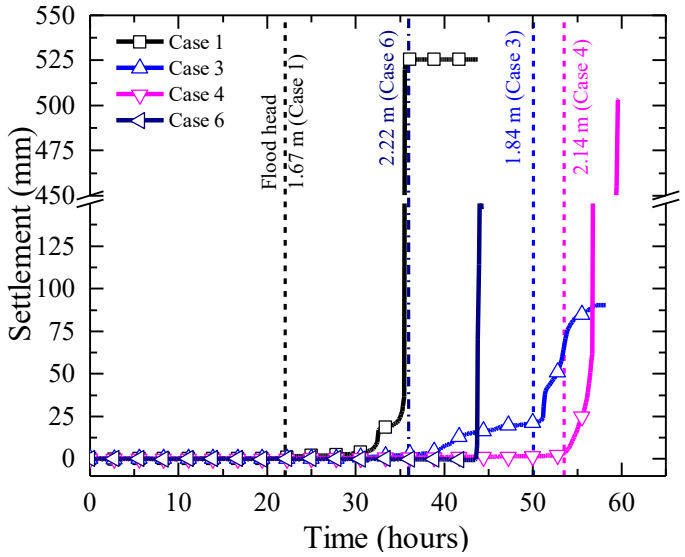

Figure 5.3 Time histories of settlement on location F

Table 5-1 Summary of the centrifugal experiment result

Cases	Initiation of failure		Occurrence of large failure	
	Seepage flow duration (hrs)	Flood head (m)	Seepage flow duration (hrs)	Flood head (m)
Case 1	22	1.67	35	2.2
Case 2	No failure			
Case 3	50	1.84	No large deformation	
Case 4	53.5	2.14	57(no complete failure)	2.3
Case 5[b]	No failure			
Case 6[b]	36	2.22	43	2.9

The result of centrifugal tests concerning the point of initiation of failure (onset of the soil movement) and occurrence of large failure (large deformation leading to change in geometry of slope) is presented in **Table 5-1**. Observation can be summarised as follows. Failure is prevented in Cases 2 and 5 completely. In Case 3, a slight movement of the slope is observed with no large deformation of the slope. In all these cases (Cases 2, 3 and 5), protection in levee is provided by steel drainage pipes. In Case 4, a more extensive movement of soil slope is observed; however, the large deformation of slope as observed in Case 1 is prevented. In Case 6, slope has large deformation compared to no significant deformation in Case 5.

Figure 5.4 (a) shows the changes in the pore water pressure at location A with increasing flood head for Case 1 (unreinforced), Case 2 (both reinforcement and drainage), and Case 4 (only reinforcement) while **Fig. 5.4(b)** shows same for Case 5 (both reinforcement and drainage) and Case 6 (only drainage). The vertical lines in the graph indicate flood water head at which the failure is initiated. The horizontal line indicates the pore water pressure at location A when the failure is initiated. In **Fig. 5.4(a)**, it is observed that, in Case 1, failure occurs when the flood water head reaches 1.67 m and pore water pressure reaches 10.6 kPa. In Case 4, failure starts when pore water pressure at location A reaches 13.3 kPa, and flood water head reaches 2.14 m. These difference in the pore water pressure at which the failure starts indicates the slope could withstand development of larger positive pore water pressure and higher flood water head with the reinforcement provided by the pipe. **Figure 5.4 (b)** shows the development of pore water pressure with the flood water head for Case 5 and Case 6. In Case 6, failure is again initiated when pore water pressure at location A reaches around 10.6 kPa as in Case 1, however, to achieve this pore water pressure, higher flood head of 2.22 m is required. It should also be taken into consideration that the failure in Case 6 starts when the flood water head has been maintained at this value (with the slight descending trend; see **Fig. 4**) for almost 20 hrs during seepage test. The pore water pressure development in Case 5 and Case 6 follows a similar trend. However, no failure occurs in Case 5, highlighting added protection by the dual function of steel drainage in Case 5. In Case 2, pore water pressure is maintained lower than the pore water pressure at the failure condition of other cases for similar flood water head, thus preventing failure.

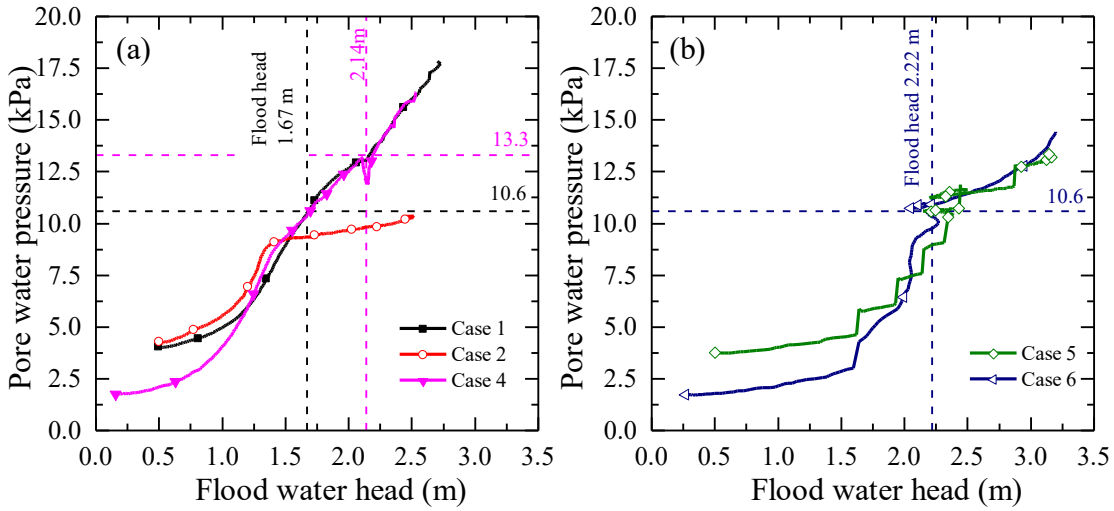

Figure 5.4 Development of pore water pressure at location A (below slope) with flood water head (a) Case 1, 2 and 4; (b) Case 5 and Case 6

5.3 Comparison of performance of levees

For the comparison of performance of levee four different cases with different level of protection is selected. In this study, Cases 1 (unreinforced), Case 3 (with steel drainage pipe), Case 4 (with only reinforcement) and Case 6 (with only drainage) are analysed. This comparison is done to understand the relative contribution of the different level protection mechanism for minimising the deformation of levee against the seepage.

Figure 5.5 shows the result of slope stability analysis performed using the Geo Studio 2012 software for Cases 1, 3, 4 and 6. For the analysis Morgenstern and Price, (1967) slope stability analysis method is used for stability analysis of levee provided with various level of protection and to calculate the factor of safety in each cases, In this analysis the pore water pressure observed in centrifuge experiment is used to determine the phreatic surface at which large failure occurs (see **Table 5-1**) and for Case 3 where no failure occurs the phreatic surface at highest supply flood head is selected. At this condition phreatic surface within levee in some extent similar in Cases 1, 4 and 6 whereas in Case 3 due to combined effect drainage and reinforcement phreatic surface is much lower. Also, the reinforcement force mobilised as observed in the experiment is used to model effect

of the reinforcement. After the analysis, the slip surface is matched with the one that observed in centrifuge experiment to validate the analysis.

Figure 5.6 shows the factor of safety for Cases 1, 3, 4 and 6 obtained from slope stability analysis. From the figure it can be observed that with the use of the steel drainage pipes in levee, factor of safety of levee can be increased significantly. Factor of safety is increased in levee with steel drainage pipes by almost 11 times compared to unreinforced case, almost by 8 times compared to levee provided with only drainage and almost by 6 times compared to the levee provided with only reinforcement.

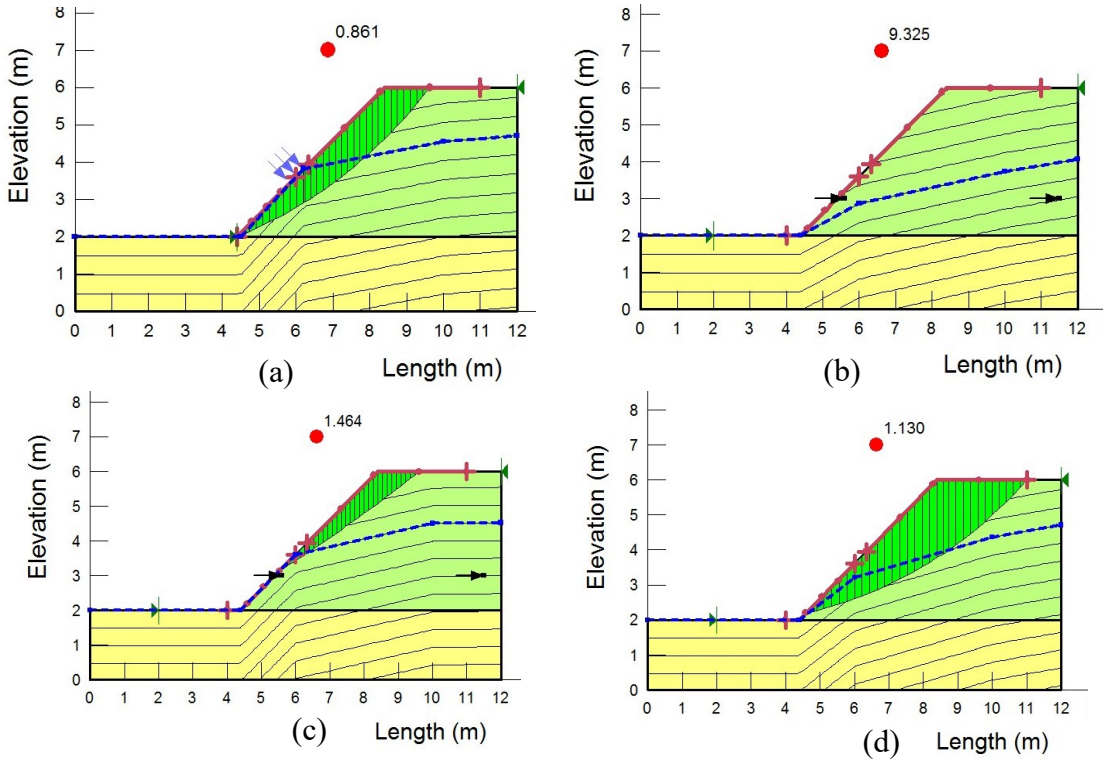

Figure 5.5 Stability analysis result using Geo studio 2012 for (a) Case 1 (b) Case 3 (c) Case 4 (d) Case 6

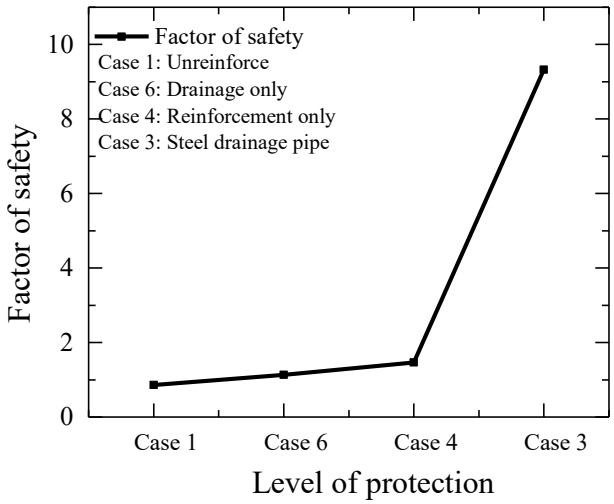

Figure 5.6 Factor of safety for different level of protection in levee

5.4 Contribution of Drainage and Reinforcement in Slope Protection

5.4.1 Drainage Contribution

The proposed steel drainage pipe, due to its tubular structure and numerous holes on the surface, enhances the drainage of the seepage water and thus limiting the rise in the pore water pressure in the slope. **Figure 5.7** shows the variation of the discharge rate with the flood water head for Cases 1-6. The discharge rate here is calculated from the change in the level of water in the drainage tank measured by PPT. For cases where drainage through the pipe is available (Cases 2, 3, 5, and 6) the discharge rate is much larger than the cases without drainage (Cases 1 and 4). It should be noted that no substantial difference in the discharge rate is observed between the cases with three drainage pipes (Cases 2 and 6) and the cases with two drainage pipes (Cases 3 and 5). This may be due to (i) the large scatter in the estimated discharge rate and (ii) more than enough capacity of the drainage pipes. In the cases with the drainage, sharp rise of the discharge rate is observed when the flood head exceeds 1.5 m. Since the pipes are installed at 1 m height from the top of foundation, the effectiveness of pipe to drain the water is observed when flood head is above the location of the pipe as shown in the **Fig. 5.7**.

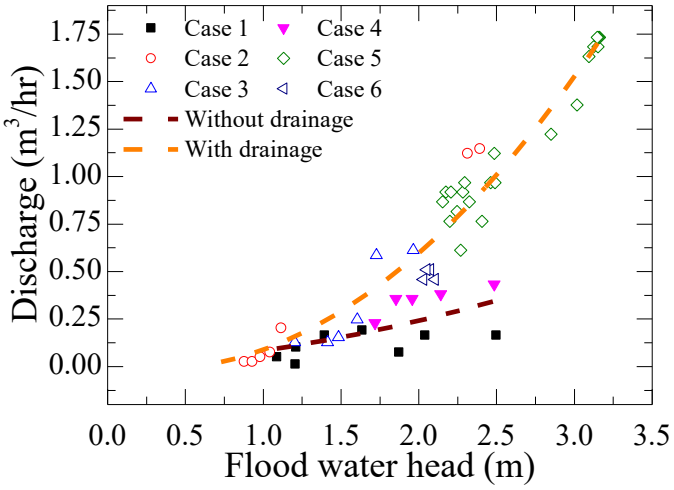

Figure 5.7 Change in discharge rate with flood water head

Figure 5.8 shows the changes in the pore water pressure at the locations A and B with the flood water head for all the cases along with pore water pressure corresponding to the fully developed steady state seepage. To obtain the pore water pressure developed at fully developed steady state seepage condition, steady state seepage analysis was performed on the levee without drainage by varying the boundary condition (flood water level). In **Fig. 5.8(a)** variation of pore water pressure at location A shows the clear distinction between the cases with drainage (Cases 2, 3, 5 and 6) and without drainage (Cases 1 and 4) as observed in discharge rate variation with flood water head. The rise of the pore water pressure at the location A is restricted in the cases with drainage. In the cases without drainage, the rise of the pore water pressure follows the similar trends and monotonically increases with flood water head and is similar to the pore water pressure corresponding to the steady state seepage flow. The increase in pore water pressure at location B with the rise of flood water head is shown in **Fig. 5.8 (b)**. In Cases 1-4, the trend of the rise is similar in all the cases regardless of with or without drainage and also is similar to the pore water pressure estimated by the steady state seepage analysis on the levee without drainage. From the graph, it can be observed that in Cases 1-4 steady state of seepage flow is achieved whereas in Cases 5-6 pore water pressure development is below the steady state condition. Thus, with drainage function in the pipe, the phreatic surface is lowered especially near the slope. The effectiveness of lowering phreatic surface decreases along the length of the pipe. The limited rise in the pore water pressure near the

slope prevented the large deformation of the slope in cases with levee provided with drainage in combination with reinforcement. In **Fig. 5.8 (a)**, it can be observed that the trend of development of pore water pressure is very similar in Cases 5 and 6, indicating the two pipes in Case 5 can sufficiently meet the drainage requirement as in Case 6 with three pipes. However, the level of the deformation in these cases is entirely different, as mentioned above. In Case 5, no significant deformation is observed as in Case 6, where large deformation was observed. This indicates that levee provided with steel drainage pipes having the combination of the drainage and reinforcement experiences superior protection than the levee provided with only drainage function. Nonetheless, the drainage pipe is effective in restricting pore water pressure buildup near the slope surface, which is crucial for slope stability and increases the resilience against the seepage flow induced failure.

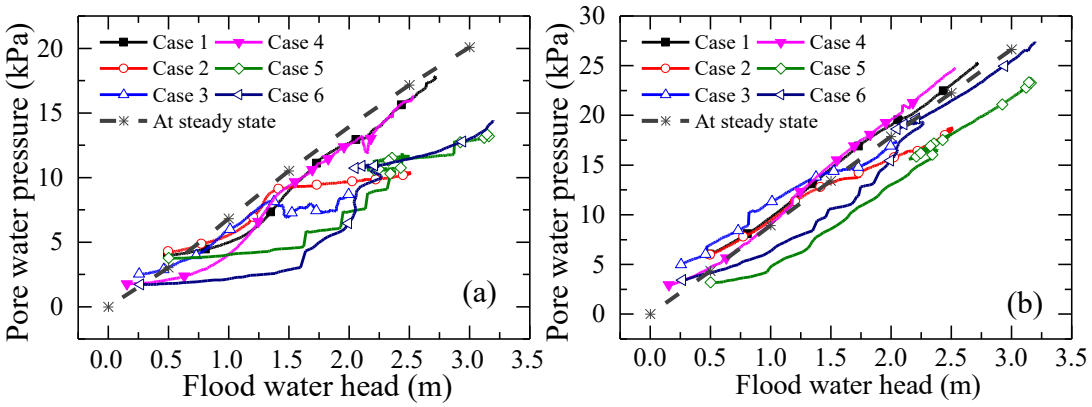

Figure 5.8 Development of pore water pressure with flood water head (a) at location A (below slope); (b) at location B (below crest).

5.4.2 Reinforcement Contribution

Steel drainage pipe by its stiffness and the special spiral blade arrangement at the end of the pipe can provide reinforcement when used in the levee. For understanding the contribution of the reinforcement of the proposed steel drainage pipe, the strain gauges to measure the axial forces and bending moment are installed in the central pipe in Cases 3 and 4.

Figure 5.9 shows the time histories of the flood-induced axial force near the facing plate (at 0.4 m from the slope surface) along with with its components, pore water pressure at locations A and B, and settlement at the location F respectively for the Case 3. The axial force is set to the zero at the beginning of the seepage test. Therefore, change in axial force is the result of soil deformation caused by seepage flow. Here, the positive value indicates the increment of the tensile force and negative value indicates the decrease of the tensile force from the initial condition, i.e. at the onset of seepage test. In **Fig. 5.9 (a),** the vertical dotted lines indicate the time with flood head at which axial force is mobilized, and slide is observed in the experiment. The axial force is mobilized when the flood water head exceeded the 1.5 m, i.e., above the location of the pipe (after 30 hrs,). This mobilization of the axial force provides the additional confinement to the soil in the shallower portion and contributes to the global stability of the slope. The axial force can be decomposed into the contribution of the end reaction (reaction at the spiral blade part) and the skin friction of the pipe surface and soil in the section without the spiral blade. The components of axial force for Case 3 are shown in **Fig. 5.9 (a)**. The end reaction here is the axial force measured at 4.4 m from the slope surface, and the skin friction in the section without the spiral blade is estimated as the difference between the axial forces measured at 0.4 m and 4.4 m from the slope surface. The pore water pressures are shown in **Fig.5.9 (b)** are measured near the points where the axial force near facing plate, i.e., at location A and end reaction, i.e., location B. Time history of the settlement is shown in **Fig.5.9 (c)** which is calculated by setting the settlement at the beginning of the rise of flood water head equal to zero.

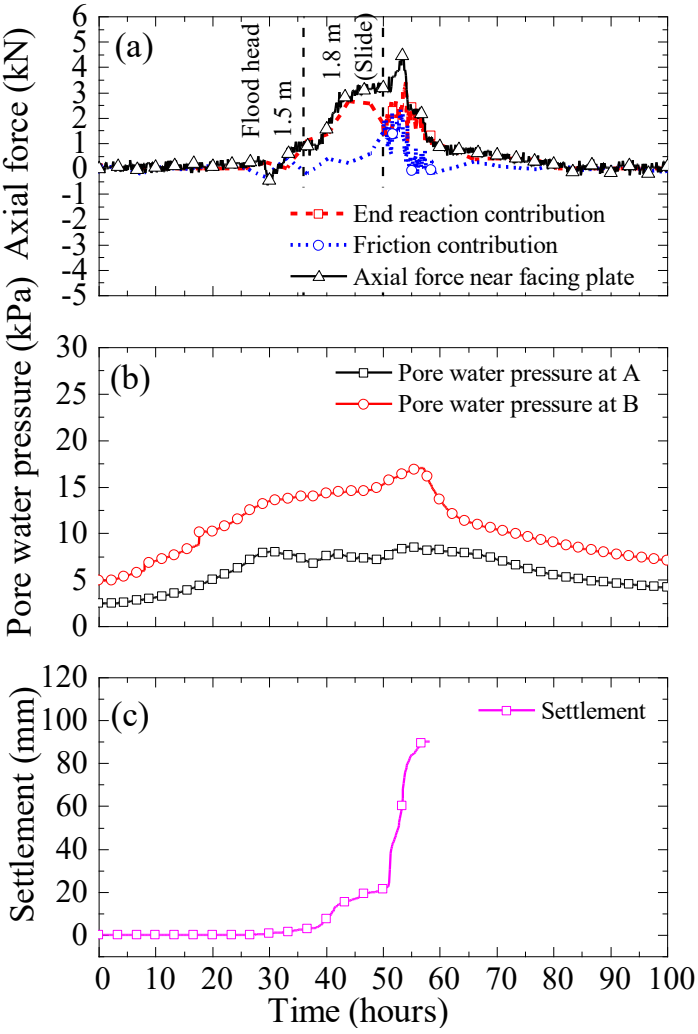

Figure 5.9 Time histories of (a) axial force with its component (b) pore water pressure at location A and B (c) settlement at location F, in Case 3

Similarly, **Fig.5.1 (a)-(c)** show the time histories the flood-induced axial force near the facing plate (at 0.4 m from the slope surface) along with its component, pore water pressure at location A and B, and settlement at location F respectively for Case 4. In **Fig. 5.1 (a),** the vertical dotted lines indicate the time with the flood head at which axial force is mobilized, and large slope failure is observed in the experiment. In Case 4, as well axial force is mobilized when the flood water head exceeded the 1.5 m (after 25 hrs)

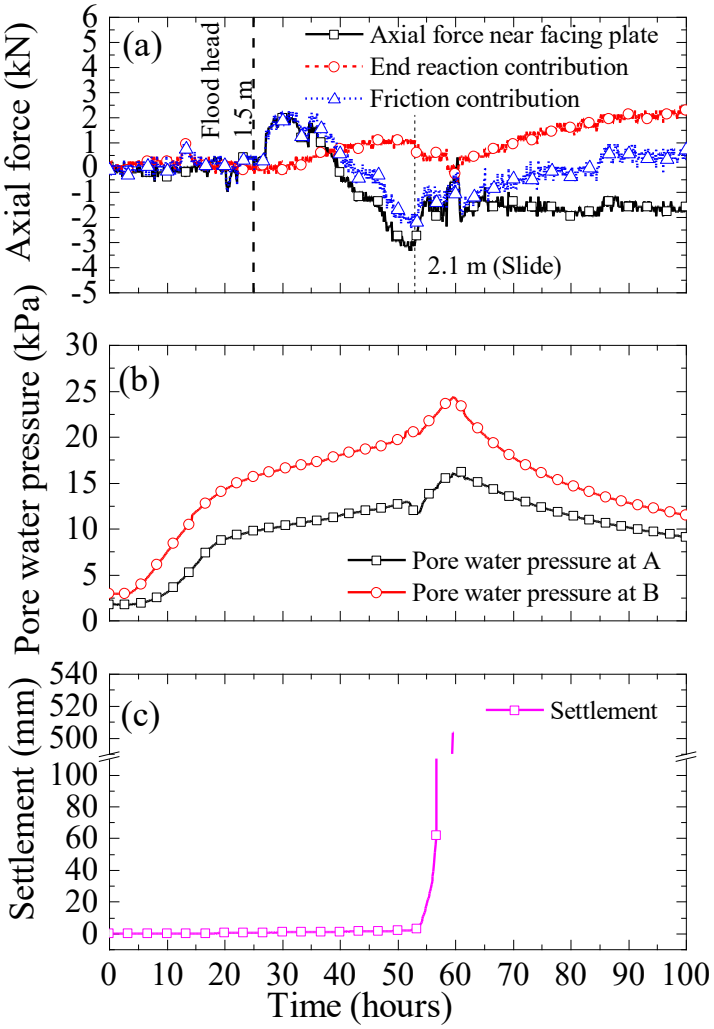

Figure 5.10 Time histories of (a) Axial force with its component (b) pore water pressure at location A and B (d) settlement at location F, in Case 4

On comparing the axial forces in two cases in **Figs. 5.9 and 5.1**, it can be found that in Case 4, the maximum axial force is smaller compared to Case 3. It should be in consideration that in Case 4, the rise of the phreatic surface is not restricted as drainage is not provided. In Case 3, when the drainage and reinforcement function are combined, the maximum axial force recorded near the facing plate is about 4.7 kN. The contribution from the skin friction in the section without the spiral blade is about 2.2 kN, and from end, reaction is 2.5 kN. In Case 4, the maximum axial force recorded near the facing plate is about 2.2 kN, which is mostly due to the contribution from the skin friction and negligible amount of the end reaction. The maximum skin friction is the same for both

cases. The end reaction contribution, however, significantly varies with the cases. The larger end reaction is mobilized when the pipe is provided with the drainage function.

The absence of the drainage function in Case 4 resulted in the higher phreatic surface. The increase in the phreatic surface in the slope surface can cause (i) decrease in the end reaction capacity which is mostly related to the rise in pore water pressure at location B; (ii) decrease in the skin friction related to high pore water pressure at location A; and (iii) cause instability of the slope due to reduction of soil resistance which is also related to pore water pressure at location A. The instability of the slope in return may cause increase in the end reaction due to increase in load retained by pipe. On observing the time histories of the pore water pressure at location A and B, and flood water head in supply tank following relation can be observed:

Case 3: Pore water pressure head at location A < Pore water pressure head at location B < Flood water head

Case 4: Pore water pressure head at location A < Pore water pressure head at location B = Flood water head

As explained in (i) above, the presence of much higher pore water pressure head at location B in Case 4 compared to Case 3, might have resulted in end reaction not being mobilized adequately in Case 4. Also, in **Fig. 5.1 (a)**, it can be observed that there is a reduction in the axial force before the large failure of the slope, i.e., before 53 hours of seepage flow, beginning at t= 40 hrs. Axial force decreases and becomes negative, i.e. tensile forces decrease from initial condition. This negative value of axial force could be due to the loss of the soil mass near the slope surface. Snapshot of the video camera record on the front slope surface shows gradual erosion of the soil and the deposition of the eroded soil near the toe of the slope as shown in **Fig.5.1. Figure 5.11** shows the start of the erosion of soil at 37 hours and soil deposited near the toe at 52 hours of seepage flow, respectively. The progression of the soil erosion also corresponds to the gradual decrease of the axial force in Case 4 and eventually negative axial force.

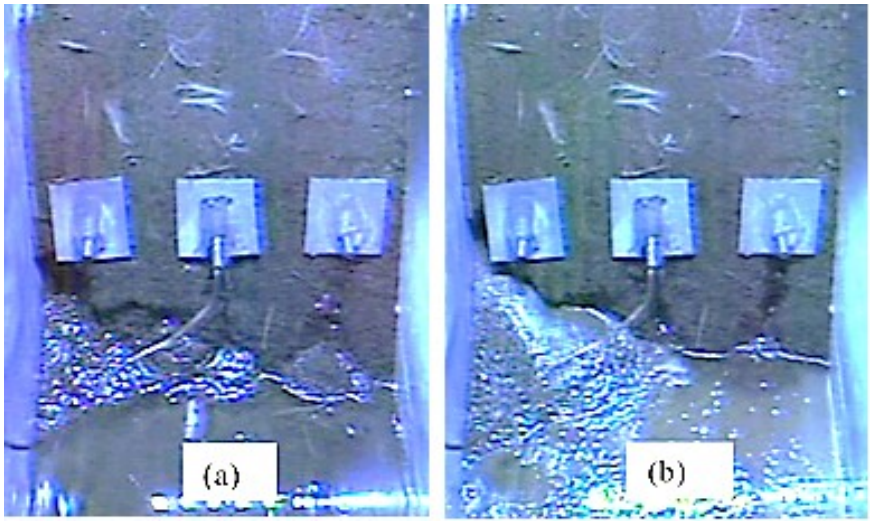

Figure 5.11 Erosion of soil near the slope surface in Case 4 (a) at 37 hours (b) 52 hours of seepage flow

The flood-induced bending moment at the different distance from slope surface along the length of the pipe at the different relevant times is plotted along with the flood-induced soil reaction on the pipe for Case 3 and Case 4 in **Fig.5.1**. Soil reaction here is the soil pressure change in response to the soil movement. The bending moment is measured by the strain gauges placed at four different locations on pipe surface, as shown earlier in Fig. 2. The embedment length of the pipe is 5.6 m. The section with the spiral blades is from 4.6 m to 5.6 m from the slope surface. Unfortunately, the strain gauges are not attached to the section with the spiral blades. The bending moment is analyzed by taking the start of the seepage flow as a datum, i.e., bending moment at the onset of seepage flow is set zero. Bending moment analyzed here is due to the soil mass movement caused due to the seepage flow. The soil reaction is calculated from weighted residual numerical differentiation as described in Brandenberg et al. (2010). The bending moment data recorded during centrifuge experiment are double differentiated using this method.

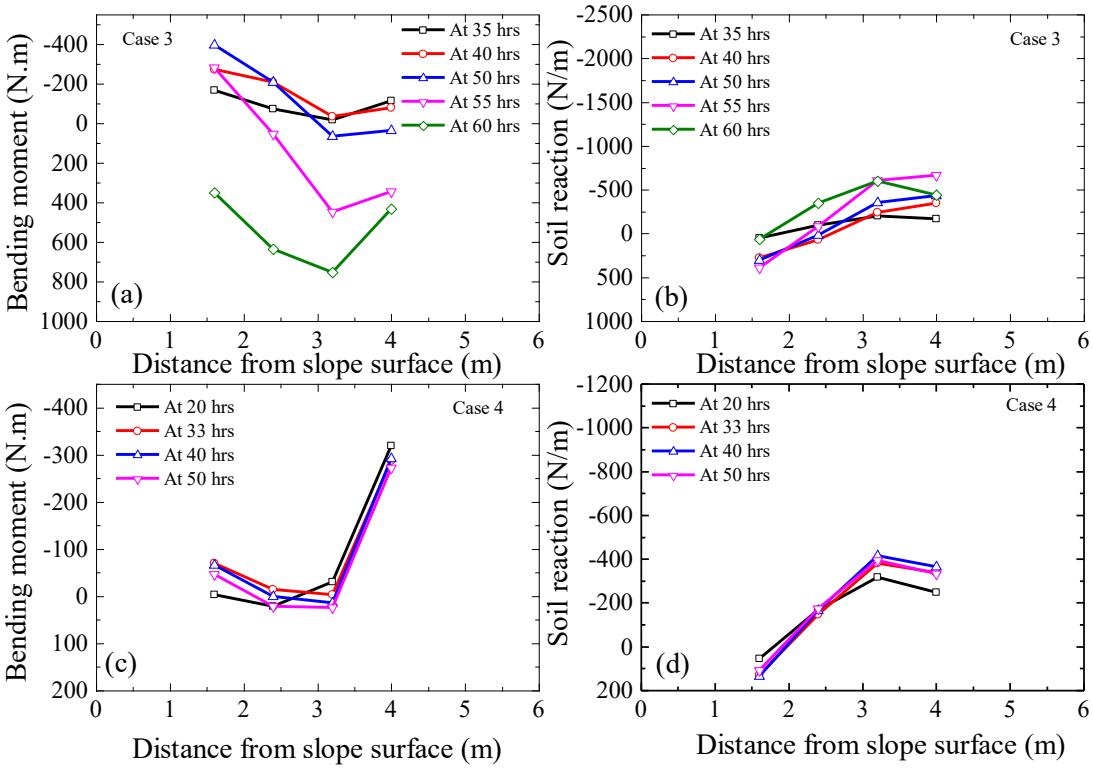

Figure 5.12 Bending moment and earth reaction along length of pipe (a) bending moment in Case 3; (b) Soil reaction in Case 3; (c) bending moment in Case 4; (d) earth reaction in Case 4

From distributions of the bending moment and soil reaction in Case 3, it can be observed that with the progression of seepage flow fluctuation in the bending moment and soil reaction is observed whereas in the Case 4 there is minimal change in soil reaction with the progression of the seepage flow. In Case 3 before the start of seepage flow, soil below the pipes was eroded near the surface, which might have resulted in loosening of soil below the pipe. This loosening of soil could have allowed the pipe to move more freely and hence more change in soil reaction with seepage flow. In Case 4, the failure is very sudden as reflected by the sharp change in settlement in time history of settlement in **Fig. 5.3**. So initially, when there is small change in settlement, bending moment is small which is followed by sudden large deformation (around 55 hrs of seepage flow) causing the bending moment observation to be out of the range.

In either case, the maximum soil reaction is less than 1 kN/m. If we consider the fact that possible static load induced by the self-weight of the soil at the middle of the section

without the spiral blades is 7.7 kN/m, it can be said that the soil reaction calculated is minimal. This suggests that the reinforcement contribution is, therefore, predominantly through the mobilization of the axial force and minimally through the bending moment with the specifications of the steel pipe used.

5.5 Discussion based on 1g physical model test

In this section, observation made in single gravity physical model test is discussed. In the single gravity model test series same flooding rate was maintained in all the test cases, which allowed fair comparison among the test cases. In this series of experiment, focus is made in understanding the reinforcement function in the pipe.

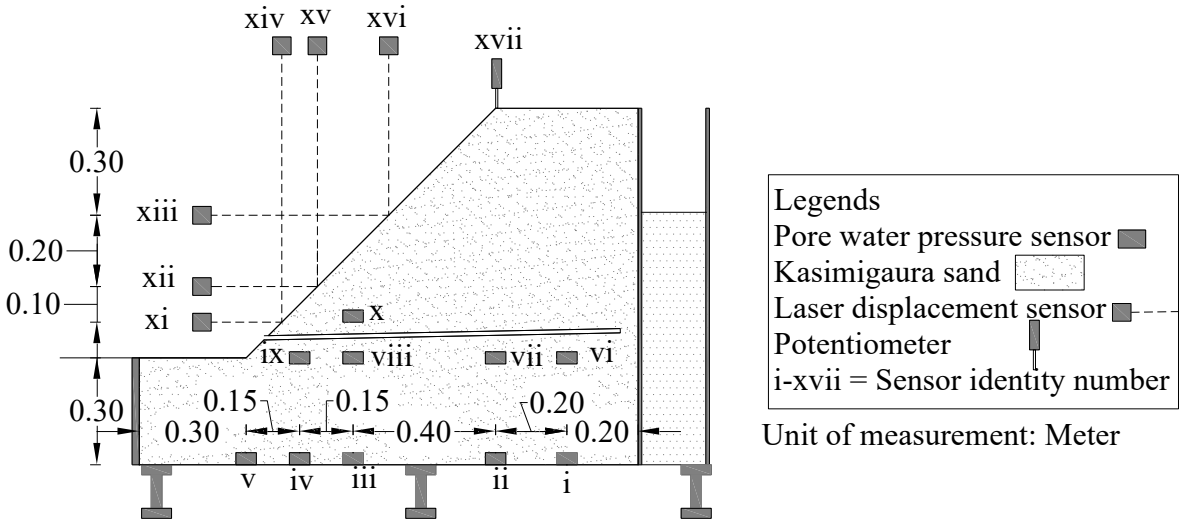

Figure 5.13 Cross-section of model ground showing the locations of sensors

In this test series, three different test conditions (Cases AT.1-AT.3) is taken into consideration. The details of the experiment are discussed in chapter 3. Performance of the model ground for these three tests is discussed based on observation of various sensors installed in the model ground. **Figure 5.13** shows the cross-section of the model ground showing the locations of the sensors. Three types of sensors are used in the model ground to capture the performance of the model ground. The details of the location of the sensors are listed on **Table 5-2**.

Table 5-2 Locations of sensors in model ground

Sensor ID number	Sensor ID	Type of sensor	Height from bottom of model	Distance from supply tank
i	01_200	Pore water pressure transducer	100 mm	200 mm
ii	01_400	Pore water pressure transducer	100 mm	400 mm
iii	01_800	Pore water pressure transducer	100 mm	800 mm
iv	01_950	Pore water pressure transducer	100 mm	950 mm
v	01_1100	Pore water pressure transducer	100 mm	1100 mm
vi	03_200	Pore water pressure transducer	300 mm	200 mm
vii	03_400	Pore water pressure transducer	300 mm	400 mm
viii	03_800	Pore water pressure transducer	300 mm	800 mm
ix	03_950	Pore water pressure transducer	300 mm	950 mm
x	04_800	Pore water pressure transducer	400 mm	800 mm
xi	LDT_H_04	Laser displacement transducer (for horizontal movement)	400 mm	1000 mm
xii	LDT_H_05	Laser displacement transducer (for horizontal movement)	500 mm	900 mm
xiii	LDT_H_07	Laser displacement transducer (for horizontal movement)	700 mm	700 mm
xiv	LDT_V_04	Laser displacement transducer (for settlement)	400 mm	1000 mm
xv	LDT_V_05	Laser displacement transducer (for settlement)	500 mm	900 mm
xvi	LDT_V_07	Laser displacement transducer (for settlement)	700 mm	700 mm
xvii	P_V_1	Potentiometer (for settlement at shoulder)	1000 mm	400 mm

5.5.1 Performance of the drainage

In this series of the experiment, Case AT.3 is provided with the steel drainage pipes having both drainage and reinforcement. Case AT.1, which is unreinforced and Case

AT.2 which case with pipe with only reinforcement function, is not provided with drainage. Here, the drainage performance of the pipe is compared by the comparison of the Case AT.1 and AT.3.

Figure 5.14 (a-e) shows the time history of the pore water pressure observations at 200 mm, 400 mm, 800 mm, 950 mm and 1100 mm respectively at the 100 mm from the bottom of the foundation. In this, both test condition flood water level is raised from 300 mm to 900 mm in steps. In each step, water is raised by 100 mm (see Fig. 3.8). From the figure, it can be observed that with the increase in the flood water level, pore water pressure in the model ground also consequently increases in the step. The increment rate of pore water pressure; however, in each step for case with the drainage and without drainage is different. At the locations near to the supply tank (at 200 mm from supply tank), pore water pressure increases by almost 1 kPa in Case AT.1 and 0.5 kPa in Case AT.3 in each step as shown in **Fig. 5.14**(a). In Case AT.1, rise is almost equal to rise in flood water level whereas because of presence of the drainage in Case AT.3, there is limited increment in pore water pressure. Maximum pore water pressure developed at this location (i.e., 200 mm from water supply tank) is reduced by 1kPa in Case AT.3 compared to Case AT.1. A similar trend is observed in all the locations. The maximum pore water pressure developed at all other locations; however, is reduced by on average 2 kPa in Case AT.3 compared to Case AT.1, as shown in **Fig. 5.1 (b-e).** Thus, the drainage pipe is most effective near the slope surface /near the toe region, which is crucial considering the stability of the levee structure. This limited rise of pore water pressure is able to prevent any deformation in Case AT.3

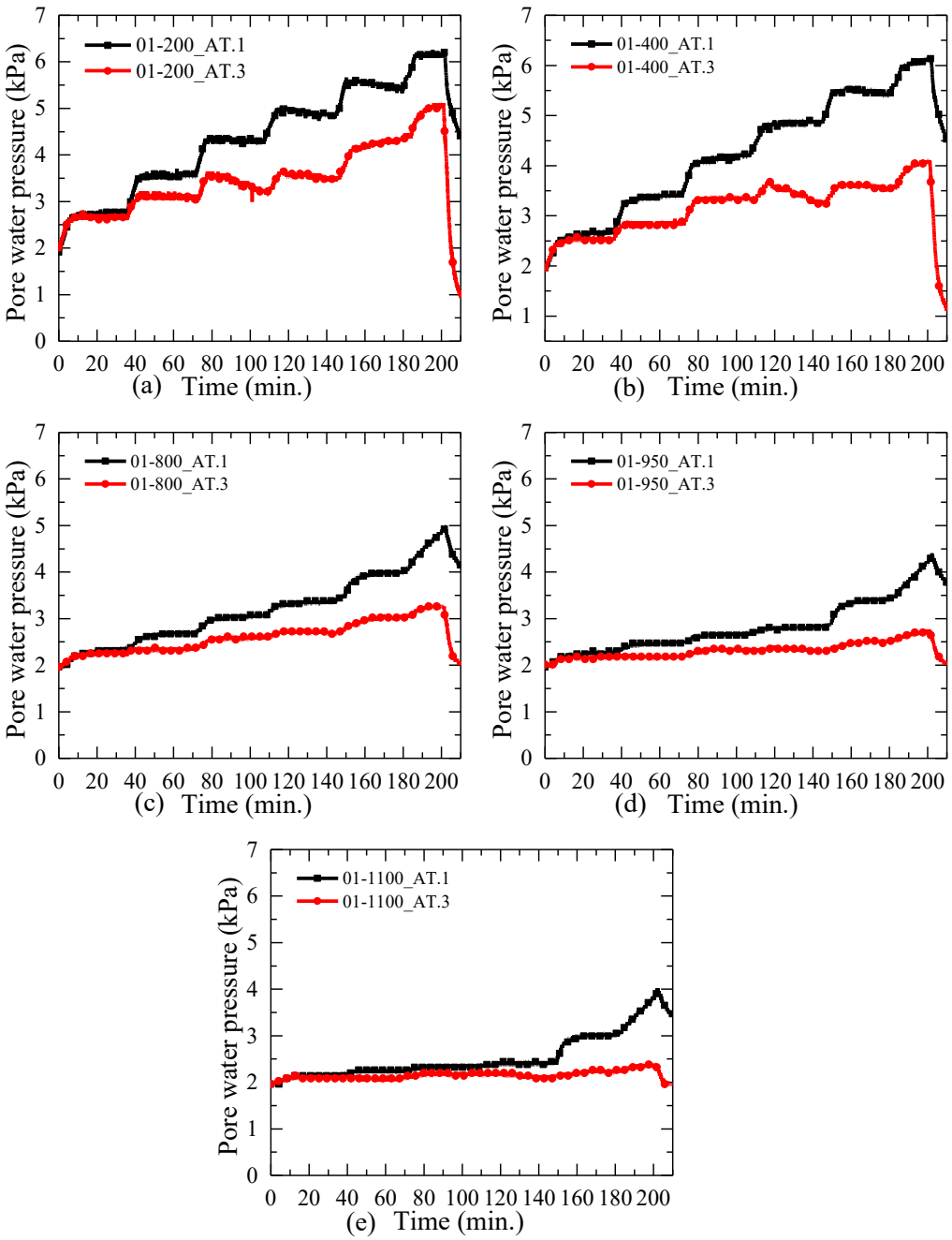

Figure 5.14 Time history of pore water pressure in Cases AT.1 and AT.3 (a) at 200 mm from supply tank (b) at 400 mm from supply tank (c) at 800 mm from supply tank (d) at 950 mm from supply tank (e) at 1100 mm from supply tank

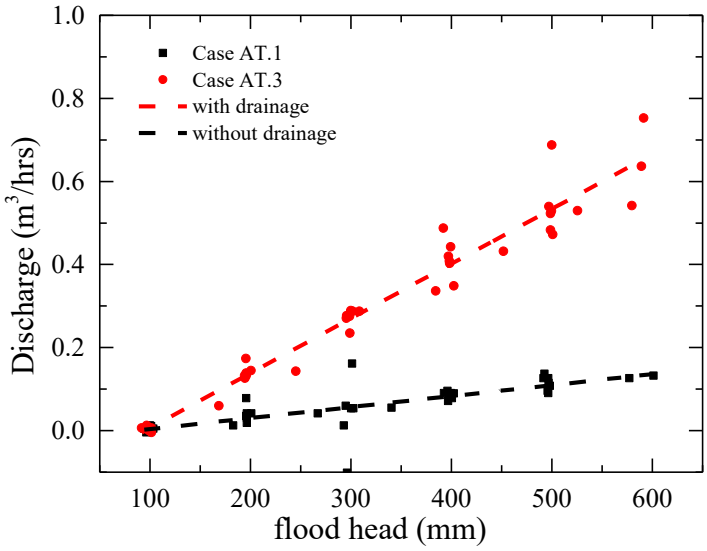

Figure 5.15 Comparison of discharge with the change in flood head for Cases AT.1 and AT.3

Figure 5.15 shows change in the discharge with change in flood head in Cases AT.1 and AT.3. Here, the flood head is the difference of flood water level and height of the foundation. The Case AT.2 is not included in comparison as the discharge rate is comparable to Case AT.1. Discharge rate increases linearly with the increase in flood head in both the cases. The discharge rate, however, is increased by almost four times in presence of the drainage. Thus with the presence of the drainage pipe, discharge of the seepage water increased significantly by the pipes, which limit the rise of the pore water pressure within the levee. This limited rise in pore water pressure caused by higher discharge rate allows the soil to remain in unsaturated condition, thus minimizing the strength loss during the flooding.

5.5.2 Performance of the reinforcement

The reinforcement performance of the pipe is discussed in two scenarios in this section. The first scenario is the case when reinforcement is provided in the model ground without the drainage and second scenario is the case when reinforcement is provided in the model ground in combination with the drainage. Cases AT.2 and AT.3 are used for discussion in this section to highlight the performance of the reinforcement in these two scenarios.

In Case AT.2 model ground showed the limited deformation with the formation of the arch above the location of the pipe when subjected to flooding as discussed in chapter 3. In Case AT.3, model ground showed no deformation when subjected same level of the flooding.

Arch is formed in model ground above the location due to the differential settlement between the location of the pipes and free field (Han and Gabr, 2002; Zhou et al., 2017). Stress ratio, which is defined as the ratio of the stress near the location of pipe and stress in the free field (in spacing between pipes) determines the height of the arch in the model ground. This differential settlement also causes the mobilization of the bending moment in the pipes. **Figure 5.16** shows the time history of the differential settlement at 0.1 m height from the toe of slope for Case AT.2 and Case AT.3, respectively. Differential settlement is calculated as the difference of vertical settlement at location of pipe at mid-span and at the free space between pipes. Vertical dashed line in **Fig. 5.16 (a)** shows the flood level at the different duration of seepage flow. From the figure, it can be observed that once the flood level reaches the 700 mm (at 80 min), there is a rise in differential settlement and sudden rise in value beyond 100 minutes of seepage flow (after 800 mm flood). The value of the differential settlement in Case AT.3 is very minimal as the model ground, in this case, did not show any significant deformation.

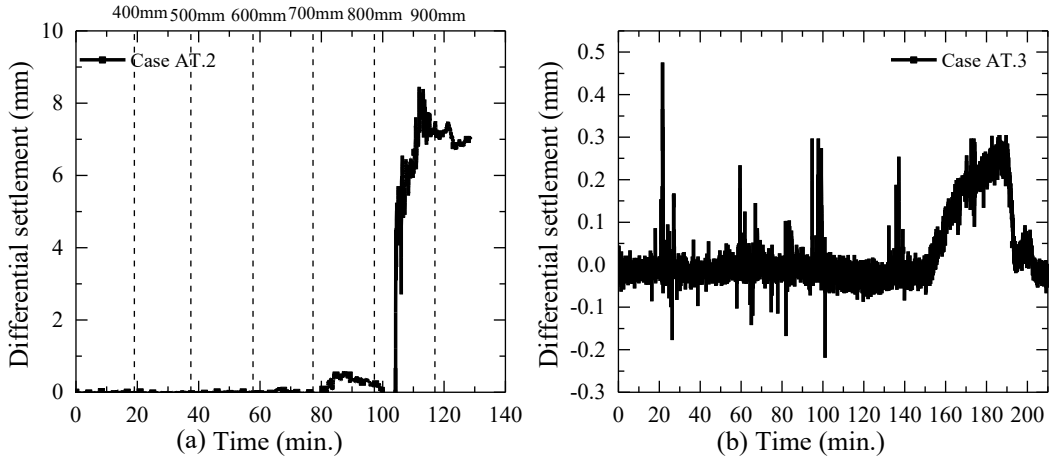

Figure 5.16 Time history of differential settlement at the height of 0.1 m from toe of slope (a) Case AT.2 (b) Case AT.3

Figure 5.17 (a-b) shows the distribution of the bending moment in pipe at different flood level in Cases AT.2 and AT.3, respectively. In his figure, the bending moment represents the change in bending moment during the seepage flow as the bending moment at the beginning of the seepage flow is considered as zero. From the figure, it can be observed that in Case AT.3, bending moment mobilization is minimal as the differential settlement. This minimal differential settlement leads to small change in bending moment in the pipe. **Figure 5.17 (a)** shows that significant bending moment is mobilized after the flood reaches 700 mm level. There is sudden and significant rise in bending moment mobilization when flood level reaches 900 mm level. This sudden rise in bending moment mobilization is in accordance with the change in the differential settlement, as shown in **Fig. 5.16 (a).** This mobilization of the bending moment in Case AT.2 restricts the collapse of slope even though the phreatic surface is located at high position in the model ground.

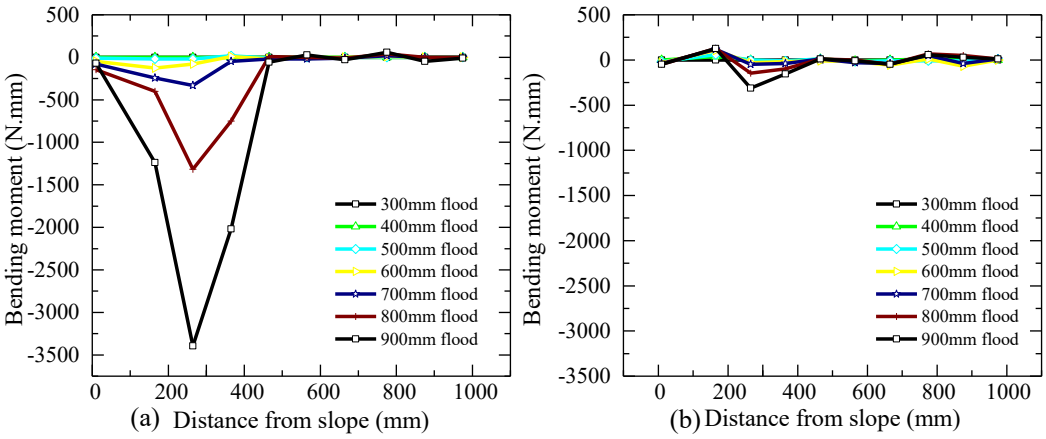

Figure 5.17 Bending moment distribution in pipe at different flood level (a) Case AT.2 (b) Case AT.3

Figure 5.18 (a-b) shows the time history of horizontal displacement at the height of 0.2 m from the toe of the slope for Case AT.2 and AT.3, respectively. Vertical dashed lines in **Fig. 5.18 (a)** indicates flood level at the different duration of seepage flow. In the figure, it can be observed that horizontal displacement in Case AT.2 increases with the time beyond the 80 minutes of seepage duration when flood level exceeds the 700 mm level.

Also, there is a sudden increase in the horizontal displacement when the flood level exceeds the 800 mm level. There is minimal change in the observation of the horizontal displacement in Case AT.3, as shown in **Fig. 5.18 (b)**

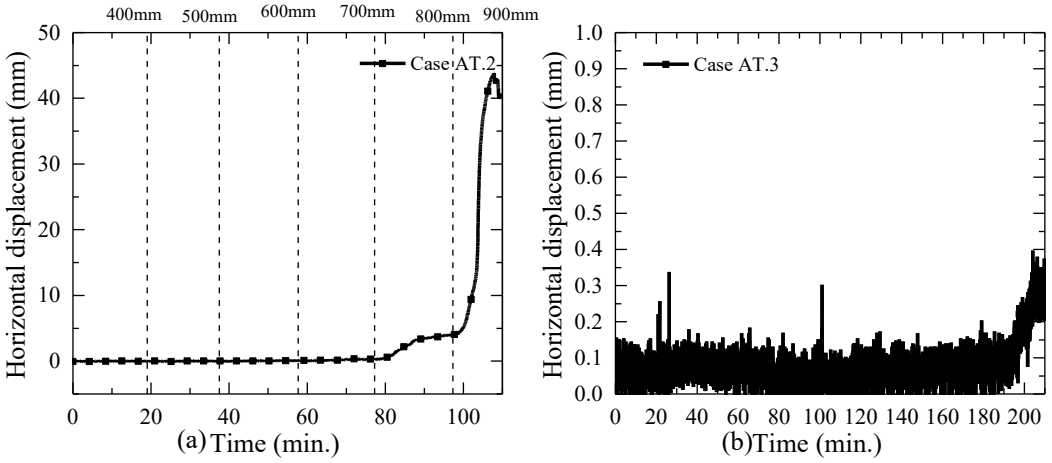

Figure 5.18 Time history of horizontal displacement at height of 0.2 m from toe of slope (a) Case AT.2 (b) Case AT.3

Figure 5.19 shows the axial force distribution in the pipe in Case AT.2 at different flood levels. Axial force here shows the change in the axial force mobilization during the seepage flow as the axial force at the beginning of seepage flow is taken as zero. The axial force increases with the increase in flood level, more significantly when the flood level is beyond level of 600 mm. There is a significant rise in maximum axial force when flood level is beyond the 800 mm flood. This change in axial force is in accordance to change in horizontal displacement, as shown in **Fig. 5.18(a)**. As the flood level increases the point of occurrence of the maximum axial force is shifted farther from the slope surface, indicating the deepening of the slip surface. This mobilization of the axial force restricts the slope movement in Case AT.2 and preventing the collapse of the soil.

Mobilization of the bending moment and axial force in Case AT.2 provides additional strength to the model ground, which prevents the complete collapse of the slope. However, the absence of the drainage results in higher phreatic surface within the levee, causing the formation of the cracks. In Case AT.3 where both drainage and reinforcement is provided, lowered phreatic surface and mobilization of the bending moment results prevention of

the deformation. Thus, pipe with dual function provides better performance against flooding compared to pipe with only reinforcement.

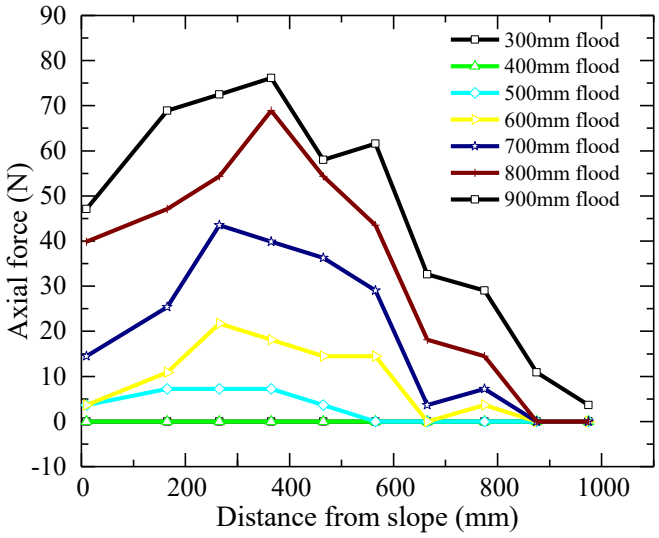

Figure 5.19 Axial force distribution in pipe at different flood level for Case AT.2

5.6 Summary

In this chapter working mechanism of steel drainage pipe which combines the drainage and reinforcement function against the flooding in sand levee with 1H: 1V slope through centrifugal tests and 1g test is discussed. One case of the unreinforced slope and additional five cases of the reinforced slope with varying level of the protection are studied in series of centrifuge test. Unreinforced slope serves as the control for other cases of the investigation. The contribution of each function of proposed steel drainage pipes in the slope protection is also investigated through the tests. From the series of centrifuge test following observations are made:

- It is found that with the rise of the pore water pressure in a sand levee during the flood, the slope experienced complete failure when no protection is provided.
- The slope with the protection exhibits increased resilience against the flood. The protected slope can withstand the higher flood water level and longer flood duration. Also, propagation of the slip surface and deformation is limited. Steel

drainage pipe with both drainage and reinforcement function is found to be more effective than the traditional method of the protection using only either drainage or reinforcement function.

- Factor of safety is increased in levee with steel drainage pipes by almost 11 times compared to unreinforced case, almost by 8 times compared to levee provided with only drainage and almost by 6 times compared to the levee provided with only reinforcement.
- The drainage function of the steel drainage pipe limits the rise of the phreatic surface in the levee through the quick drainage of the seepage water from the levee. The drainage of seepage water limits the rise of the pore water pressure, especially near the slope surface.
- Mobilization of the axial force is contributed by (i) end reaction developed due to the portion of the steel pipe with spiral blades and (ii) skin friction between the soil and pipe. End reaction is not adequately mobilized in the pipes without drainage due to the presence of the higher phreatic surface.

In the series of 1g test, three different cases are studied. One of the cases is unreinforced, and the other two cases are provided with pipe with only reinforcement and pipe with both drainage and reinforcement respectively. From this series of the experiment, following observations are made:

- The presence of the pipe cause differential settlement between free fields and place of location of the pipe, which is caused by mobilization of the bending moment.
- Bending moment mobilization cause strengthening of slope and limits the deformation. Similarly, with the horizontal movement, axial force is mobilised also contributing to the slope stability.
- Pipe when combined with both drainage and reinforcement provides maximum protection and prevents failure of the slope.

6 Effectiveness of steel drainage pipes against flooding

6.1 Introduction

In this chapter, the numerical parametric study is made to understand the comparative performance of the steel drainage pipe with the pipes with only drainage and only reinforcement. In this chapter also the effect of the permeability of the soil, flooding condition in the performance of steel drainage pipes is discussed. The influence of the arrangement of pipes and design of pipes in the overall performance of levee in flooding is also studied through the parametric numerical analysis.

In the following sections, the prototype model ground used in the series of centrifuge test is used. The model ground has the slope of the 1V:1H and the total height of the model ground are 6 m which includes the foundation of the height 2 m. The model ground is made of the Edosaki sand. The properties of the Edosaki sand used in numerical analysis are listed in **Table 6-1**. The boundary condition and the geometry of the model ground showed in **Fig. 4.1** used in this series of parametric numerical study. Reinforcement function in the slope is modeled by adding the series of the elastic member, beam elements at the location of the drain pipe. Pipes with only either of one function is also modeled using drainage or reinforcement function only. The properties of the steel drainage pipe used in the numerical analysis are listed in **Table 4-2**. Flood simulation and analysis procedure are kept the same as discussed in chapter 4.

Table 6-1 Properties of the Edosaki sand for parametric studies

Properties	Values
Soil particle density (Mg/m^3)	2.72
Average initial water content of model ground	14.7%
Angle of shearing resistance [Degree of compaction Dc= 80%] (degrees)	29
Cohesion [Dc= 80 %](kN/m^2)	2.5
Saturated hydraulic conductivity (m/s)	
Foundation	1.5E-6
Embankment	4.5E-5
SWCC parameters for van Genuchten model	
Saturated volumetric water content θ_s	0.467
Fitting parameters n	1.674
Fitting parameters α	9.223
Fitting parameters m	0.403
Dry density of embankment (Mg/m^3)	1.45
Dry density of foundation (Mg/m^3)	1.72
Poisson's ratio	0.33
Modulus of Elasticity (N/m2)	2.55E5

6.2 Performance of steel drainage pipe with pipes with only drainage and only reinforcement

In this series of the analysis, the comparative performance of the steel drainage pipes against its traditional counterpart pipes having only drainage and only reinforcement is evaluated by providing the same condition of flooding and model ground. While this comparison has been made through the series of the centrifuge test and 1 g test results, the condition for the test was not exactly the same. This difference in the test condition did not provide the fair condition for the comparison. Therefore, in the numerical analysis, a similar condition of the model ground and the flooding is established to make a fair comparison among the cases. In the analysis, four different Cases A.1, A.3, A.4, and A.6 are taken into consideration. In these four cases, different level of protection is provided, which is tabulated in **Table 6-2**.

For the flood simulation, the model flood hydrograph derived from the hydrograph recorded at Comite River at Comite, LA on August 18, 2016, is used. **Figure 6.1** shows the time history of the flood hydrograph for the USGS stream gage on the Comite River

at Comite taken on August 18, 2016, along with the flood head used for the simulation and flood head supplied in centrifuge test for Cases 1 and 6. Rate of rising of the flood head in simulation is kept similar to the hydrograph on Comite River, which is also similar to rising rate in centrifuge test in Case 6. Flood head in the numerical simulation is increased in a stepwise manner and kept constant at the maximum level for the levee of consideration.

Table 6-2 Test conditions for analysis

Cases	Level of protection	Description of protection					
		Pipe 1		Pipe 2		Pipe 3	
		R	D	R	D	R	D
Case A.1	Unreinforced	N/A	N/A	N/A	N/A	N/A	N/A
Case A.3	Steel drainage pipes	○	○	○	○	○	○
Case A.4	Only reinforcement	○	×	○	×	○	×
Case A.6	Only drainage	×	○	×	○	×	○

Note: R= reinforcement function; D= drainage function; ○ = present; × = not present
N/A= not available, pipes not used

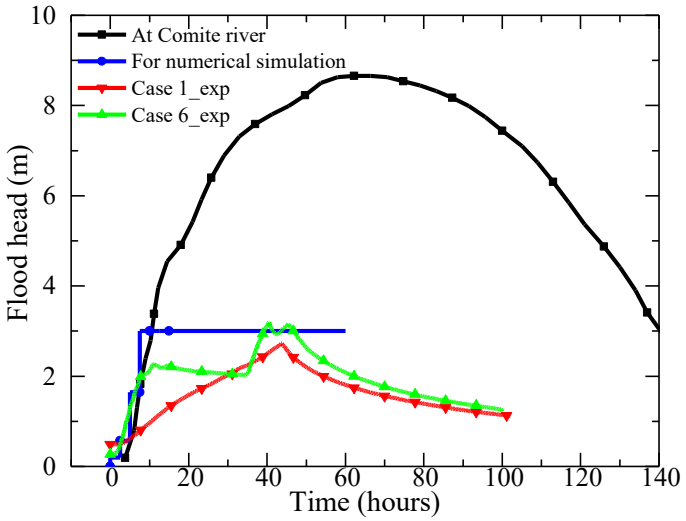

Figure 6.1 Flood approximation based on hydrograph for the USGS stream gage on the Comite River at Comite, LA. Graph taken on August 18, 2016

Figure 6.2 shows the time histories of the settlement at the shoulder of slope and horizontal displacement at the toe of the slope, respectively, for all the cases. It can be observed that with the use of protection in the river levee, the displacement is reduced significantly. The cases where the drainage is provided (Cases A.3 and A.6) both horizontal displacement and settlement are reduced significantly, highlighting the importance of the drainage function in the protection. In Case A.4 (only reinforcement), the rate of displacement increase is similar to Case A.1 (unreinforced) in the initial stage (0-15 hrs), while further increase in the displacement is restrained after that. Maximum settlement and horizontal displacement in Case A.4 are almost three times those in Case A.3 (steel drainage pipes). With the use of the only drainage (Case A.6) the settlement in the model ground is minimized to the same extent as in use of the steel drainage pipe (Case A.3). This implies that the reinforcement function is not fully utilized in Case A.3 in the scenario considered in the analysis. However, with the use of the steel drainage pipe, reinforcement may act as the backup protection in the scenario when the drainage function is disturbed possibly by blockage of pipes. The steel drainage pipes provide redundant but more reliable protection to river levee. The observation and consideration above indicate that Case A.3 (steel drainage pipe) can provide the best protection among the cases.

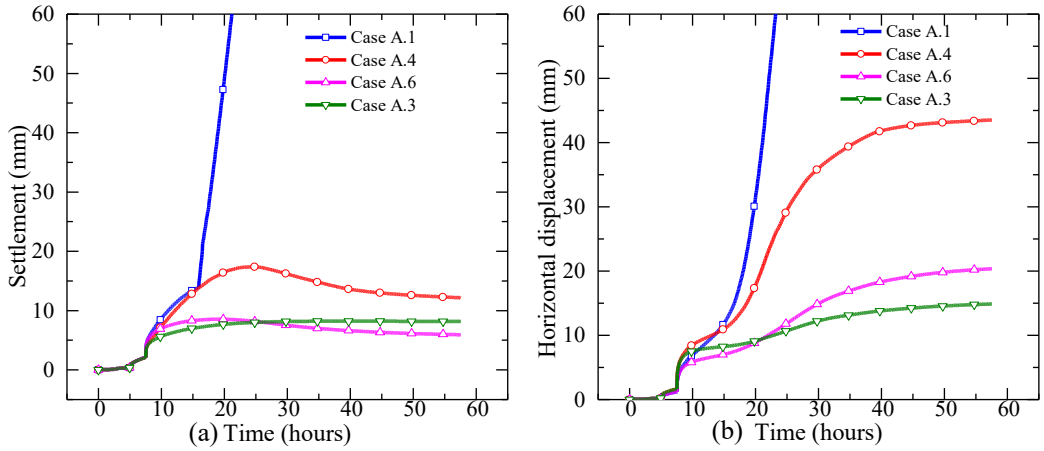

Figure 6.2 Time history of displacement for all cases (a) settlement at the shoulder of slope (b) horizontal displacement at the toe of the slope

Figure 6.3 shows the location of the phreatic surface after 40 hrs. of seepage flow for all the cases. The time duration of 40 hrs. of seepage flow is taken as a reference point to compare the phreatic surface as at this point the supply flood level is at maximum level, and change in displacement in most of the cases is stable. In the figure, it can be observed that with the presence of drainage, the location and shape of the phreatic surface in the levee is modified. The phreatic surface is at a lower position and has a concave upward shape in the cases with the drainage whereas in the absence of the drainage, the shape is concave downward and the location is high. This limited rise in phreatic surface cause limited saturation of the river levee and thus ultimately limiting deformation in cases with drainage. The presence of the reinforcement ensures the less deformation in Case A.4 (only reinforcement) compared to Case A.1 (unreinforced) even though the level of the phreatic surface is similar in both cases. Similarly, on comparing Cases A.3 and A.6, the presence of dual advantages of drainage and reinforcement in Case A.3 provides better performance than Case A.6 on minimizing the horizontal displacement.

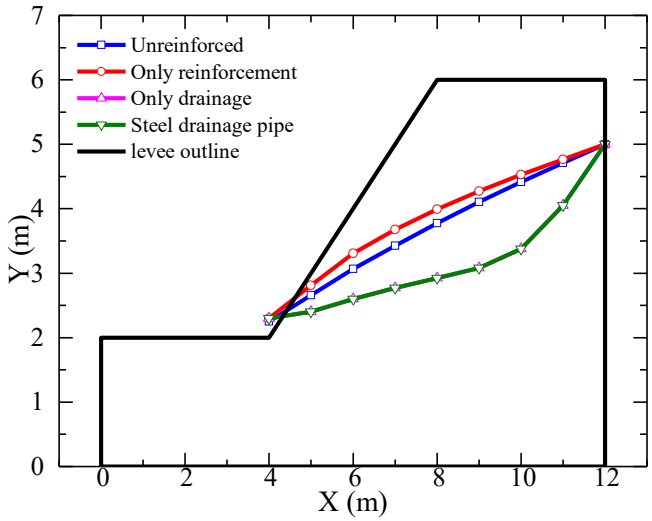

Figure 6.3. Location of phreatic surface in River levee in Cases A.1-A.4 after 40 hrs. of seepage flow

Figure 6.4 shows the axial force distribution in the pipe in Cases A.4 and A.3 (cases with only reinforcement and steel drainage pipe) at the different duration of seepage flow (10, 15, 20, 30 and 40 hrs.). Here, the axial force represents the total value of force mobilized

through the slope weight and change caused by seepage flow. **Figure 6.5** shows the location of the phreatic surface at the duration of 0, 10, 15, 20, 30, and 40 hrs. of seepage flow for Cases A.4 and Cases A.3 respectively. From the figures, it can be observed that initially at 10 hrs. of seepage flow axial force mobilized is similar in both the Cases A.4 and A.3. With the increase in the seepage flow duration location of phreatic surface changes above the location of the pipes in Case A.4, whereas there is not much change in Case A.3. This change of phreatic surface above pipe causes larger axial force mobilization is observed in Case A.4. In Case A.3, since there is not much change in the location of the phreatic surface above the pipe, axial force mobilized remains similar even after longer duration of seepage flow. Mobilization of large axial force in Case A.4 is responsible for limiting the deformation even after the rise in phreatic surface to a higher level in the river levee.

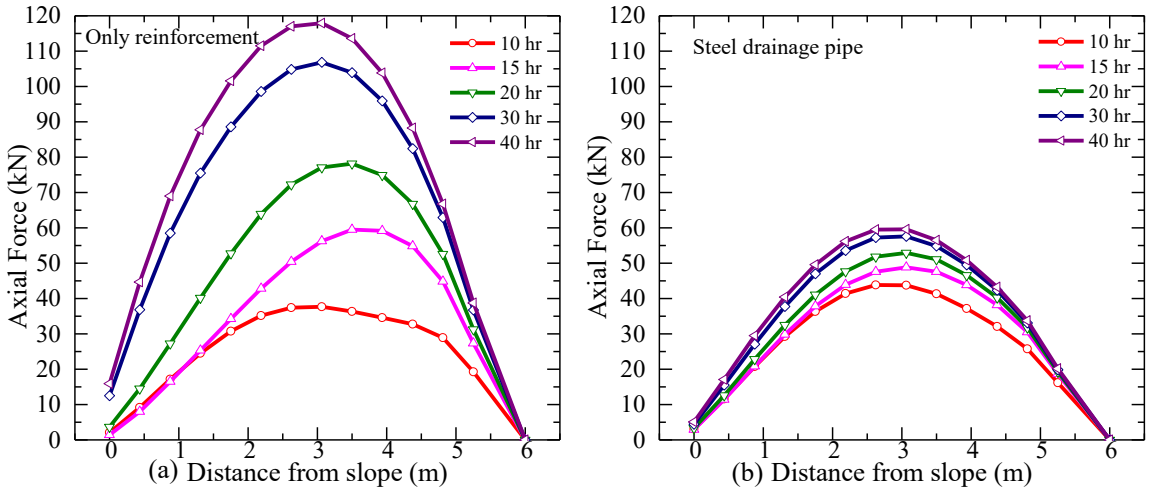

Figure 6.4. Axial force distribution in pipe (a) for Case A.4 (only reinforcement) (b) for Case A.3 (steel drainage pipe)

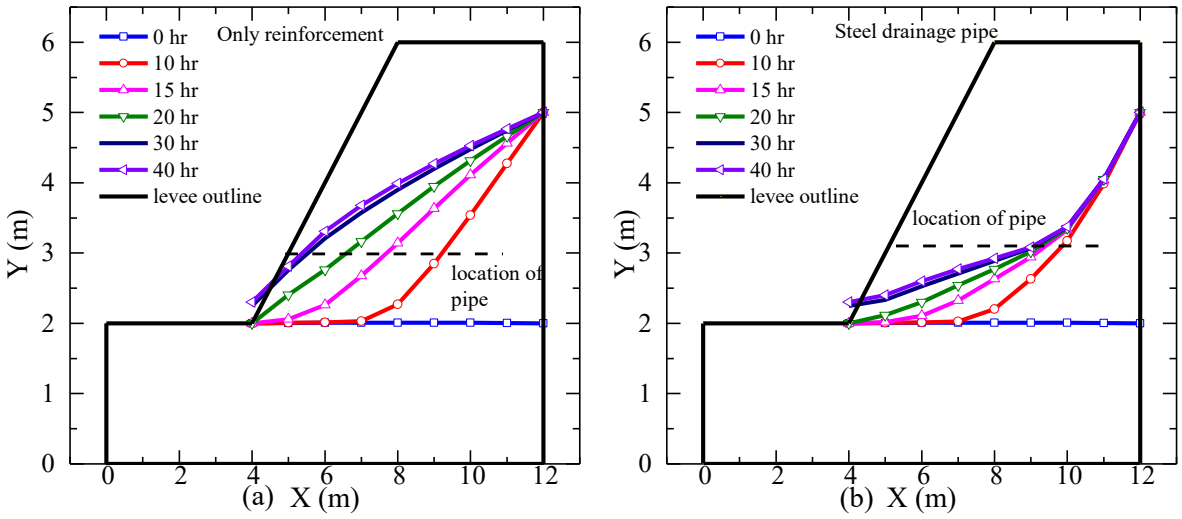

Figure 6.5 Location of phreatic surface (a) for Case A.4 (only reinforcement) (b) for Case A.3 (steel drainage pipe)

6.3 Influence of the hydraulic conductivity of soil in the performance of steel drainage pipe

Levees in generally constructed with the various types of the soil. The hydraulic conductivity of the soil varies with the type of soil. Various studies have been made to understand the effect of hydraulic conductivity of the soil in seepage induced failure of slope (Chen et al., 2009; Cho, 2014; Li et al., 2013; Rahimi et al., 2010; Santoso et al., 2011; Tsaparas et al., 2002; Zhang et al., 2015). In this series of numerical analysis, the effect of the hydraulic conductivity of the soil in the performance of levee with the steel drainage pipes is evaluated. In this series of the analysis, the hydraulic conductivity of the soil in embankment is varied in five different cases. **Table 6-3** gives the details of the values of hydraulic conductivity used in different cases. Hydraulic conductivity in analysis varies from the 4.5E-8 m/s to 4.5E-2 m/s indicating soil from fine to coarse sandy soil. In the calculation parameters of SWCC is kept same for different cases analysis.

Flood hydrograph as shown in **Fig. 6.1** is used in the numerical for all the cases. Flood is simulated in numerical analysis by increasing water level in river channel side boundary in steps. In this series of the analysis, steel drainage pipes are installed at height of 1 m

above the toe of the slope. In each cases, levee is provided with the three steel drainage pipes at the spacing of the 1 m.

Table 6-3 Hydraulic conductivity of embankment for different conditions

Cases	Hydraulic conductivity of embankment	No. of steel drainage pipes
1000k	4.5E-2 m/s	3
100k	4.5E-3 m/s	3
k	4.5E-5 m/s	3
0.01k	4.5E-7 m/s	3
0.001k	4.5E-8 m/s	3

Figure 6.6 show the time history of settlement at shoulder and horizontal displacement near toe of slope respectively for different hydraulic conductivity of soil in levee with steel drainage pipe. From the figure it can be observed that trend of rise and maximum value of the settlement and horizontal displacement is similar when hydraulic conductivity is from 4.5E-5 m/s to 4.5E-2 m/s. In the cases where the soil has lower hydraulic conductivity (4.5E-7 m/s to 4.5E-8 m/s) linear rise is a settlement and horizontal displacement is observed indicating the steady state is not achieved in the assumed seepage duration in the analysis. **Figure 6.7** shows the time history of settlement at the shoulder and horizontal displacement near the toe of slope respectively for different hydraulic conductivity of soil in the unreinforced levee. The trend and values of settlement and hydraulic conductivity in unreinforced levee and in case of levee with steel drainage pipes are very similar to each other. In these cases deformation is very small due to small change in effective stress. This indicates that levee which do not require reinforcement show small deformation with or without presence of the steel drainage pipes.

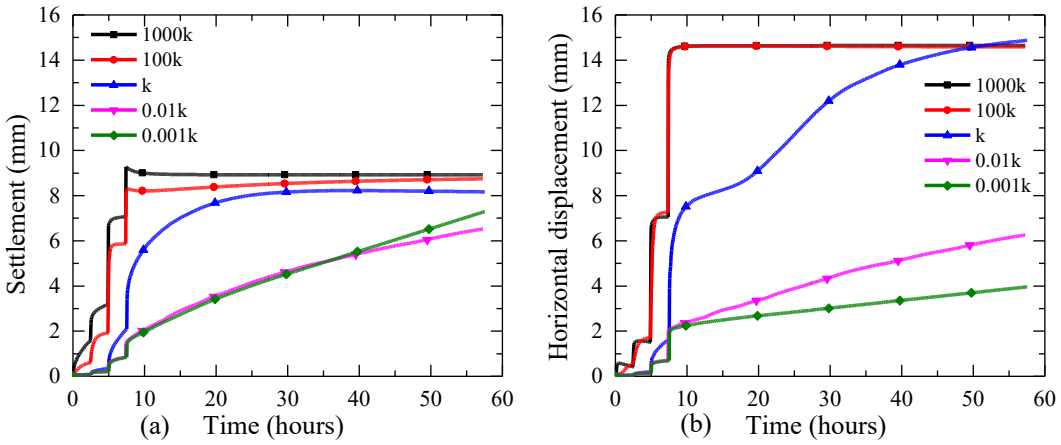

Figure 6.6 Time history of (a) settlement at the shoulder (b) horizontal displacement near the toe of slope for different hydraulic conductivity of soil in levee with steel drainage pipes

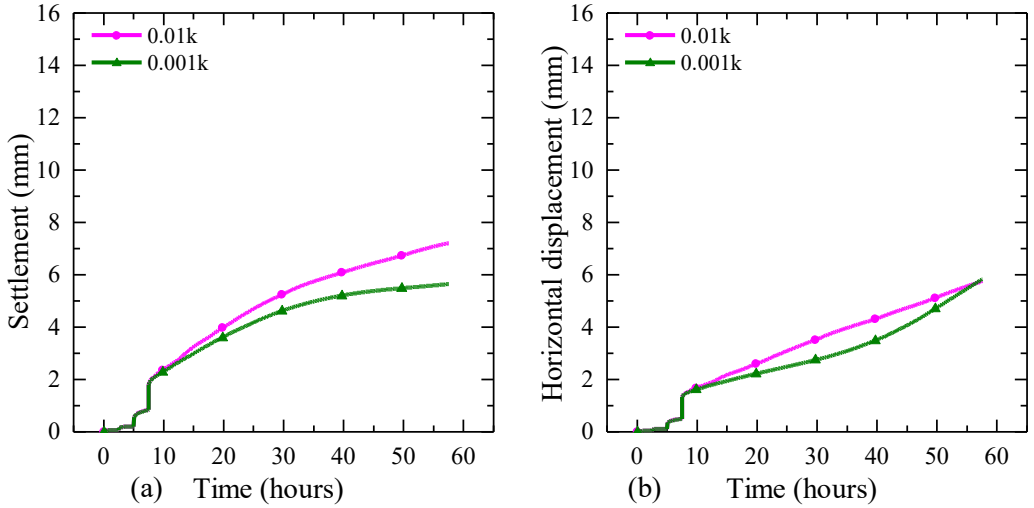

Figure 6.7 Time history of (a) settlement at the shoulder (b) horizontal displacement near the toe of slope for different hydraulic conductivity of embankment soil in the unreinforced levee

Figure 6.8 shows the time history of pore water pressure on top of foundation level at 1.6 m and 5.6 m away from the toe of the slope for different hydraulic conductivity of embankment soil in levee with steel drainage pipes. From the figure, it can be observed that near the slope, the maximum value of pore water pressure is in two groups. For higher hydraulic conductivity (4.5E-5 m/s to 4.5E-2 m/s), the maximum value is almost 6.5 kPa, and for lower hydraulic conductivity soil (4.5E-7 m/s to 4.5E-8 m/s) maximum value is

almost 2.5 kPa for considered seepage duration. Further away from the toe of the slope at 5.6 m, maximum value of pore water pressure is the same for all the cases as the influence of soil hydraulic conductivity is not fully realised in this region. Also, with the increase in hydraulic conductivity of the soil, instantaneous rise in the pore water pressure is observed.

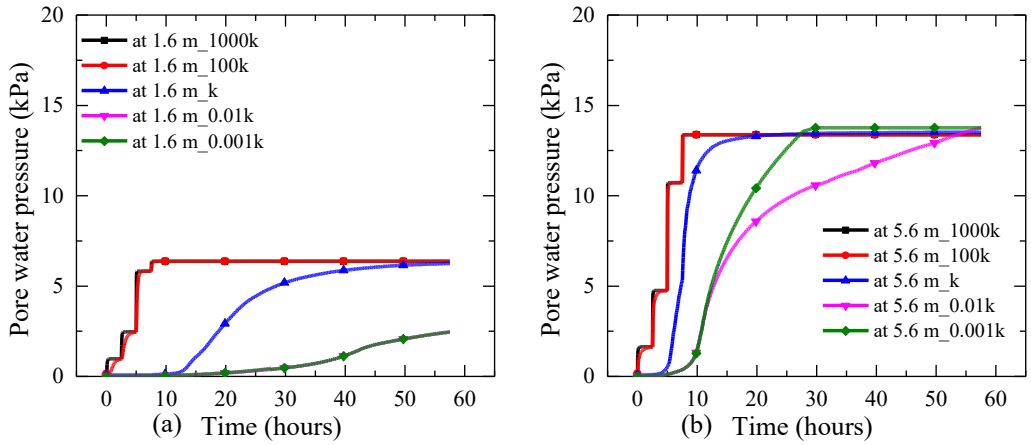

Figure 6.8 Time history of pore water pressure (a) at 1.6 m (b) at 5.6 m from the toe of slope on top of foundation for different hydraulic conductivity of embankment soil in levee with steel drainage pipes

Figure 6.9 shows the change in pore water pressure in levee provided with steel drainage pipes with increase in flood head at two different locations; at 1.6m and 5.6 m from the toe of slope for soil with different hydraulic conductivity. From the figure it can be observed that pore water pressure developed in levee is higher throughout the levee in soil with hydraulic conductivity from range 100k to 1000k (4.5E-3 m/s to 4.5E-2 m/s) for any given flood head. For the soil having hydraulic conductivity from range of k to 1000k (4.5E-5 m/s to 4.5E-2 m/s) the maximum pore water pressure developed near the toe is same and equal to 6.35 kPa. **Figure 6.10** shows the pore water pressure developed under different hydraulic conductivity of soil for different flood head at 1.6 m away from toe of slope. From the figure it can be observed that at any flood head pore water pressure developed in soil from range 100k to 1000k (4.5E-3 m/s to 4.5E-2 m/s) is constant. At higher flood head of 3.0 m maximum pore water pressure developed can be divided in

two groups; lower hydraulic conductivity soil group (4.5E-7 m/s to 4.5E-8 m/s) and higher hydraulic conductivity group (4.5E-5 m/s to 4.5E-2 m/s).

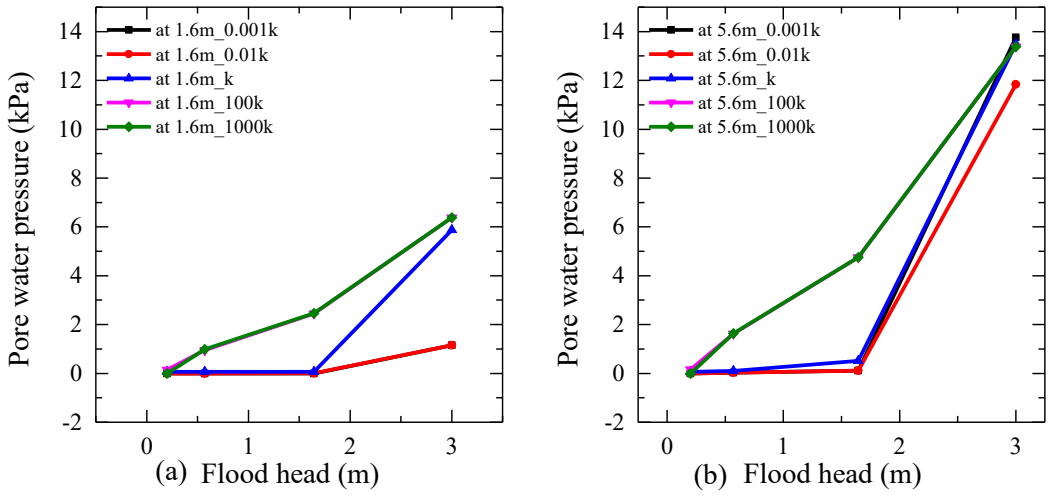

Figure 6.9 Change in pore water pressure with flood head for different hydraulic conductivity of embankment soil in levee (a) at 1.6 m (b) at 5.6 m from toe of slope

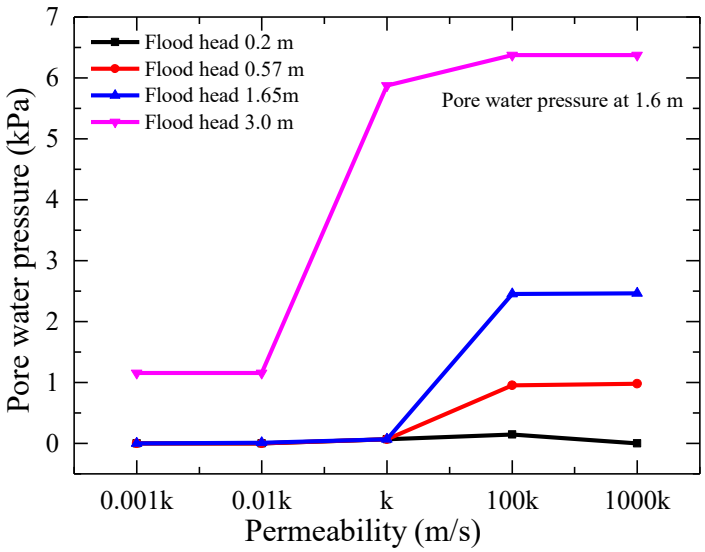

Figure 6.10 Pore water pressure development under different hydraulic conductivity of embankment soil at different supply flood head

Figure 6.11 shows the time history of pore water pressure on top of the foundation level at 1.6 m and 5.6 m away from the toe of the slope for different hydraulic conductivity of embankment soil in the unreinforced levee. On comparing the development of the pore water pressure in the unreinforced case, it can be observed that near the slope surface

maximum value of pore water pressure with and without steel drainage pipes is very similar. This inability of steel drainage pipes in lowering the pore water pressure near the slope surface in soil with lower hydraulic conductivity is the reason for no improvement in deformation with the installation of steel drainage pipes.

Thus from these series of analysis, it can be concluded that deformation in levee with steel drainage pipes made of soil with hydraulic conductivity from 4.5E-5 m/s to 4.5E-2 m/s remains consistent across different types of soil. In the soil with very low hydraulic conductivity, installation of the steel drainage pipes do not contribute to the lowering of pore water pressure and hence the deformation as well.

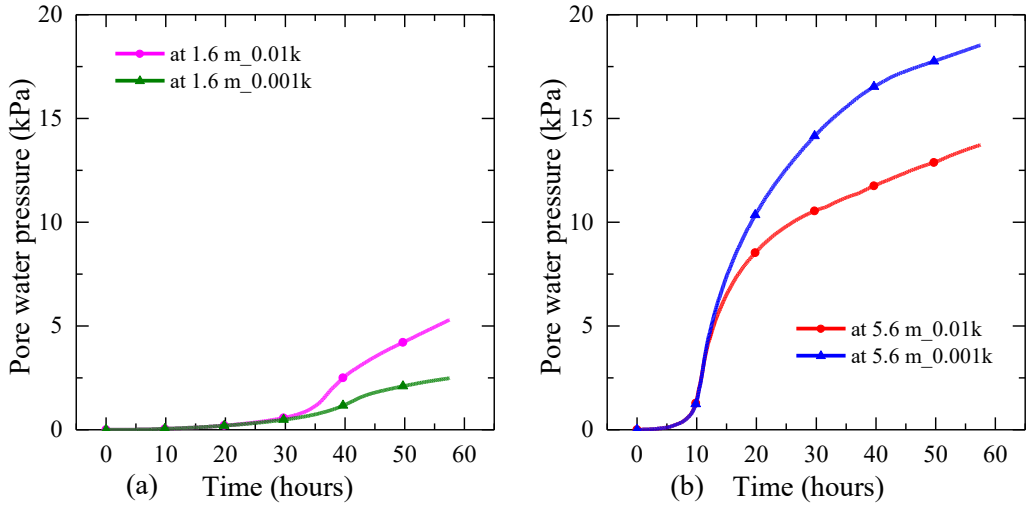

Figure 6.11 Time history of pore water pressure (a) at 1.6 m (b) at 5.6 m from the toe of slope on top of foundation for different hydraulic conductivity of embankment soil in the unreinforced levee

6.4 Influence of flooding condition in the performance of steel drainage pipe

Flood level rise within the river channel varies with the width of the river channel, the gradient of the river, and amount of rainfall. This difference in the rising rate of the flood water level causes a difference in seepage rate in the levee. Various studies have been made in the effect of seepage rate in the stability of slope (Gasmo et al., 2000; Kristo et al., 2017; Miao et al., 2018; Song et al., 2018; Sun et al., 2017). From these studies, it is

concluded that with the rise in the rate of the seepage, the stability of the slope is affected. In this section, the effect of the rising rate of the flood on the performance of the levee reinforced with steel drainage pipe is studied and compared to the unreinforced levee subjected to varying flooding conditions.

6.4.1 Unreinforced levee

In this series of the analysis, the unreinforced levee is subjected to the varying the flooding condition. The reference flood hydrograph is taken as flood applied in the unreinforced case in centrifuge test discussed in Chapter 2. The rising rate of flood in this series of analysis is varied. The rising rate of the flood is defined by the time required to reach the maximum flood level. **Table 6-4** lists out the flooding conditions for all the cases of analysis.

Table 6-4 Flooding conditions for numerical analysis for unreinforced levee

Case ID	The time required to reach maximum flood	Description
Seepage rate (t)	40 hours	Same as the centrifuge test
Seepage rate (2t)	20 hours	Maximum flood level reached in half time of the experiment
Seepage rate (10t)	4 hours	Maximum flood level reached in one-tenth of experiment
Seepage rate (inst.)	instantaneous	Maximum flood level reached instantaneously
Seepage rate (0.5t)	80 hours	Maximum flood level reached in the double time of the

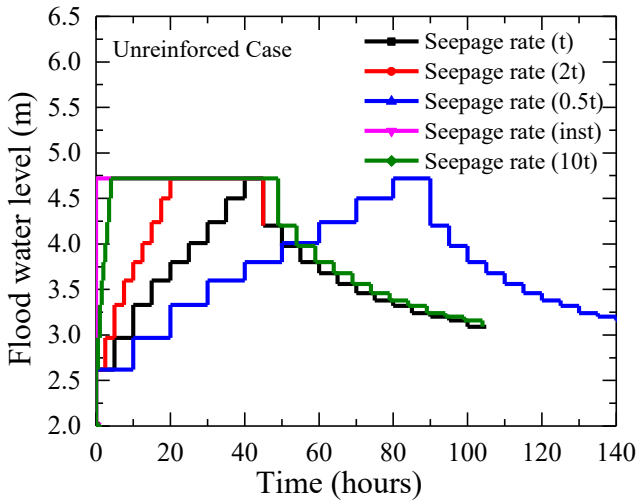

Figure 6.12 Different flood hydrograph used for analysis in the unreinforced levee

Figure 6.12 shows the flood hydrograph used for numerical analysis to study the impact of different flood rising rate in the performance of levee against the flooding. Maximum flood level for each flooding condition is kept constant for analysis. Also, the lowering speed of flood level is kept similar for all the flooding conditions. The initial condition for all the cases is all assumed to be the same. The flood level rising rate in this series of analysis varies from 0.02m/hr to instantaneous rise (infinity).

Figure 6.13 shows the change in the phreatic surface in the levee at the different duration of seepage flow for different flooding condition for the unreinforced slope. From the figure, it can be observed that even though the final phreatic surface is very similar in all the flooding condition, the progression of the phreatic surface varies significantly with the flooding condition. In cases where flood level rising rate is relatively slow (t, 2t, 0.5t), the rise in the phreatic surface is relatively uniform across the levee cross-section. Phreatic surface in such cases is linear. In cases with faster flood level rising rate (inst., 10t), the rise in the phreatic surface is not uniform across the levee cross-section. In these cases, the phreatic surface is the more curvilinear shape. While levee is subjected to quicker flood rising rate, a region near the toe is subjected to higher phreatic surface within the short duration of the seepage flow.

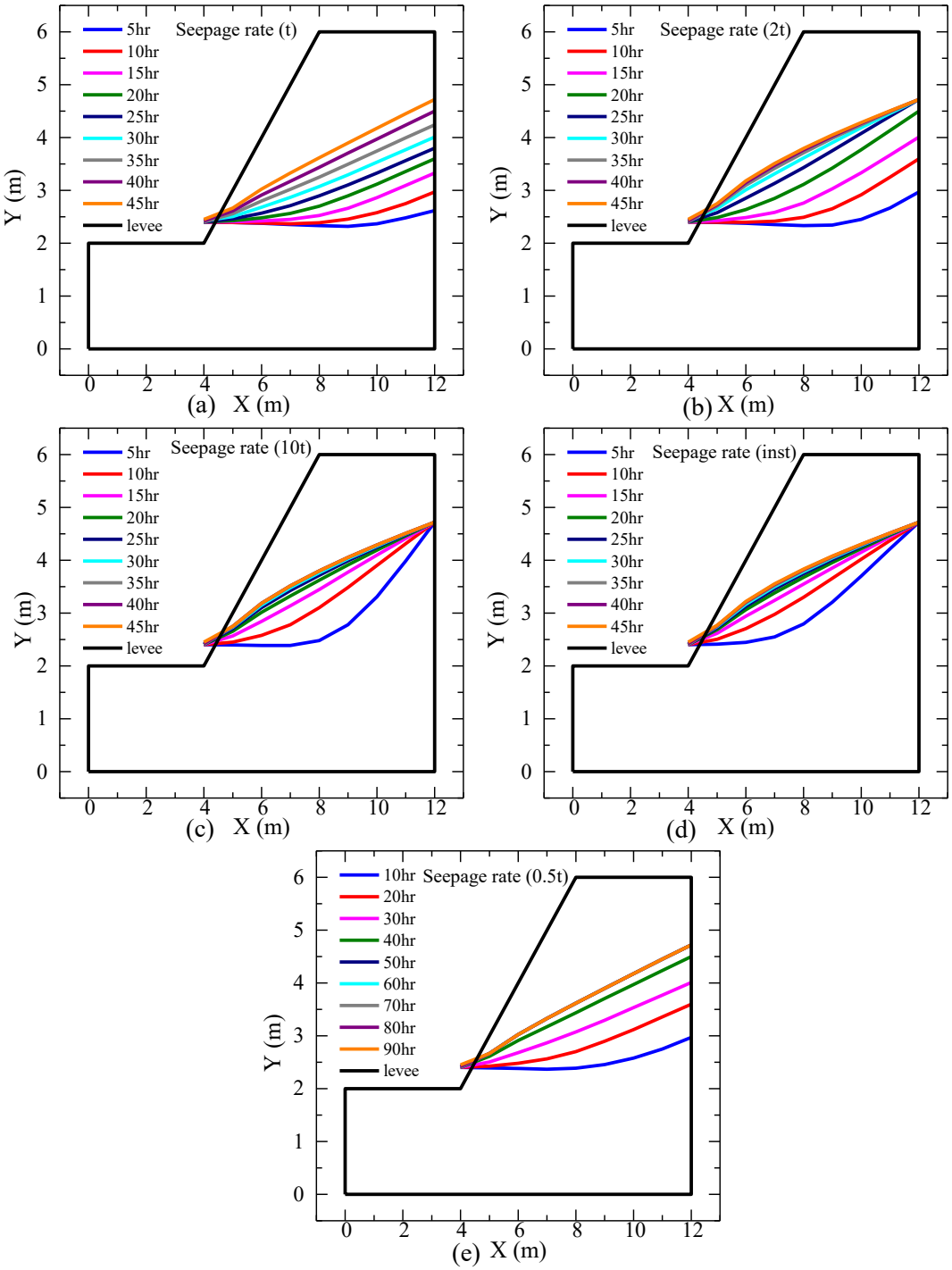

Figure 6.13 Change in phreatic surface level with seepage flow for (a) Seepage rate (t) (b) Seepage rate (2t) (c) Seepage rate (10t) (d) Seepage rate (inst) (e) Seepage rate (0.5t)

As it is established that toe region of the slope is susceptible for the initiation of the failure in unreinforced slope, this higher phreatic surface from an early stage of seepage flow makes the slope more vulnerable to the failure. The quicker the flood level rises, a larger area of the slope is below the phreatic in short span of time. Thus, a larger area of the slope is saturated in a short span of time, making the strength reduction of slope quicker.

Figure 6.14 shows the time history of the horizontal displacement near the toe of the slope for different flooding conditions in the unreinforced levee. From the figure, it can be observed that maximum horizontal displacement for quicker flood level rising rate (seepage rate inst., 10t) is very similar equal to the 150 mm and for the slower rate of rising of the flood (seepage rate t, 2t, 0.5t) maximum horizontal displacement is almost 110 mm. In addition to this from the figure, it can be observed that once horizontal displacement reaches 20 mm, there is a quick rise in horizontal displacement in Cases with seepage rate t, 2t, 10t and instantaneous. This quick rise of horizontal displacement is indicative of initiation of slope collapse. However, with a slower rise of the flood rising rate, the quick rise in horizontal displacement is observed only after the horizontal displacement reaches 40 mm. Thus, flood rising rate effects the maximum deformation in slope and also the initiation of the slope collapse.

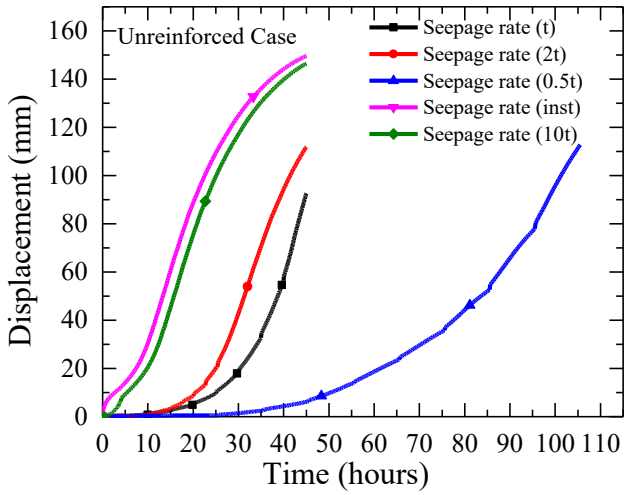

Figure 6.14 Time history horizontal displacement near the toe of the slope for different flood rising rate in unreinforced slope.

6.4.2 Levee with steel drainage pipes

Table 6-5 Flooding conditions for numerical analysis for levee with steel drainage pipes

Case ID	Time required to reach maximum flood level	Description
Seepage rate (t)	50 hours	Same as the centrifuge test
Seepage rate (2t)	25 hours	Maximum flood level reached in half time of centrifuge test
Seepage rate (10t)	5 hours	Maximum flood level reached in one-tenth of centrifuge test
Seepage rate (inst.)	instantaneous	Maximum flood level reached instantaneously
Seepage rate (0.5t)	100 hours	Maximum flood level reached in the double time of centrifuge

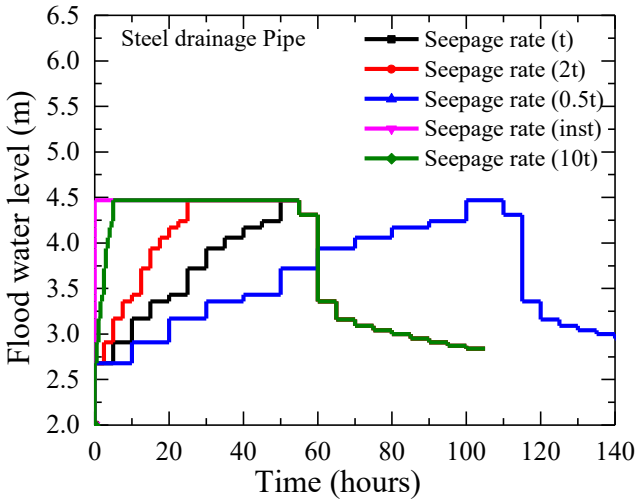

Figure 6.15 Different flood hydrograph for analysis in levee with steel drainage pipes

In this series of the analysis, levee provided with three steel drainage pipe at the height of 1 m from the toe slope at a spacing of 1 m is subjected to the varying the flooding condition. The reference flood hydrograph is taken as flood applied in the case with steel drainage pipe in centrifuge test (Case 2) discussed in chapter 2. The rising rate of the flood is varied in this series of analysis. **Table 6-5** lists out the flooding conditions for all the cases of analysis. **Figure 6.15** shows the flood hydrograph used for numerical analysis to study the impact of different flood rising rate in the performance of levee against the

flooding. Maximum flood level for each flooding condition is kept constant for analysis. Also, the lowering speed of flood level is kept similar for all the flooding conditions. The initial condition for all the cases is all assumed to be the same. The flood level rising rate in this series of analysis varies from 0.018 m/hr to instantaneous rise (infinity).

Figure 6.16 shows the change in the phreatic surface in the levee at the different duration of seepage flow for different flooding condition for the levee with steel drainage pipes. In this series of analysis, steel drainage pipe is located at the height of 3 m (i.e., 1 m above the toe of the slope). From the figure, it can be observed that even though there is a change in flooding condition progression of the phreatic surface does not change significantly with the flooding condition. Phreatic surface, especially near the slope surface, remains very similar in all condition of the flood rising rate. Also, the location of the maximum level of the phreatic surface remains consistent regardless of the change in flooding condition. Deformation behavior of the slope is dependent on the phreatic surface in the slope, thus with the use of the steel drainage pipes response of levee for varying flooding condition can be maintained consistent.

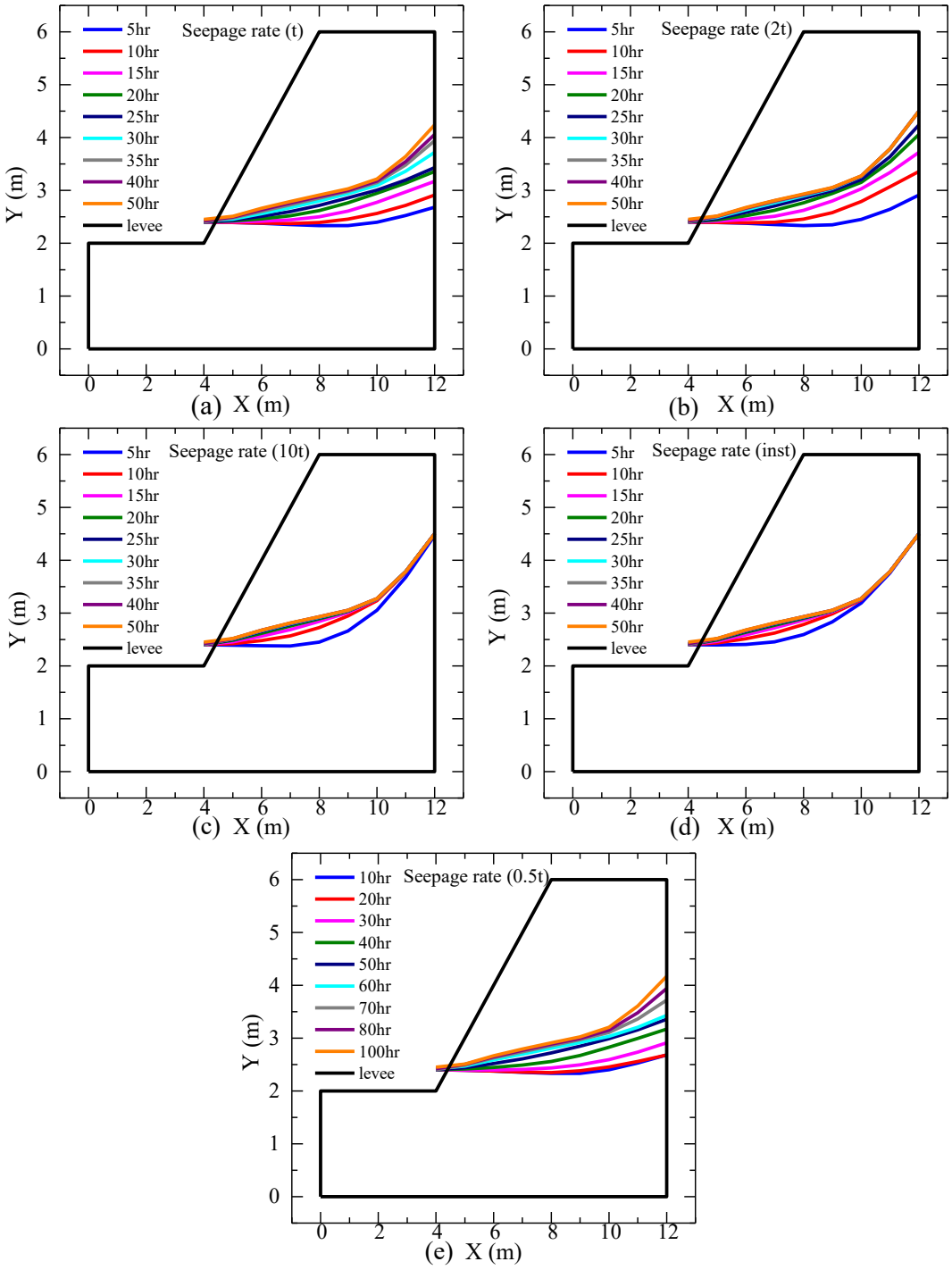

Figure 6.16 Change in phreatic surface level with seepage flow for (a) Seepage rate (t) (b) Seepage rate (2t) (c) Seepage rate (10t) (d) Seepage rate (inst) (e) Seepage rate (0.5t)

Figure 6.17 shows the time history of the horizontal displacement near the toe of the slope for different flooding conditions levee provided with steel drainage pipes. From the figure, it can be observed that the maximum value of the horizontal displacement near the toe of the slope remains constant regardless of change of the rising rate of flood level. From the figure, it can also be observed that horizontal displacement is dependent on the flood level rather than the speed of rise of flood level. Displacement at the same flood level is the same in all conditions, independent of the speed at which flood level is reached.

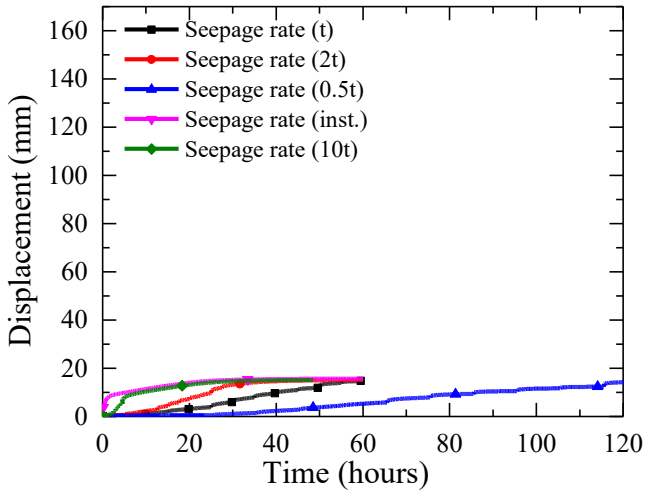

Figure 6.17 Time history horizontal displacement near the toe of the slope for different flood rising rate in unreinforced slope.

Figure 6.18 shows the pore water pressure developed at different location after 35 hours of seepage flow in unreinforced levee and levee with steel drainage pipe. In the figure it can be observed that after 35 hours of seepage flow pore water pressure developed in slope can be divided in two groups for both unreinforced and levee with steel drainage pipe. Variation of pore water pressure developed near toe of slope in unreinforced case is about 185 % whereas in levee with steel drainage pipe is about 65% with the change in speed of raising the flood. So with the use of steel drainage pipe the fluctuation of pore of water pressure with change in speed of flooding is minimized.

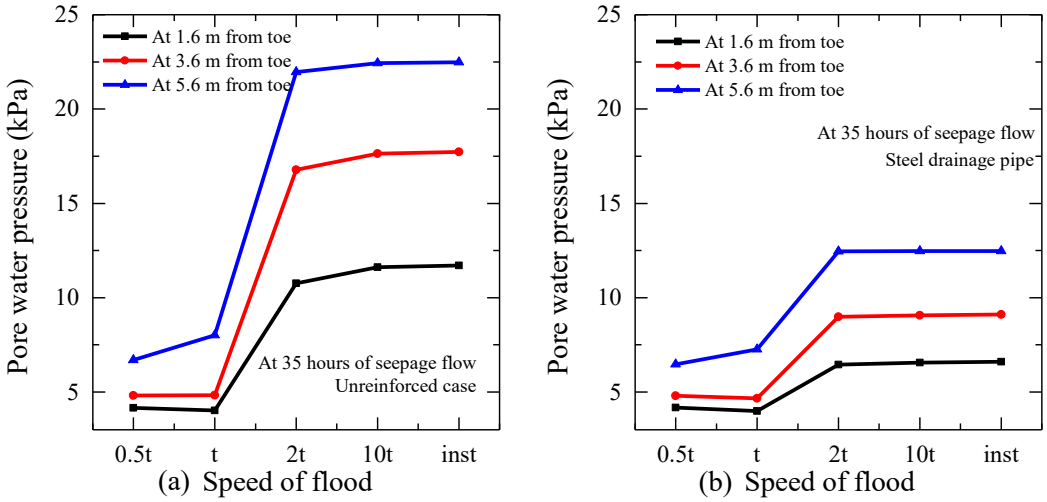

Figure 6.18 Pore water pressure at different location after 35 hours of seepage for different flooding condition in (a) unreinforced levee(b) levee with steel drainage pipes

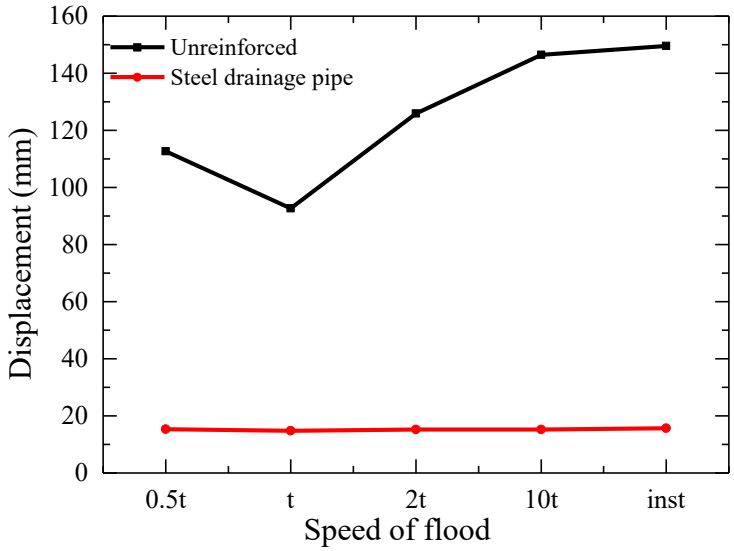

Figure 6.19 Change in maximum horizontal displacement near toe of slope with change in flooding condition in unreinforced levee and levee with steel drainage pipe

Figure 6.19 shows the change in maximum horizontal displacement near the toe of the slope with the change in the speed of raising the flood level. With the use of the steel drainage pipes in levee maximum horizontal displacement near toe becomes independent of the speed of raising the flood level. In unreinforced levee however maximum

displacement is dependent on flooding condition and maximum variation of 60% (between flood speed t and instantaneous speed) with the change in speed of raising flood level is observed.

From this series of the analysis where the speed of rising of flood level is varied in different cases, the following conclusion is obtained:

i. In unreinforced levee, speed of flooding rising level effects the progression of phreatic surface within the levee whereas in the case provided with steel drainage pipes progression is minimally affected by the speed of rising of flood level.
ii. Speed of the rise of flood level in unreinforced case cause the change in the maximum value of deformation
iii. Maximum deformation in levee with steel drainage pipe is independent of the speed of rising of flood level; rather, it is dependent on the flood level only.

6.5 Influence of the steel drainage pipe arrangement and spacing

6.5.1 Influence of arrangement of steel drainage pipes

In this series of the numerical analysis, the effect of the arrangement and spacing of steel drainage pipes in the performance of levee subjected to the flooding is evaluated. Various studies have been made to study the influence of the spacing and arrangement of drainage pipes in the hydraulic behavior of the levee subjected seepage flow (Lau and Kenney, 1984; Rahardjo et al., 2003; Resnick and Znidarcic, 1990). Also, studies have been made for the effect of the spacing and arrangement of the soil nail in control of deformation in the slope subjected to seepage flow (Cai and Ugai, 2000; Taylor et al., 2012; Wei and Cheng, 2009). From these studies, it is concluded that it is desirable that to maximize the drainage function pipe should be placed at the lower region of the slope while to maximize the reinforcement pipes/nails should be placed at mid-height of the slope. The closer spacing is desired for both drainage and reinforcement pipes. In this series of analysis, the optimum position of the steel drainage pipes having the dual function of drainage and reinforcement is investigated.

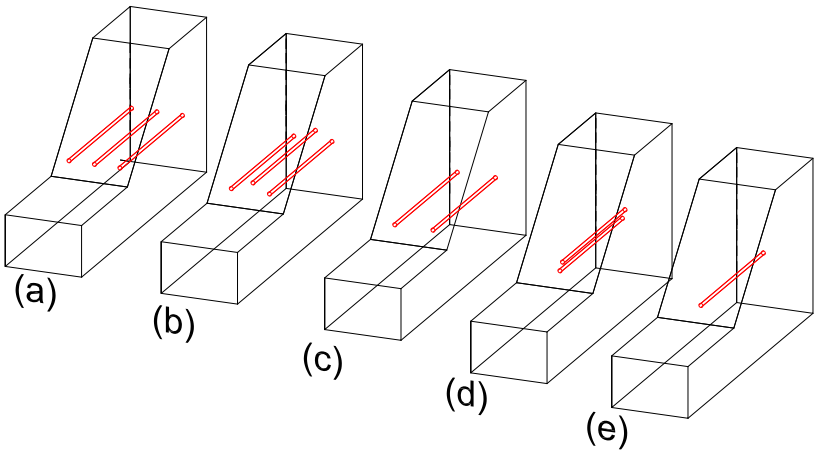

Figure 6.20 Arrangement of pipes in model ground (a) Case B.1 (b) Case B.2 (c) Case B.3 (d) Case B.4 (e) Case B.5

Table 6-6 Test conditions for analysis

Cases	No. of pipes	Height of installation	Arrangement on plan
Case B.1	3	All pipes at 1m above the toe	at a spacing of 1 m
Case B.2	3	2 pipes at 1m above the toe, 1 pipe at 1.5m above the toe	bottom pipes at a spacing of 1.5 m, an upper pipe at mid-span
Case B.3	2	All pipes at 1m above the toe	at a spacing of 1.5m
Case B.4	2	1 pipe at1m above the toe, 1 pipe at 1.5m above the toe	at mid-span
Case B.5	1	At 1m above the toe	At mid-span

In this series of the numerical analysis, five different cases, B.1-B.5 is evaluated. The details of the test conditions are presented in **Table 6-6**. **Figure 6.20** shows the arrangement of pipes in Cases B.1-B.5 in the model ground. In this series of test condition, the spacing of the pipes and the height of installation is varied. In all the test cases soil

properties are kept constant the same as used in a series of centrifuge test (refer **Table 6-1**). The model ground in all the test condition is subjected to the same flood hydrograph. Flood hydrograph shown in **Fig. 6.1** is used in the numerical analysis.

Figure 6.21 shows the time history of horizontal settlement near the toe of the slope for all Cases B.1-B.5. The trend of development of horizontal displacement is similar in all cases. Maximum horizontal displacement in the model ground varies with the cases. Maximum horizontal displacement in the model ground is dependent on the number of steel drainage pipes at the lower height. In Case B.1, three numbers of pipes are present at a lower height and thus have the lowest horizontal displacement. In Case B.2 and B.3, two pipes are present at a lower height, so the horizontal displacement is similar to each other. In Case B.2, even though the additional pipe is present at a higher level, its contribution to the reduction of horizontal displacement is not significant. A similar trend is observed in Case B.4 and B.5. Additional pipe at a higher position in Case B.4 does not have significant contribution in minimizing horizontal displacement.

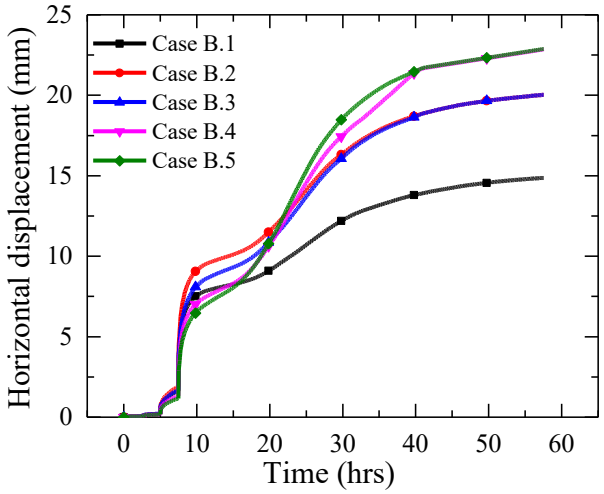

Figure 6.21 Time history of horizontal displacement near the toe of slope for all cases

Figure 6.22 shows the time history of settlement at the shoulder of the slope for all Cases B.1-B.5. The trend of change in a settlement with seepage flow is similar in all cases. Peak settlement in model ground varies with the number and arrangement of pipes. Higher the number of pipes less is the value of the peak settlement. Pipes arranged in a

row provides better minimization in settlement compared to the pipes arranged in layers if an equal number of pipes are used (Peak settlement of Case B.1< Case B.2, Case B.3<Case B.4).

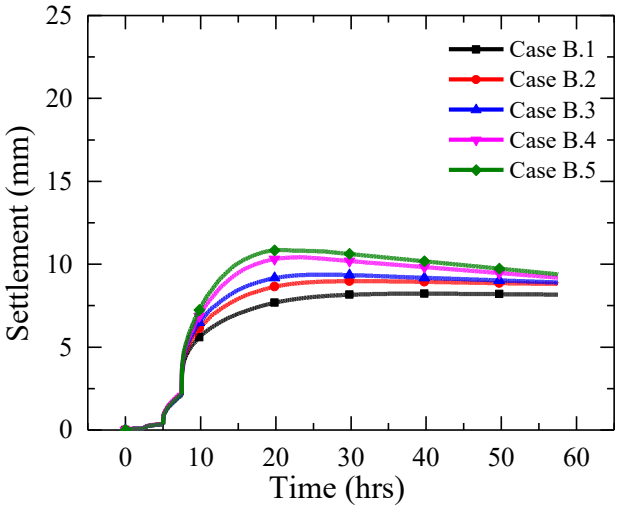

Figure 6.22 Time history of settlement at the shoulder of slope for all the cases

Figure 6.23 shows the time history of the pore water pressure on the top of the foundation at 1.6 m and 5.6 m from the toe of slope respectively for Cases B.1 –B.5. Here evaluating the time history of pore water pressure at two different locations, it can be observed as follows:

- Pore water pressure in Case B.1< CaseB.2=Case B.3< Case B.4 =Case B.5

Thus the overall drainage is governed by the pipes present at the lower height. If the pipes are present in the layer, the pipes present at the higher position in the slope do not have significant contribution in overall drainage of the slope. This hydraulic behavior is in accordance with the horizontal displacement at the toe of the slope.

Figure 6.24 shows the bending moment distribution in the pipe present at the lower elevation when the flood level is maximum in the model ground. Here the bending moment represents the total value of bending moment result of the slope weight and change caused by seepage flow. Bending moment mobilization is the result of the

differential settlement. If the differential settlement is higher, bending moment mobilization will also be higher. **Figure 6.25** (a-b) show the variation in the bending moment distribution in pipes present in different elevation in Cases B.2 and B.4, respectively. In the cases, where the pipes are present in layers (Case B.2 and B.4), bending moment mobilized in pipes present in lower elevation is less compared to other cases in which steel drainage pipe is installed in a single row. In Case B.5, only one pipe is installed, and hence the bending moment mobilized is the maximum. For cases where the pipes are present in different rows (Case B.2 and B.4), larger bending moment is mobilised in the pipes in higher elevation. Hence pipes installed at a higher elevation is more efficient in bending moment mobilization.

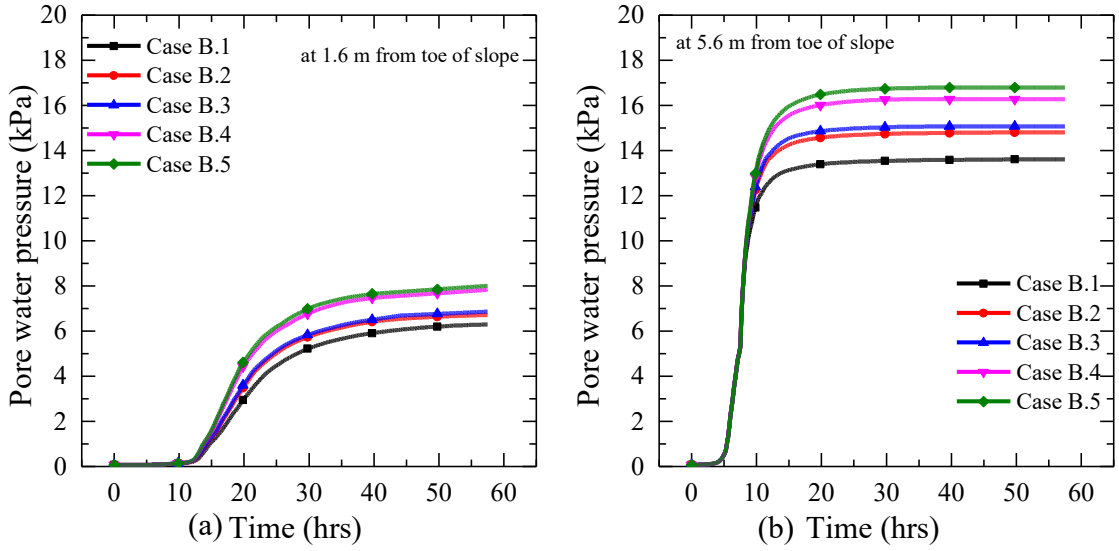

Figure 6.23 Time history of pore water pressure on top of the foundation (a) at 1.6 m from the toe of slope (b) at 5.6 m from the toe of the slope

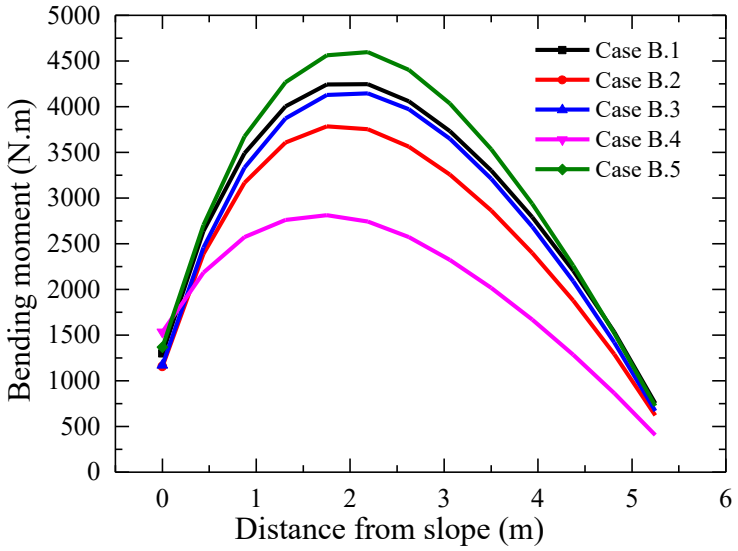

Figure 6.24 Bending moment distribution in the pipe at maximum flood level in all cases

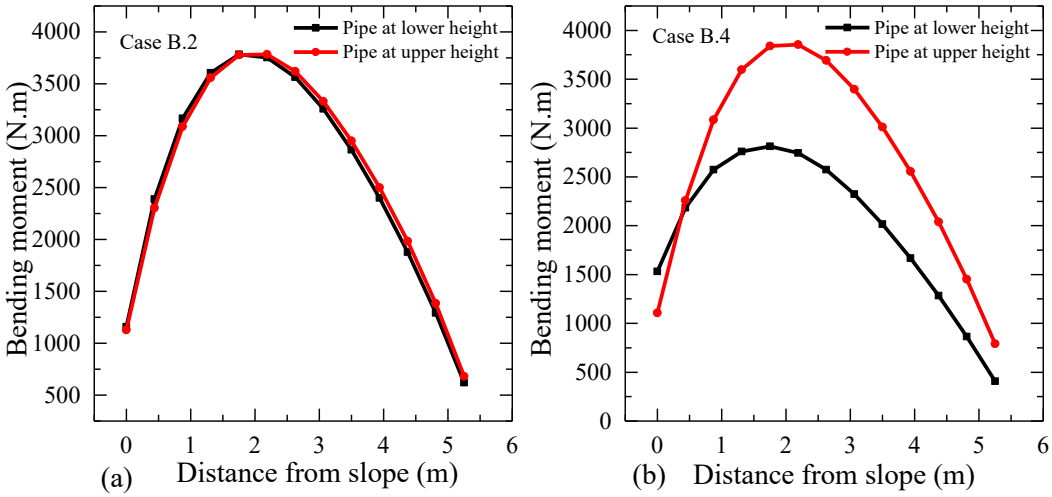

Figure 6.25 Change in distribution of bending moment in pipe installed at varying height (a) for Case B.2 (b) for Case B.4

Figure 6.26 shows the distribution of the axial force mobilized in pipe present at a lower elevation at maximum flood level for Cases B.1- B.5. **Figure 6.27 (a-b)** shows the change in the distribution of axial force in pipe installed at different elevations in Case B.2 and Case B.4, respectively. Axial force mobilized in the individual pipe is higher in the cases with a fewer number of pipes. Axial force mobilized in pipes at a higher elevation is slightly greater than pipe present at a lower elevation as shown in **Fig. 6.27.**

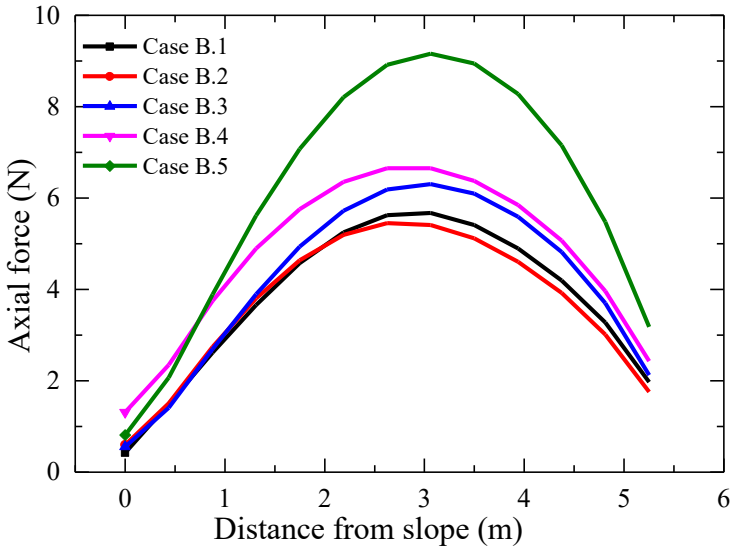

Figure 6.26 Axial force distribution in the pipe at maximum flood level in all cases

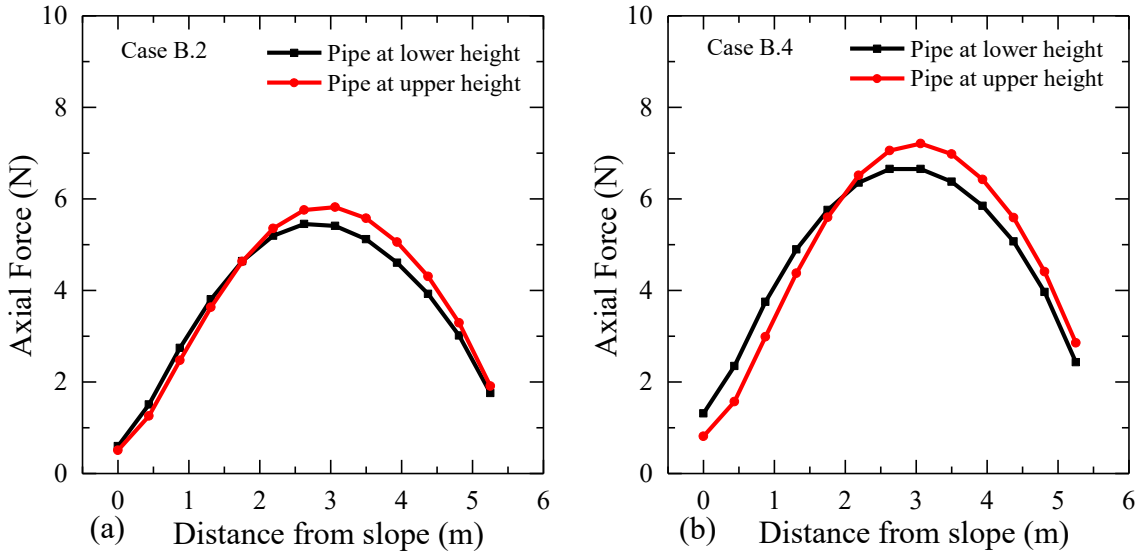

Figure 6.27 Change in distribution of axial force in pipe installed at varying height (a) for Case B.2 (b) for Case B.4

From the pore water pressure, bending moment distribution and axial force distribution it is observed that if only reinforcement function is considered the installation of pipes at mid-level of the slope is more effective whereas considering drainage function installing the pipes at a lower elevation is more effective. Installation of the pipes in the different layer will not have an additional contribution in the drainage in slope. However, the

reinforcing force mobilized in steel drainage pipes will be increased by installing the pipes in layers. The overall deformation of the slope is more controlled by the location of the phreatic surface within the slope. Thus installation of the steel drainage pipe at lower elevation would be more effective in minimizing deformation in slope subjected to flooding.

6.5.2 Influence of spacing of steel drainage pipes

In this series of analysis influence of spacing of the steel drainage pipes installed in a single row in overall deformation of the slope is evaluated. For this series of the analysis model ground of same cross section, material properties in the previous section but with longer length is taken into consideration. The length of the model ground is considered as 8 m. The model ground is subjected as the same flood hydrograph in the previous section.

Figure 6.28 shows the change in the maximum value of settlement observed at the shoulder of the slope in mid-span of the slope with the change in spacing between the steel drainage pipes. From the figure, it can be observed that for the spacing between pipes from 2 -5 m, the maximum settlement at the shoulder remain similar. For spacing lower than 2 m, there is a significant reduction in the maximum settlement and for cases with spacing greater than 5 m significant increase in the maximum settlement is observed. Thus, with very large spacing between pipes, installation of the pipes would have no contribution in minimization of deformation.

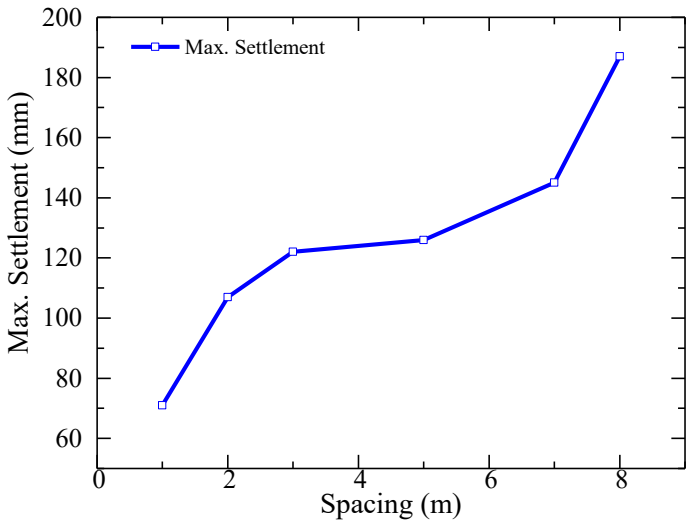

Figure 6.28 Change in the maximum settlement at the shoulder with the spacing between steel drainage pipes

6.6 Summary

In this chapter series of the parametric studies were made using the numerical analysis. From these numerical analysis following conclusion are made:

- Use of steel drainage pipe provides better protection than the pipes with only drainage and reinforcement when subjected to the same flooding.
- On comparing the pipes with only drainage and only reinforcement, pipes with drainage provide better protection against flooding.
- Deformation in levee with steel drainage pipes made of soil with hydraulic conductivity from 4.5E-5 m/s to 4.5E-2 m/s remains consistent across the range.
- In the soil with very low hydraulic conductivity, when there is small deformation installation of the steel drainage pipes do not contribute to the lowering of pore water pressure and consequently to the deformation as well.
- In unreinforced levee, speed of flooding rising level effects the progression of phreatic surface within the levee whereas in the case provided with steel drainage pipes progression is minimally affected by the speed of rising of flood level.

- Speed of the rise of flood level in unreinforced case cause the change in the maximum value of deformation
- Maximum deformation in levee with steel drainage pipe is independent of the speed of rising of flood level; rather, it is dependent on the flood level only.
- The overall deformation of the slope is more controlled by the location of the phreatic surface within the slope. Thus installation of the steel drainage pipe at lower elevation would be more effective in minimizing deformation in slope subjected to flooding.
- Closer spacing of steel drainage pipes will provide lower deformation; however, for the range of the spacing of 2-5 m model ground goes under similar deformation and at very large spacing, the installation of steel drainage pipes will provide no improvement in deformation control.

7 Conclusions and recommendations

In this study use of steel drainage pipe which is new technique to protect the levee against flooding is proposed. Through this study working mechanism of steel drainage pipes, advantages over other method of protection and the performance levee with steel drainage pipe under the various condition of flooding, material properties and arrangement are discussed through chapter 2-6. The conclusion of each chapters are present in the following section. Also recommendation to advance the knowledge gain from this study is also suggested in this chapter.

7.1 Conclusions

7.1.1 Conclusions based on Chapter 2: Centrifuge experiments and results

In this chapter, details of the centrifuge test and procedures was discussed. Series of the six different test conditions and results were discussed. This chapter was focused on simulating the realistic condition of levee subjected to flooding and behaviour of levee when provided with the protection. Conclusion from this chapter are:

- With increase in flood head, increased seepage flow cause the weakening of the slope starting from toe region which eventually cause the failure of levee.
- When levee is protected with pipes with only drainage or only reinforcement, resistance of levee against flooding is increased however is not sufficient to protect against longer and larger flood.
- From the experiment it is observed that, on the condition pore water pressure near the toe region is limited within 10 kPa, slope failure is prevented even in absence of reinforcement.
- With the use of the reinforcement, levee can with stand higher pore water pressure, however higher pore water pressure can cause erosion of soil especially near pipes. This erosion of soil near pipes creates weak zone making levees vulnerable.

7.1.2 Conclusions based on Chapter 3:1g Physical model test and results

In this chapter, the details of the single gravity experiment are discussed. In this series of the experiment, rising rate flood level is maintained equal through all test, making it possible for direct comparison among the cases which was not achieved through centrifuge test. Conclusion from this chapter are:

- Superior performance of the steel drainage pipes over pipes with only reinforcement is confirmed through test result under similar condition
- Presence of steel pipe restrict the collapse soil through the mobilisation of reinforcing force of pipe
- The presence of only reinforcement reduced the depth of the slip surface by 70% compared to unreinforced case.
- The steel drainage pipe with the presence of the drainage and reinforcement reduced the maximum pore water pressure by 19% and deformation was completely prevented.

7.1.3 Conclusions based on Chapter 4: Numerical simulation of physical model test

Numerical programme can be only used for the study of soil behaviour if it can simulate the realistic condition with the acceptable confidence. In this chapter numerical programme is validated by using the centrifuge result. The conclusions from this chapter are:

- Numerical programme is able to predict the development of pore water pressure in the model ground both in trend and magnitude
- The initiation of the failure and trend of deformation is captured by the numerical programme
- Mobilisation of the reinforcing force in pipe, lowering of the phreatic surface through drainage is well predicted by the numerical programme making it suitable for the parametric studies.

7.1.4 Conclusions based on Chapter 5: Working mechanism of steel drainage pipe

In this chapter working mechanism of steel drainage pipe which combines the drainage and reinforcement function is discussed through centrifugal tests and 1g test. The conclusion for this chapter are

- The protected slope can withstand the higher flood water level and longer flood duration. Also, propagation of the slip surface and deformation is limited.
- The drainage function of the steel drainage pipe limits the rise of the phreatic surface in the levee through the quick drainage of the seepage water from the levee. The drainage of seepage water limits the rise of the pore water pressure, especially near the slope surface.
- With the specifications of the steel pipe used in the model slope the reinforcement is provided through the mobilization of the axial force and mobilization of bending moment that provides additional confinement to the soil in the shallower portion.
- Factor of safety is increased in levee with steel drainage pipes by almost 11 times compared to unreinforced case, almost by 8 times compared to levee provided with only drainage and almost by 6 times compared to the levee provided with only reinforcement.
- Mobilization of the axial force is contributed by (i) end reaction developed due to the portion of the steel pipe with spiral blades and (ii) skin friction between the soil and pipe. End reaction is not adequately mobilized in the pipes without drainage due to the presence of the higher phreatic surface.
- From this series of the experiment, it is concluded that the presence of the pipe cause differential settlement between free fields and place of location of the pipe, which is caused by mobilization of the bending moment. Bending moment mobilization cause strengthening of slope and limits the deformation.
- Similarly, with the horizontal movement, axial force is mobilised also contributing to the slope stability. Pipe when combined with both drainage and reinforcement provides maximum protection and prevents failure of the slope.

7.1.5 Conclusions based on Chapter 6: Effectiveness of steel drainage pipes against flooding

In this chapter series of the parametric studies were made using the numerical analysis. From these numerical analysis following conclusion are made:

- Use of steel drainage pipe provides better protection than the pipes with only drainage and reinforcement when subjected to the same flooding.
- On comparing the pipes with only drainage and only reinforcement, pipes with drainage provide better protection against flooding.
- Deformation in levee with steel drainage pipes made of soil with hydraulic conductivity from 4.5E-5 m/s to 4.5E-2 m/s remains consistent across the range.
- In the soil with very low hydraulic conductivity, installation of the steel drainage pipes do not contribute to the lowering of pore water pressure and consequently to the deformation as well.
- In unreinforced levee, speed of flooding rising level effects the progression of phreatic surface within the levee whereas in the case provided with steel drainage pipes progression is minimally affected by the speed of rising of flood level.
- Speed of the rise of flood level in unreinforced case cause the change in the maximum value of deformation.
- Maximum deformation in levee with steel drainage pipe is independent of the speed of rising of flood level; rather, it is dependent on the flood level only.
- The overall deformation of the slope is more controlled by the location of the phreatic surface within the slope. Thus installation of the steel drainage pipe at lower elevation would be more effective in minimizing deformation in slope subjected to flooding.
- Closer spacing of steel drainage pipes will provide lower deformation; however, for the range of the spacing of 2-5 m model ground goes under similar deformation.
- If pipes are installed at very large spacing, the installation of steel drainage pipes will provide no improvement in deformation control.

7.2 Recommendations

River levee are very important geotechnical structures constructed on the river banks protecting settlement area and important civil infrastructure. Levees are constructed and restructured over the years, making it very heterogeneous structure. Usually levee failure are initiated from specific weak point within this heterogeneity. Also, the weakness in levee can be present in form of the cracks from the disaster such as earthquake. This study considered the homogenous levee body as the model ground having relatively steep slope. So, it would be useful to study the behaviour of non-homogenous levee with steel drainage pipe. Also, performance of steel drainage pipe on various model ground with different slope angle, with different slope height and different floods to determine the design chart would be a step further in the study.

References

Ahuja, L.R., Naney, J.W., Williams, R.D., 1985. Estimating soil water characteristics from simpler properties or limited data. Soil Sci. Soc. Am. J. 49, 1100–1105.

Allersma, H.G.B., Bartsch, M., 2004. Centrifuge tests on methods stabilizing embankments, in: Advances in Geotechnical Engineering with Emphasis on Dams, Highway Materials, and Soil Improvement. pp. 311–322.

Arya, L.M., Paris, J.F., 1981. A physioempirical model to predict the soil moisture characteristics from particle size. Soil Sci. Soc. Am. J. 45, 1023–1030.

Barden, L., Madedor, A.O., Sides, G.R., 1969. Volume change characteristics of unsaturated clay. J. Soil Mech. Found. Div. 95, 33–52.

Bea, R.G., 2008. Failure of the New Orleans 17th street canal levee and floodwall during Hurricane Katrina. Berkeley, CA.

Biot, M., 1941. General theory of three-dimensional consolidation. J. Appl. Phys. 26, 148–152.

Bishop, A., 1960. The measurement of pore pressure in the triaxial test, in: Pore Pressure and Suction in Soils. Butterworth & Company, London, Butterworth, London, pp. 38–46.

Bishop, A.W., Blight, G.E., 1963. Some aspects of effective stress in saturated and unsaturated soils. Geotechnique 13, 177–197.

Brandenberg, S.J., Wilson, D.W., Rashid, M.M., 2010. Weighted Residual Numerical Differentiation Algorithm Applied to Experimental Bending Moment Data. J. Geotech. Geoenvironmental Eng. 136, 854–863.

Brooks, R.H., Corey, A.T., 1964. Hydraulic properties of porous medium, Hydrology Paper 3. Fort Collins, Colo.

Cai, F., Ugai, K., 2003. Reinforcing mechanism of anchors in slopes: a numerical comparison of results of LEM and FEM. Int. J. Numer. Anal. Methods 27, 549–564.

Cai, F., Ugai, K., 2000. Numerical Analysis of the Stability of a Slope Reinforced with Piles. Soils Found. 40, 73–84.

Cai, F., Ugai, K., Wakai, A., Li, Q., 1998. Effects of horizontal drains on slope stability under rainfall by three-dimensional finite element analysis. Comput. Geotech. 23, 255–275.

Camici, S., Barbetta, S., Moramarco, T., 2015. Levee body vulnerability to seepage: the case study of the levee failure along the Foenna stream on 1st January 2006(central Italy). J. flood risk Manag. 8, 1–20. doi:10.1111/jfr3.12137

Cargill, K.W., Ko, H.-Y., 1983. Centrifugal modeling of transient water flow. J. Geotech. Eng. 109, 536–555.

Chappell, B., 2015. Japanese River Levee Fails; Flooding Spurs Evacuation Order For 130,000 [WWW Document]. Two W. NPR. URL https://www.npr.org/sections/thetwo-way/2015/09/10/439106520/japanese-river-levee-fails-flooding-spurs-evacuation-order-for-130-000 (accessed 10.1.15).

Chen, C.N., Chen, H.Y., 2016. Distributions of Pore Water Pressure Surround a Horizontal Drain Pipe on a Retaining Wall Under Steady State Condition. J. Mech. 29, 263–272. doi:10.1017/jmech.2012.132

Chen, R.H., Chen, A.H.P., Chen, A.K.S., Zhung, A.H.B., Chen, H.P., Zhung, Á.H.B., Chen, K.S., 2009. Simulation of a slope failure induced by rainfall infiltration. Env. Geol 58, 943–952. doi:10.1007/s00254-008-1574-8

Chen, X., Huang, J., 2011. Stability analysis of bank slope under conditions of reservoir impounding and rapid drawdown. J. Rock Mech. Geotech. Eng. 3, 429–437. doi:10.3724/SP.J.1235.2011.00429

Chin, K.B., Leong, E.C., Rahardjo, H., 2010. A simplified method to estimate the soil-

watercharacteristic curve. Can. Geotech. J. 47, 1382–1400.

Cho, S.E., 2014. Probabilistic stability analysis of rainfall-induced landslides considering spatial variability of permeability. Eng. Geol. 171, 11–20.

Choi, E.C.C., 1984. Seepage around Horizontal Drains in Hill Slopes. J. Hydraul. Eng. 109, 1363–1368. doi:10.1061/(ASCE)0733-9429(1983)109:10(1363)

Chu-Agor, M.L., Fox, G.A., Cancienne, R.M., Wilson, G.V., 2008. Seepage caused tension failures and erosion undercutting of hillslopes. J. Hydrol. 359, 247–259. doi:10.1016/j.jhydrol.2008.07.005

Colman, J., 1962. Stress strain relations for partly saturated soil. Géotechnique 12, 348–350.

Drucker, D., Prager, W., 1952. Soil mechanics and plastic analysis or limit design. Quart. Appl. Math. 10, 157–175.

Fredlund, D., Xing, A., Huang, S., 1994. Predicting the permeability function for unsaturated soils using the soil-water characteristic curve. Can. Geotech. J. 31, 533–546.

Fredlund, D.G., 1995. Prediction of the unsaturated soil functions using soil-water characteristic curve, in: Proceeding of Bengt B.Broms Symposium in Geotechnical Engineering. Singapore.

Fredlund, D.G., Morgenstern, N.R., 1977. Stress State Variables for Saturated and Unsaturated Soils. J. Geotech. Div.

Fredlund, D.G., Rahardjo, H., 1993. Soil Mechanics for Unsaturated Soils. John Wiley & Sons.

Fredlund, D.G., Rahardjo, H., Fredlund, M.D., 2012. Unsaturated soil mechanics in engineering practice. John Wiley & Sons.

Fredlund, D.G., Xing, A.A., 1994. Equations for the soil-water characteristic curve. Can.

Geotech. J. 31, 521–532.

Fredlund, M.D., Fredlund, D.G., Wilson, G.W., 1997. Prediction of the Soil-Water Characteristic Curve from Grain-Size Distribution and Volume-Mass Properties, in: Proceeding of Third Brazilian Symposium on Unsaturated Soils, Rio de Janerio, Brazil, 22-25 April. pp. 13–23.

Fung, Y.C., 1965. Foundation of solid mechanics. Prentice-Hall, Englewood Cliffs, NJ.

Gasmo, J.M., Rahardjo, H., Leong, E.C., 2000. Infiltration effects on stability of a residual soil slope. Comput. Geotech. 26, 145–165. doi:10.1016/S0266-352X(99)00035-X

Gavin, K., Xue, J., 2008. A simple method to analyze infiltration into unsaturated soil slopes. Comput. Geotech. 35, 223–230. doi:10.1016/j.compgeo.2007.04.002

Ghiassian, H., Ghareh, S., 2008. Stability of Sandy Slopes Under Seepage Conditions. Landslides 5, 397–406. doi:10.1007/s10346-008-0132-5

Hamdhan, I.N., Schweiger, H.F., 2011. Slope Stability Analysis of Unsaturated Soil with Fully Coupled Flow-Deformation Analysis, in: Mathematical Geoscience at the Crossroads of Theory and Practice. Salzburg, Austria. doi:10.5242/iamg.2011.0063

Han, J., Gabr, M.A., 2002. Numerical Analysis of Geosynthetic-Reinforced and Pile-Supported Earth Platforms over Soft Soil. J. Geotech. Geoenvironmental Eng. 128, 44–53. doi:10.1061/(asce)1090-0241(2002)128:1(44)

Heber Green, W., Ampt, G.A., 1911. Studies on Soil Phyics. J. Agric. Sci. 4, 1. doi:10.1017/S0021859600001441

Hori, T., Mohri, Y., Kohgo, Y., Matsushima, K., 2011. Model Test and Consolidation Analysis of Failure of a Loose Sandy Embankment Dam during Seepage. Soils Found. 51, 53–66. doi:10.3208/sandf.51.53

Horikoshi, K., Takahashi, A., 2015. Suffusion-induced change in spatial distribution of fine fractions in embankment subjected to seepage flow. Soils Found. 55, 1293–1304. doi:10.1016/j.sandf.2015.09.027

Jia, G.W., Zhan, T.L.T., Chen, Y.M., Fredlund, D.G., 2009. Performance of large scale slope model subjected to rising and lowering water levels. Eng. Geol. 106, 92–103.

Kasim, F.B., Fredlund, D.G., Gan, J..-M., 1998. Effect of steady state rainfall on long term matric suction condition in slopes, in: Proceeding of the Second International Conference on Unsaturated Soils. Beijing, China, pp. 78–83.

Koito, N., Horikoshi, K., Takahashi, A., 2016. Physical modelling of backward erosion piping in foundation beneath levee, in: 8th International Conference on Scour and Erosion. Taylor and Francis Group, Oxford, UK, pp. 445–451.

Kosugi, K., 1999. General model for unsaturated hydraulic conductivity for soils with lognormal pore-size distribution. Soil Sci. Soc. Am. J. 63, 270–277. doi:10.2136/sssaj1999.03615995006300020003x

Krahn, J., Fredlund, D.G., Klassen, M.J., 1989. Effect of soil suction on slope stability at Notch Hill. Can. Geotech. J. 26, 269–278. doi:10.1139/t89-036

Kristo, C., Rahardjo, H., Satyanaga, A., 2017. Effect of variations in rainfall intensity on slope stability in Singapore. Int. Soil Water Conserv. Res. 5, 258–264. doi:10.1016/j.iswcr.2017.07.001

Kumar, P.R., 2007. Scaling Laws and Experimental Modelling of Contaminant Transport Mechanism through Soils in a Geotechnical Centrifuge. Geotech. Geol. Eng. 25, 581–590. doi:10.1007/s10706-007-9131-x

Lau, K.C., Kenney, T.C., 1984. Horizontal drains to stabilize clay slopes. Can. Geotech. J. 21, 241–249. doi:10.1139/t84-027

Leong, E.C., Rahardjo, H., 1997. Review of Soil-Water Characteristic Curve Equations. J. Geotech. Geoenvironmental Eng. 123, 1106–1117. doi:10.1061/(ASCE)1090-0241(1997)123:12(1106)

Li, J., Tham, L.G., Junaideen, S.M., Yue, Z.Q., Lee, C.F., 2008. Loose Fill Slope Stabilization with Soil Nails: Full-Scale Test. J. Geotech. Geoenvironmental Eng.

134, 277–288. doi:10.1061/ASCE1090-0241(2008)134:3(277)

Li, W.C., Lee, L.M., Cai, H., Li, H.J., Dai, F.C., Wang, M.L., 2013. Combined roles of saturated permeability and rainfall characteristics on surficial failure of homogeneous soil slope. Eng. Geol. 153, 105–113. doi:10.1016/J.ENGGEO.2012.11.017

Ling, H.I., Wu, M.-H., Leshchinsky, D., Leshchinsky, B., 2009. Centrifuge Modeling of Slope Instability. J. Geotech. Geoenvironmental Eng. 135, 758–767. doi:10.1061/(ASCE)GT.1943-5606.0000024

Matyas, E.L., Radhakrishna, H.S., 1968. Volume change characteristics of partially saturated soils. Geotechnique 18, 432–448.

Miao, F., Wu, Y., Li, L., Tang, H., Li, Y., 2018. Centrifuge model test on the retrogressive landslide subjected to reservoir water level fluctuation. Eng. Geol. 245, 169–179. doi:10.1016/J.ENGGEO.2018.08.016

Morgenstern, N.R., Price, V.E., 1967. A numerical method for solving the equations of stability of general slip surfaces. Comput. J. 9, 388–393.

Ng, C.W.. C., Zhan, L.T.L., Bao, C.C.G., Fredlund, D.G., Gong, B.W., 2003. Performance of an unsaturated expansive soil slope subjected to artificial rainfall infiltration. … 53, 143–157.

Ng, C.W.W., Zhang, L.M., Wang, Y.H., 2006. The effects of soil nails in a dense steep slope subjected to rising groundwater, in: Ng, Zhang, Wang (Eds.), Physical Modelling in Geotechnics : 6th ICPMG ’06. Taylor & Francis, Hong Kong, pp. 397–401.

Nobuyuki, T., 2004. A Flash Report on flood disaster caused by a heavy rainfall in the Hokuriku region in July 2004. J. Japanese Soc. Civ. Eng. 89, 7–10.

P. Orense, R., Shimoma, S., Maeda, K., Towhata, I., 2006. Instrumented Model Slope Failure due to Water Seepage. J. Nat. Disaster Sci. 26, 15–26.

doi:10.2328/jnds.26.15

Polemio, M., Lollino, P., 2011. Failure of infrastructure embankments induced by flooding and seepage: a neglected source of hazard. Nat. Hazards Earth Syst. Sci 11, 3383–3396. doi:10.5194/nhess-11-3383-2011

Rahardjo, H., Hritzuk, K.J.J., Leong, E.C.C., Rezaur, R.B.B., 2003. Effectiveness of horizontal drains for slope stability. Eng. Geol. 69, 295–308. doi:10.1016/S0013-7952(02)00288-0

Rahardjo, H., Santoso, V.A., Leong, E.C., Ng, Y.S., Hua, C.J., 2011. Performance of Horizontal Drains in Residual Soil Slopes. Soils Found. 51, 437–447.

Rahimi, A., Rahardjo, H., Leong, E.-C., 2015. Effect of range of soil–water characteristic curve measurements on estimation of permeability function. Eng. Geol. 185, 96–104. doi:10.1016/j.enggeo.2014.11.017

Rahimi, A., Rahardjo, H., Leong, E.-C., 2010. Effect of hydraulic properties of soil on rainfall-induced slope failure. Eng. Geol. 114, 135–143.

Rangitaiki River Scheme Review- April 2017 Flood Event, 2017. . Edgecumbe. doi:https://www.boprc.govt.nz/media/773858/rangitaiki-river-scheme-review-april-2017-flood-event-final-report-as-supplied-to-by-of-plenty-regional-council.pdf

Resnick, G.S., Znidarcic, D., 1990. Centrifugal modeling of drains for slope stabilization. J. Geotech. Eng. 116, 1607–1624.

Rotte, V.M., Viswanadham, B.V.S., 2012. Performance of 2V:1H Slopes with and without Soil-Nails Subjected to Seepage: Centrifuge Study, in: GeoCongress, ASCE. pp. 643–652.

Santoso, A.M., Phoon, K.-K., Quek, S.-T., 2011. Effects of soil spatial variability on rainfall-induced landslides. Comput. Struct. 89, 893–900. doi:10.1016/J.COMPSTRUC.2011.02.016

Saran, R.K., Viswanadham, B.V.S., 2018. Centrifuge model tests on the use of geosynthetic layer as an internal drain in levees. Geotext. Geomembranes 46, 257–276. doi:10.1016/j.geotexmem.2017.12.004

Sato, T., Fukuzono, T., Ikeda, S., 2006. The Niigata flood in 2004 as a flood risk of low probability but high consequence, in: A Better Integrated Management of Disaster Risks: Toward Resilient Society to Emerging Disaster Risks in Mega-Cities. Terra, Tokyo, pp. 177–192.

Schnellmann, R., Busslinger, M., Schneider, H.R., Rahardjo, H., 2010. Effect of rising water table in an unsaturated slope. Eng. Geol. 114, 71–83. doi:10.1016/j.enggeo.2010.04.005

Song, K., Wang, F., Yi, Q., Lu, S., 2018. Landslide deformation behavior influenced by water level fluctuations of the Three Gorges Reservoir (China). Eng. Geol. 247, 58–68. doi:10.1016/J.ENGGEO.2018.10.020

Sun, G., Yang, Y., Jiang, W., Zheng, H., 2017. Effects of an increase in reservoir drawdown rate on bank slope stability: A case study at the Three Gorges Reservoir, China. Eng. Geol. 221, 61–69. doi:10.1016/J.ENGGEO.2017.02.018

Sutherland, H.J., Rechard, R.P., 1984. Centrifuge simulations of stable tailings dam. J. Geotech. Eng. 110, 390–402.

Takahashi, A., 2002. Soil-pile interaction in the liquefaction-induced lateral spreading of soils. PhD Diss. Tokyo Institute of Technology.

Takemura, J., Kondoh, M., Esaki, T., Kouda, M., Kusakabe, O., 1999. Centrifuge model tests on double propped wall excavation in soft clay. Soils Found. 39, 75–87.

Taylor, P., Maleki, M.R., Mahyar, M., 2012. Effect of nail characteristics on slope stability based on limit equilibrium and numerical methods. Geomech. Geoengin. An Int. J. 7, 197–207.

Tei, K., Taylor, R.N., Milligan, G.W.E., 1998. Centrifuge Model Tests of Nailed Soil

Slopes. Soils Found. 38, 165–177.

Terzaghi, K., 1936. The shearing resistance of saturated soils and the angle between the planes of shear, in: Proceedings of the First International Conference on Soil Mechanics.

Thusyanthan, N.I., Madabhushi, S.P.G., 2003. Scaling of Seepage Flow Velocity in Centrifuge Models.

Timpong, S., Itoh, K., Toyosawa, Y., 2007. Geotechnical centrifuge modelling of slope failure induced by ground water table change, in: Mclnnes, Jakeways, Fairbank, Mathie (Eds.), Landslide and Climate Change. Taylor and Francis Group, London, pp. 107–112.

Tsaparas, I., Rahardjo, H., Toll, D.., Leong, E.., 2002. Controlling parameters for rainfall-induced landslides. Comput. Geotech. 29, 1–27. doi:10.1016/S0266-352X(01)00019-2

Van Genuchten, M., 1980. A closed-form equation for predicting the hydraulic conductivity of unsaturated soils. Soil Sci. Soc. Am. J. 44, 892–898.

Vanapalli, S.S.K., Fredlund, D.G.G., Pufahl, D.E., Clifton, A.W., Pufahl, M.D., Clifton, A.W., 1996. Model for the prediction of shear strength with respect to soil suction. Can. Geotech. J. 33, 379–392.

Vandamme, J., Zou, Q., 2013. Investigation of slope instability induced by seepage and erosion by a particle method. Comput. Geotech. 48, 9–20. doi:10.1016/j.compgeo.2012.09.009

Wang, G., Sassa, K., 2003. Pore-pressure generation and movement of rainfall-induced landslides: effects of grain size and fine-particle content. Eng. Geol. 69, 109–125. doi:10.1016/S0013-7952(02)00268-5

Wei, W.B., Cheng, Y.M., 2009. Strength reduction analysis for slope reinforced with one row of piles. Comput. Geotech. 36, 1176–1185.

doi:10.1016/J.COMPGEO.2009.05.004

Yang, M., Deng, B., 2019. Stability study of slope reinforced with piles under steady unsaturated flow conditions. Comput. Geotech. 109, 89–98. doi:10.1016/j.compgeo.2019.01.020

Zapata, C.E., 1999. Uncertainity in soil-water-characteristic curve and impacts on unsaturated shear strength prediction. Arizona State University.

Zhan, T.L.T., Ng, C.W.W., Asce, M., 2004. Analytical Analysis of Rainfall Infiltration Mechanism in Unsaturated Soils. Int. J. Geomech. 4, 273–284. doi:10.1061/(ASCE)1532-3641(2004)4:4(273)

Zhang, J., Pu, J., Zhang, M., Qiu, T., 2001. Model Tests by Centrifuge of Soil Nail Reinforcements. J. Test. Eval. JTEVA 29, 315–328. doi:10.1520/JTE12261J

Zhang, L., Chen, Q., 2005. Predicting Bimodal Soil–Water Characteristic Curves. J. Geotech. Geoenvironmental Eng. 131, 666–670. doi:10.1061/(ASCE)1090-0241(2005)131:5(666)

Zhang, L.L., Zhang, L.M., Tang, W.H., 2015. Rainfall-induced slope failure considering variability of soil properties. Risk Var. Geotech. Eng. 215–220. doi:10.1680/ravige.34860.0022

Zhang, W.J., Maeda, K., 2014. The Model Test and SPH Simulations for Slope and Levee Failure under Heavy Rainfall Considering the Coupling of Soil, Water and Air, in: Soil Behavior and Geomechanics GSP 236. pp. 538–547. doi:10.1061/9780784413388.056

Zhou, W.-H., Lao, J.-Y., Huang, Y., Chen, R., 2017. Group effect on soil arching in geogrid-reinforced pile-supported embankments. Japanese Geotech. Soc. Spec. Publ. 5, 130–134. doi:10.3208/jgssp.v05.035

Zhou, Y.D., Cheuk, C.Y., Tham, L.G., 2009. Deformation and crack development of a nailed loose fill slope subjected to water infiltration. Landslides 6, 299–308.

doi:10.1007/s10346-009-0162-7